Mechanisms and physiological implications of mitochondrial and cellular calcium signaling

Melissa J. MacEwen

A dissertation

submitted in partial fulfillment of the

requirements for the degree of

Doctor of Philosophy

University of Washington

2023

Reading Committee:

Yasemin Sancak, Chair

Suzanne Hoppins

Philip Morgan

Program Authorized to Offer Degree:

Pharmacology

University of Washington

Abstract

Mechanisms and physiological implications of mitochondrial and cellular calcium signaling

Melissa J. MacEwen

Chair of the Supervisory Committee:

Yasemin Sancak

Department of Pharmacology

Calcium signaling is central to fields as disparate as memory formation, protein structure, and cellular migration. The five chapters of this dissertation each examine calcium signaling in a different context. First, an introduction contextualizes this dissertation in the broader history of calcium signaling and mitochondrial biology. Secondly, a review details the most salient contributions to the field of mitochondrial calcium signaling in recent years. Third, a research publication clarifies why the metazoan mitochondrial calcium uniporter (MCU) requires another protein, EMRE, to conduct calcium ions. The fourth chapter provides an overview of an ongoing project examining potential metabolic "rewiring" that enables mitochondria to produce energy and metabolites even when mitochondrial calcium signaling is compromised. Finally, the fifth chapter uses experimental biochemistry to determine which of three proposed mathematical models most accurately reflects the binding between calmodulin (CaM) and myosin light-chain kinase (MLCK).

TABLE of CONTENTS

GLOSSARY of ABBREVIATIONS

Abbreviation	Full Name
µg	Microgram
µM	Micromolar
Å	Angstrom
ATP	Adenosine triphosphate
BAT	Brown adipose tissue
Ca^{2+}	Calcium (ion)
CaM	Calmodulin
DOI	Digital object identifier
EDTA	Ethylenediaminetetraacetic acid
Em	Emission
ER	Endoplasmic reticulum
Ex	Excitation
FAO	Fatty acid oxidation
FLAG	DYKDDDDK protein affinity tag
GO	Gene ontology
IMM	Inner mitochondrial membrane
kDa	Kilodalton
KD	Knockdown
KO	Knockout
MCU	Mitochondrial calcium uniporter
MICU (1-3)	Mitochondrial calcium uptake protein (1-3)
mg	Milligram
Mg^{2+}	Magnesium (ion)
MLCK	Myosin light-chain kinase
mM	Millimolar
mPTP	Mitochondrial permeability transition pore
mtDNA	Mitochondrial DNA
Na^{+}	Sodium (ion)
NCLX	Na^{+}/Ca^{2+} exchanger
nM	Nanomolar
OMM	Outer mitochondrial membrane
OXPHOS	Oxidative phosphorylation
SD	Standard deviation
shRNA	Short hairpin RNA
TCA	Tricarboxylic acid (as in TCA cycle)
RNA-seq	RNA sequencing
rRNA	Ribosomal RNA
tRNA	Transfer RNA
VDAC	Voltage-dependent anion channel
WT	Wild type

ACKNOWLEDGEMENTS

Dr. Yasemin Sancak

Yasemin, I can't even begin to thank you for everything you have provided during these key years in your lab. It has been a thrilling adventure to join you as you get your lab off the ground. You are an incredible scientist, mentor, colleague and friend. You have pushed me to do better, and to aim higher, than I ever thought possible. From helping me pull my first publication together, to giving me the freedom to apply for fellowships, to supporting my interest in science communication, to being a sympathetic ear during the COVID-19 pandemic, few people have shaped my life quite so profoundly as you have. Your brilliance, empathy, and dedication continue to inspire me. Thank you for everything.

My thesis committee

I am incredibly grateful to my thesis committee – Dr. Sandy Bajjalieh, Dr. John Scott, Dr. Phil Morgan and Dr. Suzanne Hoppins. Your enthusiasm for my project (and Grateful Dead quotes), as well as your clear-eyed feedback for my various projects, has been invaluable. Thank you.

The University of Washington Department of Pharmacology

Science can be hard. Science can be exhausting. To be part of a department that is consistently kind, helpful and accommodating has truly been a life saver during my time as a doctoral student. I joined the Department of Pharmacology because of its highly collaborative nature, and its dedication to its students, faculty, and trainees. I was not

disappointed. My time as a student here has taught me much more than technical lab skills. By participating in such a pro-social department, I have strengthened my ability to work on a team, to focus on big picture questions that address well-crafted hypotheses, and to effectively share my ideas. We are a small department, but we are mighty, and I am proud to call the Department of Pharmacology my home. Thank you.

The Sancak Lab

Thank you as well to the rest of the Sancak Lab members. George, Tim, Nicole, Hayden, Albert, Caitlin – you are aces in my book and I treasure our time both in and out of lab. We made it through a pandemic and we're still going strong! Going to work truly is a pleasure with labmates like you, whether we're sharing methods, looking at each other's data, or enjoying a beer hour together. Thank you.

My friends

Finding and maintaining friendships in adulthood is notoriously difficult. I feel fortunate beyond measure to have the strongest friendships now, that I've had in my entire life. To my friends in the Department of Pharmacology and beyond – thank you, thank you, thank you. It is a pleasure to know you. I treasure you.

DEDICATIONS

To my mother, Jennifer MacEwen:

Sometimes, I wake up feeling like the luckiest person on Earth to have such a supportive person in my life. You have been my rock through my undergraduate degree, my time in industry, and now, a Ph.D. Your kindness and patience empowered me to push forward despite obstacles. You have cheered me on sad days, and celebrated with me on happy days. Who could ask for more?

To my father, David MacEwen:

You inspire me every day, in ways you are probably not even aware of. You push me to be brave, to dream big, and to always make time for fun along the way. Your thoughtful interest in my evolving scientific pursuits, and your constant faith in me, have helped me to achieve more than I ever thought possible. Truly. In your own words: “Shoot for the stars. Maybe land on the garage roof.” No matter where I end up, the view is always pretty good.

I love you both so much.

CHAPTER 1:

Introduction

‘‘Ja Kalzium, das ist alles![1]’’

O. Loewi, 1959

PREAMBLE

A discussion of calcium signaling risks straying into realms of exaltation that seem to border on hyperbole. In the words of Dr. Ernesto Carafoli, “At first glance…calcium could be considered both an essential mediator of activity during cell life and as a conveyor of doom at the moment of cell death. Such a view, however, would be simplistic (Carafoli, 2002).” Nevertheless, this grandiosity is fully merited: it is nearly impossible to overstate the immense importance of calcium in physiology and cell biology. From protists to primates, calcium shapes our bodies and our world. Keeping the vast, loosely defined scope of the calcium signaling field in mind, this doctoral dissertation endeavors to share the author’s contribution to this field by clarifying how calcium is utilized and regulated in several key contexts.

This dissertation contains five chapters. First, this **Introduction (Chapter One)** provides a brief overview of the fields of calcium signaling and mitochondrial biology, with an emphasis on the origins of the mitochondrial calcium signaling subfield. Because

[1] Though Otto Loewi’s proclamation literally translates to “Yes calcium, that’s all,” it is more broadly understood to mean “Calcium is everything” or “Calcium is universal” (Brini & Carafoli, 2000)

Chapter Two is a review article that focuses on mitochondrial calcium signaling, and because each of the subsequent experimental chapters contains an introduction contextualizing the relevant project, this introduction attempts to provide additional useful background information.

Chapter Two is comprised of a review concerning noteworthy developments in the field of mitochondrial calcium signaling, with a focus on the last ~5 years. The last two decades have witnessed explosive growth in this subfield and have yielded dramatic, paradigm-shifting developments in our understanding of the dynamic calcium signaling between the mitochondria and the rest of the cell. Now that many of the dominant protein players have been identified, recently published work has expanded our knowledge of the relevance of mitochondrial calcium signaling to human physiology and disease. That in mind, in the review, particular attention is paid to the physiological relevance of recent findings, as well as the primary concerns for this subfield moving forward.

The next three sections concern calcium signaling in three different experimental contexts. **Chapter Three** consists of a publication that endeavored to answer a seemingly straight-forward question: why does the metazoan mitochondrial calcium uniporter complex require the protein EMRE to function, while many other species do not? Metazoans, it bears clarifying, are organisms broadly considered “animals.” The publication of this project, which utilizes a hybrid approach of biochemistry techniques and functional testing, dovetailed tidily with a surge of publications examining the structure of the mitochondrial calcium uniporter complex and its constituent proteins. The findings of the project suggest that EMRE dependence originates in an 8-amino acid long sequence in the *Homo sapiens* MCU protein; without EMRE, this region is pliant and

blocks the exit of Ca^{2+} from the uniporter complex into the mitochondrial matrix. Because the mitochondrial calcium uniporter complex plays a role in a wide variety of human diseases in addition to regulating mitochondrial function and metabolism, this work has relevance to a wide range of future research.

Chapter Four, an intriguing project whose scope extends beyond this dissertation, centers on characterizing what we believe to be metabolic "rewiring" that occurs when mitochondrial calcium signaling is disrupted, as in the case of human disease. It has remained unclear why some mouse strains with disrupted mitochondrial calcium signaling (MCU KO) survive, while other mouse strains do not. Preliminary data collected using mass spectrometry, RNA-seq, lipidomics, and growth curve data suggests cells that survive the loss of mitochondrial calcium signaling, do so by upregulating an alternative metabolic pathway that centers on the conversion of select amino acids and lipids to propionyl-CoA and then to succinyl-CoA. In doing so, they are able to bypass steps of the citric acid cycle that are governed by mitochondrial calcium. Future work will verify and expand upon this preliminary data.

Finally, **Chapter Five** showcases a collaboration between the Sancak Lab and Dr. Joseph Dexter of Harvard University that experimentally tested several models of binding between calmodulin and myosin light-chain kinase (MLCK). Calmodulin is one of the most conserved of all proteins, and is the most conserved EF-hand protein (Carafoli & Krebs, 2016). The binding of Ca^{2+}, calmodulin, and MLCK is essential for smooth muscle contraction. Though a variety of models have been proposed for the interaction between Ca^{2+}, calmodulin and MLCK, this project was the first to test the proposed models experimentally using a FRET-based reporter system paired with a suite of wild-type and

mutant calmodulin proteins. Our findings suggest that a partially ordered binding model best explains the interaction between these proteins.

A BRIEF HISTORY OF CELLULAR CALCIUM SIGNALING RESEARCH

Research into Ca^{2+} signaling began somewhat abruptly in 1883, albeit under experimental circumstances of dubious scientific rigor. While Sidney Ringer was studying the contraction of isolated rat hearts, he suspended the cells in a saline solution that he had prepared using London tap water. When Ringer ultimately replaced the tap water with distilled water, he observed that the hearts – which had once been beating forcefully – contracted more and more weakly. They eventually stopped entirely after 20 minutes. Ringer was ultimately able to restore contraction by supplementing his suspension medium with calcium salts; the hearts had beat in the initial medium preparation, it turned out, because London has hard water (Ringer, 1883; Carafoli, 2002). Though Ca^{2+} was long believed to play structural roles in the body by forming teeth and bones, Ringer had identified a novel function for the ion: as a signaling messenger.

In some ways, the discovery of Ca^{2+} signaling was timely. By 1883, several signaling molecules had either been discovered, or were on the cusp of characterization. Claude Bernard described the “internal secretions” of ductless glands affecting the behavior of distant cells, while in 1880 Charles Darwin discovered a chemical that would later be named auxin, which regulates plant growth and shoot curvature (Nair *et al*, 2019). Ernest Starling ultimately coined the term “hormone” in 1905, to refer to “the chemical messengers which spread from cell to cell along the bloodstream [and which] may coordinate the activities and growth of different parts of the body” (Henderson, 2005; Nair

et al, 2019) In retrospective, then, it is surprising Ringer's observation went largely unnoticed and uncelebrated by his scientific peers for more than 70 years.

Interest in Ca^{2+} accelerated quickly in the 1950s due to biological discoveries that shaped the perception of the field, as well as advancements in tools to study calcium signaling. Biologically, Weber discovered that the binding of Ca^{2+} to myofibrils activates actomyosin (Weber, 1959), and a series of laboratories discovered that isolated sarcoplasmic reticulum vesicles use a system powered by ATP to accumulate Ca^{2+} (Ebashi, 1961; Ebashi, 1962; Carafoli, 2002). Troponin C was also found to be the Ca^{2+} receptor mediating myofibrillar contraction (Ebashi & Kodama, 1965). Chemically, the synthesis of EDTA and subsequent experiments characterizing the molecule's Ca^{2+}-chelating properties enabled Bozler to remove Ca^{2+} from muscle fibers (Bozler, 1954; Carafoli, 2002). This era of research gave rise to the "calcium concept" (Ebashi, 1961) and paved the way for an ongoing explosion of research characterizing the many roles of Ca^{2+}.

We now know that calcium truly does accompany cells at every step of life. From a rush of calcium signaling paired seamlessly with the fertilization of an egg, to cellular motility and cellular division, to the formation of memories, to the final destruction of apoptosis, calcium signaling underpins cellular function and behavior at every turn.

ESSENTIAL WHYS AND HOWS OF CALCIUM SIGNALING

The centrality of Ca^{2+} signaling to cellular biochemistry begs a simple question: why Ca^{2+} in particular? Though there is no shortage of physiologically useful anions and cations, Ca^{2+} became one of the dominant physiological signal carriers because of its

abundance (it is the third most abundant metal found in nature) (Carafoli & Krebs, 2016) and its unique coordination chemistry. The interactions between ions and their ligands are determined by properties including the ions' valency, ionic radius, polarizability, hydration energy, and charge density (Carafoli & Krebs, 2016). For example, though Ca^{2+} and Mg^{2+} are both divalent cations, Mg^{2+} ions are relatively small (0.65 Å) and require a fixed octahedral geometry with six coordinating ligands and minimal variability between bond lengths. Ca^{2+} is a comparatively larger ion (99 Å) and is much more flexible in its acceptable bond length and the geometry of its ligand binding. Because the regulation of Ca^{2+} within a cell or organism is almost entirely governed by the binding of Ca^{2+} to ligands, this ease of binding makes it relatively straight-forward to control Ca^{2+} levels (Carafoli & Krebs, 2016). Furthermore, calcium phosphate salts are much less soluble than magnesium phosphate salts. The precipitation of Ca^{2+} phosphate granules has been found to alter cellular Ca^{2+} signaling, lead to the formation of complexes between Ca^{2+} phosphate and DNA, promote autophagy, and alter mitochondrial functions such as oxidative phosphorylation and mitochondrial structure. These additional mechanisms of regulation would be less viable given a more soluble chemical compound such as magnesium phosphate (Malyala *et al*,2019; Chen *et al*, 2014).

Ca^{2+} was adopted early in evolutionary history as a means of regulating cellular activity. As life evolved from single cell organisms to complex, multicellular organisms, the requirement for effective cellular regulation increased in tandem. These developments were made possible in large part due to increasingly sophisticated applications of Ca^{2+} signaling. Ca^{2+} can be regulated very precisely, on both large and small scales. Throughout evolution, organisms have utilized Ca^{2+} extensively because they have found

ways to rapidly toggle Ca^{2+} signaling between an “on” and an “off” state; Ca^{2+} can be released as a flood, or it can be rapidly sequestered. As stated eloquently by David Clapham in his 2007 review, “underlying the speed and effectiveness of Ca^{2+} is the 20,000-fold gradient maintained by cells between their intracellular (~100 nM free) and extracellular (1.1-1.4 mM free) concentrations” (Clapham, 2007; Atchison & Beierwaltes, 2012). Calcium signaling is now used extensively by eukaryotes ranging from mammals, to plants, to fungi (Dominguez, 2004), and prokaryotes including both bacteria and archaea also use Ca^{2+}-centered signaling systems (Norris *et al*, 1996; Marchadier *et al*, 2016)

A variety of proteins that can bind to and/or sense Ca^{2+} are essential for Ca^{2+} signaling. These proteins enable different parts of the cell to signal to one another by binding and releasing Ca^{2+} as a messenger, buffering Ca^{2+} concentrations in different compartments of the cells, and transporting Ca^{2+} ions across membranes. By extension, a key aspect of Ca^{2+} signaling is the concept of Ca^{2+}-binding motifs – that is, specific sequences of amino acids that enable Ca^{2+} to bind to proteins for the purpose of Ca^{2+} transport and/or signaling. The well characterized EF-hand motif is a protein domain with high Ca^{2+} affinity. It is comprised of approximately 30 amino acids (Chin & Means, 2000). During Ca^{2+} binding, the Ca^{2+}-binding site undergoes a conformational change that alters protein function. This domain is highly conserved and is known to appear in more than 800 Ca^{2+}-binding proteins (Carafoli & Krebs, 2016). Of these proteins, calmodulin (CaM) is one of the most highly conserved and ubiquitously expressed across eukaryotes (Carafoli & Krebs, 2016). Another Ca^{2+} binding motif is the C2-domain, which enables proteins to interact with phospholipids in a generally Ca^{2+}-dependent manner. This

domain consists of 120-130 amino acids and is most commonly utilized in signal transduction pathways or membrane trafficking. Synaptotagmin, a Ca^{2+} sensor important to exocytosis and neurotransmitter release, is one of the best characterized C2 proteins. Unlike EF-hand proteins, which undergo a conformation change upon Ca^{2+} binding, the binding of Ca^{2+} to C2-domains leads to the protein's structural stabilization (Carafoli & Krebs, 2016; Nalefski & Falke, 1996).

Ca^{2+}-transporting proteins also play an important role in cellular Ca^{2+} signaling and regulation as they help buffer Ca^{2+} concentrations. The plasma membrane Ca^{2+} channels are regulated by a variety of mechanisms including interactions with ligands such as glutamate; the emptying of Ca^{2+} stores (as with SOCE channels); changes in membrane electrical potential (such as voltage-gated CaV channels); and interactions with environmental signals such as temperature and pH (as with transient receptor potential channels which regulate Ca^{2+}) (Carafoli & Krebs, 2016). The endoplasmic reticulum (ER) and sarcoplasmic reticulum (SR) arguably contain the most critical Ca^{2+} channels within the cell, as these organelles store and release vast amounts of Ca^{2+} in response to stimuli. Ca^{2+} ATPases (Ca^{2+} pumps) also play essential regulatory roles in the cell by clearing Ca^{2+} from the cytosol and sequestering it in either the external space or the lumen of different organelles. The PMCA pump is located in the plasma membrane, while the SPCA pump is located in the Golgi, and the powerful SERCA pump is located in the ER/SR. Essential Ca^{2+}-transporting machinery is also found within the mitochondria. The mitochondrial calcium uniporter complex, for example, enables mitochondria to transport Ca^{2+} from the cytosol into the mitochondrial matrix, while the Na^{+}/ Ca^{2+} exchanger enables mitochondria to release Ca^{2+} back into the cytosol.

MITOCHONDRIAL FORM AND FUNCTION

Mitochondria likely arose approximately 1.5 billion years ago (Spees *et al*, 2006) when a eukaryotic progenitor engulfed an alpha-proteobacterium (Martin, 2017). These origins explain eukaryotic mitochondria's spatially and functionally distinct inner and outer membranes (IMM and OMM, respectively, with the mitochondrial matrix encapsulated by the IMM), specialized transcriptional and translational machinery, and circular mitochondrial DNA (mtDNA) (**Fig. 1**). mtDNA consists of around 17,000 base pairs, which encode 37 genes. Of these genes, 13 encode proteins required for oxidative phosphorylation (OXPHOS), 22 code for transfer RNA (tRNA), one codes for a large subunit of ribosomal RNA (rRNA), and one codes for a small subunit of rRNA (Anderson *et al*, 1981).

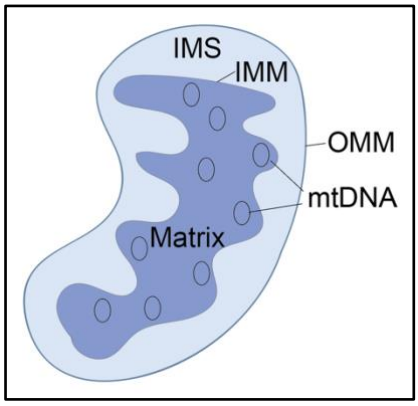

Figure 1. Mitochondrial structure Mitochondria consist of an outer mitochondrial membrane (OMM) and an inner mitochondrial membrane (IMM), with an intermembrane space (IMS) between them. Within the IMM is the mitochondrial matrix, which contains the circular mitochondrial DNA (mtDNA).

As their relationship with the rest of the cell evolved, mitochondria ceded the vast majority of their genetic information to the nucleus. They compensate for this loss by employing an elaborate, tightly regulated protein import system. Indeed, despite the small size of the mitochondrial genome, proteomic analyses have revealed that mammalian mitochondria contain approximately 1500 different proteins (Pfanner *et al*, 2019). Nuclear-encoded proteins destined for the mitochondria often feature a mitochondrial import signal termed a presequence (Mossman *et al*, 2012). Following cytosolic translation, these

precursor proteins are stabilized, protected from aggregation, and escorted through the cytosol to the mitochondria by chaperones (Stuart *et al*, 1994). Precursor proteins are then translocated across the outer mitochondrial membrane before being transported to their final destination by chaperones and cleaved to a mature form by specific presequence peptidases (Mossman *et al* 2012; Stuart *et al*, 1994). Proper localization and folding of mitochondrial proteins are vitally important to the health of the mitochondria and the cell. As such, mitochondria are in constant, precise communication with the rest of the cell so that the needs of the cell and mitochondria can be effectively met in response to changing circumstances.

Mitochondria are best known as producers of cellular energy and their ability to efficiently produce ATP is indeed unparalleled. While cytosolic glycolysis[2] can produce a total of two ATP molecules per initial molecule of glucose, mitochondrial OXPHOS[3] can produce upwards of 36-38 molecules of ATP – about 95% of the cell's energy (Tzameli, 2012). This staggering ATP production depends on proper cooperation of the citric acid cycle[4] and OXPHOS. These two processes overlap tightly, as products from the citric acid cycle are necessary for the proper functioning of OXPHOS. The citric acid cycle is comprised of a "cycle" of enzymes which break carbon chains into smaller and smaller components, yielding three NADH, one $FADH_2$, and one GTP molecule per "turn" of the cycle, in addition to CO_2 and H_2O waste. Notably, NADH and $FADH_2$ are subsequently utilized during OXPHOS. OXPHOS centers on the electron transport chain – a series of protein complexes (complexes one through four) embedded in the inner mitochondrial

[2] Glycolysis is considered anaerobic respiration, as it can proceed without oxygen
[3] OXPHOS is considered aerobic respiration, as it requires oxygen
[4] Other names for the citric acid cycle include the Krebs cycle and the tricarboxylic acid cycle (TCA cycle)

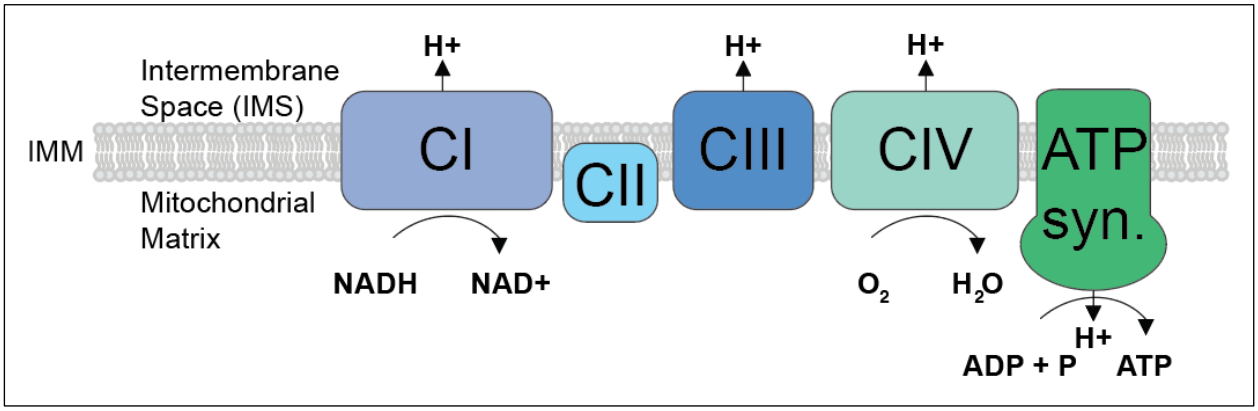

Figure 2. Mitochondrial oxidative phosphorylation (OXPHOS) depends on the protein complexes of the electron transport chain. Mitochondria rely heavily on the electron transport chain for energy (ATP) production. This chain straddles the IMM and consists of four protein complexes, labeled CI-CIV. ATP synthase catalyzes the synthesis of ATP from ADP; this synthesis is dependent on the electrochemical gradient generated by the electron transport chain.

membrane. Receipt of NADH, $FADH_2$, and succinate from the citric acid cycle enables a steady flow of electrons through this chain of protein structures, culminating in the production of ATP by the churning of ATP synthase at the end, as well as the final acceptance of an electron by oxygen, yielding water (**Fig. 2**).

The production of energy from glycolysis and OXPHOS necessitates a careful balance of factors, and takes into account cellular energy needs, available nutrients, and conditions of cellular stress. For example, although glucose is regarded as the canonical source of cellular energy, mitochondria are also capable of catabolizing amino acids (Wu, 2009), pyrimidines (Nyhan, 2005), and fatty acids (Houten *et al*, 2015) for the production of energy and useful metabolites. Ca^{2+} is one of the means by which mitochondrial energy production is regulated. With regard to the citric acid cycle, pyruvate dehydrogenase (PDH), NAD^+-dependent isocitrate dehydrogenase (DH), and 2-oxoglutarate dehydrogenase (part of the oxoglutarate dehydrogenase complex, OGDC), are each activated by Ca^{2+}, and elevated Ca^{2+} concentrations in the mitochondrial matrix can cause the citric acid cycle to proceed more quickly (Traaseth *et al*, 2004; Wan *et al*, 1989).

In addition to their key role in cellular energy production, mitochondria are increasingly regarded as sophisticated signaling platforms that play essential roles in cellular functions including protein homeostasis, immunity, cell signaling, and apoptosis. Ca^{2+} signaling has emerged as a critical means for the mitochondria to respond to changing mitochondrial and cellular needs.

The mid 20th century marked the beginning of scientific interest in mitochondrial Ca^{2+} signaling, although it would take decades for this work to reach maturity. Following a series of experiments demonstrating mitochondrial swelling the presence of Ca^{2+} (Raaflaub, 1953; Hunter, 1963; Cooper & Tapley, 1956), and mitochondrial Ca^{2+} uptake from homogenized heart tissue (Slater & Cleland, 1953), isolated kidney mitochondria were found to use energy to accumulate large amounts of Ca^{2+} (Vasington & Murphy, 1962; Deluca & Engstrom, 1961). This discovery marked a major turning point in the field, as it linked mitochondrial Ca^{2+} signaling with the activity of the respiratory chain.

Mitochondrial Ca^{2+} signaling is now known to regulate Ca^{2+} signaling between the endoplasmic reticulum, cytosol, and mitochondria. It also regulates cellular bioenergetics, apoptosis, mitochondrial shape, and cellular movement (Zhao *et al*, 2019; Koval *et al*, 2019; Giorgio *et al*, 2018; Chakraborty *et al*, 2017; Bick *et al*, 2017; Prudent *et al*, 2016; Murphy *et al*, 2014). At the organismal level, mitochondrial Ca^{2+} uptake influences muscle health, tissue regeneration, and insulin secretion (Musa *et al*, 2019; Antony *et al*, 2016; Mammucari *et al*, 2015; Logan *et al*, 2014; Quan *et al*, 2015). Altered cellular Ca^{2+} is broadly associated with cellular dysfunction and death in vulnerable cells including neurons (Zaichik *et al*, 2017). Furthermore, altered MCU-mediated mitochondrial Ca^{2+} signaling is involved in a variety of human neurodegenerative diseases, including

Parkinson's disease, Alzheimer's disease, and hereditary spastic paraplegia (Zaichik *et al*, 2017; Supnet *et al*, 2010; Patron *et al*, 2018). Remarkably, most of the protein machinery required for mitochondrial Ca^{2+} uptake was only characterized within the past 10-15 years. Ca^{2+} ions enter the mitochondria through a protein channel called the mitochondrial calcium uniporter (MCU) that spans the inner membrane of the organelle (Chaudhuri *et al*, 2013; Mallilankaraman *et al*, 2012; Alam *et al*, 2012). MCU is part of a larger protein complex composed of five main proteins: pore-forming subunit MCU, and regulatory proteins EMRE, MICU1, MICU2, and MCUb (MacEwen *et al*, 2020; Lambert *et al*, 2019) (**Fig. 3**). The uniporter itself has also been implicated in a variety of human diseases (Logan *et al*, 2014; Musa *et al*, 2019). Continuing to characterize the relationship between the proteins of the uniporter complex and human disease, remains a top priority of the field.

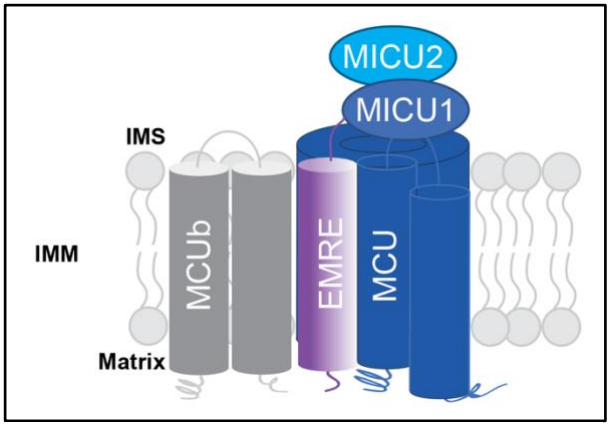

Figure 3. The mitochondrial uniporter complex is essential for mitochondrial calcium signaling. The uniporter complex is a protein localized to the IMM. It consists of pore-forming MCU, a 10-kDa protein called EMRE which is essential for calcium conductance, and MICU1 and MICU2, which dissociate during calcium signaling events. MCU. MCUb is a non-pore-forming protein that is sometimes incorporated into the uniporter complex. It negatively regulates uniporter complex function.

CLOSING THOUGHTS

Each chapter of this dissertation centers on mitochondrial and/or cellular Ca^{2+} signaling in some way. I hope the offerings within the following chapters are useful contributions to these remarkable fields, and that they help similarly interested researchers on their way.

REFERENCES

- Alam MR, Groschner LN, Parichatikanond W, *et al* (2012) Mitochondrial Ca^{2+} uptake 1 (MICU1) and mitochondrial Ca^{2+} uniporter (MCU) contribute to metabolism-secretion coupling in clonal pancreatic β-cells. *J Biol Chem* 287: 34445-34454. doi:10.1074/jbc.M112.392084
- Anderson S, Bankier AT, Barrell BG, *et al* (1981) Sequence and organization of the human mitochondrial genome. *Nature* 290: 457-465. doi:10.1038/290457a0
- Antony AN, Paillard M, Moffat C, *et al* (2016) MICU1 regulation of mitochondrial Ca(2+) uptake dictates survival and tissue regeneration *Nat Commun*. 7: 10955. Published 2016 Mar 9. doi:10.1038/ncomms10955
- Atchison DK, Beierwaltes WH. The influence of extracellular and intracellular calcium on the secretion of renin. *Pflugers Arch*. 2013;465(1):59-69. doi:10.1007/s00424-012-1107-x
- Bick AG, Wakimoto H, Kamer KJ, *et al* (2017) Cardiovascular homeostasis dependence on MICU2, a regulatory subunit of the mitochondrial calcium uniporter. *Proc Natl Acad Sci U S A* 114: E9096-E9104. doi:10.1073/pnas.1711303114
- Bozler E (1954) Relaxation in extracted muscle fibers. *J Gen Physiol* 38: 149-159. doi:10.1085/jgp.38.2.149
- Brini M, Carafoli E (2000) Calcium signalling: a historical account, recent developments and future perspectives. *Cell Mol Life Sci* 57: 354-370. doi:10.1007/PL00000698

- Carafoli E (2002) Calcium signaling: a tale for all seasons. *Proc Natl Acad Sci U S A* 99: 1115-1122. doi:10.1073/pnas.032427999
- Carafoli E, Krebs J (2016) Why Calcium? How Calcium Became the Best Communicator. *J Biol Chem* 291: 20849-20857. doi:10.1074/jbc.R116.735894
- Chakraborty PK, Mustafi SB, Xiong X, *et al* (2017) MICU1 drives glycolysis and chemoresistance in ovarian cancer. *Nat Commun* 8: 14634. Published 2017 May 22. doi:10.1038/ncomms14634
- Chaudhuri D, Sancak Y, Mootha VK, Clapham DE (2013) MCU encodes the pore conducting mitochondrial calcium currents. *Elife* 2: e00704. Published 2013 Jun 4. doi:10.7554/eLife.00704
- Chen X, Khambu B, Zhang H, *et al* (2014) Autophagy induced by calcium phosphate precipitates targets damaged endosomes. *J Biol Chem* 289:11162-11174. doi:10.1074/jbc.M113.531855
- Chin D, Means AR (2000) Calmodulin: a prototypical calcium sensor [published correction appears in Trends Cell Biol 2000 Oct;10(10):428]. *Trends Cell Biol* 10: 322-328. doi:10.1016/s0962-8924(00)01800-6
- Clapham DE (2007) Calcium signaling. *Cell* 131:1047-1058. doi:10.1016/j.cell.2007.11.028
- Cooper C, Tapley DF (1956) Effect of thyroxine on the swelling of mitochondria isolated from various tissues of the rat. *Nature* 178: 1119. doi:10.1038/1781119a0
- Deluca HF, Engstrom GW (1961) Calcium uptake by rat kidney mitochondria. *Proc Natl Acad Sci U S A* 47(11): 1744-1750. doi:10.1073/pnas.47.11.1744

- Dominguez DC (2004) Calcium signalling in bacteria. *Mol Microbiol*. 54: 291-297. doi:10.1111/j.1365-2958.2004.04276.x
- Ebashi S (1961) Calcium binding activity of vesicular relaxing factor. *J Chir (Paris)* 82: 236-244. doi:10.1093/oxfordjournals.jbchem.a127439
- Ebashi S, Lipmann F (1962) ADENOSINE TRIPHOSPHATE-LINKED CONCENTRATION OF CALCIUM IONS IN A PARTICULATE FRACTION OF RABBIT MUSCLE. *J Cell Biol* 14: 389-400. doi:10.1083/jcb.14.3.389
- Ebashi S, Kodama A (1965) A new protein factor promoting aggregation of tropomyosin. *J Biochem* 58: 107-108. doi:10.1093/oxfordjournals.jbchem.a128157
- Giorgio, Valentina *et al* (2018) “Calcium and regulation of the mitochondrial permeability transition.” *Cell calcium* vol. 70: 56-63. doi:10.1016/j.ceca.2017.05.004
- Henderson J (2005) Ernest Starling and 'Hormones': an historical commentary. *J Endocrinol*. 184: 5-10. doi:10.1677/joe.1.06000
- Houten SM, Violante S, Ventura FV, Wanders RJ (2016) The Biochemistry and Physiology of Mitochondrial Fatty Acid β-Oxidation and Its Genetic Disorders. *Annu Rev Physiol* 78: 23-44. doi:10.1146/annurev-physiol-021115-105045
- Hunter FE Jr, Gebicki JM, Hoffsten PE, Weinstein J, Scott A (1963) Swelling and lysis of rat liver mitochondria induced by ferrous ions. *J Biol Chem* 238: 828-835.
- Koval OM, Nguyen EK, Santhana V, *et al* (2019) Loss of MCU prevents mitochondrial fusion in G_1-S phase and blocks cell cycle progression and

proliferation. *Sci Signal* 12(579): eaav1439. Published 2019 Apr 30. doi:10.1126/scisignal.aav1439

- Lambert JP, Luongo TS, Tomar D, *et al* (2019) MCUB Regulates the Molecular Composition of the Mitochondrial Calcium Uniporter Channel to Limit Mitochondrial Calcium Overload During Stress. *Circulation* 140(21): 1720-1733. doi:10.1161/CIRCULATIONAHA.118.037968
- Logan CV, Szabadkai G, Sharpe JA, *et al* (2014) Loss-of-function mutations in MICU1 cause a brain and muscle disorder linked to primary alterations in mitochondrial calcium signaling. *Nat Genet* 46: 188-193. doi:10.1038/ng.2851
- MacEwen MJ, Markhard AL, Bozbeyoglu M, *et al* (2020) Evolutionary divergence reveals the molecular basis of EMRE dependence of the human MCU. *Life Sci Alliance*. 3: e202000718. Published 2020 Aug 7. doi:10.26508/lsa.202000718
- Mallilankaraman, Karthik *et al* (2012) “MICU1 is an essential gatekeeper for MCU-mediated mitochondrial Ca(2+) uptake that regulates cell survival.” *Cell* vol. 151,3 (2012): 630-44. doi:10.1016/j.cell.2012.10.011
- Malyala S, Zhang Y, Strubbe JO, Bazil JN (2019) Calcium phosphate precipitation inhibits mitochondrial energy metabolism. *PLoS Comput Biol*. 15: e1006719. Published 2019 Jan 7. doi:10.1371/journal.pcbi.1006719
- Mammucari C, Gherardi G, Zamparo I, *et al* (2015) The mitochondrial calcium uniporter controls skeletal muscle trophism in vivo. *Cell Rep* 10: 1269-1279. doi:10.1016/j.celrep.2015.01.056

- Marchadier E, Oates ME, Fang H, Donoghue PC, Hetherington AM, Gough J (2016) Evolution of the Calcium-Based Intracellular Signaling System. *Genome Biol Evol* 8: 2118-2132. Published 2016 Jul 14. doi:10.1093/gbe/evw139
- Martin WF (2017) Physiology, anaerobes, and the origin of mitosing cells 50 years on. *J Theor Biol* 434: 2-10. doi:10.1016/j.jtbi.2017.01.004
- Mossmann D, Meisinger C, Vögtle FN (2012) Processing of mitochondrial presequences. *Biochim Biophys Acta* 1819: 1098-1106. doi:10.1016/j.bbagrm.2011.11.007
- Murphy E, Pan X, Nguyen T, Liu J, Holmström KM, Finkel T (2014) Unresolved questions from the analysis of mice lacking MCU expression. *Biochem Biophys Res Commun* 449: 384-385. doi:10.1016/j.bbrc.2014.04.144
- Musa S, Eyaid W, Kamer K, *et al* (2019) A Middle Eastern Founder Mutation Expands the Genotypic and Phenotypic Spectrum of Mitochondrial MICU1 Deficiency: A Report of 13 Patients. *JIMD Rep* 43: 79-83. doi:10.1007/8904_2018_107
- Nair A, Chauhan P, Saha B, Kubatzky KF (2019) Conceptual Evolution of Cell Signaling. *Int J Mol Sci* 20: 3292. doi:10.3390/ijms20133292
- Nyhan WL (2005) Disorders of purine and pyrimidine metabolism. *Mol Genet Metab* 86: 25-33. doi:10.1016/j.ymgme.2005.07.027
- Nalefski EA, Falke JJ (1996) The C2 domain calcium-binding motif: structural and functional diversity. *Protein Sci* 5: 2375-2390. doi:10.1002/pro.5560051201
- Norris V, Grant S, Freestone P, *et al* (1996) Calcium signalling in bacteria. *J Bacteriol* 178: 3677-3682. doi:10.1128/jb.178.13.3677-3682.1996

- Patron M, Sprenger HG, Langer T (2018) m-AAA proteases, mitochondrial calcium homeostasis and neurodegeneration. *Cell Res* 28: 296-306. doi:10.1038/cr.2018.17
- Pfanner N, Warscheid B, Wiedemann N (2019) Mitochondrial proteins: from biogenesis to functional networks [published correction appears in Nat Rev Mol Cell Biol. 2021 May;22(5):367]. *Nat Rev Mol Cell Biol* 20: 267-284. doi:10.1038/s41580-018-0092-0
- Prudent J, Popgeorgiev N, Gadet R, Deygas M, Rimokh R, Gillet G (2016) Mitochondrial Ca^{2+} uptake controls actin cytoskeleton dynamics during cell migration. *Sci Rep*. 2016;6: 36570. doi:10.1038/srep36570
- Quan X, Nguyen TT, Choi SK, *et al* (2015) Essential role of mitochondrial Ca^{2+} uniporter in the generation of mitochondrial pH gradient and metabolism-secretion coupling in insulin-releasing cells. *J Biol Chem* 290: 4086-4096. doi:10.1074/jbc.M114.632547
- Raaflaub J (1953) Die Schwellung isolierter Leberzellmitochondrien und ihre physikalisch-chemische Beeinflussbarkeit [Swelling of isolated mitochondria of the liver and their susceptibility to physicochemical influences]. *Helv Physiol Pharmacol Acta* 11: 142-156.
- Ringer S (1883) A third contribution regarding the Influence of the Inorganic Constituents of the Blood on the Ventricular Contraction. *J Physiol* 4: 222-225. doi:10.1113/jphysiol.1883.sp000127

- Slater EC, Cleland KW (1953) The effect of calcium on the respiratory and phosphorylative activities of heart-muscle sarcosomes. *Biochem J* 55: 566-590. doi:10.1042/bj0550566
- Spees JL, Olson SD, Whitney MJ, Prockop DJ (2006) Mitochondrial transfer between cells can rescue aerobic respiration. *Proc Natl Acad Sci U S A* 103: 1283-1288. doi:10.1073/pnas.0510511103
- Stuart RA, Cyr DM, Craig EA, Neupert W (1994) Mitochondrial molecular chaperones: their role in protein translocation. *Trends Biochem Sci* 19: 87-92. doi:10.1016/0968-0004(94)90041-8
- Supnet C, Bezprozvanny I (2010) Neuronal calcium signaling, mitochondrial dysfunction, and Alzheimer's disease. *J Alzheimers Dis* 20 Suppl 2(Suppl 2): S487-S498. doi:10.3233/JAD-2010-100306
- Traaseth N, Elfering S, Solien J, Haynes V, Giulivi C (2004) Role of calcium signaling in the activation of mitochondrial nitric oxide synthase and citric acid cycle. *Biochim Biophys Acta* 1658: 64-71. doi:10.1016/j.bbabio.2004.04.015
- Tzameli I (2012) The evolving role of mitochondria in metabolism. *Trends Endocrinol Metab* 23: 417-419. doi:10.1016/j.tem.2012.07.008
- Vasington FD, Murphy JV (1962) Ca ion uptake by rat kidney mitochondria and its dependence on respiration and phosphorylation. *J Biol Chem* 237: 2670-2677.
- Wan B, LaNoue KF, Cheung JY, Scaduto RC Jr (1989) Regulation of citric acid cycle by calcium. *J Biol Chem* 264: 13430-13439.
- Weber A (1959) On the role of calcium in the activity of adenosine 5'-triphosphate hydrolysis by actomyosin. *J Biol Chem* 234: 2764-2769.

- Wu G (2009) Amino acids: metabolism, functions, and nutrition. *Amino Acids* 37: 1-17. doi:10.1007/s00726-009-0269-0
- Zaichick SV, McGrath KM, Caraveo G (2017) The role of Ca^{2+} signaling in Parkinson's disease. *Dis Model Mech* 10: 519-535. doi:10.1242/dmm.028738
- Zhao H, Li T, Wang K, *et al* (2019) AMPK-mediated activation of MCU stimulates mitochondrial Ca^{2+} entry to promote mitotic progression. *Nat Cell Biol* 21: 476-486. doi:10.1038/s41556-019-0296-3

CHAPTER 2:

Beyond the Matrix:

Structural and Physiological Advancements in Mitochondrial Calcium Signaling

Melissa JS MacEwen[1], Yasemin Sancak[1]

Biochemical Society Transactions

Accepted 10 March 2023

[1]Department of Pharmacology, University of Washington, Seattle, WA, USA

Correspondence: sancak@uw.edu

ABSTRACT

Mitochondrial calcium (Ca^{2+}) signaling has long been known to regulate diverse cellular functions, ranging from ATP production via oxidative phosphorylation, to cytoplasmic Ca^{2+} signaling to apoptosis. Central to mitochondrial Ca^{2+} signaling is the mitochondrial Ca^{2+} uniporter complex (MCUC) which enables Ca^{2+} flux from the cytosol into the mitochondrial matrix. Several pivotal discoveries over the past fifteen years have clarified the identity of the proteins comprising MCUC. Here, we provide an overview of the literature on mitochondrial Ca^{2+} biology and highlight recent findings on the high-resolution structure, dynamic regulation, and new functions of MCUC. We discuss the importance of these findings for human health and the therapeutic potential of targeting mitochondrial Ca^{2+} signaling

INTRODUCTION

Mitochondrial calcium (Ca^{2+}) uptake was first observed as an *in vitro* phenomenon in the early 1960s (Deluca & Engstrom, 1961; Vasington & Murphy, 1962). It was quickly recognized as an important regulator of mitochondrial bioenergetics through Ca^{2+}-mediated activation of the TCA cycle. This foundational work paved the way for decades of research on the functions of mitochondrial Ca^{2+} uptake in physiology and diseases. Yet, the molecular identity of the uniporter remained a mystery for decades. The proteins responsible for mitochondrial Ca^{2+} influx into the mitochondrial matrix—the mitochondrial calcium uniporter (MCU) and its regulatory proteins—was identified over the last 13 years. These discoveries dramatically accelerated efforts to understand the regulation and function of mitochondrial Ca^{2+} uptake. Ca^{2+} influx across the inner mitochondrial membrane (IMM) is now recognized to govern numerous aspects of biology, ranging from ATP production via oxidative phosphorylation to cytoplasmic Ca^{2+} signaling in a variety of

tissues (Dedkova & Blatter, 2013; Kamer & Mootha, 2015; Nicholls, 2009; Rizzuto *et al*., 2012), to regulation of immunological synapses (Quintana & Hoth, 2012). High mitochondrial matrix [Ca^{2+}] can also lead to opening of the mitochondrial permeability transition pore (mPTP), a structure that is responsible for rapid release of Ca^{2+} and other small molecules from the mitochondrial matrix to the cytosol, which can cause cell death (Giorgi *et al*., 2012). Mitochondrial Ca^{2+} signaling has also been found to play a significant role in human diseases including neurological disorders such as amyotrophic lateral sclerosis, Friedreich's ataxia, Charcot-Marie-Tooth (Rodriguez *et al*., 2022), Alzheimer's disease (Calvo-Rodriguez *et al*., 2020), as well as heart failure (Boyman *et al*., 2015) and lysosomal storage disorders (Peng *et al*., 2020).

The field of mitochondrial Ca^{2+} biology continues to advance rapidly. Here, we review recent publications centered on the mitochondrial calcium uniporter, with an emphasis on its structure, novel regulatory mechanisms, and its emerging roles in development, mitochondrial diseases and immunity. We contextualize these findings in the broader field, while emphasizing publications from the past five years. Many excellent reviews concerning the biology of mitochondrial Ca^{2+} signaling were published within this same time frame. Of note are those concerning the mechanisms of mitochondrial Ca^{2+} signaling in health and disease, as well as those exploring the role of mitochondrial Ca^{2+} signaling in cardiac disease, diabetes, cellular senescence, cancer, and neurodegeneration. We encourage the reader to pursue these reviews to gain an even deeper understanding of this rich field (Ahumada-Castro *et al*., 2021; Alevriadou *et al*., 2021; Arnst *et al*., 2022; Boyman *et al*., 2021; Calvo-Rodriguez *et al*., 2021; Modesti *et al*., 2021; Murphy *et al*., 2021).

MECHANISMS OF MITOCHONDRIAL Ca^{2+} INFLUX, EFFLUX, AND SEQUESTRATION

To maintain homeostasis, mitochondria must precisely balance the influx, sequestration, and release of Ca^{2+} into and from the mitochondrial matrix. Characterizing the machinery and chemistry central to these processes has clarified the regulation and biological implications of mitochondrial Ca^{2+} cycling and signaling. The main players of mitochondrial Ca^{2+} homeostasis are shown in **Figure 1** and described in more detail below.

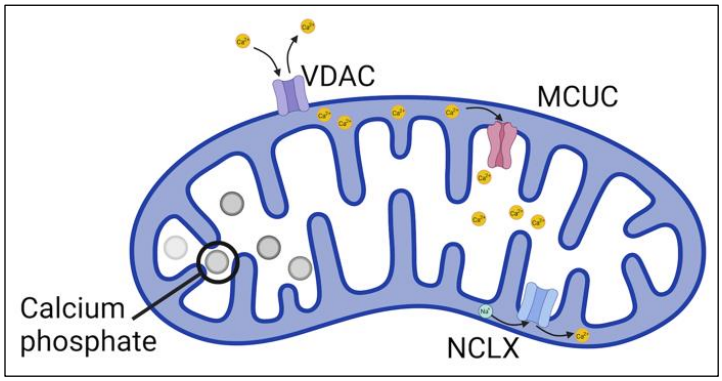

Figure 1: Mechanisms of mitochondrial Ca^{2+} influx, efflux, and sequestration. Mitochondria are organelles with an outer mitochondrial membrane (OMM) and inner mitochondrial membrane (IMM). Ca^{2+} ions likely diffuse through the OMM via VDAC proteins. Bulk transport of Ca^{2+} across the IMM and into the mitochondrial matrix requires the mitochondrial calcium uniporter complex (MCUC), a highly selective ion channel. NCLX, a Ca^{2+} / Na^{+} exchanger enables the majority of Ca^{2+} efflux from the mitochondria. Ca^{2+} is shown in yellow, while Na^{+} is shown in teal.

Mechanisms Of Influx

Mitochondrial Ca^{2+} uptake from the cytosol to the mitochondrial matrix faces two primary physical barriers: the outer mitochondrial membrane (OMM) and the inner mitochondrial membrane (IMM). Ca^{2+} transport across the OMM remains poorly understood as the OMM is not believed to have a specific Ca^{2+} transporter (Hajnoczky *et al*., 2002). Rather, the voltage-dependent anion channel (VDAC) is believed to passively permit the diffusion of metabolites and solutes such as Ca^{2+}. VDAC was recently demonstrated to form multi-protein complexes with the Ca^{2+} channels of other organelles, thus facilitating highly efficient Ca^{2+} transfer through the OMM (Rosencrans *et al*., 2021).

Once past the OMM, the vast majority of Ca^{2+} travels from the intermembrane space (IMS) to the mitochondrial matrix via rapid bulk entry through the mitochondrial calcium uniporter (MCU). MCU is a pore-forming protein that resides in the IMM and is

the eponymous protein of the mitochondrial calcium uniporter complex (MCUC). MCU-facilitated Ca^{2+} flux is dependent on mitochondrial membrane potential. The uniporter is a Ca^{2+} selective channel, and patch-clamp experiments of the IMM reveal that it has a Ca^{2+} affinity of 2 nM or less (Kirichok *et al*., 2004).

Additional core MCUC proteins include Mitochondrial Calcium Uptake (MICU) homologs MICU1-3, Essential MCU Regulator (EMRE), and MCUb. The MICU proteins play distinct, crucial roles in setting the threshold for uniporter Ca^{2+} uptake and its potentiation. They also contribute to specific Ca^{2+} regulation of the channel through their EF-hand Ca^{2+}-binding domains (Csordas *et al*., 2013; de la Fuente *et al*., 2014; Foskett *et al*., 2014; Kamer *et al*., 2018; Liu *et al*., 2016; Perocchi *et al*., 2010; Plovanich *et al*., 2013; Zhuo *et al*., 2021). The consensus of the field is that, when the cytosolic [Ca^{2+}] is low, MICU1 blocks the MCU pore to prevent mitochondrial Ca^{2+} overload (Csordas *et al*., 2013; Liu *et al.*, 2016; Perocchi *et al*., 2010; Pinton *et al*., 2008). When IMS [Ca^{2+}] increases, Ca^{2+} binds to the EF-hands of the MICU proteins. MICU1 – which forms a disulfide-bonded heterodimer with either MICU2 or MICU3 – then dissociates from MCU, enabling Ca^{2+} conductance. Recent structural work supports this consensus, as discussed in detail below. EMRE, a small transmembrane protein, is required for both MCU-MICU1 interaction and Ca^{2+} conductance through MCU (Kovacs-Bogdan *et al*., 2014; Sancak *et al.*, 2013; Tsai *et al*., 2016). MCUb is a paralog of MCU, but it does not form a functional Ca^{2+} channel and seems to have a negative regulatory role in the MCUC. MICU3, a MICU1 paralog, is mostly found in brain tissue and enhances Ca^{2+} uptake in neuronal mitochondria (Patron *et al*., 2019) **(Figure 2)**.

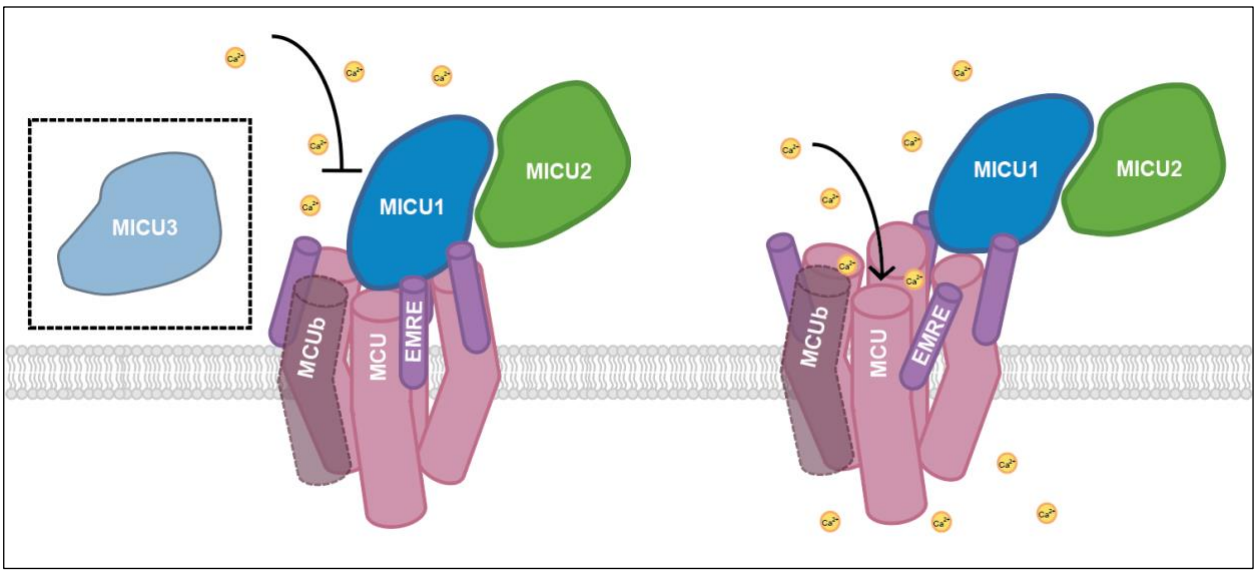

Figure 2: The Mitochondrial Calcium Uniporter Complex.
The mitochondrial calcium uniporter complex (MCUC) is composed of membrane proteins MCU, EMRE and IMS-localized proteins MICU1 and MICU2. MCUb, a paralog of MCU, and MICU3, a paralog of MICU1/MICU2, are less commonly incorporated into MCUC. MCU is the pore-forming protein and requires EMRE to form a functional channel in multicellular and some unicellular organisms. The incorporation of MCUb into the MCUC modulates mitochondrial Ca^{2+} flux and prevents mitochondrial Ca^{2+} overload. The MICU proteins – MICU1, MICU2, and MICU3 – block the entrance of Ca^{2+} into the pore, except during Ca^{2+} signaling events. During signaling events, the MICU proteins dissociate from the MCUC pore, remaining tethered via MICU1-EMRE binding. MICU1 forms a disulfide-bonded heterodimer with either MICU2 or MICU3, though MICU3 has only been identified in brain tissue. Arrows indicate the presence or absence of Ca^{2+} transport, with MCUC illustrated in a closed, non-conductive conformation (left) or an open, Ca^{2+}-conducting conformation (right).

Structural and biochemical studies have shown that MCU and its associated proteins form a form the MCUC, a large holocomplex whose structure and interactions are discussed in detail below. Two other IMM proteins, Mitochondrial Calcium Uniporter Regulator 1 (MCUR1) and Solute Carrier 25A23, also regulate the activity of the uniporter despite not being part of the core complex (Hoffman *et al*., 2014; Tomar *et al*., 2016). MCUR1 is a scaffold protein that binds to MCU and EMRE and is required for MCUC assembly. SLC25A23 augments mitochondrial Ca^{2+} uptake, however the exact mechanism of this regulation remains elusive.

Mechanisms Of Calcium Efflux and Sequestration

Matrix Ca^{2+} is maintained at a far lower resting concentration than the concentration reached after a Ca^{2+} signaling event (Finkel *et al*., 2015). This regulation is crucial; excessive mitochondrial Ca^{2+} accumulation can be hazardous, as it can lead to mitochondrial Ca^{2+} overload or opening of the permeability transition pore (Parks *et al*., 2018). To restore resting Ca^{2+} levels, exchangers and antiporters facilitate the exit of Ca^{2+} from mitochondria. The Na^{+}/ Ca^{2+} exchanger NCLX is the dominant Ca^{2+} efflux pathway (Assali *et al*., 2020). NCLX is expressed on the IMM of many tissues, in an expression pattern similar to that of MCU (Boyman *et al*., 2013; Palty *et al*., 2010). Ca^{2+} ions are also stored as calcium phosphate deposits in the mitochondrial matrix. Fast sequestration of Ca^{2+} in the form of calcium phosphate after mitochondrial Ca^{2+} entry is thought to play an important role in reduction of the effective concentration of free matrix [Ca^{2+}]. These deposits are also thought to serve as Ca^{2+} reservoirs that can be mobilized if needed. Although the function of mitochondrial calcium phosphate deposits is still under debate, their visualization using cryo-scanning transmission electron tomography shows that these deposits form independently of MCU, disappear if mitochondrial membrane potential is lost, and do not preferentially form in mitochondria in a particular cellular location (Wolf *et al*., 2017).

HIGH-RESOLUTION UNIPORTER STRUCTURES UNVEIL NEW REGULATORS AND MECHANISMS

A remarkable series of studies have recently shed light on the structures of the individual proteins of the MCUC, as well as the uniporter holocomplex in its Ca^{2+} -bound and Ca^{2+}-free states (Zhuo *et al*., 2021; Baradaran *et al*., 2018; Fan *et al*., 2018; Nguyen *et al*., 2018; Yoo *et al*., 2018; Kamer *et al.*, 2019; Wu *et al*., 2020; Wang *et al*., 2019). By defining specific interactions of the uniporter proteins and identifying a lipid molecule that

interacts with the uniporter channel, these publications have helped to develop a more refined model of uniporter regulation and the functions of its individual subunits.

In the wake of these publications and their predecessors, the following is clear: MCU is a transmembrane protein that spans the IMM and contains two transmembrane-spanning helices, TM1 and TM2. TM2 of MCU forms the protein's Ca^{2+}-conducting pore. Although MCU was known to oligomerize prior to 2018 (Kovacs-Bogdan *et al*., 2014; Lee *et al*., 2015), cryo-EM structures established the presence of a "dimer of dimer" structure composed of four MCU protomers (Baradaran *et al*., 2018; Fan *et al*., 2018; Nguyen *et al*., 2018; Yoo *et al*., 2018), with different symmetric arrangements of the soluble and transmembrane domains (Yoo *et al*., 2018). There are four EMRE subunits per functional channel. Structurally, EMRE participates in the formation of functional channels by interacting with MCU at the matrix channel opening. This interaction stabilizes a region at the inner leaflet of the IMM, which is otherwise flexible. This region is proposed to occlude the matrix side of the Ca^{2+} pore, preventing escape of Ca^{2+} ions into the matrix and regulating channel gating through binding-induced structural changes in the channel (Wang *et al*., 2019; Van Keuren *et al*., 2020). Related work from our laboratory independently validated several of these structural findings biochemically, by using a suite of protein chimeras composed of domains from *H. sapiens* MCU (HsMCU) and *D. discoideum* MCU (DdMCU) (MacEwen *et al*., 2020). *D. discoideum* MCU is functional in the absence of EMRE, which enabled us to characterize the aspects of HsMCU that make it dependent on EMRE for Ca^{2+} conductance. This work led to the identification of a 10-amino acid region in HsMCU that renders it EMRE-dependent; we termed this region EMRE dependence domain (EDD). This biochemically identified EDD region overlaps

with a 6-amino acid stretch first identified by Wang *et al.* in a mammalian EMRE-MCU structure that they show is important for EMRE function (Wang *et al*., 2019).

A second function of EMRE is facilitating the interaction of MICU1 with MCU through EMRE's positively charged DDD domain that faces the IMS. Using structural data from the MICU1-MICU2 heterodimer and *in vitro* binding experiments, Wu *et al.* showed that the DDD domain interacts with a Ca^{2+}-induced alkaline stretch in MICU1 (Wu *et al*., 2020). This Ca^{2+}-enhanced interaction between EMRE and MICU1 is thought to prevent complete dissociation of MICU1 from the complex in the presence of Ca^{2+}. Two publications also suggested another important function of the EMRE-MICU1 interaction: potentiation of uniporter activity (Zhuo *et al*., 2021; Garg *et al*., 2021). The authors propose that, by binding to EMRE when Ca^{2+} is present, MICU1 alters MCU-EMRE interaction, which results in increased uniporter conductance.

CONTROLLING MCUC COMPOSITION AND STABILITY TO TUNE MITOCHONDRIAL Ca^{2+} UPTAKE

The activity of the uniporter varies across physiological conditions and cell types (Fieni *et al*., 2012). Recent work highlighted the importance of two primary modes of fine-tuning uniporter activity: steady state differences in the expression of MCUC proteins across tissues; and regulation of MCUC proteins in response to stress, disease, or other alterations to cellular or organismal physiology.

MCU and MICU1 are posttranslationally modified in response to various stimuli, which lead to changes in uniporter activity and have been reviewed before (Nemani *et al.*, 2018). Here, we focus on new research indicating that changes to uniporter subunit composition or altered stability of the complex is a novel mode of uniporter regulation. Such changes often happen at the level of individual complex proteins, and can have

dramatic, long-lasting effects on cellular and tissue wide Ca^{2+} signaling and metabolism. For example, during chronic stress, increased MCUb incorporation into the complex limits mitochondrial Ca^{2+} overload and counteracts mitochondrial damage, as seen in mice in response to cardiac injury (Lambert *et al*., 2019). Consistent with this observation, Huo *et al.* demonstrated that cardiomyocyte- specific MCUb knockout mice exhibited increased pathological cardiac remodeling and infarct expansion following ischemic injury. This same group found the inverse in cardiomyocyte specific MCUb overexpressing mice, highlighting the importance of proper uniporter composition for homeostasis (Huo *et al*., 2020).

A similar mechanism of altered uniporter composition is observed in failing human heart tissue. The relative mRNA abundance of MICU1 to MCU is tissue-specific and is particularly low in cardiac muscle. During heart failure, MICU1/2 expression increases, while MCU expression stays the same. This altered composition likely changes the gating and activity of the uniporter in failing human hearts and may contribute to decreased cardiac contractile function in heart failure (Paillard *et al*., 2022). MICU3 is another uniporter regulatory protein whose presence in the complex substantially alters the physiological performance of specific tissues. MICU3 is a paralog of MICU1 and MICU2. It is mostly found in the brain and binds specifically to MICU1 to enhance Ca^{2+} uptake (Patron *et al*., 2019). If MICU3 is silenced in primary cortical neurons, the Ca^{2+} signals spurred by synaptic activity are impaired. Finally, increased MICU1 expression and ensuing changes in Ca^{2+} signaling and metabolism are important for fibroblast to myofibroblast differentiation (Lombardi *et al*., 2019).

The precise regulation of EMRE has important consequences for human health. Under normal physiological conditions, EMRE that does not complex with MCU is rapidly degraded by the m-AAA protease (Tsai *et al*., 2017). This process is essential to maintaining the balance of MCU-EMRE that are assembled with an adequate ratio of MICU1/MICU2 “gatekeeper subunits (Konig *et al*., 2016). Mutations in mitochondrial m-AAA proteases, which are linked to neurodegeneration in spinocerebellar ataxia (SCA28) and hereditary spastic paraplegia (HSP7), lead to accumulation of EMRE and formation of excess MCU-EMRE complexes that are not gated by MICUs. This eventually leads to unregulated mitochondrial Ca^{2+} entry and overload. This has been proposed to contribute to neurodegeneration in these debilitating diseases.

The stability of MCU is also carefully regulated, as recently shown by two elegant studies. In 2020, using functional experiments in a yeast heterologous uniporter expression system, Ghosh *et al.* showed that cardiolipin plays an essential role in stabilizing MCU (Ghosh *et al*., 2020). This finding may clarify the pathologically low cardiolipin and uniporter levels observed in patients with Barth syndrome, a disease characterized by partial loss of cardiolipin. Furthermore, Dr. Chaudhuri and coworkers discovered a novel link between OXPHOS function and MCU. In healthy cells, reactive oxygen species that leak from Complex I of the electron transport chain damage MCU and lead to its degradation. In Complex I deficiency, MCU is stabilized, and the number of functional uniporter channels increases, leading to an increase in overall MCUC activity. Most importantly, the authors showed that uniporter function prolongs survival of OXPHOS-deficient mice and *Drosophila*, thereby identifying a previously unknown function for the uniporter (Balderas *et al*., 2022).

EXPANDING THE FUNCTIONS OF MITOCHONDRIAL Ca^{2+} FLUX

Targeted perturbation of mitochondrial Ca^{2+} flux in animal models and phenotypes of patients with uniporter gene mutations highlight the importance of this pathway in development, immunity, neuromuscular system and metabolic health. Likely due to highly tissue-specific nature of Ca^{2+} signaling and mitochondrial functions, uniporter activity has been shown to regulate distinct pathways across different tissue types. Despite this functional diversity, altered uniporter regulation fundamentally produces a phenotype through either altered metabolic regulation, and/or altered cellular Ca^{2+} signaling. Here, we non-exhaustively highlight recent findings on the physiological roles of the mitochondrial calcium uptake.

Emerging Roles of The Uniporter in Early Development and Differentiation

The first report of MCU knockout (KO) mice was somewhat of a surprise for mitochondrial community: loss of MCU was compatible with life, but only on a mixed background (Pan *et al*., 2013). Since then, the same phenotype of viability on a mixed background has been shown for EMRE KO mice (Liu *et al*., 2020). MCU loss is also tolerated in the fly and the worm (Fieni *et al*., 2012; Alvarez-Illera *et al*., 2020). That said, loss of MCU does cause reduced viability in the mouse. The knockout mice are observed at much lower ratios than expected from a heterozygous mating (Murphy *et al*., 2014). This suggests the presence of modifiers (genetic or environmental) that allow survival of animals past a certain developmental stage in the absence of mitochondrial Ca^{2+} uptake. Important roles for mitochondrial Ca^{2+} uptake in early development were recently shown in different model organisms and systems. In *Xenopus* eggs, early cell divisions after fertilization require ROS generated by the mitochondria, which is fueled by MCU-mediated mitochondrial Ca^{2+} uptake (Han *et al*., 2018). Modulation of MCU activity is also

observed in human embryonic stem cells (hESCs): repression of MICU1 by Foxd1 is essential for proper differentiation of hESCs into induced pluripotent stem cells (hiPSCs) (Shanmughapriya *et al*., 2018). The authors in this study conclude that the presence of MICU1 modulates periodic cytosolic Ca^{2+} oscillations necessary for differentiation. These new roles of the uniporter in early development help explain the viability (albeit low) of MCU KO animals on a mixed background. Nevertheless, how MCU knockout animals survive, and what type of compensatory changes take place in these survivors, is still unknown.

Although no MCU mutation has ever been identified in humans, a recent preprint by Bulthuis *et al.* reported two patients with EMRE mutations that lead to a loss of EMRE protein (Bulthuis *et al*., 2022). Muscle breakdown was a common phenotype observed in both patients, who otherwise showed diverse symptoms. In addition, several patients with MICU1 mutations have been reported to date (OMIM #615673), most of which present with neuromuscular problems. A neuron-specific MICU1 KO mouse model recapitulates the phenotypes observed in patients and whole body MICU1 KO mice, suggesting that neuronal abnormalities are the main cause of the observed phenotypes in patients (Singh *et al*., 2022). Nevertheless, phenotypic diversity observed in humans again underlines the importance of other modifiers and compensatory mechanisms in mitochondrial Ca^{2+} regulation. For example, the appearance and bodyweight of MICU1 knockout mice become more similar to wild type mice over time due to downregulation of EMRE expression (Liu *et al*., 2016).

Emerging Tissue-specific Roles of The Uniporter

Several recent studies highlight the diverse, tissue-specific functions of the uniporter. They also point to a need for further research on uniporter regulation and function, as several contradictory phenotypes associated with the uniporter have been reported. For example, in a 2020 publication, Flicker *et al.* generated a brown adipose tissue (BAT)-specific MCU knockout mouse and reported that MCU is not required for brown fat energetics (Flicker *et al*., 2019). By contrast, Xue *et al.* found that in the BAT, the uniporter function is important for thermogenesis in response to cold (Xue *et al*., 2022). The authors suggested that these disparities are due to the differences in the genetic background of the mice used in these two papers, but they could also stem from experimental differences such as fasting before cold exposure in the second study. In addition, several papers reported contradicting phenotypes associated with loss of uniporter function in the heart. As proposed by Garbincius *et al.*, some of these differences can be attributed to cellular adaptations in response to chronic loss of uniporter function but are absent in its acute inhibition (Garbincius *et al*., 2020).

The importance of metabolism, mitochondria and cellular Ca^{2+} signaling for proper functioning of the innate immunity are well appreciated (Weinberg *et al*., 2015). The uniporter sits at the intersection of these regulators, and several papers showed important roles of the uniporter in different aspects of cellular responses to pathogens. In neutrophils, activation of mitochondrial Ca^{2+} uptake stimulates cell polarization and chemotaxis, which are required for effective removal of pathogenic species (Zheng *et al*., 2017). In addition, increased uniporter function is associated with phagocytosis-induced activation of NLRP3 inflammasome in macrophages (Dong *et al*., 2022). Conversely, reduced uniporter activity due to MCUb expression decreases inflammation in

macrophages (Feno *et al*., 2021). Moreover, in epithelial cells that express pathogenic cystic fibrosis receptor, bacterial infection activates NLRP3 in an MCU-dependent manner (Rimessi *et al*., 2015). Even though MCU activation is associated with worse cellular outcomes and more pathogen survival in the literature so far, whether modulating its activity pharmacologically would be beneficial or damaging to the cells is likely to depend on many factors at play, such as the duration of infection and detrimental effects of prolonged inflammation.

CONCLUDING REMARKS

Identification of the MCUC protein components accelerated research on numerous aspects of uniporter biology and led to exciting discoveries on the structure, regulation, function of the uniporter, as well as its roles in diseases. Nevertheless, several fundamental questions about mitochondrial Ca^{2+} signaling and MCUC regulation remain unanswered. For example, the presence of yet-uncharacterized, uniporter-independent mitochondrial Ca^{2+}-entry pathways has been reported (Bisbach *et al*., 2020; Hamilton *et al*., 2018). Identification of these pathways could alter our understanding of how mitochondrial Ca^{2+} signaling reflects and responds to mitochondrial and cellular needs. Furthermore, upstream signals that change MCUC protein transcription or the generation of alternative splice variants remain to be characterized and may help explain tissue-specific differences in uniporter function (Vecellio *et al*., 2016).

Finally, while mitochondrial Ca^{2+} signaling is generally considered necessary for proper mitochondrial and cellular health, the viability of MCU KO cells in mixed background mice suggests that the loss of uniporter function may be tolerated in normal tissues and may even have protective effects in the context of Ca^{2+}-induced mitochondrial damage, as observed in hereditary ataxias. Though the therapeutic potential of MCUC

inhibition is made uncertain by the diverse roles of mitochondrial Ca^{2+} flux in different tissues and the cellular adaptations to altered uniporter function, the MCUC remains a promising therapeutic target. The field of mitochondrial Ca^{2+} signaling continues to develop rapidly and deepen our understanding of the mitochondria's role in health and disease. We look forward to what is to come.

FUNDING

MJSM was supported by NIH grant 1F31AG072716-01A1. YS is supported by NIH grant DP2ES032761 and is a Pew Biomedical Scholar.

ACKNOWLEDGEMENTS

We thank Timothy Locke and David Shechner for critical reading of the manuscript and suggestions.

REFERENCES

- Ahumada-Castro, U., Puebla-Huerta, A., Cuevas-Espinoza, V., Lovy, A., and Cardenas, J.C. (2021). Keeping zombies alive: The ER-mitochondria Ca(2+) transfer in cellular senescence. Biochim Biophys Acta Mol Cell Res 1868, 119099. 10.1016/j.bbamcr.2021.119099.
- Alvarez-Illera, P., Garcia-Casas, P., Fonteriz, R.I., Montero, M., and Alvarez, J. (2020). Mitochondrial Ca(2+) Dynamics in MCU Knockout C. elegans Worms. Int J Mol Sci 21. 10.3390/ijms21228622.
- Alevriadou, B.R., Patel, A., Noble, M., Ghosh, S., Gohil, V.M., Stathopulos, P.B., and Madesh, M. (2021). Molecular nature and physiological role of the mitochondrial calcium uniporter channel. Am J Physiol Cell Physiol 320, C465-C482. 10.1152/ajpcell.00502.2020.

- Arnst, N., Redolfi, N., Lia, A., Bedetta, M., Greotti, E., and Pizzo, P. (2022). Mitochondrial Ca(2+) Signaling and Bioenergetics in Alzheimer's Disease. Biomedicines 10. 10.3390/biomedicines10123025.
- Assali, E.A., Jones, A.E., Veliova, M., Acin-Perez, R., Taha, M., Miller, N., Shum, M., Oliveira, M.F., Las, G., Liesa, M., et al. (2020). NCLX prevents cell death during adrenergic activation of the brown adipose tissue. Nat Commun 11, 3347. 10.1038/s41467-020-16572-3.
- Balderas, E., Eberhardt, D.R., Lee, S., Pleinis, J.M., Sommakia, S., Balynas, A.M., Yin, X., Parker, M.C., Maguire, C.T., Cho, S., et al. (2022). Mitochondrial calcium uniporter stabilization preserves energetic homeostasis during Complex I impairment. Nat Commun 13, 2769. 10.1038/s41467-022-30236-4.
- Baradaran, R., Wang, C., Siliciano, A.F., and Long, S.B. (2018). Cryo-EM structures of fungal and metazoan mitochondrial calcium uniporters. Nature 559, 580-584. 10.1038/s41586-018-0331-8.
- Bisbach, C.M., Hutto, R.A., Poria, D., Cleghorn, W.M., Abbas, F., Vinberg, F., Kefalov, V.J., Hurley, J.B., and Brockerhoff, S.E. (2020). Mitochondrial Calcium Uniporter (MCU) deficiency reveals an alternate path for Ca(2+) uptake in photoreceptor mitochondria. Sci Rep 10, 16041. 10.1038/s41598-020-72708-x.
- Boyman, L., Greiser, M., and Lederer, W.J. (2021). Calcium influx through the mitochondrial calcium uniporter holocomplex, MCU(cx). J Mol Cell Cardiol 151, 145-154. 10.1016/j.yjmcc.2020.10.015.

- Boyman, L., Williams, G.S., and Lederer, W.J. (2015). The growing importance of mitochondrial calcium in health and disease. Proc Natl Acad Sci U S A 112, 11150-11151. 10.1073/pnas.1514284112.
- Boyman, L., Williams, G.S., Khananshvili, D., Sekler, I., and Lederer, W.J. (2013). NCLX: the mitochondrial sodium calcium exchanger. J Mol Cell Cardiol 59, 205-213. 10.1016/j.yjmcc.2013.03.012.
- Bulthuis, E.P., Adjobo-Hermans, M.J.W., de Potter, B., Hoogstraten, S., Wezendonk, L.H.T., Tutakhel, O.A.Z., Wintjes, L.T., van den Heuvel, B., Willems, P.H.G.M., Kamsteeg, E.-J., et al. (2022). SMDT1 variants impair EMRE-mediated mitochondrial calcium uptake in patients with muscle involvement. bioRxiv, 2022.2010.2031.514480. 10.1101/2022.10.31.514480.
- Calvo-Rodriguez, M., and Bacskai, B.J. (2021). Mitochondria and Calcium in Alzheimer's Disease: From Cell Signaling to Neuronal Cell Death. Trends Neurosci 44, 136-151. 10.1016/j.tins.2020.10.004.
- Calvo-Rodriguez, M., Hou, S.S., Snyder, A.C., Kharitonova, E.K., Russ, A.N., Das, S., Fan, Z., Muzikansky, A., Garcia-Alloza, M., Serrano-Pozo, A., et al. (2020). Increased mitochondrial calcium levels associated with neuronal death in a mouse model of Alzheimer's disease. Nat Commun 11, 2146. 10.1038/s41467-020-16074-2.
- Csordas, G., Golenar, T., Seifert, E.L., Kamer, K.J., Sancak, Y., Perocchi, F., Moffat, C., Weaver, D., Perez, S.F., Bogorad, R., et al. (2013). MICU1 controls both the threshold and cooperative activation of the mitochondrial Ca(2)(+) uniporter. Cell Metab 17, 976-987. 10.1016/j.cmet.2013.04.020.

- de la Fuente, S., Matesanz-Isabel, J., Fonteriz, R.I., Montero, M., and Alvarez, J. (2014). Dynamics of mitochondrial Ca2+ uptake in MICU1-knockdown cells. Biochem J 458, 33-40. 10.1042/BJ20131025.
- Dedkova, E.N., and Blatter, L.A. (2013). Calcium signaling in cardiac mitochondria. J Mol Cell Cardiol 58, 125-133. 10.1016/j.yjmcc.2012.12.021.
- Deluca, H.F., and Engstrom, G.W. (1961). Calcium uptake by rat kidney mitochondria. Proc Natl Acad Sci U S A 47, 1744-1750. 10.1073/pnas.47.11.1744.
- Dong, H., Zhao, B., Chen, J., Liu, Z., Li, X., Li, L., and Wen, H. (2022). Mitochondrial calcium uniporter promotes phagocytosis-dependent activation of the NLRP3 inflammasome. Proc Natl Acad Sci U S A 119, e2123247119. 10.1073/pnas.2123247119.
- Fan, C., Fan, M., Orlando, B.J., Fastman, N.M., Zhang, J., Xu, Y., Chambers, M.G., Xu, X., Perry, K., Liao, M., and Feng, L. (2018). X-ray and cryo-EM structures of the mitochondrial calcium uniporter. Nature 559, 575-579. 10.1038/s41586-018-0330-9.
- Feno, S., Munari, F., Reane, D.V., Gissi, R., Hoang, D.H., Castegna, A., Chazaud, B., Viola, A., Rizzuto, R., and Raffaello, A. (2021). The dominant-negative mitochondrial calcium uniporter subunit MCUb drives macrophage polarization during skeletal muscle regeneration. Sci Signal 14, eabf3838. 10.1126/scisignal.abf3838.
- Fieni, F., Lee, S.B., Jan, Y.N., and Kirichok, Y. (2012). Activity of the mitochondrial calcium uniporter varies greatly between tissues. Nat Commun 3, 1317. 10.1038/ncomms2325.

- Finkel, T., Menazza, S., Holmstrom, K.M., Parks, R.J., Liu, J., Sun, J., Liu, J., Pan, X., and Murphy, E. (2015). The ins and outs of mitochondrial calcium. Circ Res 116, 1810-1819. 10.1161/CIRCRESAHA.116.305484.
- Flicker, D., Sancak, Y., Mick, E., Goldberger, O., and Mootha, V.K. (2019). Exploring the In Vivo Role of the Mitochondrial Calcium Uniporter in Brown Fat Bioenergetics. Cell Rep 27, 1364-1375 e1365. 10.1016/j.celrep.2019.04.013.
- Foskett, J.K., and Madesh, M. (2014). Regulation of the mitochondrial Ca(2+) uniporter by MICU1 and MICU2. Biochem Biophys Res Commun 449, 377-383. 10.1016/j.bbrc.2014.04.146.
- Garbincius, J.F., Luongo, T.S., and Elrod, J.W. (2020). The debate continues - What is the role of MCU and mitochondrial calcium uptake in the heart? J Mol Cell Cardiol 143, 163-174. 10.1016/j.yjmcc.2020.04.029.
- Garg, V., Suzuki, J., Paranjpe, I., Unsulangi, T., Boyman, L., Milescu, L.S., Lederer, W.J., and Kirichok, Y. (2021). The mechanism of MICU-dependent gating of the mitochondrial Ca(2+)uniporter. Elife 10. 10.7554/eLife.69312.
- Ghosh, S., Basu Ball, W., Madaris, T.R., Srikantan, S., Madesh, M., Mootha, V.K., and Gohil, V.M. (2020). An essential role for cardiolipin in the stability and function of the mitochondrial calcium uniporter. Proc Natl Acad Sci U S A 117, 16383-16390. 10.1073/pnas.2000640117.
- Giorgi, C., Baldassari, F., Bononi, A., Bonora, M., De Marchi, E., Marchi, S., Missiroli, S., Patergnani, S., Rimessi, A., Suski, J.M., et al. (2012). Mitochondrial Ca(2+) and apoptosis. Cell Calcium 52, 36-43. 10.1016/j.ceca.2012.02.008.

- Hajnoczky, G., Csordas, G., and Yi, M. (2002). Old players in a new role: mitochondria-associated membranes, VDAC, and ryanodine receptors as contributors to calcium signal propagation from endoplasmic reticulum to the mitochondria. Cell Calcium 32, 363-377. 10.1016/s0143416002001872.
- Hamilton, J., Brustovetsky, T., Rysted, J.E., Lin, Z., Usachev, Y.M., and Brustovetsky, N. (2018). Deletion of mitochondrial calcium uniporter incompletely inhibits calcium uptake and induction of the permeability transition pore in brain mitochondria. J Biol Chem 293, 15652-15663. 10.1074/jbc.RA118.002926.
- Han, Y., Ishibashi, S., Iglesias-Gonzalez, J., Chen, Y., Love, N.R., and Amaya, E. (2018). Ca(2+)-Induced Mitochondrial ROS Regulate the Early Embryonic Cell Cycle. Cell Rep 22, 218-231. 10.1016/j.celrep.2017.12.042.
- Hoffman, N.E., Chandramoorthy, H.C., Shanmughapriya, S., Zhang, X.Q., Vallem, S., Doonan, P.J., Malliankaraman, K., Guo, S., Rajan, S., Elrod, J.W., et al. (2014). SLC25A23 augments mitochondrial Ca(2)(+) uptake, interacts with MCU, and induces oxidative stress-mediated cell death. Mol Biol Cell 25, 936-947. 10.1091/mbc.E13-08-0502.
- Huo, J., Lu, S., Kwong, J.Q., Bround, M.J., Grimes, K.M., Sargent, M.A., Brown, M.E., Davis, M.E., Bers, D.M., and Molkentin, J.D. (2020). MCUb Induction Protects the Heart From Postischemic Remodeling. Circ Res 127, 379-390. 10.1161/CIRCRESAHA.119.316369.
- Kamer, K.J., Jiang, W., Kaushik, V.K., Mootha, V.K., and Grabarek, Z. (2019). Crystal structure of MICU2 and comparison with MICU1 reveal insights into the

uniporter gating mechanism. Proc Natl Acad Sci U S A 116, 3546-3555. 10.1073/pnas.1817759116.

- Kamer, K.J., and Mootha, V.K. (2015). The molecular era of the mitochondrial calcium uniporter. Nat Rev Mol Cell Biol 16, 545-553. 10.1038/nrm4039.
- Kamer, K.J., Sancak, Y., Fomina, Y., Meisel, J.D., Chaudhuri, D., Grabarek, Z., and Mootha, V.K. (2018). MICU1 imparts the mitochondrial uniporter with the ability to discriminate between Ca(2+) and Mn(2+). Proc Natl Acad Sci U S A 115, E7960-E7969. 10.1073/pnas.1807811115.
- Kirichok, Y., Krapivinsky, G., and Clapham, D.E. (2004). The mitochondrial calcium uniporter is a highly selective ion channel. Nature 427, 360-364. 10.1038/nature02246.
- Konig, T., Troder, S.E., Bakka, K., Korwitz, A., Richter-Dennerlein, R., Lampe, P.A., Patron, M., Muhlmeister, M., Guerrero-Castillo, S., Brandt, U., et al. (2016). The m-AAA Protease Associated with Neurodegeneration Limits MCU Activity in Mitochondria. Mol Cell 64, 148-162. 10.1016/j.molcel.2016.08.020.
- Kovacs-Bogdan, E., Sancak, Y., Kamer, K.J., Plovanich, M., Jambhekar, A., Huber, R.J., Myre, M.A., Blower, M.D., and Mootha, V.K. (2014). Reconstitution of the mitochondrial calcium uniporter in yeast. Proc Natl Acad Sci U S A 111, 8985-8990. 10.1073/pnas.1400514111.
- Lambert, J.P., Luongo, T.S., Tomar, D., Jadiya, P., Gao, E., Zhang, X., Lucchese, A.M., Kolmetzky, D.W., Shah, N.S., and Elrod, J.W. (2019). MCUB Regulates the Molecular Composition of the Mitochondrial Calcium Uniporter Channel to Limit

Mitochondrial Calcium Overload During Stress. Circulation 140, 1720-1733. 10.1161/CIRCULATIONAHA.118.037968.

- Lee, Y., Min, C.K., Kim, T.G., Song, H.K., Lim, Y., Kim, D., Shin, K., Kang, M., Kang, J.Y., Youn, H.S., et al. (2015). Structure and function of the N-terminal domain of the human mitochondrial calcium uniporter. EMBO Rep 16, 1318-1333. 10.15252/embr.201540436.
- Liu, J.C., Liu, J., Holmstrom, K.M., Menazza, S., Parks, R.J., Fergusson, M.M., Yu, Z.X., Springer, D.A., Halsey, C., Liu, C., et al. (2016). MICU1 Serves as a Molecular Gatekeeper to Prevent In Vivo Mitochondrial Calcium Overload. Cell Rep 16, 1561-1573. 10.1016/j.celrep.2016.07.011.
- Liu, J.C., Syder, N.C., Ghorashi, N.S., Willingham, T.B., Parks, R.J., Sun, J., Fergusson, M.M., Liu, J., Holmstrom, K.M., Menazza, S., et al. (2020). EMRE is essential for mitochondrial calcium uniporter activity in a mouse model. JCI Insight 5. 10.1172/jci.insight.134063.
- Lombardi, A.A., Gibb, A.A., Arif, E., Kolmetzky, D.W., Tomar, D., Luongo, T.S., Jadiya, P., Murray, E.K., Lorkiewicz, P.K., Hajnoczky, G., et al. (2019). Mitochondrial calcium exchange links metabolism with the epigenome to control cellular differentiation. Nat Commun 10, 4509. 10.1038/s41467-019-12103-x.
- MacEwen, M.J., Markhard, A.L., Bozbeyoglu, M., Bradford, F., Goldberger, O., Mootha, V.K., and Sancak, Y. (2020). Evolutionary divergence reveals the molecular basis of EMRE dependence of the human MCU. Life Sci Alliance 3. 10.26508/lsa.202000718.

- Modesti, L., Danese, A., Angela Maria Vitto, V., Ramaccini, D., Aguiari, G., Gafa, R., Lanza, G., Giorgi, C., and Pinton, P. (2021). Mitochondrial Ca(2+) Signaling in Health, Disease and Therapy. Cells 10. 10.3390/cells10061317.
- Murphy, E., Pan, X., Nguyen, T., Liu, J., Holmstrom, K.M., and Finkel, T. (2014). Unresolved questions from the analysis of mice lacking MCU expression. Biochem Biophys Res Commun 449, 384-385. 10.1016/j.bbrc.2014.04.144.
- Murphy, E., and Steenbergen, C. (2021). Regulation of Mitochondrial Ca(2+) Uptake. Annu Rev Physiol 83, 107-126. 10.1146/annurev-physiol-031920-092419.
- Nemani, N., Shanmughapriya, S., and Madesh, M. (2018). Molecular regulation of MCU: Implications in physiology and disease. Cell Calcium 74, 86-93. 10.1016/j.ceca.2018.06.006.
- Nguyen, N.X., Armache, J.P., Lee, C., Yang, Y., Zeng, W., Mootha, V.K., Cheng, Y., Bai, X.C., and Jiang, Y. (2018). Cryo-EM structure of a fungal mitochondrial calcium uniporter. Nature 559, 570-574. 10.1038/s41586-018-0333-6.
- Nicholls, D.G. (2009). Mitochondrial calcium function and dysfunction in the central nervous system. Biochim Biophys Acta 1787, 1416-1424. 10.1016/j.bbabio.2009.03.010.
- Paillard, M., Huang, K.T., Weaver, D., Lambert, J.P., Elrod, J.W., and Hajnoczky, G. (2022). Altered composition of the mitochondrial Ca(2+)uniporter in the failing human heart. Cell Calcium 105, 102618. 10.1016/j.ceca.2022.102618.
- Palty, R., Silverman, W.F., Hershfinkel, M., Caporale, T., Sensi, S.L., Parnis, J., Nolte, C., Fishman, D., Shoshan-Barmatz, V., Herrmann, S., et al. (2010). NCLX

is an essential component of mitochondrial Na+/Ca2+ exchange. Proc Natl Acad Sci U S A 107, 436-441. 10.1073/pnas.0908099107.

- Pan, X., Liu, J., Nguyen, T., Liu, C., Sun, J., Teng, Y., Fergusson, M.M., Rovira, II, Allen, M., Springer, D.A., et al. (2013). The physiological role of mitochondrial calcium revealed by mice lacking the mitochondrial calcium uniporter. Nat Cell Biol 15, 1464-1472. 10.1038/ncb2868.
- Parks, R.J., Murphy, E., and Liu, J.C. (2018). Mitochondrial Permeability Transition Pore and Calcium Handling. Methods Mol Biol 1782, 187-196. 10.1007/978-1-4939-7831-1_11.
- Patron, M., Granatiero, V., Espino, J., Rizzuto, R., and De Stefani, D. (2019). MICU3 is a tissue-specific enhancer of mitochondrial calcium uptake. Cell Death Differ 26, 179-195. 10.1038/s41418-018-0113-8.
- Peng, W., Wong, Y.C., and Krainc, D. (2020). Mitochondria-lysosome contacts regulate mitochondrial Ca(2+) dynamics via lysosomal TRPML1. Proc Natl Acad Sci U S A 117, 19266-19275. 10.1073/pnas.2003236117.
- Perocchi, F., Gohil, V.M., Girgis, H.S., Bao, X.R., McCombs, J.E., Palmer, A.E., and Mootha, V.K. (2010). MICU1 encodes a mitochondrial EF hand protein required for Ca(2+) uptake. Nature 467, 291-296. 10.1038/nature09358.
- Pinton, P., Giorgi, C., Siviero, R., Zecchini, E., and Rizzuto, R. (2008). Calcium and apoptosis: ER-mitochondria Ca2+ transfer in the control of apoptosis. Oncogene 27, 6407-6418. 10.1038/onc.2008.308.
- Plovanich, M., Bogorad, R.L., Sancak, Y., Kamer, K.J., Strittmatter, L., Li, A.A., Girgis, H.S., Kuchimanchi, S., De Groot, J., Speciner, L., et al. (2013). MICU2, a

paralog of MICU1, resides within the mitochondrial uniporter complex to regulate calcium handling. PLoS One 8, e55785. 10.1371/journal.pone.0055785.

- Quintana, A., and Hoth, M. (2012). Mitochondrial dynamics and their impact on T cell function. Cell Calcium 52, 57-63. 10.1016/j.ceca.2012.02.005.
- Rimessi, A., Bezzerri, V., Patergnani, S., Marchi, S., Cabrini, G., and Pinton, P. (2015). Mitochondrial Ca2+-dependent NLRP3 activation exacerbates the Pseudomonas aeruginosa-driven inflammatory response in cystic fibrosis. Nat Commun 6, 6201. 10.1038/ncomms7201.
- Rizzuto, R., De Stefani, D., Raffaello, A., and Mammucari, C. (2012). Mitochondria as sensors and regulators of calcium signalling. Nat Rev Mol Cell Biol 13, 566-578. 10.1038/nrm3412.
- Rodriguez, L.R., Lapena-Luzon, T., Beneto, N., Beltran-Beltran, V., Pallardo, F.V., Gonzalez-Cabo, P., and Navarro, J.A. (2022). Therapeutic Strategies Targeting Mitochondrial Calcium Signaling: A New Hope for Neurological Diseases? Antioxidants (Basel) 11. 10.3390/antiox11010165.
- Rosencrans, W.M., Rajendran, M., Bezrukov, S.M., and Rostovtseva, T.K. (2021). VDAC regulation of mitochondrial calcium flux: From channel biophysics to disease. Cell Calcium 94, 102356. 10.1016/j.ceca.2021.102356.
- Sancak, Y., Markhard, A.L., Kitami, T., Kovacs-Bogdan, E., Kamer, K.J., Udeshi, N.D., Carr, S.A., Chaudhuri, D., Clapham, D.E., Li, A.A., et al. (2013). EMRE is an essential component of the mitochondrial calcium uniporter complex. Science 342, 1379-1382. 10.1126/science.1242993.

- Shanmughapriya, S., Tomar, D., Dong, Z., Slovik, K.J., Nemani, N., Natarajaseenivasan, K., Carvalho, E., Lu, C., Corrigan, K., Garikipati, V.N.S., et al. (2018). FOXD1-dependent MICU1 expression regulates mitochondrial activity and cell differentiation. Nat Commun 9, 3449. 10.1038/s41467-018-05856-4.
- Singh, R., Bartok, A., Paillard, M., Tyburski, A., Elliott, M., and Hajnoczky, G. (2022). Uncontrolled mitochondrial calcium uptake underlies the pathogenesis of neurodegeneration in MICU1-deficient mice and patients. Sci Adv 8, eabj4716. 10.1126/sciadv.abj4716.
- Tomar, D., Dong, Z., Shanmughapriya, S., Koch, D.A., Thomas, T., Hoffman, N.E., Timbalia, S.A., Goldman, S.J., Breves, S.L., Corbally, D.P., et al. (2016). MCUR1 Is a Scaffold Factor for the MCU Complex Function and Promotes Mitochondrial Bioenergetics. Cell Rep 15, 1673-1685. 10.1016/j.celrep.2016.04.050.
- Tsai, C.W., Wu, Y., Pao, P.C., Phillips, C.B., Williams, C., Miller, C., Ranaghan, M., and Tsai, M.F. (2017). Proteolytic control of the mitochondrial calcium uniporter complex. Proc Natl Acad Sci U S A 114, 4388-4393. 10.1073/pnas.1702938114.
- Tsai, M.F., Phillips, C.B., Ranaghan, M., Tsai, C.W., Wu, Y., Willliams, C., and Miller, C. (2016). Dual functions of a small regulatory subunit in the mitochondrial calcium uniporter complex. Elife 5. 10.7554/eLife.15545.
- Van Keuren, A.M., Tsai, C.W., Balderas, E., Rodriguez, M.X., Chaudhuri, D., and Tsai, M.F. (2020). Mechanisms of EMRE-Dependent MCU Opening in the Mitochondrial Calcium Uniporter Complex. Cell Rep 33, 108486. 10.1016/j.celrep.2020.108486.

- Vasington, F.D., and Murphy, J.V. (1962). Ca ion uptake by rat kidney mitochondria and its dependence on respiration and phosphorylation. J Biol Chem 237, 2670-2677.
- Vecellio Reane, D., Vallese, F., Checchetto, V., Acquasaliente, L., Butera, G., De Filippis, V., Szabo, I., Zanotti, G., Rizzuto, R., and Raffaello, A. (2016). A MICU1 Splice Variant Confers High Sensitivity to the Mitochondrial Ca(2+) Uptake Machinery of Skeletal Muscle. Mol Cell 64, 760-773. 10.1016/j.molcel.2016.10.001.
- Wang, Y., Nguyen, N.X., She, J., Zeng, W., Yang, Y., Bai, X.C., and Jiang, Y. (2019). Structural Mechanism of EMRE-Dependent Gating of the Human Mitochondrial Calcium Uniporter. Cell 177, 1252-1261 e1213. 10.1016/j.cell.2019.03.050.
- Weinberg, S.E., Sena, L.A., and Chandel, N.S. (2015). Mitochondria in the regulation of innate and adaptive immunity. Immunity 42, 406-417. 10.1016/j.immuni.2015.02.002.
- Wolf, S.G., Mutsafi, Y., Dadosh, T., Ilani, T., Lansky, Z., Horowitz, B., Rubin, S., Elbaum, M., and Fass, D. (2017). 3D visualization of mitochondrial solid-phase calcium stores in whole cells. Elife 6. 10.7554/eLife.29929.
- Wu, W., Shen, Q., Zhang, R., Qiu, Z., Wang, Y., Zheng, J., and Jia, Z. (2020). The structure of the MICU1-MICU2 complex unveils the regulation of the mitochondrial calcium uniporter. EMBO J 39, e104285. 10.15252/embj.2019104285.
- Xue, K., Wu, D., Wang, Y., Zhao, Y., Shen, H., Yao, J., Huang, X., Li, X., Zhou, Z., Wang, Z., and Qiu, Y. (2022). The mitochondrial calcium uniporter engages UCP1

to form a thermoporter that promotes thermogenesis. Cell Metab 34, 1325-1341 e1326. 10.1016/j.cmet.2022.07.011.

- Yoo, J., Wu, M., Yin, Y., Herzik, M.A., Jr., Lander, G.C., and Lee, S.Y. (2018). Cryo-EM structure of a mitochondrial calcium uniporter. Science 361, 506-511. 10.1126/science.aar4056.
- Zheng, X., Chen, M., Meng, X., Chu, X., Cai, C., and Zou, F. (2017). Phosphorylation of dynamin-related protein 1 at Ser616 regulates mitochondrial fission and is involved in mitochondrial calcium uniporter-mediated neutrophil polarization and chemotaxis. Mol Immunol 87, 23-32. 10.1016/j.molimm.2017.03.019.
- Zhuo, W., Zhou, H., Guo, R., Yi, J., Zhang, L., Yu, L., Sui, Y., Zeng, W., Wang, P., and Yang, M. (2021). Structure of intact human MCU supercomplex with the auxiliary MICU subunits. Protein Cell 12, 220-229. 10.1007/s13238-020-00776-w.

CHAPTER 3:

Evolutionary divergence reveals the molecular basis of EMRE dependence of the human MCU

Melissa JS MacEwen[1,*], Andrew L Markhard[2,*], Mert Bozbeyoglu[2], Forrest Bradford[1], Olga Goldberger[2], Vamsi K Mootha[2,3,4] , Yasemin Sancak[1]

Life Science Alliance

Published 7 August 2020

DOI: 10.26508/lsa.202000718

[1]Department of Pharmacology, University of Washington, Seattle, WA, USA

[2]Howard Hughes Medical Institute and Department of Molecular Biology, Massachusetts General Hospital, Boston, MA, USA

[3]Broad Institute, Cambridge, MA, USA

[4]Department of Systems Biology, Harvard Medical School, Boston, MA, USA

Correspondence: sancak@uw.edu; vamsi@hms.harvard.edu
*Melissa JS MacEwen and Andrew L Markhard contributed equally to this work

ABSTRACT

The mitochondrial calcium uniporter (MCU) is a calcium-activated calcium channel critical for signaling and bioenergetics. MCU, the pore-forming subunit of the uniporter, contains two transmembrane domains and is found in all major eukaryotic taxa. In amoeba and fungi, MCU homologs are sufficient to form a functional calcium channel, whereas human MCU exhibits a strict requirement for the metazoan protein essential MCU regulator (EMRE) for conductance. Here, we exploit this evolutionary divergence to decipher the molecular basis of human MCU's dependence on EMRE. By systematically generating chimeric proteins that consist of EMRE-independent *Dictyostelium discoideum* MCU and *Homo sapiens* MCU (HsMCU), we converged on a stretch of 10 amino acids in *D. discoideum* MCU that can be transplanted to HsMCU to render it EMRE independent. We call this region in human MCU the EMRE dependence domain (EDD). Cross-linking experiments show that EMRE directly interacts with HsMCU at its transmembrane domains as well as the EDD. Our results suggest that EMRE stabilizes the EDD of MCU, permitting both channel opening and calcium conductance, consistent with recently published structures of MCU-EMRE.

INTRODUCTION

Mitochondria play central roles in diverse cellular processes including metabolism, signaling, and cell death. Calcium (Ca^{2+}) signaling is critical for coordination of cellular needs with mitochondrial outputs by regulating the activity of the tricarboxylic acid cycle, activity of mitochondrial metabolite carriers, and triggering the mitochondrial permeability transition pore (Denton, 2009; Del Arco *et al.*, 2016; Giorgio *et al.*, 2018). This coordination is partially mediated by entry of Ca^{2+} into the mitochondrial matrix from the

cytosol during a Ca^{2+} signaling event. Perturbation of mitochondrial Ca^{2+} uptake is associated with a plethora of cellular and systemic pathologies, ranging from abnormal mitochondrial movement and shape, to immune dysfunction, cell cycle progression, and neuromuscular disease (Logan *et al.*, 2014; Mammucari *et al.*, 2015; Prudent *et al.*, 2016; Mammucari *et al.*, 2018; Paupe & Prudent, 2018; Koval *et al.*, 2019; Zhao *et al.*, 2019).

The mitochondrial Ca^{2+} uniporter complex, a multi-subunit protein assembly that resides in the inner mitochondrial membrane (IMM) is responsible for bulk entry of Ca^{2+} ions into the mitochondrial matrix (Deluca & Engstrom, 1961; Vasington & Murphy, 1962; Carafoli & Lehninger, 1971; Kirichok *et al.*, 2004). An ~35-kD protein termed mitochondrial calcium uniporter (MCU) is the defining component of the uniporter complex and serves as its pore (Baughman *et al.*, 2011; De Stefani *et al.*, 2011; Chaudhuri *et al.*, 2013; Kovacs-Bogdan *et al.*, 2014). MCU is a transmembrane protein with two membrane-spanning helices (TM1 and TM2), a short linker region facing the intermembrane space (IMS) with a highly conserved “DIME” motif, a large amino terminal domain that assumes a β-grasp fold (Lee *et al.*, 2015, 2016), and a carboxyl terminal region that is mostly helical (Oxenoid *et al.*, 2016; Baradaran *et al.*, 2018; Fan *et al.*, 2018; Nguyen *et al.*, 2018; Yoo *et al.*, 2018). Functional and structural studies have shown that TM2 forms the Ca^{2+}-conducting pore of the channel, whereas the N-terminal domain is mostly dispensable for Ca^{2+} conductance and is likely to play a regulatory role (Lee *et al.*, 2015; Oxenoid *et al.*, 2016). In animals, MCU nucleates other proteins (MCUb, MICU1, MICU2, MICU3, and essential MCU regulator [EMRE]) that regulate different aspects of uniporter function. MICU1, MICU2, and MICU3 are EF-hand containing Ca^{2+}-binding proteins that localize to the IMS of the mitochondria. MICU homologs are not necessary for Ca^{2+} conductance

by the uniporter, but rather, they play crucial roles in setting the threshold for Ca^{2+} uptake (Perocchi *et al.*, 2010; Mallilankaraman *et al.*, 2012; Csordas *et al.*, 2013; Plovanich *et al.*, 2013; de la Fuente *et al.*, 2014; Foskett & Madesh, 2014; Patron *et al.*, 2014; Liu *et al.*, 2016; Kamer *et al.*, 2018). In certain cell types, however, loss of MICU1 homologs leads to loss of other uniporter components, including MCU, leading to a decrease in uniporter activity (Plovanich *et al.*, 2013). MCUb is a paralog of MCU and is thought to be a negative regulator of MCU because of its inability to form a functional Ca^{2+} channel (Raffaello *et al.*, 2013).

EMRE is a single-pass transmembrane protein that was the last essential component of the uniporter to be identified, in part because of its curious evolutionary distribution (Sancak *et al.*, 2013). MCU and MICU1 homologs tend to be found in all major eukaryotic taxa, with lineage-specific losses (Bick *et al.*, 2012). Saccharomyces cerevisiae, for example, has completely lost both MICU1 and MCU, and in fact, this evolutionary diversity formed the basis for the initial discovery of MICU1 (Perocchi *et al.*, 2010). After the initial molecular identification of the uniporter machinery, our efforts to functionally reconstitute uniporter activity in yeast mitochondria using human MCU alone failed, for reasons that were not clear. This led to the search for additional missing components of the uniporter complex, leading to the identification of EMRE, which is lacking in most fungi but present in all metazoans and in extant members of the out-group of metazoans and fungi (Sancak *et al.*, 2013). In these species, EMRE fulfills two important functions. First, the C-terminal domain of EMRE is crucial for MCU–MICU1 interaction (Sancak *et al.*, 2013; Tsai *et al.*, 2016). Second, EMRE is strictly required for mitochondrial Ca^{2+} uptake (Sancak *et al.*, 2013; Kovacs-Bogdan *et al.*, 2014; Tsai *et al.*,

2016). Hence, in metazoans, MCU and EMRE are both necessary and sufficient for reconstituting the pore activity of the uniporter.

Here, we exploited the evolutionary divergence of EMRE to understand its role in the uniporter complex. We previously showed that in amoeba *Dictyostelium discoideum*, there are no EMRE homologs, and *D. discoideum* MCU (DdMCU) forms a functional uniporter by itself (Kovacs-Bogdan *et al.*, 2014). We reasoned that sequence elements that confer EMRE-independent activity to DdMCU could be swapped from DdMCU to *Homo sapiens* MCU (HsMCU) to render it "EMRE independent." To this end, we systematically generated HsMCU–DdMCU chimeric proteins and tested their ability to conduct Ca^{2+} in human cells lacking EMRE. These efforts led to the identification of a 10-amino acid–long region in HsMCU that determines its EMRE dependence. We call this region of MCU its EMRE dependence domain (EDD). Using copper-mediated cysteine cross-linking experiments, we show that EMRE interacts with both transmembrane domains of MCU (TM1 and TM2) as well as its EDD. Interestingly, EDD, which is C-terminal to the pore-forming TM2, appears flexible in published high-resolution fungal MCU structures (Fan *et al.*, 2018; Nguyen *et al.*, 2018; Yoo *et al.*, 2018) and partially overlaps with the EMRE-MCU interaction domain identified in a high-resolution cryo-EM structure of human MCU-EMRE (Wang *et al.*, 2019). Our data suggest that EMRE stabilizes this region through direct binding, which may lead to an open conformation of the pore at the matrix side to enable exit of Ca^{2+}, consistent with recently reported structural data (Wang *et al.*, 2019).

RESULTS

Carboxyl-terminal domain of EMRE faces the IMS and mediates MICU1–EMRE interaction

EMRE is a small transmembrane protein that resides in the IMM and has been shown to have two distinct functions in the uniporter. First, EMRE facilitates the interaction of MCU with MICU1. Second, it is required for Ca^{2+} conductance through human MCU. It was essential to clarify EMRE's membrane topology to understand the mechanisms of these two functions. Previous experimental studies reported contradictory results on the topology of EMRE (Tsai *et al.*, 2016; Vais *et al.*, 2016; Yamamoto *et al.*, 2016). We wanted to determine EMRE's topology using two complementary methods. To this end, we first generated EMRE KO cell lines that stably express EMRE protein tagged with FLAG at its carboxyl terminus (C-terminus) (EMRE-FLAG). When expressed at near endogenous levels, EMRE- FLAG rescued the mitochondrial Ca^{2+} uptake defect observed in EMRE KO cells to the same extent as untagged EMRE protein (**Fig 1A**) in a permeabilized cell mitochondrial Ca^{2+} uptake assay. Furthermore, EMRE-FLAG immunoprecipitated endogenous MCU and MICU1 (**Fig 1B**), showing that the C-terminal tag did not perturb EMRE's function or interaction with other uniporter proteins.

To determine the membrane topology of EMRE, we first used a proteinase accessibility assay. Mitochondria isolated from EMRE- FLAG expressing EMRE KO cells were incubated with proteinase K (PK) in the presence of increasing concentrations of

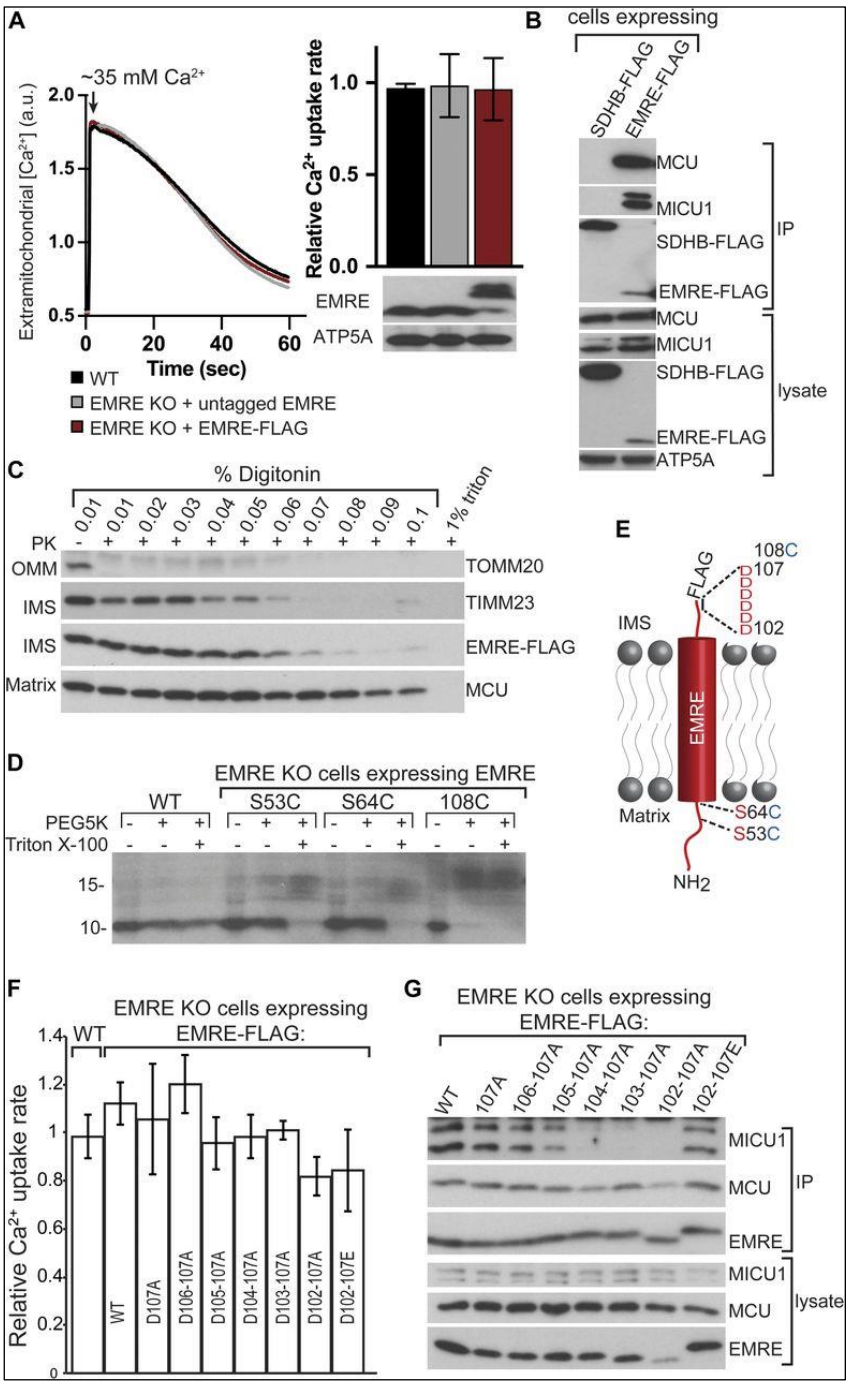

Figure 1. EMRE CAD faces the intermembrane space and mediates EMRE–MICU1 interaction.

(A) Tagging EMRE with a FLAG epitope tag at its C terminus does not impair its function. HEK293T cells expressing indicated proteins were permeabilized and mitochondrial Ca^{2+} uptake was measured by monitoring extramitochondrial Ca^{2+} clearance. Bar graph shows quantification of Ca^{2+} uptake rates and Western blot shows EMRE expression. (n = 4). ATP5A serves as loading control. **(B)** C-terminal FLAG tag does not impair EMRE–MCU and EMRE–MICU1 interactions. EMRE FLAG and control SDHB-FLAG were immunoprecipitated, and immunoprecipitates were blotted for MCU and MICU1. ATP5A serves as loading control. **(C)** Proteinase K treatment of isolated mitochondria in the presence of increased detergent concentration. EMRE-FLAG is degraded by proteinase K at the same detergent concentration as TIMM23, an inner mitochondrial membrane protein. **(D)** Mitochondria were isolated from WT or EMRE KO cells that stably express the indicated proteins. Mitoplasts (mitochondria without outer membranes) were prepared and treated with PEG5K-maleimide. A 5-kD mass addition to EMRE protein was detected by Western blotting. **(D, E)** Schematic shows EMRE membrane topology and the position of the amino acids that were mutated to cysteines for PEGylation experiments shown in **(D)**. EMRE aa 64–85 were predicted to form its transmembrane domain using TMHMM (Sonnhammer *et al.*, 1998). **(F)** EMRE DDD domain is not required for mitochondrial calcium uptake. Mitochondrial calcium uptake rates of WT and EMRE KO cells stably expressing the indicated proteins (n = 4). **(G)** Charge- conserving mutations of the six aspartic acids of EMRE to glutamic acid restores EMRE–MICU1 interaction. WT EMRE–FLAG or EMRE–FLAG with the indicated mutations were stably expressed in EMRE KO cells, immunoprecipitated, and immunoprecipitates were subjected to Western blotting to detect EMRE–MICU1 interaction. Data information: In **(A, F)**, data are presented as mean ± SD.

digitonin, and degradation of EMRE-FLAG was monitored using Western blotting. The

FLAG tag disappeared at the same digitonin concentration as IMS protein TIMM23, suggesting that the C terminus of EMRE faces the IMS (**Fig 1C**). Next, we confirmed N-in C-out topology of EMRE by using an orthogonal approach that uses the addition of a 5-kD mass to cysteine residues using polyethylene glycol (PEG)-maleimide (PEG5K). In this assay, cysteine residues that are in the matrix are shielded from membrane-impermeable PEG5K. Wild-type EMRE does not contain any cysteines, so we mutated S53 or S64—amino acids that are N-terminal to the predicted transmembrane domain (aa 65–84)—to cysteine (S53C or S64C). We also added a cysteine residue at EMRE's C terminus after the last amino acid (EMRE 108C). Expression of WT, S53C, S64C, or 108C EMRE in EMRE KO cells rescued the mitochondrial Ca^{2+} uptake defect of these cells (**Fig S1**), suggesting that these mutations do not perturb protein function and topology. Mitoplasts (mitochondria without an outer membrane) prepared from EMRE KO cells that express wild type, S53C, S63C, or 108C EMRE were treated with PEG5K-maleimide. An ~5-kD shift in the molecular weight of EMRE was detected only with the EMRE 108C protein, suggesting that 53C and 64C are in the matrix. When PEG5K was added in the presence of a small amount

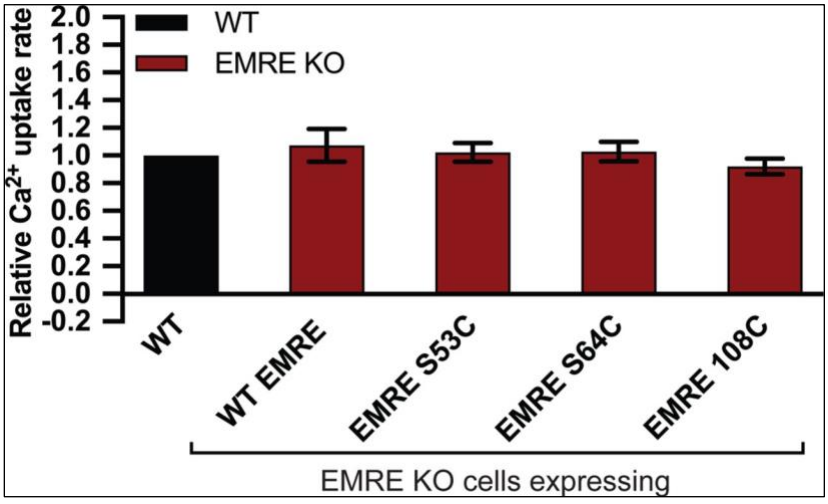

Figure S1. EMRE S53C, S64C, and 108C are functional proteins.
Mutation of EMRE S53 and S64C to cysteine or addition of a cysteine at the C terminus of EMRE does not impair its function. HEK293T cells expressing indicated proteins were permeabilized and mitochondrial Ca2+ uptake was measured by monitoring extramitochondrial Ca2+ clearance. Bar graph shows quantification of Ca2+ uptake rates relative to WT HEK293T cells (n = 4). Data information: data are presented as mean ± SD.

of detergent to disrupt the inner membrane, all three cysteine-containing proteins were PEGylated, showing that the lack of modification of 53C and 64C was not due to their inaccessibility to PEG5K-maleimide in the complex (**Fig 1D**). These findings are consistent with previous results and confirm that EMRE's N terminus faces the matrix and its C terminus acidic domain (CAD) faces the IMM (**Fig 1E**) (Sancak *et al.*, 2013; Tsai *et al.*, 2016; Yamamoto *et al.*, 2016).

CAD has a high percentage of negatively charged aspartic acid (D) and glutamic acid (E) (10/22 amino acids, ~45%). Notably, the presence of five or more D or E at the end of the protein is conserved across species and is a defining feature of EMRE (Sancak *et al.*, 2013). CAD has been shown to be important for the interaction of EMRE with MICU1. We asked whether EMRE–MICU1 interaction is mainly mediated by the negative charges in this region and whether CAD also plays a role in Ca^{2+} conductance. To test these, we mutated the six Ds (D102 to D107) to alanine (A) and expressed these mutant proteins in EMRE KO cells as FLAG-tagged proteins. Loss of negative charge in this region did not perturb mitochondrial Ca^{2+} uptake (**Fig 1F**) (Tsai *et al.*, 2016; Vais *et al.*, 2016; Yamamoto *et al.*, 2016). However, we did see a decrease in the amount of MICU1 that immunoprecipitated with EMRE as the number of alanines increased in this region. EMRE–MICU1 interaction was restored when Ds were mutated to similarly charged Es (**Fig 1G**). These results show that the negative charge of CAD is dispensable for Ca^{2+} conductance by MCU but is critical for EMRE–MICU1 interaction.

Identification of the EDD of HsMCU

EMRE likely arose in early evolution of opisthokonts and is found in all metazoans. Its loss leads to a complete loss of mitochondrial Ca^{2+} uptake (Sancak *et al.*, 2013), but

the molecular basis for this requirement is not known. We previously showed that amoeba *D. discoideum* does not have an EMRE homolog and that *D. discoideum* MCU (DdMCU) forms a functional Ca^{2+} channel by itself (Kovacs-Bogdan *et al.*, 2014). In contrast, to be able to conduct Ca^{2+}, human MCU (HsMCU) requires co-expression of EMRE (Kovacs-Bogdan *et al.*, 2014). The EMRE dependence of MCU does not appear to be related to proper MCU folding or mitochondrial localization, as MCU forms higher order oligomers with correct membrane topology in the absence of EMRE (Kovacs-Bogdan *et al.*, 2014). We hypothesized that EMRE plays an important role in Ca^{2+} permeation of the human uniporter and exploited the evolutionary divergence of EMRE dependence of DdMCU and HsMCU to understand the molecular details of EMRE function. First, we compared the predicted secondary structures of DdMCU and HsMCU (**Fig 2A**). The predicted secondary structures of the two MCU proteins were most divergent at their N termini. To test whether the DdMCU N terminus domain would be sufficient to confer EMRE independence to HsMCU, we generated a chimeric protein, chimera 1, as shown in **Fig 2B**. We expressed chimera 1 in MCU KO HEK293T cells to determine whether it would form a functional protein, and in EMRE KO HEK293T cells to determine whether it would function independently of EMRE in our permeabilized cell mitochondrial Ca^{2+} uptake assay. Chimera 1 formed a functional channel in MCU KO cells; however, its activity was still dependent on the presence of EMRE (**Fig 2B**).

These results suggested that the two transmembrane domains or the C terminus domain of HsMCU might be critical for its EMRE dependence. To test this, we generated chimeras 2–6 and determined their function and EMRE dependence. Chimeras 2 and 3 did not form functional Ca^{2+} channels (**Fig 2C**). Chimera 4 showed reduced, but EMRE-

dependent uniporter activity (**Fig 2C**), suggesting that the TM domains of HsMCU are involved in its EMRE dependence. Chimeras 5 and 6, on the other hand, showed EMRE-independent Ca^{2+} uptake (**Fig 2C**). Both of these chimeras contain the two predicted C-

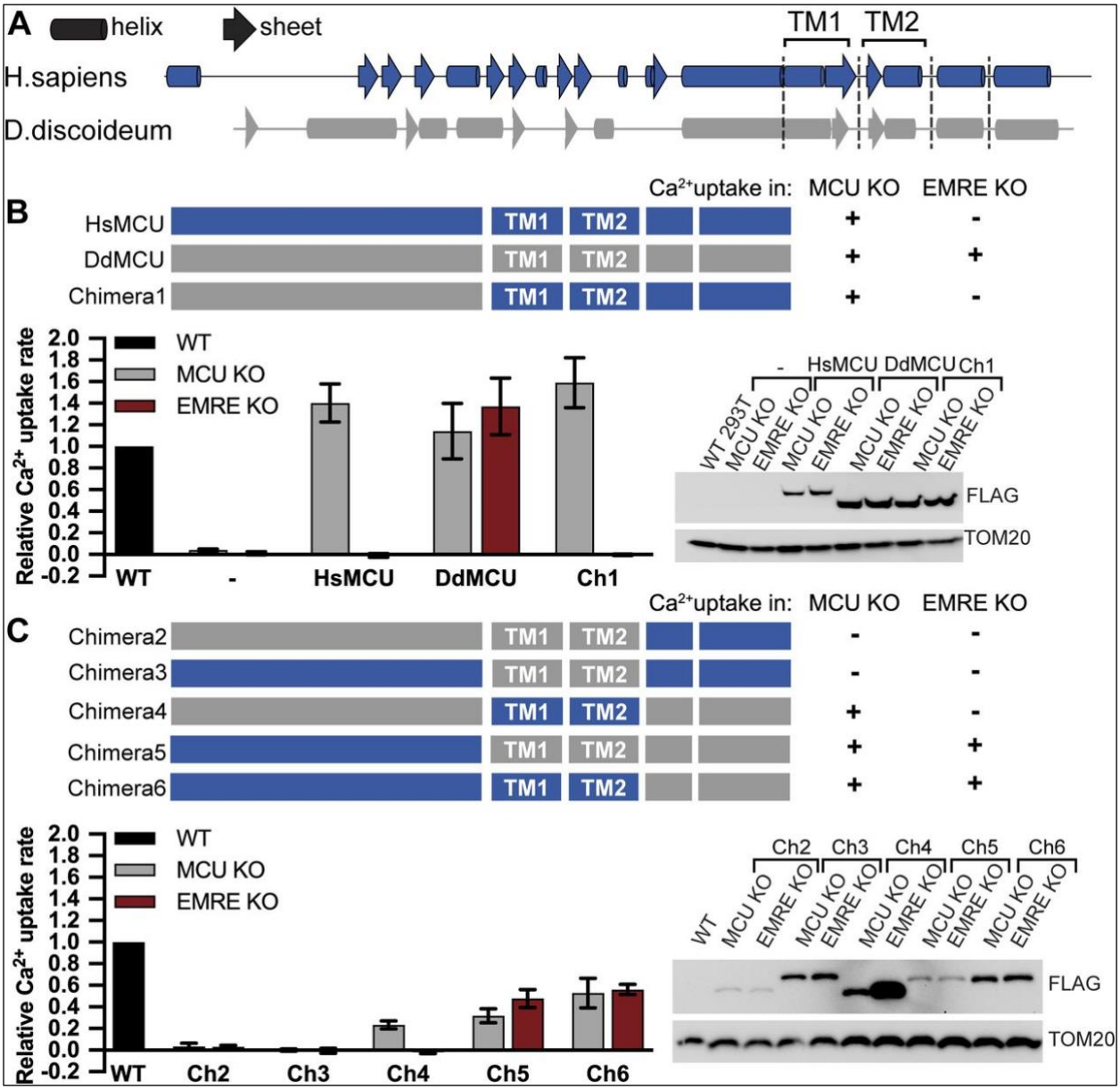

Figure 2. Carboxyl-terminal helices of Dictyostelium discoideum MCU (DdMCU) confer EMRE-independent Ca2+ uptake to Homo sapiens MCU (HsMCU).
(A) Schematic shows helices and sheets of HsMCU and DdMCU as predicted by PSIPRED. Two transmembrane domains are labeled. **(B, C)** Schematic summarizes the domain structure of HsMCU, DdMCU, and the chimeric proteins. FLAG-tagged proteins were stably expressed in MCU KO and EMRE KO HEK293T cells. Mitochondrial Ca2+ uptake rates in control WT and chimera expressing cells were measured and normalized to those of WT cells (n = 3–4). Expression of chimeras was detected by Western blotting using anti-FLAG antibody. TOM20 serves as loading control. Data information: in **(B, C)**, data are presented as mean ± SD.

terminal helices from DdMCU. To determine whether one of these predicted helices might be the critical domain for EMRE-independent Ca^{2+} uptake, we generated chimeras 7 and 8. Surprisingly, chimera 7 was functional to the same extent both in MCU KO and EMRE KO cells. In addition, chimera 8, despite its poor expression, supported mitochondrial

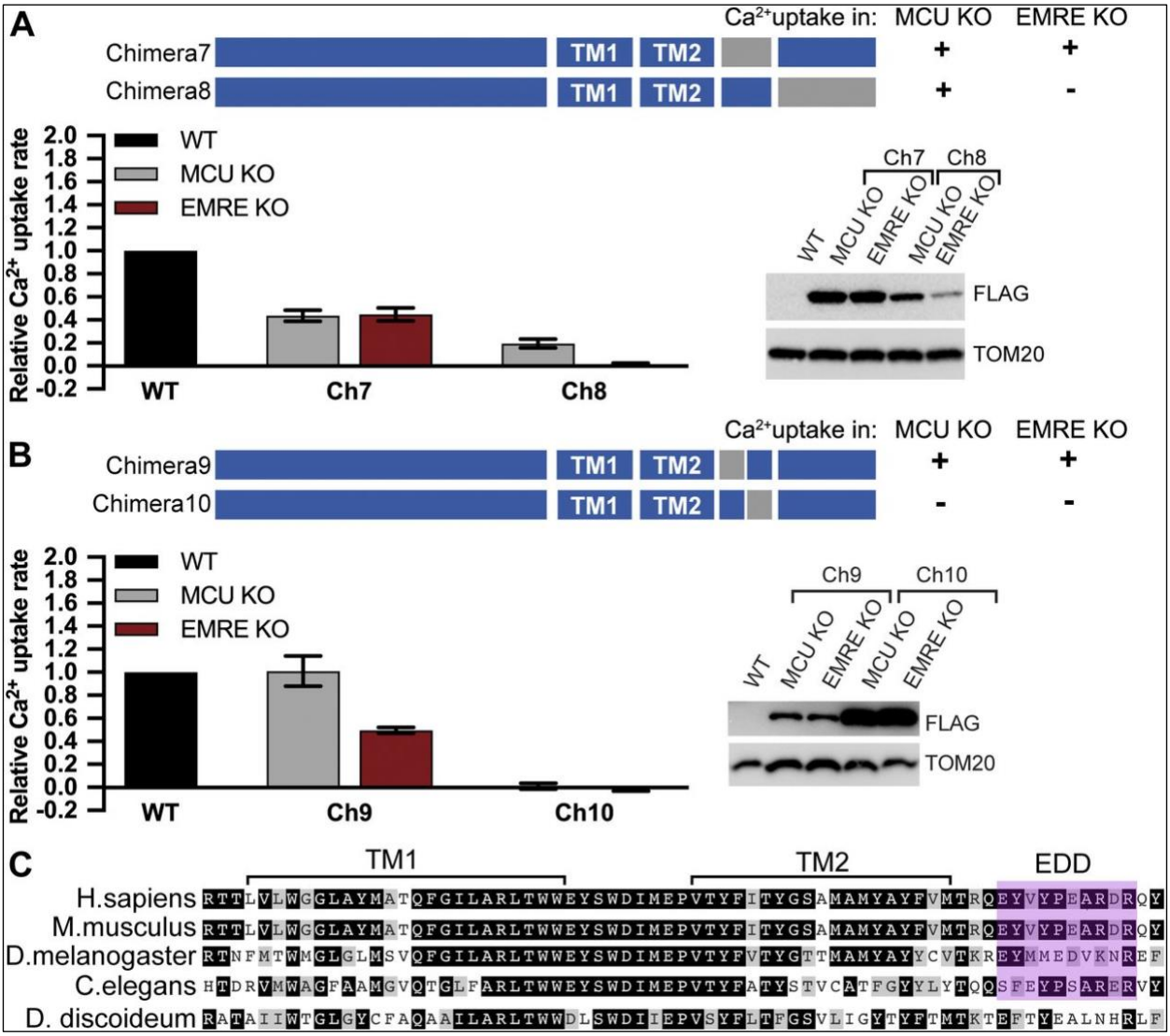

Figure 3. EMRE dependence domain of Homo sapiens MCU is a 10- amino acid–long region located C-terminal to TM2.

(A, B) Schematic summarizes the domain structure of chimeric proteins. FLAG-tagged proteins were stably expressed in mitochondrial calcium uniporter (MCU) KO and EMRE KO HEK293T cells. Mitochondrial Ca^{2+} uptake rates in control WT and chimera expressing cells were measured and normalized to those of WT cells (n = 3–4). **(C)** Alignment of MCU protein from indicated species was done using CLUSTALW and amino acids were color-coded using BoxShade. Black boxes show identical amino acids, gray boxes show similar amino acids. TM1, TM2 and EMRE dependence domain are indicated. Data information: In **(A, B)**, data are presented as mean ± SD.

Ca^{2+} uptake, and its activity was EMRE dependent (**Fig 3A**). The helical region that defines chimera 7 is composed of 23 amino acids. We further divided this region into two halves at conserved amino acids to generate chimeras 9 and 10 (**Figs 3B** and **S2**). Chimera 10 did not support mitochondrial Ca^{2+} uptake, but chimera 9 formed an EMRE-independent Ca^{2+} channel (**Fig 3B**). The chimera 9 region originating from DdMCU is 10 amino acids long and is located directly after the pore forming TM (TM2) of HsMCU. We term this 10-amino acid region of MCU (aa288–aa297) the EDD (**Fig 3C**).

During our analysis, we noticed that the expression levels of the chimeric proteins varied (**Figs 2B** and **C**, **3A** and **B**, and **S3A**). However, we did not observe a correlation between the expression level of a particular chimera and the rate of mitochondrial Ca^{2+} uptake in cells that express the chimeric proteins (for example, compare the chimera 4 and 5 in **Fig 2C**). In these experiments, chimeric proteins were stably expressed in cells using lentivirus-mediated integration of the corresponding cDNAs into the genome. To

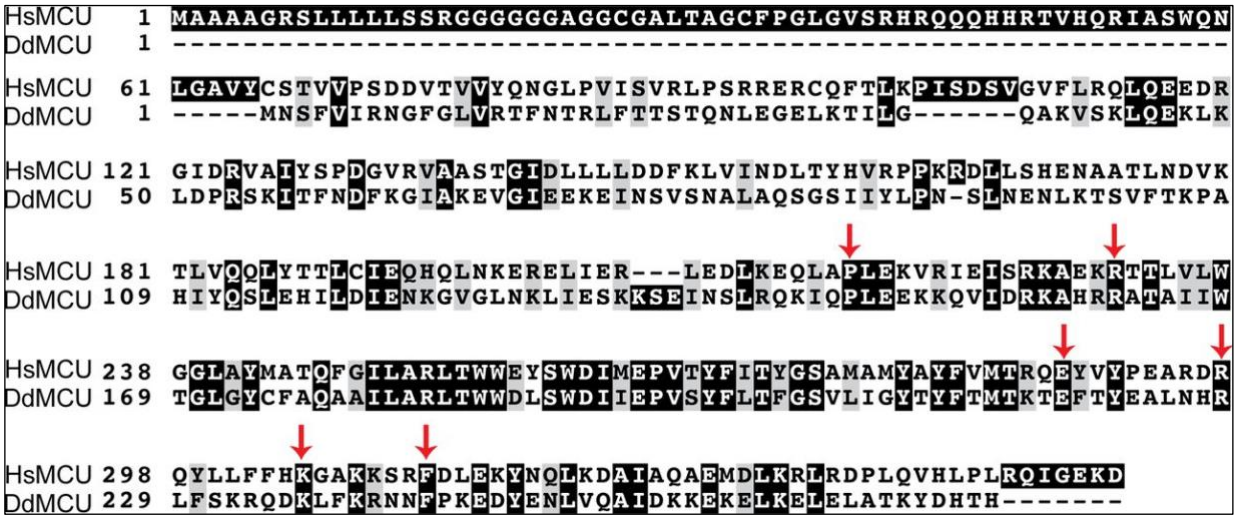

Figure S2. *Homo sapiens* MCU–*Dictyostelium discoideum* MCU (HsMCU–DdMCU) chimera break points.
Arrowheads point to the conserved amino acids of HsMCU and DdMCU that were chosen as break points in chimeras. Alignment of HsMCU and DdMCU was done using CLUSTALW, and amino acids were color coded using BoxShade. Black boxes show identical amino acids and gray boxes show similar amino acids.

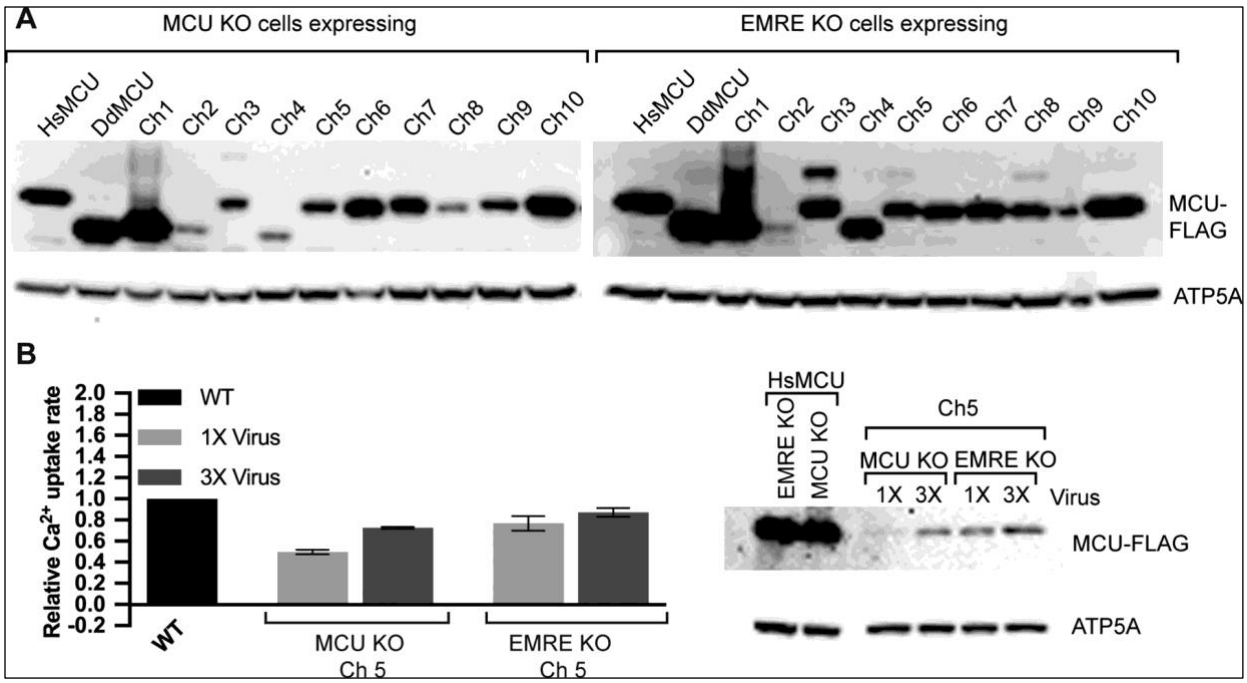

Figure S3. Comparison of Homo sapiens MCU–Dictyostelium discoideum MCU chimera protein expression and function.
(A) Mitochondrial calcium uniporter (MCU) KO or EMRE KO cells that stably express the indicated FLAG-tagged proteins were lysed, and lysates were analyzed by Western blotting using anti-FLAG antibody. ATP5A serves as loading control. **(B)** MCU KO and EMRE KO cells were infected with virus as described in material and methods to generate 1× infected cells after puromycin selection. The same cells were infected again with twice the amount of original virus to produce 3× infected cells. Mitochondrial Ca^{2+} uptake rates of control WT, 1× infected and 3× infected cells were measured. Bar graph shows mitochondrial Ca^{2+} uptake rates relative to WT control cells (n = 3). Western blot shows expression levels of FLAG-tagged *H. sapiens* MCU and chimera 5. ATP5A serves as loading control. **(B)** Data information: in **(B)**, data are presented as mean ± SD.

eliminate the possibility that low protein expression was due to low virus titer, we picked chimera 5, a chimera that expressed poorly but formed functional channels, and reinfected cells with virus. We observed a slight increase in protein expression and a concomitant increase in Ca^{2+} uptake rates. However, chimera 5 still expressed at lower levels than HsMCU (**Fig S3B**). This suggests that chimeric proteins may be inherently unstable. Consequently, we cannot determine whether low Ca^{2+} uptake rates of chimeras compared to HsMCU are due to their channel properties or their expression levels. Nevertheless, expression of a particular chimeric protein in MCU KO and EMRE KO cells were mostly comparable, allowing us to determine their EMRE dependence. Expression

of HsMCU–DdMCU chimeras did not alter mitochondrial membrane potential, suggesting that lack of mitochondrial Ca^{2+} uptake after expression of some chimeras was not secondary to perturbed mitochondrial health (**Fig S4**). Example mitochondrial Ca^{2+} uptake data for HsMCU, DdMCU, and chimeras in MCU KO and EMRE KO cells are shown in **Fig S5** and sequences of the chimeric proteins used are provided (**Supplemental Data 1, following Methods section**).

MCU TM1, TM2, and EDD interact with EMRE

Our functional experiments highlighted the importance of MCU TM domains and EDD for the EMRE dependence of human MCU. To complement these experiments and to determine if these domains are also important for EMRE–MCU physical interaction, we performed immunoprecipitation experiments using chimeras that formed functional channels and showed good protein expression (chimeras 1, 5, 6, 7, and 9). To further normalize protein expression levels, we transiently expressed control HsMCU, DdMCU, or chimeras, together with untagged EMRE in MCU KO cells. We treated these cells with amine-reactive cross-linker dithiobis (succinimidyl propionate) (DSP) before cell lysis to stabilize protein–protein interactions. We then immunoprecipitated MCU-FLAG. Chimera 5 did not interact with EMRE; chimeras 6 and 7 showed reduced EMRE interaction; chimeras 1 and 9 showed wild-type levels of EMRE–MCU interaction (**Fig 4A** and **B**). Consistent with stabilization of EMRE protein when bound to MCU, chimeras that showed better EMRE interaction also had more EMRE protein in the lysate (**Fig 4A**). These experiments suggested that MCU TM1, TM2, and the helical region that includes the EDD are important for EMRE–MCU binding. To determine if EMRE directly interacts with HsMCU in TM1, TM2, and EDD, we performed cysteine cross-linking experiments. Two

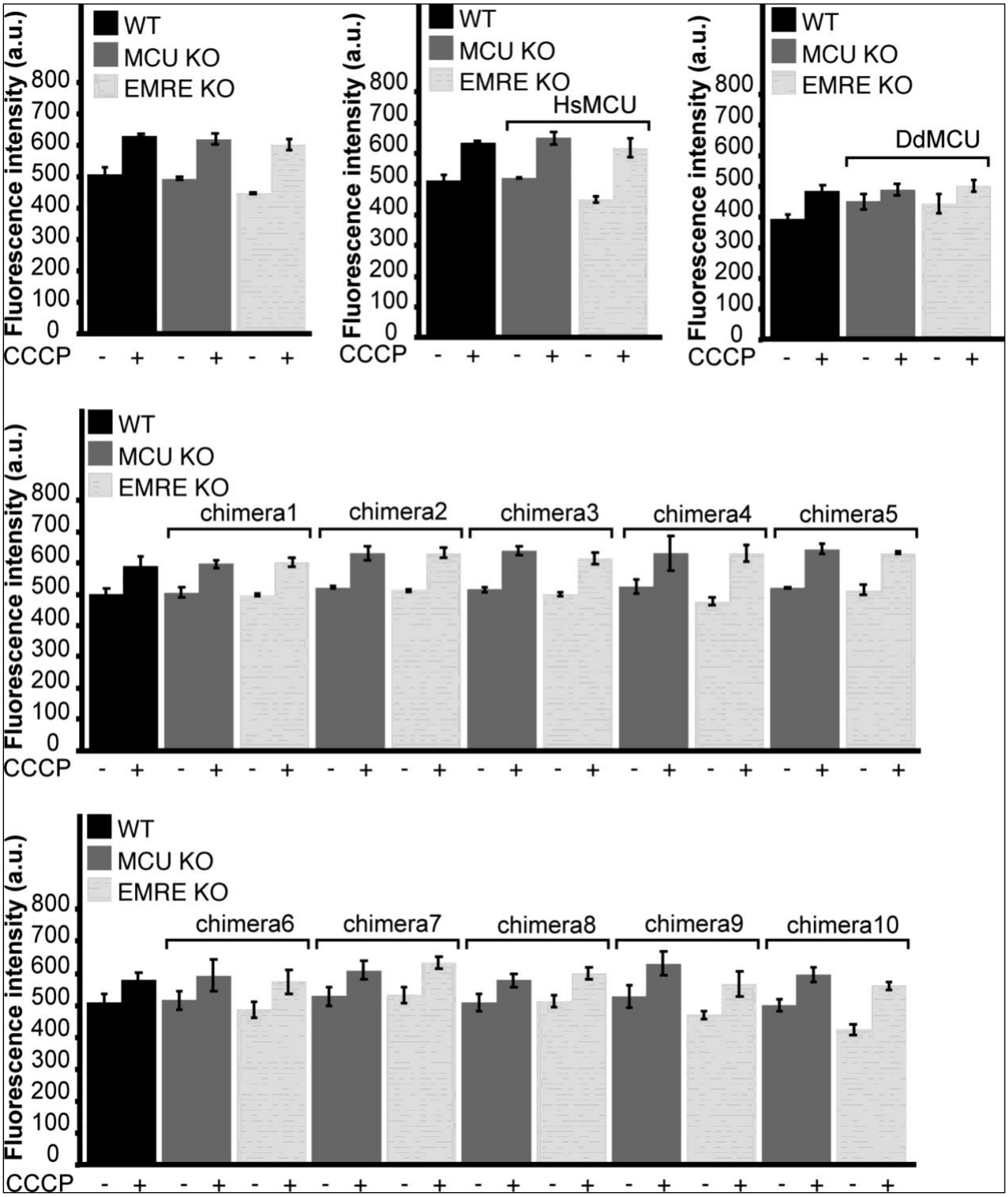

Figure S4. Expression of *Homo sapiens* MCU, *Dictyostelium discoideum* MCU, or chimeras do not alter mitochondrial membrane potential.
Control WT, MCU KO, or EMRE KO cells expressing the indicated proteins were permeabilized and incubated with TMRM. TMRM fluorescence was measured in the absence and presence of uncoupler CCCP. All cells showed comparable mitochondrial membrane potential (n = 3). Data information: Data are presented as mean ± SD.

amino acids on each trans-membrane domain of MCU were selected and mutated to

cysteine. We also mutated several consecutive EMRE amino acids to cysteines and performed a partial cysteine-scanning experiment. First, we co-expressed MCU and

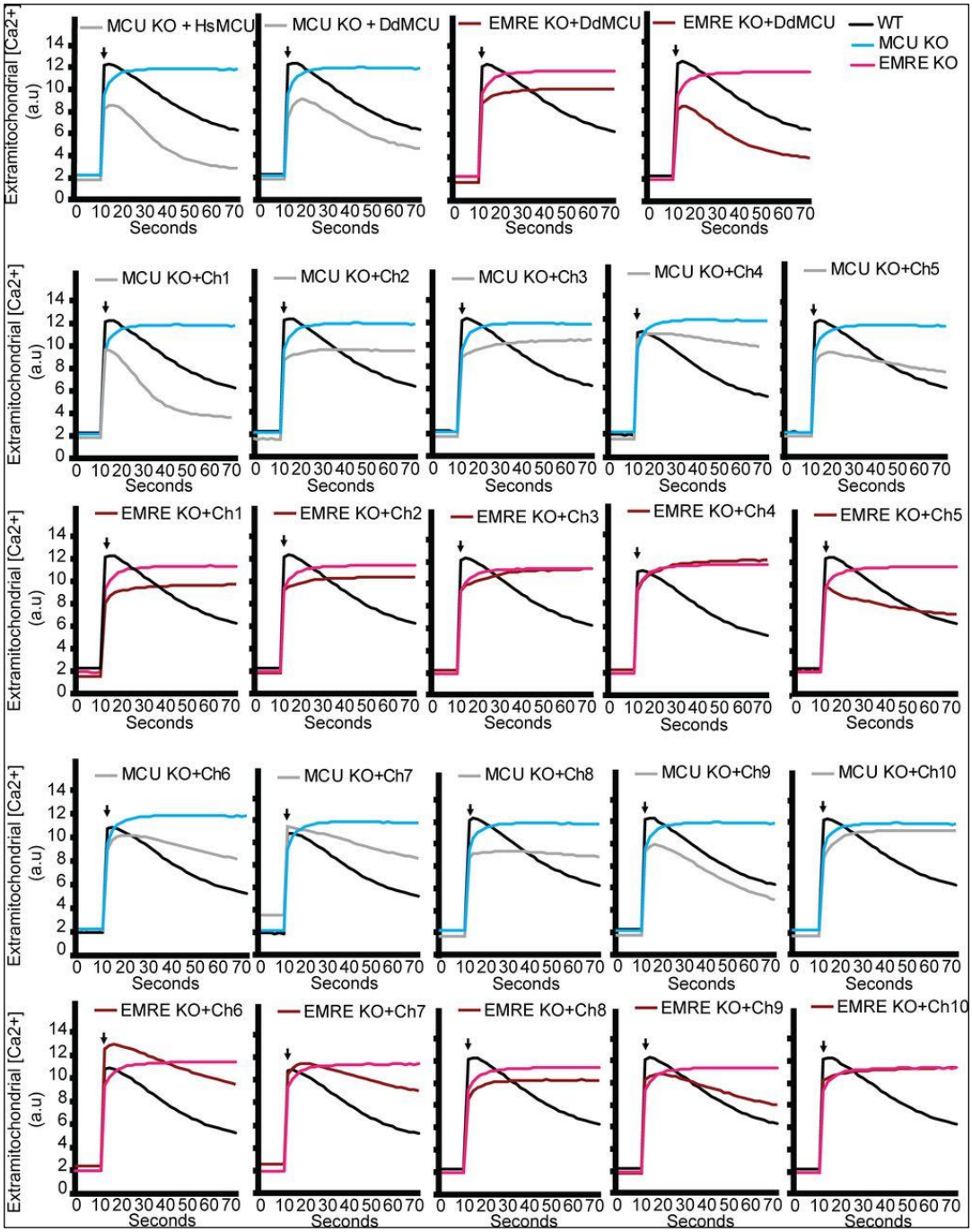

Figure S5. Representative mitochondrial Ca2+ uptake traces.
WT, mitochondrial calcium uniporter (MCU) KO, or EMRE KO HEK293T cell expressing the indicated proteins were permeabilized and mitochondrial Ca2+ uptake was measured by monitoring extramitochondrial Ca2+ clearance. The arrows indicate addition of Ca2+. Each graph shows data from WT and MCU KO or EMRE KO cells, in addition to data from cell lines that express the indicated chimeras.

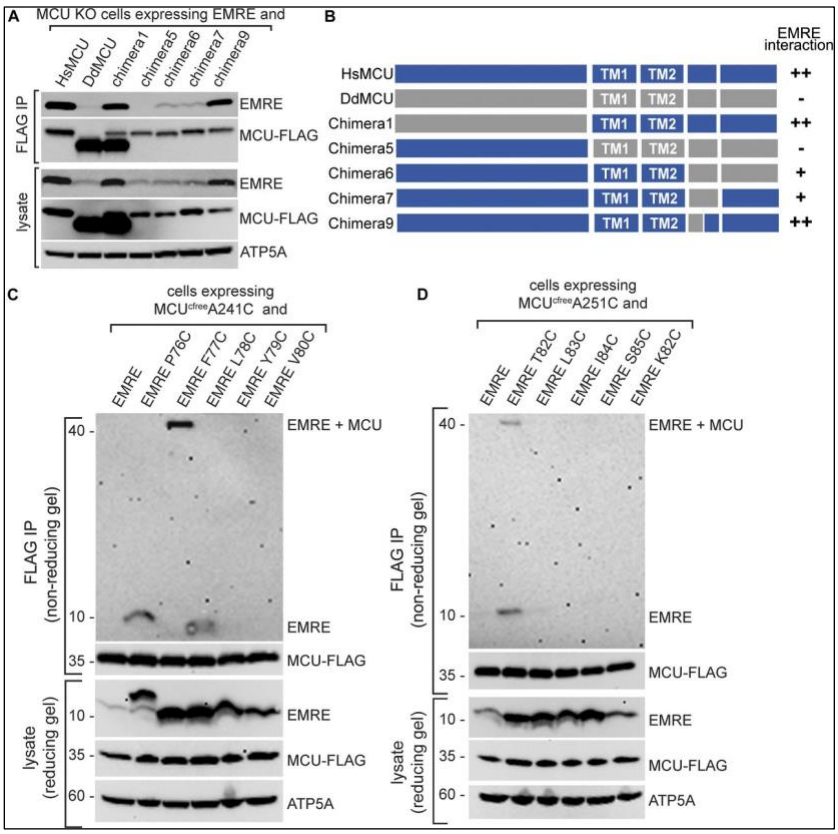

Figure 4. EMRE directly interacts with TM1 of mitochondrial calcium uniporter (MCU).
(A) MCU TM and C-terminal helices are required for EMRE–MCU interaction. Untagged EMRE and indicated FLAG-tagged MCU proteins were co-expressed in MCU KO HEK293T cells by transient transfection, FLAG-tagged proteins were immunoprecipitated and immunoprecipitates were analyzed for the presence of EMRE by Western blotting. ATP5A serves as loading control. EMRE–MCU interaction was evident both in immunoprecipitates and in lysates through stabilization of EMRE. **(B)** Schematic summarizes EMRE-chimera binding data and highlights the importance of MCU TM and C-terminal helices for EMR–EMCU interaction. **(C, D)** EMRE–*Homo sapiens* MCU cysteine cross-linking experiments show direct binding of MCU TM1 residues A241 and A251 to EMRE F77 and T82, respectively. **(C, D)** *H. sapiens* MCU that contains only one cysteine at amino acid 241 **(C)** or 251 **(D)** were stably co-expressed with indicated EMRE proteins. WT EMRE does not contain any cysteines and served as a control. Mitochondria were isolated from cells, and cysteine–cysteine cross-linking was induced using copper phenanthroline. MCU-FLAG was immunoprecipitated and the presence of an ~40 kD cross-linked EMRE-MCU band was detected under non-reducing conditions by Western blotting. Lysates were prepared in parallel under reducing conditions and were blotted to detect indicated proteins. ATP5A serves as loading control. Numbers indicate the locations of molecular weight standards.

EMRE proteins that contain one cysteine residue each, as well as control cysteine-free MCU, in MCU KO cells and confirmed that they are functional (**Fig S6A**). WT EMRE does not contain any cysteine residues and served as an additional control. Then, we performed copper-mediated cysteine cross- linking experiments in mitochondria isolated from these cells, immunoprecipitated MCU, and determined the presence of EMRE–MCU cross-linked protein product using non-reducing gel electrophoresis followed by Western blotting. Our results showed that MCU TM1 residue A241C cross-links with

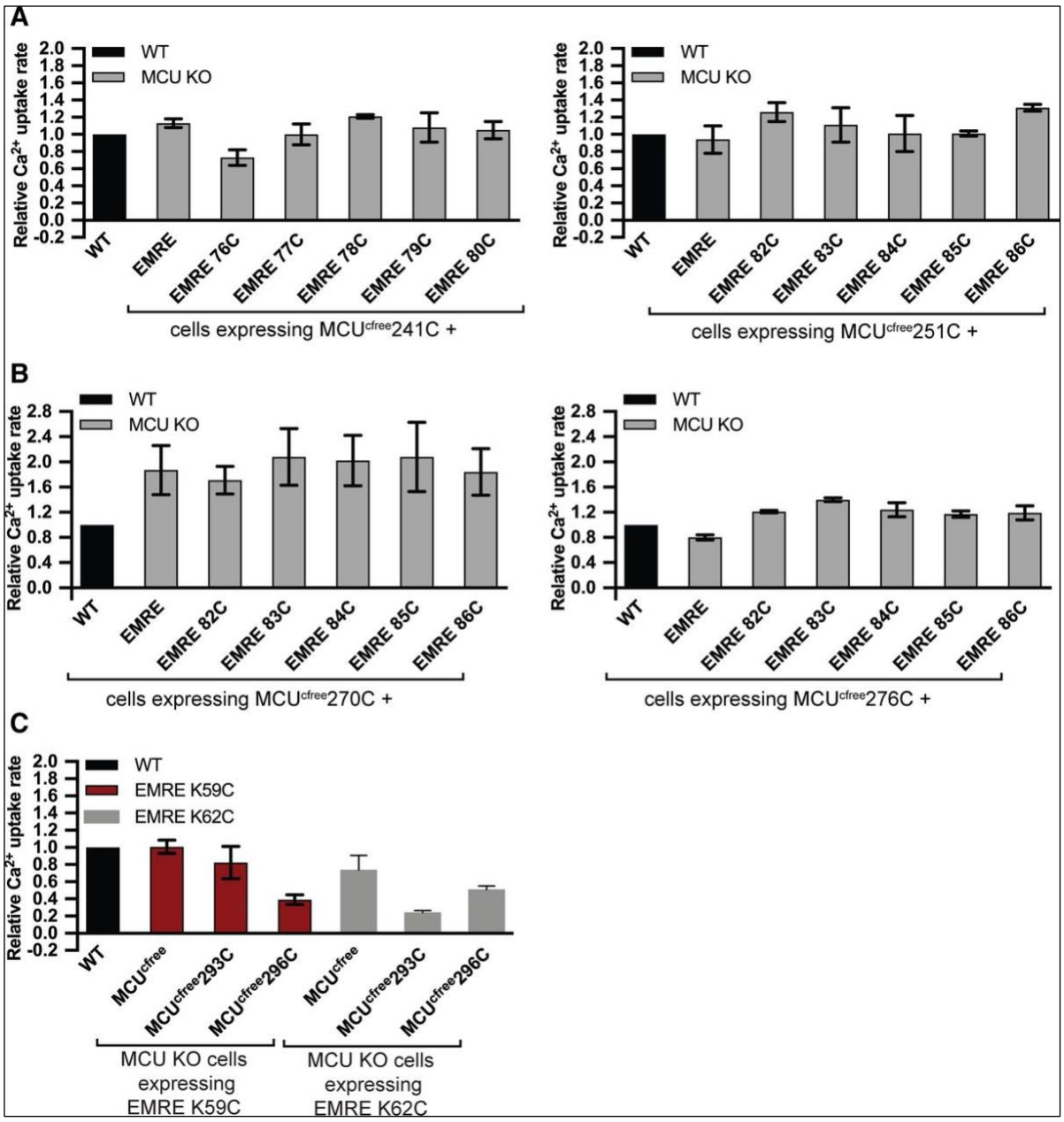

Figure S6. Functional characterization of mitochondrial calcium uniporter (MCU) and EMRE proteins used for cysteine cross-linking experiments.

(A, B, C) MCU KO HEK293T cells expressing indicated proteins were permeabilized and mitochondrial Ca^{2+} uptake was measured by monitoring extramitochondrial Ca^{2+} clearance. Bar graphs show Ca^{2+} uptake rates relative to control WT cells (n = 3–4). (A, B, C) MCU–EMRE cross-linking in TM1 of MCU **(A)**, in TM2 or MCU **(B)**, in EMRE-dependence domain of MCU **(C)** are shown. Data information: data are presented as mean ± SD.

EMRE F77C, but not with four other EMRE residues near F77C (**Fig 4C**). Similarly, MCU TM1 residue A251C specifically cross-linked to EMRE T82C (**Fig 4D**). To determine if EMRE also interacts with the pore-forming TM2 of MCU, we performed similar cross-

linking experiments with MCU I270C and MCU M276C. MCU KO cells expressing these MCU and EMRE cysteine cross-linked residues showed Ca^{2+} uptake, showing that cysteine substitutions did not alter protein function (**Fig S6B**). MCU I270C cross-linked to EMRE I84C (**Fig 5A**) and MCU M276C cross-linked to EMRE P76C (**Fig 5B**). Collectively, these findings confirm the inter- action that was observed between MCU TM1 and EMRE previously (Tsai *et al.*, 2016) and establish that the pore-forming TM2 of MCU also interacts with EMRE, both within and outside the MCU–EMRE interaction domain defined by the MCU–EMRE structure (Wang *et al.*, 2019).

Finally, we performed cysteine cross-linking experiments between amino acids in EDD (MCU E293 and D296) and the N-terminal domain of EMRE that faces the mitochondrial matrix (K59 and K62). First, we confirmed that cysteine substitutions did not alter the function of MCU or EMRE (**Fig S6C**). Both MCU residues in EDD cross-linked to both EMRE residues (**Fig 5C**). **Fig 5D** shows a schematic of MCU and EMRE amino acids that cross-linked. To gain insight for functional significance of EDD for uniporter function, we identified and highlighted the sequences that correspond to EDD in the four fungal MCU homologs whose high-resolution structures have been published (**Fig S7**). Surprisingly, this region appeared flexible in fungal MCU, which have slow calcium conductance rates compared to human uniporter (Carafoli & Lehninger, 1971; Goncalves *et al.*, 2015; Fan *et al.*, 2018; Nguyen *et al.*, 2018; Wettmarshausen *et al.*, 2018; Pittis *et al.*, 2020 Preprint). Based on this observation and our cross-linking data, we posit that binding of EMRE stabilizes this otherwise flexible region at the matrix opening of the channel and allows exit of Ca^{2+} ions from the pore.

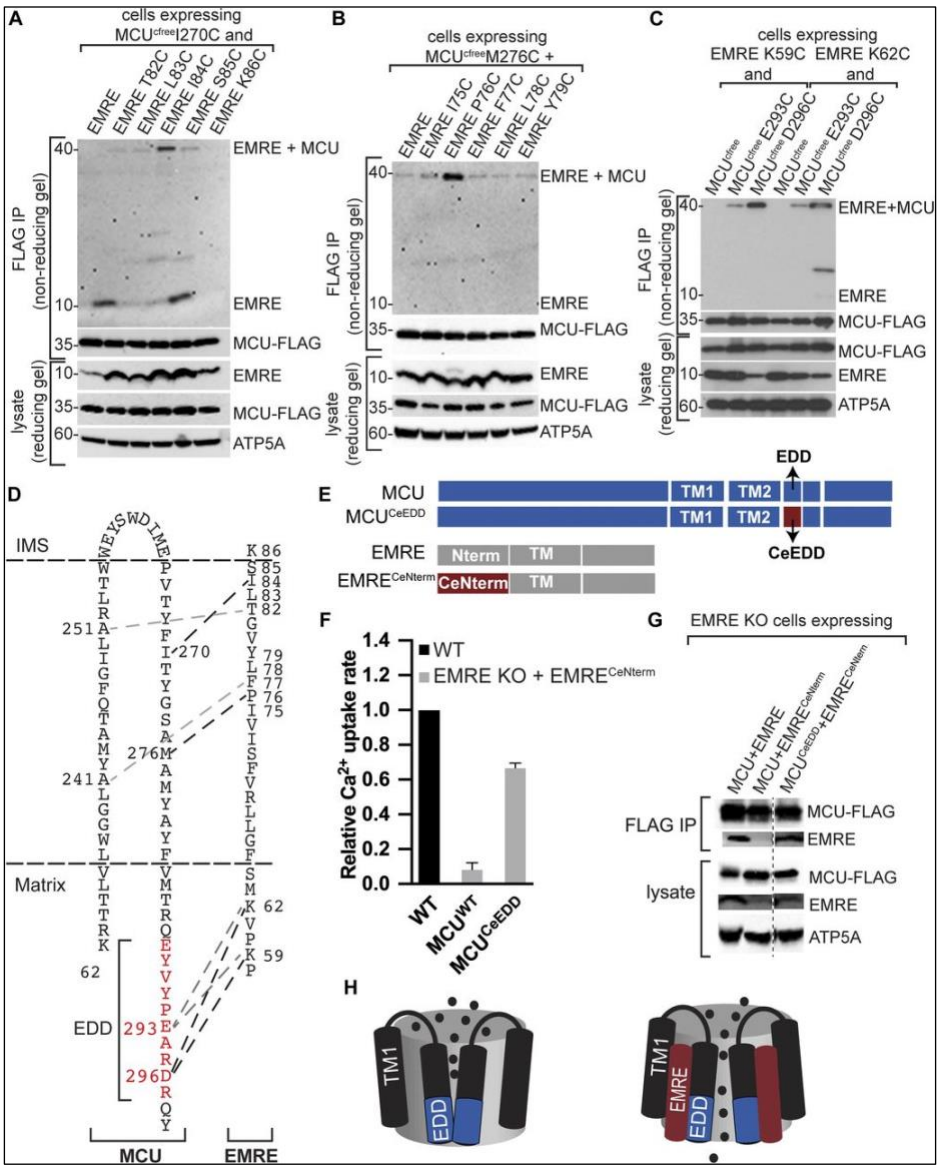

Figure 5. EMRE directly interacts with TM2 and EMRE dependence domain (EDD) of mitochondrial calcium uniporter (MCU).
(A, B) EMRE–*Homo sapiens* MCU (HsMCU) cysteine cross-linking experiment shows direct binding of MCU TM2 residues I270 and M276C to EMRE I84 and P76, respectively. **(A, B)** HsMCU that contains only one cysteine at amino acid 270 **(A)** 276 **(B)** was stably co-expressed with indicated EMRE proteins in MCU KO cells. WT EMRE does not contain any cysteines and served as a control. Mitochondria were isolated from cells and cysteine–cysteine cross-linking was induced using copper phenanthroline. MCU-FLAG was immunoprecipitated and the presence of an ~40 kD cross-linked EMRE–MCU band was detected under non-reducing conditions by Western blotting using EMRE antibody. Lysates were prepared in parallel under reducing conditions and were blotted to detect indicated proteins. ATP5A serves as loading control. Numbers indicate the locations of molecular weight standards. **(C)** EMRE–HsMCU cysteine cross-linking experiments show direct binding of MCU EDD residues E293 and D296 to EMRE K59 and K62. Cross-linking and sample processing were performed as in **(A)**. **(D)** Schematic showing MCU and EMRE amino acids that directly interact with each other in the membrane and in the matrix. EDD is shown in red. **(E)** Schematic showing HsMCU, HsMCU with *Caenorhabditis elegans* MCU EDD, Hs EMRE, and HsEMRE with *C. elegans* EMRE N-terminal domain. These constructs were used in **(F, G)**. **(F)** Mitochondrial Ca^{2+} uptake rates in control WT or EMRE KO cells stably expressing HsEMRECeNterm together with HsMCU or HsMCUCeEDD were measured and normalized to those of WT cells (n = 3–4). MCU forms a functional channel only if its EDD interacts with EMRE. **(G)** MCU–FLAG was immunoprecipitated from EMRE KO cells that stably express HsMCU or HsMCUCeEDD with HsEMRE or HsEMRECeNterm after DSP-mediated cross-linking. Immunoprecipitates and lysates were analyzed with Western blotting for the presence of indicated proteins. An interaction with MCU and EMRE was observed only if EDD and EMRE originated from the same species. **(H)** Model shows the proposed mechanism of EMRE function in the uniporter. In the absence of EMRE, Ca^{2+} ions cannot exit the channel because of blockage of the pore by EDD. Binding of EMRE leads to a conformational change in EDD and allows exit of Ca^{2+} ions into the matrix. Data information: in **(F)**, data are presented as mean ± SD.

Previous studies suggested that a small portion of N-terminal domain of EMRE is

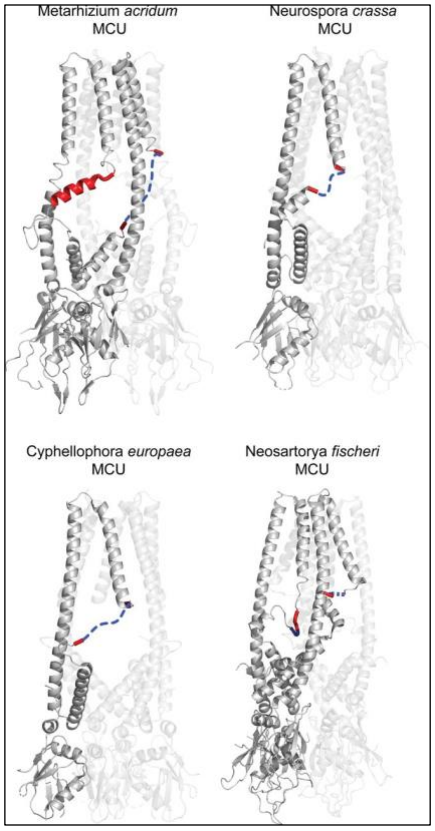

Figure S7. The region homologous to EMRE dependence domain (EDD) appears flexible in fungi.
High-resolution structures of mitochondrial calcium uniporter (MCU) tetramers from four different fungal species are shown. The region that is homologous to EDD or amino acids that surround the EDD in these structures are shown in red. Dotted blue lines show amino acids that are omitted in these structures, all of which overlap with EDD. In the *Metarhizium acridum* MCU structure, one MCU chain shows alpha helical EDD, whereas the same region in the neighboring chain is not structured. Protein Data Bank IDs of these structures are as follows: *M. acridum* (6C5W); *N. crassa* (5KUJ); *N. fischeri* (6D7W); *C. europaea* (6DNF).

dispensable for MCU–EMRE interaction (Tsai *et al.*, 2016). However, in contrast, our cross-linking data show that the N terminus of EMRE directly interacts with MCU. To determine the importance of this region for uniporter function and the stability of EMRE–MCU interaction, we generated chimeric proteins using HsMCU, HsEMRE, *Caenorhabditis elegans* MCU, and *C. elegans* EMRE (CeEMRE) as shown in **Fig 5E**. When expressed in MCU KO cells, *C. elegans* MCU and CeEMRE form a functional channel, but HsMCU and CeEMRE are not compatible (Tsai *et al.*, 2016). Sequence alignment of MCU and EMRE from human and *C. elegans* are shown in **Fig S8**. This system allowed us to test whether the EDD and N terminus of EMRE contribute to MCU–EMRE interaction and channel function by generating chimeric *C. elegans* and human proteins. HsEMRE with CeEMRE N terminal domain (HsEMRECeNterm) did not bind to HsMCU. When HsEMRECeNterm was expressed with HsMCU with CeEDD (HsMCUCeEDD), the two proteins interacted and supported mitochondrial Ca^{2+} uptake (**Fig 5F** and **G**). We conclude that EDD and EMRE N-terminus interactions are necessary to form a stable association between MCU and EMRE and to form a functional pore.

Figure S8. Alignment of human and *Caenorhabditis elegans* mitochondrial calcium uniporter (MCU) TM1, TM2, and EMRE dependence domain, and EMRE N-terminal domain.
Alignments of MCU or EMRE from human and *C. elegans* were done using CLUSTALW, and amino acids were color coded using BoxShade. Black boxes show identical amino acids and gray boxes show similar amino acids. Purple box indicates EMRE dependence domain. Arrowheads indicate *Homo sapiens* MCU and HsEMRE amino acids that cross-link.

Based on our functional and interaction data, we propose a mechanism of EMRE regulation of the mitochondrial Ca^{2+} channel that is consistent with high-resolution MCU-EMRE structure (Wang *et al.*, 2019) and previous functional studies (Sancak *et al.*, 2013): when MCU is expressed in the absence of EMRE, there is no calcium transport, likely because the EDD is flexible and prevents Ca^{2+} exit from the pore. Co-expression of MCU and EMRE are necessary and sufficient for calcium transport (Kovacs-Bogdan *et al.*, 2014), likely because EMRE binds to the transmembrane domains and EDD of MCU, changes the EDD conformation, permitting exit of Ca^{2+} ions (**Fig 5H**).

DISCUSSION

Perturbation of uniporter function is associated with a number of cellular and systemic defects, ranging from altered cell cycle progression and mitochondrial dynamics to skeletal muscle myopathy and neurodegenerative disease (Kamer & Mootha, 2015; Chakraborty *et al.*, 2017; Musa *et al.*, 2019). EMRE has emerged as a core component of the animal mitochondrial Ca^{2+} uniporters whose expression is under transcriptional and posttranslational control (Konig *et al.*, 2016; Munch & Harper, 2016; Tsai *et al.*, 2017). For example, accumulation of EMRE protein in the absence of mitochondrial AAA-

proteases AFG3L2 and SPG7, whose mutations are associated with spinocerebellar ataxia and hereditary spastic paraplegia, is responsible for mitochondrial Ca^{2+} overload and may contribute to neuronal loss (Konig *et al.*, 2016). In addition, in a mouse model of neuromuscular disease caused by MICU1 deficiency, decreased EMRE expression over time correlated with improved health (Liu *et al.*, 2016). These observations highlight the importance of EMRE in physiology and disease.

Here, we exploited evolutionary divergence of mitochondrial Ca^{2+} uniporter composition to understand the function of EMRE, which is required for the human uniporter but not found in most fungi or other taxa. Functional experiments using chimeric proteins that consist of human HsMCU (which is EMRE dependent) and Dictyostelium DdMCU (which operates independent of EMRE) revealed the presence of a region in MCU that we named EDD. We also show that EMRE makes direct contacts with the two TM domains of MCU as well as with EDD. Interestingly, the region that corresponds to EDD appears flexible in previously published high-resolution structures of fungal MCU homologs (Baradaran *et al.*, 2018; Fan *et al*, 2018; Nguyen *et al.*, 2018) and partially overlaps with the juxtamembrane loop identified to be important to stabilize channel opening in structural studies (Wang *et al.*, 2019). In species that do not have EMRE, it is plausible that lipids or other currently unknown proteins may fulfill the same function. It is notable that fungal MCU homologs appear to have extremely low conductance, as initially documented by Lehninger and colleagues (Carafoli & Lehninger, 1971) and later by others (Goncalves *et al.*, 2015; Fan *et al*, 2018; Nguyen *et al.*, 2018; Wettmarshausen *et al.*, 2018; Pittis *et al.*, 2020 Preprint). In contrast, we have shown that the uniporter of

animals and those from Dictyostelium exhibit extremely high conductance (Kovacs-Bogdan *et al.*, 2014).

In our experimental system, the measured activity of a chimeric protein is a function of its expression, channel properties, and its effect on mitochondrial membrane potential and mitochondrial health. We did not observe perturbed membrane potential in cells that express chimeras. However, it is possible that some chimeras exhibit reduced mitochondrial uptake compared with HsMCU or DdMCU because their stable expression causes mitochondrial Ca^{2+} overload or alters mitochondrial Ca^{2+} storage capacity or Ca^{2+} extrusion from the mitochondria. Despite having variable expression levels of HsMCU, DdMCU, and chimeras, expression of a particular chimera was comparable in MCU KO and EMRE KO cells, with the exception of chimera 4. This enables us to determine EMRE dependence of a chimera by comparing Ca^{2+} uptake rates in MCU KO and EMRE KO cells, independent of how its expression compares with that of HsMCU.

Our data show that EMRE directly interacts with MCU in TM1, TM2, and EDD. Importantly, comparison of chimera 7 and chimera 9 immunoprecipitation data (**Fig 4A**) suggests that the region defined by chimera 10 might also be important for EMRE–MCU binding. However, chimera 10 was not functional, and we did not pursue this chimera for protein–protein interaction experiments because of the possibility that it is not folded properly. In addition, although EDD is the smallest region that we tested that enabled EMRE-independent Ca^{2+} uptake, it is evident in our data that the presence of EMRE can increase Ca^{2+} uptake rates by chimera 9. Thus, we note that the data presented here are consistent with additional, extended interactions between EMRE and MCU in the matrix.

Notably, our functional data and model for the role of EMRE in Ca^{2+} conductance appear to be generally in good agreement with a high-resolution structure of MCU–EMRE that was contemporary with the preprint version of this article (Wang *et al.*, 2019). Wang *et al.* (2019) also conclude that EMRE enables Ca^{2+} conductance by modulating the conformation of MCU distal to the Ca^{2+} pore. Both studies have also converged on an overlapping region of MCU that confers EMRE dependence: Wang *et al.* (2019) spotlighted a six-amino acid–long region (aa 285–aa 291) in HsMCU, whereas we defined EDD as MCU aa 288–aa 297 using evolutionary divergence and systematic domain swapping. Future studies will determine whether addition of aa 285–aa 287 to EDD will augment its activity. In addition, both our experimental data and those published by Wang *et al.* (2019) show that EMRE interacts with MCU TM1 and TM2. However, our data show robust cross-linking between TM2 and EMRE amino acids that appear farther apart than cross-linking distance in the structure. At present, we cannot reconcile this experimental finding with the structure. Although the cross-linking could be spurious, our results are robust and raise the possibility that there may be additional conformational states of the complex that are not reflected in the structure, or cysteine cross-linking may be capturing dynamics that occur in the complex's native environment (Bass *et al.*, 2007).

What is the evolutionary significance of EMRE? Curiously, based on functional data, Dictyostelium and fungal MCU appear to be able to adopt an open conformation when expressed (Kovacs-Bogdan *et al.*, 2014; Baradaran *et al.*, 2018; Fan *et al.*, 2018; Nguyen *et al.*, 2018; Yoo *et al.*, 2018), whereas human MCU when expressed on its own adopts a closed conformation. Dictyostelium MCU displays a much higher rate of calcium uptake than those from fungi and comparable with human MCU and EMRE (Kovacs-

Bogdan *et al.*, 2014). The current work suggests that the EDD of MCU is responsible for maintaining the closed state, but in a manner that is dependent on EMRE. Given that MICU1/2 interacts with EMRE, it is conceivable that EMRE mediates acute allosteric control at the exit site. Over longer time scales, the expression level of EMRE has emerged as an important determinant of uniporter activity (Konig *et al.*, 2016; Tsai *et al.*, 2017) with relevance to human disease. Collectively, these findings suggest that this evolutionary innovation may have emerged to confer an added layer of acute or chronic regulation to the uniporter. Future structural and functional studies will be required to fully decipher the mechanisms by which the uniporter is regulated across different eukaryotes.

METHODS AND MATERIALS

Cell culture

- DMEM; Thermo Fisher Scientific, Cat. no. 11-965-118
- FBS; Life Technologies, Cat. no. 26140087
- GlutaMAX; Thermo Fisher Scientific, Cat. no. 35-050-061
- Trypsin; Gibco, Cat. no. 12605-010
- PBS; Thermo Fisher Scientific, Cat. no. 20012050
- Penicillin/streptomycin solution; VWR Cat. no. 45000-652
- Genlantis MycoScope PCR Detection Kit; VWR Cat. no. 10497-508

HEK293T cells were acquired from the Sabatini Lab at the Whitehead Institute for Biomedical Research. They were grown in DMEM medium supplemented with 1× GlutaMAX and 10% FBS. The cells were tested for mycoplasma every 3 mo using the Genlantis MycoScope PCR Detection Kit and were confirmed to be free of mycoplasma contamination. The identity of the HEK293T cells was confirmed using short tandem

repeat analysis. The HEK293T cell line has the following short tandem repeat profile: TH01 (7, 9.3); D21S11 (28, 29, 30.2); D5S818 (7, 8, 9); D13S317 (11, 12, 13, 14, 15); D7S820 (11); D16S539 (9, 13); CSF1PO (11, 12, 13); Amelogenin (X); vWA (16, 18, 19, 20); TPOX (11). This profile matches 100% to HEK293T cell line profile (CRL-3216; ATCC) if the Alternative Master's algorithm is used, and 83% if the Tanabe algorithm is used.

Gel electrophoresis and Western blotting Antibodies and dilution used for experiments

- MCU antibody; Sigma-Aldrich, Cat. no. HPA016480-100UL (1:2,000)
- DYKDDDDK Tag Rabbit antibody; Cell Signaling Technology, Cat. no. 14793S (1:3,000)
- EMRE antibody; Bethyl Laboratories, Cat. no. A300-BL19208 (1:1,000)
- ATP5A antibody; Abcam Biochemicals, Cat. no. ab14748 (1:5,000)
- TOM20 antibody; Cell Signaling Technology, Cat. no. 42406S (1:5,000)
- HRP-linked antirabbit secondary antibody; Cell Signaling Technology Cat. no. 7074S (1:10,000)
- HRP-linked anti-mouse secondary antibody; Cell Signaling Technology Cat. no. 7076S (1:10,000)

Gel electrophoresis

- 10× Tris/Glycine Buffer; Boston BioProducts Cat. no. BP-150-4L
- Novex WedgeWell 16% Tris-Glycine Gel; Invitrogen Cat. no. XP00165BOX
- Novex 12% Tris-Glycine Mini Gels, WedgeWell format, 15-well; Thermo Fisher Scientific Cat. no. XP00125BOX

Western blotting

- 10× TBST-Standard (10× w/1% Tween-20, pH 7.4); Boston Bio- Products Cat. no. IBB-580-4L
- Ethanol, 200 proof (100%); Thermo Fisher Scientific Cat. no. 04- 355-450
- Trans-Blot Turbo 5× Transfer Buffer; Bio-Rad Cat. no. 10026938
- Powdered fat-free milk; Kroger brand, Cat. no. G500A554
- Trans-Blot Turbo RTA Mini PVDF Transfer Kit; Bio-Rad Cat. no. 1704272
- Transfer apparatus for SDS–PAGE; Bio-Rad Trans-Blot Turbo Transfer System

For MCU-FLAG and ATP5A; Bio-Rad Mixed Molecular Weight Protein Transfer setting (7 min, 1.3 A, 25 V)

For TOM20; Bio-Rad Low Molecular Weight Protein Transfer setting (5 min, 1.3 A, 25 V)

- Blot imager: iBrightCL1000
- Automated Western Blot Development Processor: Precision Bio- systems BlotCycler, Model W5 100-12VAC; S/N 394387
- Clarity Max Western ECL Substrate; Bio-Rad Cat. no. 1705062
- Clarity Western ECL Substrate; Bio-Rad Cat. no. 170-5060

After transfer, the membranes were briefly washed with TBST and incubated with 5% milk in TBST (wt/vol) for 30 min. They were then incubated overnight with primary antibodies diluted in 5% milk in TBST (wt/vol). Afterward, all membranes were washed with TBST three times, 5 min each, and incubated for 1 h with secondary antibody diluted in 5% milk in TBST at room temperature. The membranes were then washed four times, 5 min each, using a Precision Biosystems BlotCycler. Membranes were developed using Bio-Rad ECL substrate.

Transfer and PFA cross-linking of EMRE blots

- Transfer apparatus for SDS–PAGE; Bio-Rad Trans-Blot Turbo Transfer System

A custom 3-min transfer protocol with constant 1.3 A and 25 V was used for EMRE Western blotting

- 16% Paraformaldehyde aqueous solution; EMS/Thermo Fisher Scientific Cat. no. 50-980-487
- PBS; Thermo Fisher Scientific, Cat. no. 20012050

Protocol and reagents adapted from (Suzuki *et al.*, 2008). Immediately after transfer of proteins from the electrophoresis gel to a 0.22-μm polyvinylidene difluoride (PVDF) membrane, membranes that were to be immunoblotted for EMRE were soaked in a solution of 0.4% PFA in PBS for 30 min without agitation. The membranes were then blocked and immunoblotted normally, as described above.

Cell lysis, sample preparation, and immunoprecipitation

- Bradford Dye Reagent; Bio-Rad, Cat. no. 5000205
- Spectrophotometer; Spectronic Instruments, Genesys 5
- Protease inhibitors; Sigma-Aldrich, Cat. no. 5892953001
- Lysis buffer reagents:
- HEPES–KOH

    HEPES; Sigma-Aldrich Cat. no. H3375-1KG

    KOH; Sigma Millipore Cat. no. 1050121000

- NaCl; Sigma-Aldrich Cat. no. 746398-5KG
- EDTA; Sigma-Aldrich, Cat. no. 607-429-00-8
- Triton X-100; Sigma-Aldrich, Cat. no. X100-1L
- DDM; Sigma-Aldrich, Cat. no. D4641-5G

Reducing sample buffer, pH 6.8:

- SDS; Sigma-Aldrich Cat. no. L4509-1KG
- BME/2-mercaptoethanol; Sigma-Aldrich Cat. no. M3148-25ML Glycerol; Sigma-Aldrich Cat. no. G5516-1L
- Tris–HCl:

  Trizma base; Sigma-Aldrich Cat. no. RDD008
- Bromophenol Blue; VWR Cat. no. 97061-690

Non-reducing sample buffer, pH 6.8: same as “reducing sample buffer,” but without BME. For standard lysis, cell plates were placed on ice and washed with cold PBS, which was then aspirated. Cells were harvested in lysis buffer supplemented with 1% Triton X-100 (with 0.2% DDM if lysates were also used for immunoprecipitation) and proteases inhibitors; the volume of lysis buffer used varied based on downstream uses. Cells were triturated in tubes and then centrifuged at 17,000g for 10 min. Cell supernatant was quantified using a Bradford protein assay and a spectrophotometer. Sample preparation varied based on downstream applications.

Membrane potential measurements

- Digitonin; Thermo Fisher Scientific, Cat. no. BN2006
- L-Glutamic acid; Sigma-Aldrich Cat. no. G1251-1KG
- L-(-)-Malic Acid; Sigma-Aldrich Cat. no. M7397-25G
- KCl buffer: KCl; Sigma-Aldrich, Cat. no. 793590-1KG; K2HPO4; Sigma-Aldrich, Cat. no. P3786-1KG

MgCl2; Sigma-Aldrich, Cat. no. M8266-1KG (not MgCl2 hexahydrate?) HEPES; Sigma-Aldrich, Cat. no. H3375-1KG

- EGTA; Sigma-Aldrich Cat. no. E3889
- Carbonyl cyanide 3-chlorophenylhydrazone; Sigma-Aldrich Cat. no. C2759-250MG
- TMRM reagent; Thermo Fisher Scientific Cat. no. I34361
- Black 96-well plates; Greiner Bio-One Cat. no. 655076

Protocol and reagents adapted from Kovacs-Bogdan *et al.* (2014). Tetramethyl rhodamine methyl ester (TMRM) was used to assess the membrane potential of permeabilized cells. 1 million HEK293T cells were spun down at 800g for 3 min in 1.5 ml microcentrifuge tubes, washed with 1 ml of PBS, and spun down again for 1 min at 800g. PBS was aspirated and cells were permeabilized in 150 µl KCl buffer (125 mM KCl, 2 mM K2HPO4, 1 mM MgCl2, and 20 mM HEPES at pH 7.2, 0.005% digitonin) that was supplemented with 500 nM TMRM and 5 mM glutamate/malate from a 500 mM G/M stock solution that was filtered and stored at −20°C. Cell suspension was transferred to a black-bottom 96-well plate. Two readings of each sample were taken using a BioTek Synergy H1 microplate reader at room temperature. For each, a 540-nm excitation and 590-nm emission were recorded. The first reading was taken after cells' suspension in permeabilization buffer, to establish a baseline. Membrane potential was dissipated with the addition of 1 µM CCCP, and a second reading was taken after a 3-min incubation period. Each cell line was tested three times on the same day, for a total of six readings: three readings before the addition of CCCP (first readings), and three readings after the addition of CCCP (second readings). For the purposes of data analysis, the mean of the three "first" readings was calculated, as was the mean of the three "second" readings for each cell line. The error bars report the SD of these readings.

Cloning

cDNA encoding for the chimeric proteins were generated by gene synthesis, cloned into pLYS1 (#19319; Addgene), or pLYS5 (#50054; Addgene) plasmids using NheI/EcoRI restriction sites.

MCU without any cysteines was generated by gene synthesis, and cysteine coding nucleotides at the desired locations were introduced by mutagenesis.

The sequences of all genes used in this study were verified by sequencing using CMV forward primer and custom designed re- verse primer (TCTCGCACATTCTTCACGTC).

HEK293T EMRE knockout cell line production

- eSpCas9(1.1) plasmid; Addgene plasmid #71814
- QIAquick PCR Purification Kit; QIAGEN, Cat. no. 28106
- dNTP set, PCR grade; QIAGEN, Cat. no. 201913
- QIAprep Spin Miniprep Kit; QIAGEN, Cat. no. 27106
- Q5 High Fidality DNA polymerase; QIAGEN Cat. no. M0491S
- HsEMRE gRNA: GCCGGAGCCTGGTACCGTCG

MCU KO cell line was described before (Sancak *et al.*, 2013). EMRE gRNA was cloned into a gRNA expression plasmid. 600,000 cells growing on six-well plates were transfected with 250 ng of gRNA expression plasmid and 1 µg of eSpCas9(1.1) plasmid. 2 d later, cells were diluted at 1 cell/well and plated on 96-well plates to obtain single cell clones. EMRE KO cell clones were verified by Western blotting, functional assays, and by sequencing.

Lentivirus production and infection

- X-treme(GENE) 9 DNA Transfection Reagent; Sigma-Aldrich, Cat. no. 6365779001
- psPax2; Addgene Cat. no. 12260
- VSV-G; Addgene, Cat. no. 8454
- Puromycin dihydrochloride; VWR, Cat. no. 62111-170
- Hygromycin B Solution; VWR, Cat. no. 45000-806
- Hexadimethrine bromide/polybrene; Sigma-Aldrich Cat. no. H9268-10G
- DMEM; Thermo Fisher Scientific, Cat. no. 11-965-118
- Filter; VWR, Cat. no. 28145-505
- Syringe; VWR, Cat. no. 28200-042

Lentivirus production: 1 million HEK293T cells were plated in 6-cm plates in 5 ml of media. 1 d later, the cells were transfected with viral mix. To prepare the viral mix, 100 ng VSV-G, 900 ng psPax2, 1 µg viral plasmid, dH2O to 10 µl, and 150 µl DMEM mixed with 6 µl X-treme(GENE) and incubated for 30 min at room temperature before being added to the cells and mixed. 2 d later, the medium—which now contained the virus of interest—was filtered through a 0.45 µm sterile filter attached to a syringe. The virus was stored at −80°C until use.

Lentivirus infection: 250K HEK293T cells were plated in a six-well dish containing 2 ml media. The following day, 200 µl of the virus-containing media and 2 µl of polybrene from an 8-mg/ml stock solution was added to a final concentration of 8 µg/ml. Polybrene stock solution was prepared in water, filter sterilized and stored at −20°C for long term storage and at 4°C for short term storage. 2 d later, the cells were split and transferred to 10 cm tissue culture plates and selected. Chimera cell lines were selected using 1 µg/ml

puromycin from a 1 mg/ml puromycin stock solution that was prepared in water, filter-sterilized, and stored at −20°C for long-term storage and at 4°C for short-term storage. Copper-mediated cysteine cross-linking cell lines infected with cysteine point mutations in MCU were se- lected using 100 µg/ml from a 50 mg/ml hygromycin stock solution that was prepared in water, filter sterilized, and stored at 4°C.

Transient transfection of functional chimeras and EMRE

- X-treme(GENE) 9 DNA Transfection Reagent; Sigma-Aldrich, Cat. no. 6365779001
- DMEM; Thermo Fisher Scientific, Cat. no. 11-965-118

Two million cells of each functional chimera were plated in seven 10-cm plates. The next day, the cells were transiently transfected with functional chimeras and wild-type EMRE. To prepare the transient transfection mix, 1 µg chimera plasmid, 2 µg EMRE plasmid, dH2O to 10 µl, and 150 µl DMEM mixed with 6 µl X-treme(GENE) and incubated for 30 min at room temperature before being added to the cells and mixed. 2 d after transient transfection, the cells were DSP cross-linked as described below and lysed as described above. A small fraction of the lysate was used to prepare samples at 1 µg/µl of protein concentration in reducing sample buffer for Western blot analysis of lysates. Lysate was then immunoprecipitated as described below. After immunoprecipitation, all samples were prepared in reducing conditions, electrophoresed, and Western blotted normally.

Calcium uptake in permeabilized HEK-293T cells

- Digitonin; Thermo Fisher Scientific, Cat. no. BN2006
- Oregon Green 488 Bapta-6F; Invitrogen, Cat. no. O23990
- L-Glutamic acid; Sigma-Aldrich Cat. no. G1251-1KG

- L-(-)-Malic Acid; Sigma-Aldrich Cat. no. M7397-25G
- KCl buffer:

    KCl; Sigma-Aldrich, Cat. no. 793590-1KG

    K2HPO4 Sigma-Aldrich, Cat. no. P3786-1KG

    MgCl2 Sigma-Aldrich, Cat. no. M8266-1KG

    HEPES Sigma-Aldrich, Cat. no. H3375-1KG
- EGTA; Sigma-Aldrich Cat. no. E3889

Protocol and reagents adapted from Sancak *et al.* (2013). HEK- 293T cells grown in 10-cm tissue culture plates were trypsinized and resuspended in 10 ml of prepared media. 1 million HEK-293T cells transferred to microcentrifuge tubes and spun down for 3 min at 800g at room temperature to pellet cells. Cells were washed with PBS once and resuspended in KCl buffer (125 mM KCl, 2 mM K2HPO4, 1 mM MgCl2, 20 mM HEPES, pH 7.2), supplemented with 5 mM glutamate/malate from a 500 mM G/M stock solution that was filtered and stored at −20°C, 0.005% digitonin, and 1 µM Oregon Green Bapta 6F.

For **Fig 1**, fluorescence was monitored every 0.2 s at room temperature using a Perkin-Elmer Envision plate reader before and after injection of 50 µM CaCl2 using FITC filter sets (485 excitation and 535 emission). Calcium uptake rates were calculated using the linear fit of uptake curves between 20 and 30 s.

For all other figures, fluorescence was monitored for 78 s every 2 s at room temperature (~25°C) using a BioTek Synergy H1 microplate reader before and after injection of 50 µM CaCl2 from a 500-µM stock prepared in dH2O. Fluorescence was recorded using a fluorescent green filter set to 485/20 excitation, 528/20 emission. Calcium uptake rates

were calculated using the linear fit of uptake curves between 20 and 30 s after calcium injection. A maximum of eight samples were assayed together, including one wild- type HEK293T control per assay run. To calculate calcium uptake rates relative to wild type, the wild-type rate for each sample set was set at 100%. Calculating Experimental calcium uptake rate yielded the relative calcium uptake rate. For each figure, each proportional experimental calcium uptake rate is plotted relative to its corresponding wild type calcium uptake rate.

Crude mitochondria preparation

- 27.5-gauge needle; VWR, Cat. no. BD305109
- 1 mL syringe; BD Biosciences, Cat. no. 309659
- PBS; Thermo Fisher Scientific, Cat. no. 20012050

Cells were grown to confluency in 10-cm tissue culture plates. Cell culture medium was aspirated, and the culture plates were rinsed with 4°C PBS. PBS was aspirated and cells were harvested in fresh PBS. The cells were passed in and out of a 1-ml syringe through a 27.5-gauge needle 12 times. The disrupted mixture was then spun at 800g for 5 min, 4°C, to pellet nuclei and intact cells. The supernatant was then spun at 8,000g for 5 min, 4°C, to pellet mitochondria. The resulting supernatant was then aspirated. The pellet was used for downstream applications.

Immunoprecipitation

- Anti-FLAG M2 Affinity Gel, Sigma-Aldrich Cat. no. A2220-5ML Cells were grown to confluence in 10-cm tissue culture plates.

Cell culture media was aspirated, and the culture plates were rinsed with 4°C PBS. PBS was aspirated and cells were harvested and lysed on ice in 700-ml lysis buffer

(supplemented with 1% Triton and protease inhibitors). Cells were spun for 10 min at 4°C, maximum speed. The protein concentration was determined using a Bradford assay. A small fraction of the lysate was used to prepare samples at 1 µg/µl of protein concentration in reducing sample buffer for Western blot analysis of lysates. Between 1 and 3 mg of protein was used for IP experiments. Lysates were incubated with 10 µl of anti-FLAG M2 affinity gel beads (from the gel's 1:1 bead:glycerol slurry). Beads were washed three times beforehand with 1 ml 1% Triton lysis buffer. Volumes of all IP samples were standardized. IP samples were rocked on a nutator for 2–4 h at 4°C. Following aspiration of unbound lysate, samples were washed with 1 ml 1% Triton lysis buffer three times before mixing with sample buffer (reducing or non-reducing, depending on application) and boiled for 5 min at 95°C.

DSP cross-linking

- DSP; Thermo Fisher Scientific, Cat. no. 22585
- DMSO; Sigma-Aldrich, Cat. no. D8418-500ML
- Trizma base; Sigma-Aldrich Cat. no. RDD008

DSP was dissolved in DMSO to a final concentration of 250 mg/ml to make a 250× stock solution for the in-cell cross-linking assay. 40 µl of DSP solution was then added to confluent cells growing in 10 cm plates in 10 ml media. After swirling DSP to mix it into the media, cells were incubated at room temperature for 3 min. The reaction was quenched by adding 1 ml 1M Tris, pH 8.0, to the plates and swirling again. The medium was aspirated, plates were washed with 4°C PBS, and cells were lysed using 1% Triton lysis buffer (50 mM HEPES KOH, pH 7.4, 150 mM NaCl, 5 mM EDTA, and 1% Triton). MCU was immunoprecipitated as described above.

Copper-mediated cysteine cross-linking

- Anti-FLAG M2 Affinity Gel; Sigma-Aldrich Cat. no. A2220-5ML
- Phenanthroline; Sigma-Aldrich, Cat. no. 131377-5G
- CuSO4; Sigma-Aldrich, Cat. no. 6365779001
- EDTA; Sigma-Aldrich, Cat. no. 607-429-00-8

Cu(II)-(1,10-phenanthroline)3 was prepared in PBS by combining 100 µM CuSO4 + 300 µM phenanthroline (8 ml PBS + 0.8 µl 1M CuSO4 + 80 µl 30 mM phenanthroline). Crude mitochondria were resuspended in 250 µl copper phenanthroline solution and incubated for 20 min at room temperature. The cross-linking reaction was stopped by the addition of 10 mM EDTA from a 500 mM stock prepared in dH2O, pH 8. Mitochondria were spun and pelleted at 8,000g for 5 min, and supernatant was as- pirated with a needle and discarded. Mitochondria were then lysed with 200 µl 4°C lysis buffer (50 mM HEPES KOH, pH 7.4, 150 mM NaCl, 5 mM EDTA, and 1% Triton, protease inhibitors). A small fraction of the lysate was used to prepare samples at 1 µg/µl protein concentration in reducing sample buffer for Western blot analysis of lysates. 150–200 µg lysate protein was affinity-purified as described above under “Immu- noprecipitation.” After immunoprecipitation and washing, the beads were boiled with 20 µl non-reducing 2.5× sample buffer. 18 µl of the resulting samples were electrophoresed under non-reducing conditions and Western blotted to detect EMRE; 2 µl of each sample was separated, mixed with 18 µl 2.5× sample buffer, electrophoresed under non- reducing conditions, and Western blotted to detect MCU-FLAG.

Mitoplast preparation and PEG5K-Maleimide conjugation

- PEG5K-maleimide; Sigma-Aldrich, Cat. no. 363187, 10 mM stock solution was prepared in DMSO

Crude mitochondria were prepared in PBS from one confluent 15- cm plate of cells using a 27.5-g needle as described. To prepare mitoplasts, 450 µg of crude mitochondrial prep was resuspended in 375 µl of cold dH2O and incubated on ice for 10 min to swell. After 10 min, 125 µl of 4× respiration buffer was added (4× respiration buffer: 548 mM KCl, 40 mM HEPES, pH 7.2, 10 mM MgCl2), and the tubes were vortexed briefly. The samples were spun down for 3 min at 4°C at 800g, resuspended in 1× respiration buffer to 3 µg/µl. 10 µl of this mitoplast preparation was incubated with 1 mM PEG5K-maleimide dissolved in DMSO in 30 µl final volume for 30 min at RT in 1× respiration buffer, in the absence or presence of 1 µl of 10% Triton X-100 dissolved in dH2O. Reaction was stopped by addition of 6 µl of 5× SDS sample buffer. The lysates were subjected to SDS–PAGE and Western blotting.

PK treatment of crude mitochondrial preparations

- PK; Sigma-Aldrich, Cat. no. P2308, prepared in IBc buffer as a 1,000× stock solution
- PMSF; Sigma-Aldrich, Cat. no. P7626, prepared in ethanol as a 100× stock solution.

20 µg of crude mitochondria isolated from cultured cells as de- scribed were treated with 100 µg/ml of PK in the presence of increasing concentrations of digitonin in 30 ml of final volume in IBc buffer for 15 min at room temperature, 7 mM of PMSF was added inactivate PK for 5 min. 5 ml of 5× SDS sample buffer was added, samples were boiled, and 5–10 µl was loaded on a Tris–glycine gel for Western blotting.

BN-PAGE

- Running Buffers; Invitrogen NativePAGE Novex Bis-Tris Gel Sys- tem, Cat. no. BN1001BOX, BN1002BOX, and BN1004BOX
- Protein Standard; Invitrogen NativeMARK Unstained Protein Standard, Cat. no. LC0725
- 3–12% Bis-Tris Gel; NativePAGE 3–12% Bis-Tris Gel, Cat. no. BN1003BOX

Protocol and reagents were adapted from Sancak *et al.* (2013). Gel electrophoresis running buffers were prepared according to the manufacturer's protocol for the Invitrogen NativePAGE Novex Bis-Tris Gel System. Running buffers were cooled to 4°C before use, and electrophoresis was performed at 4°C. Invitrogen NativeMark Un- stained Protein Standard was used to estimate molecular weight. Gels were run at 40 V for 30 min. Voltage was then increased to 100 V for 1 h, and subsequently to 250 V for 90 min. When the dye front had traveled through ~1/3 of the gel, electrophoresis was paused, and the Dark Blue Cathode Buffer was replaced with Light Blue Cathode Buffer, as per the manufacturer's protocol.

Blue native PAGE transfer

- Transfer apparatus; Bio-Rad Trans-Blot SD cell
- Blotting paper; Bio-Rad extra thick blot paper, Cat. no. 1703965
- Acetic acid; Thermo Fisher Scientific, Cat. no. A38C-212
- Ethanol: 200 proof (100%); Thermo Fisher Scientific Cat. no. 04- 355-450

Protocol and reagents adapted from Sancak *et al.* (2013). After electrophoresis was complete, the gels were transferred to Bio-Rad Mini-size 0.22 μm PVDF membranes in Invitrogen Novex Tris–glycine transfer buffer at 0.18 A for 20 min, using a Bio-Rad

TransBlot SD Semi-Dry Transfer Cell and extra thick blotting paper. Membranes were incubated in 8% acetic acid while shaking for 15 min to fix the proteins. The membranes were rinsed with dH2O for 5 min, and then air-dried. Once dry, the membranes were rehydrated with ethanol. The membranes were then blocked with 5% milk in TBST (wt/vol) and immunoblotted using FLAG antibody as described above. Finally, the same membranes were probed for ATP5A (a mouse antibody) as described above, as a loading control.

DATA REPORTING AND STATISTICAL ANALYSIS

No statistical methods were used to predetermine sample size. The experiments were not randomized. The investigators were not blinded to allocation during experiments and outcome assessment. All quantitative experiments are presented as means ± SD of at least three independent biological experiments (as indicated).

ADDITIONAL SUPPLEMENTARY MATERIALS

Supplemental Data 1

- *H. sapiens* DNA and amino acid sequences are in UPPERCASE characters.
- *D. discoideum* or *C. elegans* DNA and amino acid sequences are **in lowercase, bold characters**.
- For MCU chimeras, chimera breakpoints are highlighted in red.
- For each construct, both DNA sequence and amino acid sequence are shown
- FLAG tag sequence is highlighted in green.
- 3X GGS linker sequence between MCU and FLAG tag is highlighted in blue.

HsMCU:

ATGGCGGCCGCCGCAGGTAGATCGCTCCTGCTGCTCCTCTCCTCTCGGGGCGGC

GGCGGCGGGGGCGCCGGCGGCTGCGGGGCGCTGACTGCCGGCTGCTTCCCTGG

GCTGGGCGTCAGCCGCCACCGGCAGCAGCAGCACCACCGGACGGTACACCAGA

GGATCGCTTCCTGGCAGAATTTGGGAGCTGTTTATTGCAGCACTGTTGTGCCCTCT

GATGATGTTACAGTGGTTTATCAAAATGGGTTACCTGTGATATCTGTGAGGCTACC

ATCCCGGCGTGAACGCTGTCAGTTCACACTCAAGCCTATCTCTGACTCTGTTGGTG

TATTTTTACGACAACTGCAAGAAGAGGATCGGGGAATTGACAGAGTTGCTATCTAT

TCACCAGATGGTGTTCGCGTTGCTGCTTCAACAGGAATAGACCTCCTCCTCCTTGA

TGACTTTAAGCTGGTCATTAATGACTTAACATACCACGTACGACCACCAAAAAGAG

ACCTCTTAAGTCATGAAAATGCAGCAACGCTGAATGATGTAAAGACATTGGTCCAG

CAACTATACACCACACTGTGCATTGAGCAGCACCAGTTAAACAAGGAAAGGGAGCT

TATTGAAAGACTAGAGGATCTCAAAGAGCAGCTGGCTCCCCTGGAAAAGGTACGA

ATTGAGATTAGCAGAAAAGCTGAGAAGAGGACCACTTTGGTGCTATGGGGTGGCC

TTGCCTACATGGCCACACAGTTTGGCATTTTGGCCCGGCTTACCTGGTGGGAATAT

TCCTGGGACATCATGGAGCCAGTAACATACTTCATCACTTATGGAAGTGCCATGGC

AATGTATGCATATTTTGTAATGACACGCCAGGAATATGTTTATCCAGAAGCCAGAGA

CAGACAATACTTACTATTTTTCCATAAAGGAGCCAAAAAGTCACGTTTTGACCTAGA

GAAATACAATCAACTCAAGGATGCAATTGCTCAGGCAGAAATGGACCTTAAGAGAC

TGAGAGACCCATTACAAGTACATCTGCCTCTCCGACAAATTGGTGAAAAAGATTCT

AGAGGTGGATCTGGTGGATCTGGTGGATCTATGGATTACAAGGATGACGATGACA

AG*

MAAAAGRSLLLLLSSRGGGGGGAGGCGALTAGCFPGLGVSRHRQQQHHRTVHQRIA
SWQNLGAVYCSTVVPSDDVTVVYQNGLPVISVRLPSRRERCQFTLKPISDSVGVFLRQ
LQEEDRGIDRVAIYSPDGVRVAASTGIDLLLLDDFKLVINDLTYHVRPPKRDLLSHENAA
TLNDVKTLVQQLYTTLCIEQHQLNKERELIERLEDLKEQLAPLEKVRIEISRKAEKRTTLV
LWGGLAYMATQFGILARLTWWEYSWDIMEPVTYFITYGSAMAMYAYFVMTRQEYVYP
EARDRQYLLFFHKGAKKSRFDLEKYNQLKDAIAQAEMDLKRLRDPLQVHLPLRQIGEK
DSRGGSGGSGGSMDYKDDDDK*

DdMCU:

atgaatagcttcgtgatcaggaacggcttcggcctcgtcaggaccttcaacaccaggctgtttaccacctccacc
cagaacctggagggcgagctcaaaaccatcctcggccaggccaaggtcagcaagctgcaggaaaagctga
agctggatcccaggtccaagatcaccttcaacgacttcaagggcatcgccaaggaggtgggcatcgaggaga
aggaaatcaacagcgtcagcaacgccctggctcaatccggctccatcatctacctgcctaactccctgaacga
gaacctgaagacctccgtgttcaccaagcccgcccatatctaccagtccctcgaacacatcctggacatcgaga
acaagggcgtgggcctgaataagctgatcgagtccaagaaatccgagatcaatagcctgaggcagaagatcc
agcccctggaggagaagaagcaggtgatcgacagaaaggcccacaggagggccaccgctatcatctggac
cggactcggctattgcttcgcccaggccgccattctggctaggctcacctggtgggacctctcctgggacatcat
cgagcccgtgagctacttcctgaccttcggctccgtcctgatcggctacacctacttcaccatgaccaagaccga
gttcacctacgaggctctcaaccataggctgttcagcaagaggcaggacaagctgttcaaaagaaacaacttcc
ctaaggaggactacgagaacctcgtgcaggccatcgacaagaaggagaaggagctcaaggagctcgagctc
gccacaaagtacgatcacacccaccccgggGGTGGATCTGGTGGATCTGGTGGATCTATGG
ATTACAAGGATGACGATGACAAG*****

mnsfvirngfglvrtfntrlfttstqnlegelktilgqakvsklqeklkldprskitfndfkgiakevgieekeinsvsna

laqsgsiiylpnslnenlktsvftkpahiyqslehildienkgvglnklieskkseinslrqkiqPleekkqvidrkah

rRataiiwtglgycfaqaailarltwwdlswdiiepvsyfltfgsvligytyftmtktEftyealnhRlfskrqdKlfkr

nnFpkedyenlvqaidkkekelkelelatkydhthpgGGSGGSGGSMDYKDDDDK*

Chimera 1

atgaatagcttcgtgatcaggaacggcttcggcctcgtcaggaccttcaacaccaggctgtttaccacctccacc

cagaacctggagggcgagctcaaaaccatcctcggccaggccaaggtcagcaagctgcaggaaaagctga

agctggatcccaggtccaagatcaccttcaacgacttcaagggcatcgccaaggaggtgggcatcgaggaga

aggaaatcaacagcgtcagcaacgccctggctcaatccggctccatcatctacctgcctaactccctgaacga

gaacctgaagacctccgtgttcaccaagcccgcccatatctaccagtccctcgaacacatcctggacatcgaga

acaagggcgtgggcctgaataagctgatcgagtccaagaaatccgagatcaatagcctgaggcagaagatcc

agCCCCTGGAAAAGGTACGAATTGAGATTAGCAGAAAAGCTGAGAAGAGGACCACT

TTGGTGCTATGGGGTGGCCTTGCCTACATGGCCACACAGTTTGGCATTTTGGCCC

GGCTTACCTGGTGGGAATATTCCTGGGACATCATGGAGCCAGTAACATACTTCATC

ACTTATGGAAGTGCCATGGCAATGTATGCATATTTTGTAATGACACGCCAGGAATA

TGTTTATCCAGAAGCCAGAGACAGACAATACTTACTATTTTTCCATAAAGGAGCCAA

AAAGTCACGTTTTGACCTAGAGAAATACAATCAACTCAAGGATGCAATTGCTCAGG

CAGAAATGGACCTTAAGAGACTGAGAGACCCATTACAAGTACATCTGCCTCTCCGA

CAAATTGGTGAAAAAGATCCCGGGGGTGGATCTGGTGGATCTGGTGGATCTATGG

ATTACAAGGATGACGATGACAAG*

mnsfvirngfglvrtfntrlfttstqnlegelktilgqakvsklqeklkldprskitfndfkgiakevgieekeinsvsna

laqsgsiiylpnslnenlktsvftkpahiyqslehildienkgvglnklieskkseinslrqkiqPLEKVRIEISRK

AEKRTTLVLWGGLAYMATQFGILARLTWWEYSWDIMEPVTYFITYGSAMAMYAYFVM

TRQEYVYPEARDRQYLLFFHKGAKKSRFDLEKYNQLKDAIAQAEMDLKRLRDPLQVHL

PLRQIGEKDPGGGSGGSGGSMDYKDDDDK*

Chimera 2

atgaatagcttcgtgatcaggaacggcttcggcctcgtcaggaccttcaacaccaggctgtttaccacctccacc

cagaacctggagggcgagctcaaaaccatcctcggccaggccaaggtcagcaagctgcaggaaaagctga

agctggatcccaggtacaagatcaccttcaacgacttcaagggcatcgccaaggaggtgggcatcgaggaga

aggaaatcaacagcgtcagcaacgccctggctcaatccggctccatcatctacctgcctaactccctgaacga

gaacctgaagacctccgtgttcaccaagcccgcccatatctaccagtccctcgaacacatcctggacatcgaga

acaagggcgtgggcctgaataagctgatcgagtccaagaaatccgagatcaatagcctgaggcagaagatcc

agcccctggaggagaagaagcaggtgatcgacagaaaggcccacaggagggccaccgctatcatctggac

cggactcggctattgcttcgcccaggccgccattctggctaggctcacctggtgggacctctcctgggacatcat

cgagcccgtgagctacttcctgaccttcggctccgtcctgatcggctacacctacttcacnatgaccaagaccGG

AATATGTTTATCCAGAAGCCAGAGACAGACAATACTTACTATTTTTCCATAAAGGAG

CCAAAAAGTCACGTTTTGACCTAGAGAAATACAATCAACTCAAGGATGCAATTGCT

CAGGCAGAAATGGACCTTAAGAGACTGAGAGACCCATTACAAGTACATCTGCCTCT

CCGACAAATTGGTGAAAAAGATCCCGGGGGTGGATCTGGTGGATCTGGTGGATCT

ATGGATTACAAGGATGACGATGACAAG*

mnsfvirngfglvrtfntrlfttstqnlegelktilgqakvsklqeklkldprykitfndfkgiakevgieekeinsvsna

laqsgsiiylpnslnenlktsvftkpahiyqslehildienkgvglnklieskkseinslrqkiqPleekkqvidrkah

rRataiiwtglgycfaqaailarltwwdlswdiiepvsyfltfgsvligytyftmtktEYVYPEARDRQYLLFF

HKGAKKSRFDLEKYNQLKDAIAQAEMDLKRLRDPLQVHLPLRQIGEKDPGGGSGGSG

GSMDYKDDDDK*

Chimera 3

ATGGCAGCTGCAGAAGGTAGATCGCTACTGCTACTCCTATCCTCTCGGGGAGGTG

GAGGTGGAGGTGCCGGAGGTTGCGGGACGCTGACTGCCGGCTGCTTCCCTGGGC

TGGGCGTCAGCCGCCACCGGCAGCAGCAGCACCACCGGACGGTACACCAGAGGA

TCGCTTCCTGGCAGAATTTGGGAGCTGTTTATTGCAGCACTGTTGTGCCCTCTGAT

GATGTTACAGTGGTTTATCAAAATGGGTTACCTGTGATATCTGTGAGGCTACCATC

CCGGCGTGAACGCTGTCAGTTCACACTCAAGCCTATCTCTGACTCTGTTGGTGTAT

TTTTACGACAACTGCAAGAAGAGGATCGGGGAATTGACAGAGTTGCTATCTATTCA

CCAGATGGTGTTCGCGTTGCTGCTTCAACAGGAATAGACCTCCTCCTCCTTGATGA

CTTTAAGCTGGTCATTAATGACTTAACATACCACGTACGACCACCAAAAAGAGACC

TCTTAAGTCATGAAAATGCAGCAACGCTGAATGATGTAAAGACATTGGTCCAGCAA

CTATACACCACACTGTGCATTGAGCAGCACCAGTTAAACAAGGAAAGGGAGCTTAT

TGAAAGACTAGAGGATCTCAAAGAGCAGCTGGCTCCCCTGGAAAAGGTACGAATT

GAGATTAGCAGAAAAGCTGAGAAGAGG**gccaccgctatcatctggaccggactcggctattgctt**

cgcccaggccgccattctggctaggctcacctggtgggacctctcctgggacatcatcgagcccgtgagctact

tcctgaccttcggctccgtcctgatcggctacacctacttcaccatgaccaagaccgagTATGTTTATCCA

GAAGCCAGAGACAGACAATACTTACTATTTTTCCATAAAGGAGCCAAAAAGTCACG

TTTTGACCTAGAGAAATACAATCAACTCAAGGATGCAATTGCTCAGGCAGAAATGG

ACCTTAAGAGACTGAGAGACCCATTACAAGTACATCTGCCTCTCCGACAAATTGGT

GAAAAAGATCCCGGGGGTGGATCTGGTGGATCTGGTGGATCTATGGATTACAAGG

ATGACGATGACAAG*

MAAAEGRSLLLLLSSRGGGGGGAGGCGTLTAGCFPGLGVSRHRQQQHHRTVHQRIA

SWQNLGAVYCSTVVPSDDVTVVYQNGLPVISVRLPSRRERCQFTLKPISDSVGVFLRQ

LQEEDRGIDRVAIYSPDGVRVAASTGIDLLLLDDFKLVINDLTYHVRPPKRDLLSHENAA

TLNDVKTLVQQLYTTLCIEQHQLNKERELIERLEDLKEQLAPLEKVRIEISRKAEK**Rataii**

wtglgycfaqaailarltwwdlswdiiepvsyfltfgsvligytyftmtktEYVYPEARDRQYLLFFHKGAK

KSRFDLEKYNQLKDAIAQAEMDLKRLRDPLQVHLPLRQIGEKDPGGGSGGSGGSMDY

KDDDDK*

Chimera 4

atgaatagcttcgtgatcaggaacggcttcggcctcgtcaggaccttcaacaccaggctgtttaccacctccacc

cagaacctggagggcgagctcaaaaccatcctcggccaggccaaggtcagcaagctgcaggaaaagctga

agctggatcccaggtccaagatcaccttcaacgacttcaagggcatcgccaaggaggtgggcatcgaggaga

aggaaatcaacagcgtcagcaacgccctggctcaatccggctccatcatctacctgcctaactccctgaacga

gaacctgaagacctccgtgttcaccaagcccgcccatatctaccagtccctcgaacacatcctggacatcgaga

acaagggcgtgggcctgaataagctgatcgagtccaagaaatccgagatcaatagcctgaggcagaagatcc

agcccctggaggagaagaagcaggtgatcgacagaaaggcccacagGAGGACCACTTTGGTGCT

ATGGGGTGGCCTTGCCTACATGGCCACACAGTTTGGCATTTTGGCCCGGCTTACC

TGGTGGGAATATTCCTGGGACATCATGGAGCCAGTAACATACTTCATCACTTATGG

AAGTGCCATGGCAATGTATGCATATTTTGTAATGACACGCCAGGAAT**tcacctacgagg**

ctctcaaccataggctgttcagcaagaggcaggacaagctgttcaaaagaaacaacttccctaaggaggacta

cgagaacctcgtgcaggccatcgacaagaaggagaaggagctcaaggagctcgagctcgccacaaagtac

gatcacacccaccccgggGGTGGATCTGGTGGATCTGGTGGATCTATGGATTACAAGGA

TGACGATGACAAG*

mnsfvirngfglvrtfntrlfttstqnlegelktilgqakvsklqeklkldprskitfndfkgiakevgieekeinsvsna

laqsgsiiylpnslnenlktsvftkpahiyqslehildienkgvglnklieskkseinslrqkiqPleekkqvidrkah

rRTTLVLWGGLAYMATQFGILARLTWWEYSWDIMEPVTYFITYGSAMAMYAYFVMTRQ

Eftyealnh**R**lfskrqd**K**lfkrnn**F**pkedyenlvqaidkkekelkelelatkydhthpgGGSGGSGGSMD

YKDDDDK*

Chimera 5:

ATGGCAGCTGCAGCAGGTAGATCGCTACTGCTACTCCTATCCTCTCGGGGAGGTG

GAGGTGGAGGTGCCGGAGGTTGCGGGACGCTGACTGCCGGCTGCTTCCCTGGGC

TGGGCGTCAGCCGCCACCGGCAGCAGCAGCACCACCGGACGGTACACCAGAGGA

TCGCTTCCTGGCAGAATTTGGGAGCTGTTTATTGCAGCACTGTTGTGCCCTCTGAT

GATGTTACAGTGGTTTATCAAAATGGGTTACCTGTGATATCTGTGAGGCTACCATC

CCGGCGTGAACGCTGTCAGTTCACACTCAAGCCTATCTCTGACTCTGTTGGTGTAT

TTTTACGACAACTGCAAGAAGAGGATCGGGGAATTGACAGAGTTGCTATCTATTCA

CCAGATGGTGTTCGCGTTGCTGCTTCAACAGGAATAGACCTCCTCCTCCTTGATGA

CTTTAAGCTGGTCATTAATGACTTAACATACCACGTACGACCACCAAAAAGAGACC

TCTTAAGTCATGAAAATGCAGCAACGCTGAATGATGTAAAGACATTGGTCCAGCAA

CTATACACCACACTGTGCATTGAGCAGCACCAGTTAAACAAGGAAAGGGAGCTTAT

TGAAAGACTAGAGGATCTCAAAGAGCAGCTGGCTCCCCTGGA**ggagaagaagcaggtg**

atcgacagaaaggcccacaggagggccaccgctatcatctggaccggactcggctattgcttcgcccaggcc

gccattctggctaggctcacctggtgggacctctcctgggacatcatcgagcccgtgagctacttcctgaccttc

ggctcngtcctgatcggctacacctacttcaccatgaccaagaccgagttcacctacgaggctctcaaccatag

gctgttcagcaagaggcaggacaagctgttcaaaagaaacaacttccctaaggaggactacgagaacctcgtg

caggccatcgacaagaaggagaaggagctcaaggagctcgagctcgccacaaagtacgatcacacccacc

ccgggGGTGGATCTGGTGGATCTGGTGGATCTATGGATTACAAGGATGACGATGAC

AAG*

MAAAAGRSLLLLLSSRGGGGGGAGGCGTLTAGCFPGLGVSRHRQQQHHRTVHQRIA

SWQNLGAVYCSTVVPSDDVTVVYQNGLPVISVRLPSRRERCQFTLKPISDSVGVFLRQ

LQEEDRGIDRVAIYSPDGVRVAASTGIDLLLLDDFKLVINDLTYHVRPPKRDLLSHENAA

TLNDVKTLVQQLYTTLCIEQHQLNKERELIERLEDLKEQLAPLE**ekkqvidrkahrRataiiwtg**

lgycfaqaailarltwwdlswdiiepvsyfltfgsvligytyftmtktEftyealnhRlfskrqdKlfkrnnFpkedy

enlvqaidkkekelkelelatkydhthpgGGSGGSGGSMDYKDDDDK*

Chimera 6:

ATGGCAGCTGCAGCAGGTCGATCGCTACTGCTACTCCTATCCTCTCGGGGAGGTG

GAGGTGGAGGTGCCGGAGGTTGCGGGACGCTGACTGCCGGCTGCTTCCCTGGGC

TGGGCGTCAGCCGCCACCGGCAGCAGCAGCACCACCGGACGGTACACCAGAGGA

TCGCTTCCTGGCAGAATTTGGGAGCTGTTTATTGCAGCACTGTTGTGCCCTCTGAT

GATGTTACAGTGGTTTATCAAAATGGGTTACCTGTGATATCTGTGAGGCTACCATC

CCGGCGTGAACGCTGTCAGTTCACACTCAAGCCTATCTCTGACTCTGTTGGTGTAT

TTTTACGACAACTGCAAGAAGAGGATCGGGGAATTGACAGAGTTGCTATCTATTCA

CCAGATGGTGTTCGCGTTGCTGCTTCAACAGGAATAGACCTCCTCCTCCTTGATGA

CTTTAAGCTGGTCATTAATGACTTAACATACCACGTACGACCACCAAAAAGAGACC

TCTTAAGTCATGAAAATGCAGCAACGCTGAATGATGTAAAGACATTGGTCCAGCAA

CTATACACCACACTGTGCATTGAGCAGCACCAGTTAAACAAGGAAAGGGAGCTTAT

TGAAAGACTAGAGGATCTCAAAGAGCAGCTGGCTCCCCTGGAAAAGGTACGAATT

GAGATTAGCAGAAAAGCTGAGAAGAGGACCACTTTGGTGCTATGGGGTGGCCTTG

CCTACATGGCCACACAGTTTGGCATTTTGGCCCGGCTTACCTGGTGGGAATATTCT

TGGGACATCATGGAGCCAGTAACATACTTCATCACTTATGGAAGTGCCATGGCAAT

GTATGCATATTTTGTAATGACACGCCAGGA**gttcacctacgaggctctcaaccataggctgttca**

gcaagaggcaggacaagctgttcaaaagaaacaacttccctaaggaggactacgagaacctcgtgcaggcc

atcgacaagaaggagaaggagctcaaggagctcgagctcgccacaaagtacgatcacacccaccccgggG

GTGGATCTGGTGGATCTGGTGGATCTATGGATTACAAGGATGACGATGACAAG*

MAAAAGRSLLLLLSSRGGGGGGAGGCGTLTAGCFPGLGVSRHRQQQHHRTVHQRIA

SWQNLGAVYCSTVVPSDDVTVVYQNGLPVISVRLPSRRERCQFTLKPISDSVGVFLRQ

LQEEDRGIDRVAIYSPDGVRVAASTGIDLLLLDDFKLVINDLTYHVRPPKRDLLSHENAA

TLNDVKTLVQQLYTTLCIEQHQLNKERELIERLEDLKEQLAPLEKVRIEISRKAEKRTTLV

LWGGLAYMATQFGILARLTWWEYSWDIMEPVTYFITYGSAMAMYAYFVMTRQE**ftyeal**

nhRlfskrqdKlfkrnnFpkedyenlvqaidkkekelkelelatkydhthpgGGSGGSGGSMDYKDDD

DK*

Chimera 7:

ATGGCAGCTGCAGCAGGTAGATCGCTACTGCTACTCCTATCCTCTCGGGGAGGTG

GAGGTGGAGGTGCCGGAGGTTGCGGGACGCTGACTGCCGGCTGCTTCCCTGGGC

TGGGCGTCAGCCGCCACCGGCAGCAGCAGCACCACCGGACGGTACACCAGAGGA

TCGCTTCCTGGCAGAATTTGGGAGCTGTTTATTGCAGCACTGTTGTGCCCTCTGAT

GATGTTACAGTGGTTTATCAAAATGGGTTACCTGTGATATCTGTGAGGCTACCATC

CCGGCGTGAACGCTGTCAGTTCACACTCAAGCCTATCTCTGACTCTGTTGGTGTAT

TTTTACGACAACTGCAAGAAGAGGATCGGGGAATTGACAGAGTTGCTATCTATTCA

CCAGATGGTGTTCGCGTTGCTGCTTCAACAGGAATAGACCTCCTCCTCCTTGATGA

CTTTAAGCTGGTCATTAATGACTTAACATACCACGTACGACCACCAAAAAGAGACC

TCTTAAGTCATGAAAATGCAGCAACGCTGAATGATGTAAAGACATTGGTCCAGCAA

CTATACACCACACTGTGCATTGAGCAGCACCAGTTAAACAAGGAAAGGGAGCTTAT

TGAAAGACTAGAGGATCTCAAAGAGCAGCTGGCTCCCCTGGAAAAGGTACGAATT

GAGATTAGCAGAAAAGCTGAGAAGAGGACCACTTTGGTGCTATGGGGTGGCCTTG

CCTACATGGCCACACAGTTTGGCATTTTGGCCCGGCTTACCTGGTGGGAATATTCC

TGGGACATCATGGAGCCAGTAACATACTTCATCACTTATGGAAGTGCCATGGCAAT

GTATGCATATTTTGTAATGACACGCCAGGA**gttcacctacgaggctctcaaccataggctgttca**

gcaagaggcaggacaagctgttcaaaagaaacaacttcGACCTAGAGAAATACAATCAACTCAA

GGATGCAATTGCTCAGGCAGAAATGGACCTTAAGAGACTGAGAGACCCATTACAA

GTACATCTGCCTCTCCGACAAATTGGTGAAAAAGATCCCGGGGGTGGATCTGGTG

GATCTGGTGGATCTATGGATTACAAGGATGACGATGACAAG*

MAAAAGRSLLLLLSSRGGGGGGAGGCGTLTAGCFPGLGVSRHRQQQHHRTVHQRIA

SWQNLGAVYCSTVVPSDDVTVVYQNGLPVISVRLPSRRERCQFTLKPISDSVGVFLRQ

LQEEDRGIDRVAIYSPDGVRVAASTGIDLLLLDDFKLVINDLTYHVRPPKRDLLSHENAA

TLNDVKTLVQQLYTTLCIEQHQLNKERELIERLEDLKEQLAPLEKVRIEISRKAEKRTTLV

LWGGLAYMATQFGILARLTWWEYSWDIMEPVTYFITYGSAMAMYAYFVMTRQE**ftyeal**

nhRlfskrqdKlfkrnnFDLEKYNQLKDAIAQAEMDLKRLRDPLQVHLPLRQIGEKDPGGGS

GGSGGSMDYKDDDDK*

Chimera 8:

ATGGCAGCTGCAGCAGGTAGATCGCTACTGCTACTCCTATCCTCTCGGGGAGGTG

GAGGTGGAGGTGCCGGAGGTTGCGGGACGCTGACTGCCGGCTGCTTCCCTGGGC

TGGGCGTCAGCCGCCACCGGCAGCAGCAGCACCACCGGACGGTACACCAGAGGA

TCGCTTCCTGGCAGAATTTGGGAGCTGTTTATTGCAGCACTGTTGTGCCCTCTGAT

GATGTTACAGTGGTTTATCAAAATGGGTTACCTGTGATATCTGTGAGGCTACCATC

CCGGCGTGAACGCTGTCAGTTCACACTCAAGCCTATCTCTGACTCTGTTGGTGTAT

TTTTACGACAACTGCAAGAAGAGGATCGGGGAATTGACAGAGTTGCTATCTATTCA

CCAGATGGTGTTCGCGTTGCTGCTTCAACAGGAATAGACCTCCTCCTCCTTGATGA

CTTTAAGCTGGTCATTAATGACTTAACATACCACGTACGACCACCAAAAAGAGACC

TCTTAAGTCATGAAAATGCAGCAACGCTGAATGATGTAAAGACATTGGTCCAGCAA

CTATACACCACACTGTGCATTGAGCAGCACCAGTTAAACAAGGAAAGGGAGCTTAT

TGAAAGACTAGAGGATCTCAAAGAGCAGCTGGCTCCCCTGGAAAAGGTACGAATT

GAGATTAGCAGAAAAGCTGAGAAGAGGACCACTTTGGTGCTATGGGGTGGCCTTG

CCTACATGGCCACACAGTTTGGCATTTTGGCCCGGCTTACCTGGTGGGAATATTCC

TGGGACATCATGGAGCCAGTAACATACTTCATCACTTATGGAAGTGCCATGGCAAT

GTATGCATATTTTGTAATGACACGCCAGGAATATGTTTATCCAGAAGCCAGAGACA

GACAATACTTACTATTTTTCCATAAAGGAGCCAAAAAGTCACGTTTT**cctaaggaggact**

acgagaacctcgtgcaggccatcgacaagaaggagaaggagctcaaggagctcgagctcgccacaaagta

cgatcacacccaccccgggGGTGGATCTGGTGGATCTGGTGGATCTATGGATTACAAGG

ATGACGATGACAAG*

MAAAAGRXLLLLLSSRGGGGGGAGGCGTLTAGCFPGLGVSRHRQQQHHRTVHQRIA

SWQNLGAVYCSTVVPSDDVTVVYQNGLPVISVRLPSRRERCQFTLKPISDSVGVFLRQ

LQEEDRGIDRVAIYSPDGVRVAASTGIDLLLLDDFKLVINDLTYHVRPPKRDLLSHENAA

TLNDVKTLVQQLYTTLCIEQHQLNKERELIERLEDLKEQLAPLEKVRIEISRKAEKRTTLV

LWGGLAYMATQFGILARLTWWEYSWDIMEPVTYFITYGSAMAMYAYFVMTRQEYVYP

EARDRQYLLFFHKGAKKSRF**pkedyenlvqaidkkekelkelelatkydhthpg**GGSGGSGGSM

DYKDDDDK*

Chimera 9

ATGGCAGCTGCAGCAGGTAGATCGCTACTGCTACTCCTATCCTCTCGGGGAGGTG

GAGGTGGAGGTGCCGGAGGTTGCGGGACGCTGACTGCCGGCTGCTTCCCTGGGC

TGGGCGTCAGCCGCCACCGGCAGCAGCAGCACCACCGGACGGTACACCAGAGGA

TCGCTTCCTGGCAGAATTTGGGAGCTGTTTATTGCAGCACTGTTGTGCCCTCTGAT

GATGTTACAGTGGTTTATCAAAATGGGTTACCTGTGATATCTGTGAGGCTACCATC

CCGGCGTGAACGCTGTCAGTTCACACTCAAGCCTATCTCTGACTCTGTTGGTGTAT

TTTTACGACAACTGCAAGAAGAGGATCGGGGAATTGACAGAGTTGCTATCTATTCA

CCAGATGGTGTTCGCGTTGCTGCTTCAACAGGAATAGACCTCCTCCTCCTTGATGA

CTTTAAGCTGGTCATTAATGACTTAACATACCACGTACGACCACCAAAAAGAGACC

TCTTAAGTCATGAAAATGCAGCAACGCTGAATGATGTAAAGACATTGGTCCAGCAA

CTATACACCACACTGTGCATTGAGCAGCACCAGTTAAACAAGGAAAGGGAGCTTAT

TGAAAGACTAGAGGATCTCAAAGAGCAGCTGGCTCCCCTGGAAAAGGTACGAATT

GAGATTAGCAGAAAAGCTGAGAAGAGGACCACTTTGGTGCTATGGGGTGGCCTTG

CCTACATGGCCACACAGTTTGGCATTTTGGCCCGGCTTACCTGGTGGGAATATTCC

TGGGACATCATGGAGCCAGTAACATACTTCATCACTTATGGAAGTGCCATGGCAAT

GTATGCATATTTTGTAATGACACGCCAGGAAT**tcacctacgaggctctcaaccat**AGACAAT

ACTTACTATTTTTCCATAAAGGAGCCAAAAAGTCACGTTTTGACCTAGAGAAATACA

ATCAACTCAAGGATGCAATTGCTCAGGCAGAAATGGACCTTAAGAGACTGAGAGAC

CCATTACAAGTACATCTGCCTCTCCGACAAATTGGTGAAAAAGATCCCGGGGGTG

GATCTGGTGGATCTGGTGGATCTATGGATTACAAGGATGACGATGACAAG*

MAAAAGRSLLLLLSSRGGGGGGAGGCGTLTAGCFPGLGVSRHRQQQHHRTVHQRIA

SWQNLGAVYCSTVVPSDDVTVVYQNGLPVISVRLPSRRERCQFTLKPISDSVGVFLRQ

LQEEDRGIDRVAIYSPDGVRVAASTGIDLLLLDDFKLVINDLTYHVRPPKRDLLSHENAA

TLNDVKTLVQQLYTTLCIEQHQLNKERELIERLEDLKEQLAPLEKVRIEISRKAEKRTTLV

LWGGLAYMATQFGILARLTWWEYSWDIMEPVTYFITYGSAMAMYAYFVMTRQE**ftyeal**

nhRQYLLFFHKGAKKSRFDLEKYNQLKDAIAQAEMDLKRLRDPLQVHLPLRQIGEKDP

GGGSGGSGGSMDYKDDDDK*

Chimera 10:

ATGGCAGCTGCAGCAGGTAGATCGCTACTGCTACTCCTATCCTCTCGGGGAGGTG

GAGGTGGAGGTGCCGGAGGTTGCGGGACGCTGACTGCCGGCTGCTTCCCTGGGC

TGGGCGTCAGCCGCCACCGGCAGCAGCAGCACCACCGGACGGTACACCAGAGGA

TCGCTTCCTGGCAGAATTTGGGAGCTGTTTATTGCAGCACTGTTGTGCCCTCTGAT

GATGTTACAGTGGTTTATCAAAATGGGTTACCTGTGATATCTGTGAGGCTACCATC

CCGGCGTGAACGCTGTCAGTTCACACTCAAGCCTATCTCTGACTCTGTTGGTGTAT

TTTTACGACAACTGCAAGAAGAGGATCGGGGAATTGACAGAGTTGCTATCTATTCA

CCAGATGGTGTTCGCGTTGCTGCTTCAACAGGAATAGACCTCCTCCTCCTTGATGA

CTTTAAGCTGGTCATTAATGACTTAACATACCACGTACGACCACCAAAAAGAGACC

TCTTAAGTCATGAAAATGCAGCAACGCTGAATGATGTAAAGACATTGGTCCAGCAA

CTATACACCACACTGTGCATTGAGCAGCACCAGTTAAACAAGGAAAGGGAGCTTAT

TGAAAGACTAGAGGATCTCAAAGAGCAGCTGGCTCCCCTGGAAAAGGTACGAATT

GAGATTAGCAGAAAAGCTGAGAAGAGGACCACTTTGGTGCTATGGGGTGGCCTTG

CCTACATGGCCACACAGTTTGGCATTTTGGCCCGGCTTACCTGGTGGGAATATTCC

TGGGACATCATGGAGCCAGTAACATACTTCATCACTTATGGAAGTGCCATGGCAAT

GTATGCATATTTTGTAATGACACGCCAGGAATATGTTTATCCAGAAGCCAGAGACA

GAC**tgttcagcaagaggcaggac**AAAGGAGCCAAAAAGTCACGTTTTGACCTAGAGAAAT

ACAATCAACTCAAGGATGCAATTGCTCAGGCAGAAATGGACCTTAAGAGACTGAGA

GACCCATTACAAGTACATCTGCCTCTCCGACAAATTGGTGAAAAAGATCCCGGGG

GTGGATCTGGTGGATCTGGTGGATCTATGGATTACAAGGATGACGATGACAAG*

MAAAAGRSLLLLLSSRGGGGGGAGGCGTLTAGCFPGLGVSRHRQQQHHRTVHQRIA

SWQNLGAVYCSTVVPSDDVTVVYQNGLPVISVRLPSRRERCQFTLKPISDSVGVFLRQ

LQEEDRGIDRVAIYSPDGVRVAASTGIDLLLLDDFKLVINDLTYHVRPPKRDLLSHENAA

TLNDVKTLVQQLYTTLCIEQHQLNKERELIERLEDLKEQLAPLEKVRIEISRKAEKRTTLV

LWGGLAYMATQFGILARLTWWEYSWDIMEPVTYFITYGSAMAMYAYFVMTRQEYVYP

EARDR**lfskrqd**KGAKKSRFDLEKYNQLKDAIAQAEMDLKRLRDPLQVHLPLRQIGEKDP

GGGGSGGSGGSMDYKDDDDK*

HsMCU^{CeEDD}

ATGGCGGCCGCCGCAGGTAGATCGCTCCTGCTGCTCCTCTCCTCTCGGGGCGGC

GGCGGCGGGGGCGCCGGCGGCTGCGGGGCGCTGACTGCCGGCTGCTTCCCTGG

GCTGGGCGTCAGCCGCCACCGGCAGCAGCAGCACCACCGGACGGTACACCAGA

GGATCGCTTCCTGGCAGAATTTGGGAGCTGTTTATTGCAGCACTGTTGTGCCCTCT

GATGATGTTACAGTGGTTTATCAAAATGGGTTACCTGTGATATCTGTGAGGCTACC

ATCCCGGCGTGAACGCTGTCAGTTCACACTCAAGCCTATCTCTGACTCTGTTGGTG

TATTTTTACGACAACTGCAAGAAGAGGATCGGGGAATTGACAGAGTTGCTATCTAT

TCACCAGATGGTGTTCGCGTTGCTGCTTCAACAGGAATAGACCTCCTCCTCCTTGA

TGACTTTAAGCTGGTCATTAATGACTTAACATACCACGTACGACCACCAAAAAGAG

ACCTCTTAAGTCATGAAAATGCAGCAACGCTGAATGATGTAAAGACATTGGTCCAG

CAACTATACACCACACTGTGCATTGAGCAGCACCAGTTAAACAAGGAAAGGGAGCT

TATTGAAAGACTAGAGGATCTCAAAGAGCAGCTGGCTCCCCTGGAAAAGGTACGA

ATTGAGATTAGCAGAAAAGCTGAGAAGAGGACCACTTTGGTGCTATGGGGTGGCC

TTGCCTACATGGCCACACAGTTTGGCATTTTGGCCCGGCTTACCTGGTGGGAATAT

TCCTGGGACATCATGGAGCCAGTAACATACTTCATCACTTATGGAAGTGCCATGGC

AATGTATGCATATTTTGTAATGACACGCCAG**tcatttgaatatccaagtgccagagaaaga**CAA

TACTTACTATTTTTCCATAAAGGAGCCAAAAAGTCACGTTTTGACCTAGAGAAATAC

AATCAACTCAAGGATGCAATTGCTCAGGCAGAAATGGACCTTAAGAGACTGAGAGA

CCCATTACAAGTACATCTGCCTCTCCGACAAATTGGTGAAAAAGATCCCGGGGGTG

GATCTGGTGGATCTGGTGGATCTATGGATTACAAGGATGACGATGACAAG

MAAAAGRSLLLLLSSRGGGGGGAGGCGALTAGCFPGLGVSRHRQQQHHRTVHQRIA

SWQNLGAVYCSTVVPSDDVTVVYQNGLPVISVRLPSRRERCQFTLKPISDSVGVFLRQ

LQEEDRGIDRVAIYSPDGVRVAASTGIDLLLLDDFKLVINDLTYHVRPPKRDLLSHENAA

TLNDVKTLVQQLYTTLCIEQHQLNKERELIERLEDLKEQLAPLEKVRIEISRKAEKRTTLV

LWGGLAYMATQFGILARLTWWEYSWDIMEPVTYFITYGSAMAMYAYFVMTRQ**sfeyps**

areRQYLLFFHKGAKKSRFDLEKYNQLKDAIAQAEMDLKRLRDPLQVHLPLRQIGEKDP

GGGSGGSGGSMDYKDDDDK

HsEMRE$^{\text{CeNterm}}$

atgaccagcaagaccgtgttccagaacgccttcaagaccttcctggacttcgccatcaacagcctgcccagca

cccagggcggcctgaacatcaccgccaccgcccccggcggcgtgggccagaggcccttcaccaacaaggc

cggcCTTCTCCGTGTGTTCTCCATTGTGATCCCCTTTCTCTATGTCGGGACACTCAT

TAGCAAAAATTTCGCGGCACTATTAGAGGAACATGACATTTTTGTTCCAGAGGATG

ATGATGATGATGAC

mtsktvfqnafktfldfainslpstqgglnitatapggvgqrpftnkagLLRVFSIVIPFLYVGTLISKNFAA

LLEEHDIFVPEDDDDDD

Cysteine-free MCU

ATGGCGGCCGCCGCAGGTAGATCGCTCCTGCTGCTCCTCTCCTCTCGGGGAGGT

GGAGGTGGAGGTGCAGGAGGTGGAGGTGCGCTGACTGCCGGCGGATTCCCTGG

GCTGGGCGTCAGCCGCCACCGGCAGCAGCAGCACCACCGGACGGTACACCAGA

GGATCGCTTCCTGGCAGAATTTGGGAGCTGTTTATTACAGCACTGTTGTGCCCTCT

GATGATGTTACAGTGGTTTATCAAAATGGGTTACCTGTGATATCTGTGAGGCTACC

ATCCCGGCGTGAACGCGGTCAGTTCACACTCAAGCCTATCTCTGACTCTGTTGGTG

TATTTTTACGACAACTGCAAGAAGAGGATCGGGGAATTGACAGAGTTGCTATCTAT

TCACCAGATGGTGTTCGCGTTGCTGCTTCAACAGGAATAGACCTCCTCCTCCTTGA

TGACTTTAAGCTGGTCATTAATGACTTAACATACCACGTACGACCACCAAAAAGAG

ACCTCTTAAGTCATGAAAATGCAGCAACGCTGAATGATGTAAAGACATTGGTCCAG

CAACTATACACCACACTGCGCATTGAGCAGCACCAGTTAAACAAGGAAAGGGAGC

TTATTGAAAGACTAGAGGATCTCAAAGAGCAGCTGGCTCCCCTGGAAAAGGTACG

AATTGAGATTAGCAGAAAAGCTGAGAAGAGGACCACACTAGTGCTATGGGGTGGC

CTTGCCTACATGGCCACACAGTTTGGCATTTTGGCCCGGCTTACCTGGTGGGAATA

TTCCTGGGACATCATGGAGCCAGTAACATACTTCATCACTTATGGAAGTGCCATGG

CAATGTATGCATATTTTGTAATGACACGCCAGGAATATGTTTATCCAGAAGCCAGA

GACAGACAATACTTACTATTTTTCCATAAAGGAGCCAAAAAGTCACGTTTTGACCTA

GAGAAATACAATCAACTCAAGGATGCAATTGCTCAGGCAGAAATGGACCTTAAGAG

ACTGAGAGACCCATTACAAGTACATCTGCCTCTCCGACAAATTGGTGAAAAAGAT

MAAAAGRSLLLLLSSRGGGGGGAGGGGALTAGGFPGLGVSRHRQQQHHRTVHQRIA

SWQNLGAVYYSTVVPSDDVTVVYQNGLPVISVRLPSRRERGQFTLKPISDSVGVFLRQ

LQEEDRGIDRVAIYSPDGVRVAASTGIDLLLLDDFKLVINDLTYHVRPPKRDLLSHENAA
TLNDVKTLVQQLYTTLRIEQHQLNKERELIERLEDLKEQLAPLEKVRIEISRKAEKRTTLV
LWGGLAYMATQFGILARLTWWEYSWDIMEPVTYFITYGSAMAMYAYFVMTRQEYVYP
EARDRQYLLFFHKGAKKSRFDLEKYNQLKDAIAQAEMDLKRLRDPLQVHLPLRQIGEK
DPGGGSG

ACKNOWLEDGEMENTS

We thank Jason McCoy and all members of the Mootha and Sancak laboratories for critical reading of the manuscript. We also thank David M Shechner for help with Pymol, analysis of published MCU structures, and with gRNA expression advice. MJS MacEwen was supported by T32GM007750. This work was supported by grants from the National Institutes of Health (R01HL130143, R01AR071942) to VK Mootha. VK Mootha is an Investigator of the Howard Hughes Medical Institute.

AUTHOR CONTRIBUTIONS

- MJS MacEwen: conceptualization, data curation, formal analysis, validation, visualization, methodology, and writing: original draft, review, and editing.
- AL Markhard: data curation, investigation, and methodology.
- M Bozbeyoglu: data curation and investigation.
- F Bradford: data curation and investigation.
- O Goldberger: resources, data curation, and investigation.
- VK Mootha: conceptualization, funding acquisition, investigation, and writing—original draft, review, and editing.

- Y Sancak: conceptualization, data curation, formal analysis, supervision, funding acquisition, validation, investigation, visualization, methodology, and writing—original draft, review, and editing.

CONFLICT OF INTEREST STATEMENT

VK Mootha is a paid advisor to Janssen Pharmaceuticals and 5am Ventures.

REFERENCES

- Baradaran R, Wang C, Siliciano AF, Long SB (2018) Cryo-EM structures of fungal and metazoan mitochondrial calcium uniporters. Nature 559: 580–584. doi:10.1038/s41586-018-0331-8
- Bass RB, Butler SL, Chervitz SA, Gloor SL, Falke JJ (2007) Use of site-directed cysteine and disulfide chemistry to probe protein structure and dynamics: Applications to soluble and transmembrane receptors of bacterial chemotaxis. Methods Enzymol 423: 25–51. doi:10.1016/s0076- 6879(07)23002-2
- Baughman JM, Perocchi F, Girgis HS, Plovanich M, Belcher-Timme CA, Sancak Y, Bao XR, Strittmatter L, Goldberger O, Bogorad RL, *et al* (2011) Integrative genomics identifies MCU as an essential component of the mitochondrial calcium uniporter. Nature 476: 341–345. doi:10.1038/ nature10234
- Bick AG, Calvo SE, Mootha VK (2012) Evolutionary diversity of the mitochondrial calcium uniporter. Science 336: 886. doi:10.1126/ science.1214977
- Carafoli E, Lehninger AL (1971) A survey of the interaction of calcium ions with mitochondria from different tissues and species. Biochem J 122: 681–690. doi:10.1042/bj1220681

- Chakraborty PK, Mustafi SB, Xiong X, Dwivedi SKD, Nesin V, Saha S, Zhang M, Dhanasekaran D, Jayaraman M, Mannel R, *et al* (2017) MICU1 drives glycolysis and chemoresistance in ovarian cancer. Nat Commun 8: 14634. doi:10.1038/ncomms14634
- Chaudhuri D, Sancak Y, Mootha VK, Clapham DE (2013) MCU encodes the pore conducting mitochondrial calcium currents. Elife 2: e00704. doi:10.7554/elife.00704
- Csordas G, Golenar T, Seifert EL, Kamer KJ, Sancak Y, Perocchi F, Moffat C, Weaver D, de la Fuente Perez S, Bogorad R, *et al* (2013) MICU1 controls both the threshold and cooperative activation of the mitochondrial Ca(2+) uniporter. Cell Metab 17: 976–987. doi:10.1016/j.cmet.2013.04.020
- de la Fuente S, Matesanz-Isabel J, Fonteriz RI, Montero M, Alvarez J (2014) Dynamics of mitochondrial Ca^{2+} uptake in MICU1-knockdown cells. Biochem J 458: 33–40. doi:10.1042/bj20131025
- De Stefani D, Raffaello A, Teardo E, Szabo I, Rizzuto R (2011) A forty-kilodalton protein of the inner membrane is the mitochondrial calcium uniporter. Nature 476: 336–340. doi:10.1038/nature10230
- Del Arco A, Contreras L, Pardo B, Satrustegui J (2016) Calcium regulation of mitochondrial carriers. Biochim Biophys Acta 1863: 2413–2421. doi:10.1016/j.bbamcr.2016.03.024
- Deluca HF, Engstrom GW (1961) Calcium uptake by rat kidney mitochondria. Proc Natl Acad Sci U S A 47: 1744–1750. doi:10.1073/pnas.47.11.1744

- Denton RM (2009) Regulation of mitochondrial dehydrogenases by calcium ions. Biochim Biophys Acta 1787: 1309–1316. doi:10.1016/j.bbabio. 2009.01.005
- Fan C, Fan M, Orlando BJ, Fastman NM, Zhang J, Xu Y, Chambers MG, Xu X, Perry K, Liao M, *et al* (2018) X-ray and cryo-EM structures of the mitochondrial calcium uniporter. Nature 559: 575–579. doi:10.1038/ s41586-018-0330-9
- Foskett JK, Madesh M (2014) Regulation of the mitochondrial Ca uniporter by MICU1 and MICU2. Biochem Biophys Res Commun 449: 377–383. doi:10.1016/j.bbrc.2014.04.146
- Giorgio V, Guo L, Bassot C, Petronilli V, Bernardi P (2018) Calcium and regulation of the mitochondrial permeability transition. Cell Calcium 70: 56–63. doi:10.1016/j.ceca.2017.05.004
- Goncalves AP, Cordeiro JM, Monteiro J, Lucchi C, Correia-de-Sa P, Videira A (2015) Involvement of mitochondrial proteins in calcium signaling and cell death induced by staurosporine in Neurospora crassa. Biochim Biophys Acta 1847: 1064–1074. doi:10.1016/j.bbabio.2015.05.011
- Kamer KJ, Mootha VK (2015) The molecular era of the mitochondrial calcium uniporter. Nat Rev Mol Cell Biol 16: 545–553. doi:10.1038/nrm4039
- Kamer KJ, Sancak Y, Fomina Y, Meisel JD, Chaudhuri D, Grabarek Z, Mootha VK (2018) MICU1 imparts the mitochondrial uniporter with the ability to discriminate between Ca(2+) and Mn(2+). Proc Natl Acad Sci U S A 115: E7960–E7969. doi:10.1073/pnas.1807811115

- Kirichok Y, Krapivinsky G, Clapham DE (2004) The mitochondrial calcium uniporter is a highly selective ion channel. Nature 427: 360–364. doi:10.1038/nature02246
- Konig T, Troder SE, Bakka K, Korwitz A, Richter-Dennerlein R, Lampe PA, Patron M, Muhlmeister M, Guerrero-Castillo S, Brandt U, *et al* (2016) The m- AAA protease associated with neurodegeneration limits MCU activity in mitochondria. Mol Cell 64: 148–162. doi:10.1016/j.molcel.2016.08.020
- Kovacs-Bogdan E, Sancak Y, Kamer KJ, Plovanich M, Jambhekar A, Huber RJ, Myre MA, Blower MD, Mootha VK (2014) Reconstitution of the mitochondrial calcium uniporter in yeast. Proc Natl Acad Sci U S A 111: 8985–8990. doi:10.1073/pnas.1400514111
- Koval OM, Nguyen EK, Santhana V, Fidler TP, Sebag SC, Rasmussen TP, Mittauer DJ, Strack S, Goswami PC, Abel ED, *et al* (2019) Loss of MCU prevents mitochondrial fusion in G1-S phase and blocks cell cycle progression and proliferation. Sci Signal 12: eaav1439. doi:10.1126/ scisignal.aav1439
- Lee SK, Shanmughapriya S, Mok MCY, Dong Z, Tomar D, Carvalho E, Rajan S, Junop MS, Madesh M, Stathopulos PB (2016) Structural insights into mitochondrial calcium uniporter regulation by divalent cations. Cell Chem Biol 23: 1157–1169. doi:10.1016/j.chembiol.2016.07.012
- Lee Y, Min CK, Kim TG, Song HK, Lim Y, Kim D, Shin K, Kang M, Kang JY, Youn HS, *et al* (2015) Structure and function of the N-terminal domain of the human mitochondrial calcium uniporter. EMBO Rep 16: 1318–1333. doi:10.15252/embr.201540436

- Liu JC, Liu J, Holmstrom KM, Menazza S, Parks RJ, Fergusson MM, Yu ZX, Springer DA, Halsey C, Liu C, *et al* (2016) MICU1 serves as a molecular gatekeeper to prevent in vivo mitochondrial calcium overload. Cell Rep 16: 1561–1573. doi:10.1016/j.celrep.2016.07.011
- Logan CV, Szabadkai G, Sharpe JA, Parry DA, Torelli S, Childs AM, Kriek M, Phadke R, Johnson CA, Roberts NY, *et al* (2014) Loss-of-function mutations in MICU1 cause a brain and muscle disorder linked to primary alterations in mitochondrial calcium signaling. Nat Genet 46: 188–193. doi:10.1038/ng.2851
- Mallilankaraman K, Doonan P, Cardenas C, Chandramoorthy HC, Muller M, Miller R, Hoffman NE, Gandhirajan RK, Molgo J, Birnbaum MJ, *et al* (2012) MICU1 is an essential gatekeeper for MCU-mediated mitochondrial Ca(2+) uptake that regulates cell survival. Cell 151: 630–644. doi:10.1016/j.cell.2012.10.011
- Mammucari C, Gherardi G, Zamparo I, Raffaello A, Boncompagni S, Chemello F, Cagnin S, Braga A, Zanin S, Pallafacchina G, *et al* (2015) The mitochondrial calcium uniporter controls skeletal muscle trophism in vivo. Cell Rep 10: 1269–1279. doi:10.1016/j.celrep.2015.01.056
- Mammucari C, Raffaello A, Vecellio Reane D, Gherardi G, De Mario A, Rizzuto R (2018) Mitochondrial calcium uptake in organ physiology: From molecular mechanism to animal models. Pflugers Arch 470: 1165–1179. doi:10.1007/s00424-018-2123-2
- Munch C, Harper JW (2016) Mitochondrial unfolded protein response controls matrix pre-RNA processing and translation. Nature 534: 710–713. doi:10.1038/nature18302

- Musa S, Eyaid W, Kamer K, Ali R, Al-Mureikhi M, Shahbeck N, Al Mesaifri F, Makhseed N, Mohamed Z, AlShehhi WA, *et al* (2019) A Middle Eastern founder mutation expands the genotypic and phenotypic spectrum of mitochondrial MICU1 deficiency: A report of 13 patients. JIMD Rep 43: 79–83. doi:10.1007/8904_2018_107
- Nguyen NX, Armache JP, Lee C, Yang Y, Zeng W, Mootha VK, Cheng Y, Bai XC, Jiang Y (2018) Cryo-EM structure of a fungal mitochondrial calcium uniporter. Nature 559: 570–574. doi:10.1038/s41586-018-0333-6
- Oxenoid K, Dong Y, Cao C, Cui T, Sancak Y, Markhard AL, Grabarek Z, Kong L, Liu Z, Ouyang B, *et al* (2016) Architecture of the mitochondrial calcium uniporter. Nature 533: 269–273. doi:10.1038/nature17656
- Patron M, Checchetto V, Raffaello A, Teardo E, Reane DV, Mantoan M, Granatiero V, Szabo I, De Stefani D, Rizzuto R (2014) MICU1 and MICU2 finely tune the mitochondrial Ca^{2+} uniporter by exerting opposite effects on MCU activity. Mol Cell 53: 726–737. doi:10.1016/ j.molcel.2014.01.013
- Paupe V, Prudent J (2018) New insights into the role of mitochondrial calcium homeostasis in cell migration. Biochem Biophys Res Commun 500: 75–86. doi:10.1016/j.bbrc.2017.05.039
- Perocchi F, Gohil VM, Girgis HS, Bao XR, McCombs JE, Palmer AE, Mootha VK (2010) MICU1 encodes a mitochondrial EF hand protein required for Ca(2+) uptake. Nature 467: 291–296. doi:10.1038/nature09358
- Pittis AA, Goh V, Cebrian-Serrano A, Wettmarshausen J, Perocchi F, Gabaldón T (2020) Discovery of EMRE in fungi resolves the true evolutionary history of the

mitochondrial calcium uniporter. BioRxiv: doi:10.1101/ 2020.03.24.006015 (Preprint posted March 25, 2020).

- Plovanich M, Bogorad RL, Sancak Y, Kamer KJ, Strittmatter L, Li AA, Girgis HS, Kuchimanchi S, De Groot J, Speciner L, *et al* (2013) MICU2, a paralog of MICU1, resides within the mitochondrial uniporter complex to regulate calcium handling. PLoS One 8: e55785. doi:10.1371/ journal.pone.0055785
- Prudent J, Popgeorgiev N, Gadet R, Deygas M, Rimokh R, Gillet G (2016) Mitochondrial Ca(2+) uptake controls actin cytoskeleton dynamics during cell migration. Sci Rep 6: 36570. doi:10.1038/srep36570
- Raffaello A, De Stefani D, Sabbadin D, Teardo E, Merli G, Picard A, Checchetto V, Moro S, Szabo I, Rizzuto R (2013) The mitochondrial calcium uniporter is a multimer that can include a dominant-negative pore- forming subunit. EMBO J 32: 2362–2376. doi:10.1038/emboj.2013.157
- Sancak Y, Markhard AL, Kitami T, Kovacs-Bogdan E, Kamer KJ, Udeshi ND, Carr SA, Chaudhuri D, Clapham DE, Li AA, *et al* (2013) EMRE is an essential component of the mitochondrial calcium uniporter complex. Science 342: 1379–1382. doi:10.1126/science.1242993
- Sonnhammer EL, von Heijne G, Krogh A (1998) A hidden Markov model for predicting transmembrane helices in protein sequences. Proc Int Conf Intell Syst Mol Biol 6: 175–182.
- Suzuki Y, Takeda Y, Ikuta T (2008) Immunoblotting conditions for human hemoglobin chains. Anal Biochem 378: 218–220. doi:10.1016/ j.ab.2008.04.008

- Tsai CW, Wu Y, Pao PC, Phillips CB, Williams C, Miller C, Ranaghan M, Tsai MF (2017) Proteolytic control of the mitochondrial calcium uniporter complex. Proc Natl Acad Sci U S A 114: 4388–4393. doi:10.1073/ pnas.1702938114
- Tsai MF, Phillips CB, Ranaghan M, Tsai CW, Wu Y, Willliams C, Miller C (2016) Dual functions of a small regulatory subunit in the mitochondrial calcium uniporter complex. Elife 5: e15545. doi:10.7554/elife.15545
- Vais H, Mallilankaraman K, Mak DD, Hoff H, Payne R, Tanis JE, Foskett JK (2016) EMRE is a matrix Ca(2+) sensor that governs gatekeeping of the mitochondrial Ca(2+) uniporter. Cell Rep 14: 403–410. doi:10.1016/ j.celrep.2015.12.054
- Vasington FD, Murphy JV (1962) Ca ion uptake by rat kidney mitochondria and its dependence on respiration and phosphorylation. J Biol Chem 237: 2670–2677.
- Wang Y, Nguyen NX, She J, Zeng W, Yang Y, Bai XC, Jiang Y (2019) Structural mechanism of EMRE-dependent gating of the human mitochondrial calcium uniporter. Cell 177: 1252–1261.e13. doi:10.1016/j.cell.2019.03.050
- Wettmarshausen J, Goh V, Huang KT, Arduino DM, Tripathi U, Leimpek A, Cheng Y, Pittis AA, Gabaldon T, Mokranjac D, *et al* (2018) MICU1 confers protection from MCU-dependent manganese toxicity. Cell Rep 25: 1425–1435.e7. doi:10.1016/j.celrep.2018.10.037
- Yamamoto T, Yamagoshi R, Harada K, Kawano M, Minami N, Ido Y, Kuwahara K, Fujita A, Ozono M, Watanabe A, *et al* (2016) Analysis of the structure and function of EMRE in a yeast expression system. Biochim Biophys Acta 1857: 831–839. doi:10.1016/j.bbabio.2016.03.019

- Yoo J, Wu M, Yin Y, Herzik MA Jr., Lander GC, Lee SY (2018) Cryo-EM structure of a mitochondrial calcium uniporter. Science 361: 506–511. doi:10.1126/science.aar4056
- Zhao H, Li T, Wang K, Zhao F, Chen J, Xu G, Zhao J, Li T, Chen L, Li L, *et al* (2019) AMPK-mediated activation of MCU stimulates mitochondrial Ca(2+) entry to promote mitotic progression. Nat Cell Biol 21: 476–486. doi:10.1038/s41556-019-0296-3

CHAPTER 4:

Loss of mitochondrial calcium signaling triggers a TCA cycle bypass mechanism

Melissa JS MacEwen[1], Tim Locke[1], Tanmay Sapre[1], Ekin Gokcumen[2], Shao-En Ong[1], Yasemin Sancak[1]

Unpublished; project is ongoing

[1]Department of Pharmacology, University of Washington, Seattle, WA, USA
[2]Department of Chemistry, University at Buffalo, Buffalo, NY, USA

Correspondence: sancak@uw.edu; mjsmacewen@gmail.com

ABSTRACT

Mitochondrial calcium signaling is a dynamic process that enables constant communication between the mitochondria and the rest of the cell. On a molecular level, this calcium signaling centers on mitochondrial calcium uptake into the mitochondrial matrix through the mitochondrial calcium uniporter (MCU), and mitochondrial calcium release through the mitochondrial Na^+/Ca^{2+} exchanger (NCLX). Mitochondrial calcium signaling mediates a range of cellular functions and is essential in ensuring that mitochondrial energy and metabolite production is synchronized with the needs of the rest of the cell. This is reflected by the fact that multiple mitochondrial matrix enzymes essential to the citric acid cycle are regulated by calcium. Though it is known that elevated mitochondrial matrix calcium can drive the "speed" of the citric acid cycle, and that the presence or absence of mitochondrial Ca^{2+} can determine which carbon sources are metabolized for energy, the specific metabolic pathways utilized following a loss of mitochondrial Ca^{2+} signaling are poorly characterized. Here, we identify a metabolic "bypass" mechanism that is responsive to altered regulation of citric acid cycle enzymes by calcium. This work sheds light on how MCU knockout organisms are able to survive without experiencing a catastrophic energy crisis, and reveals a therapeutic approach that may be useful in the treatment of some forms of cancer.

INTRODUCTION

Mitochondrial calcium signaling is an essential regulator of cellular function. By mediating communication between the mitochondria and the rest of the cell, mitochondrial calcium ensures that mitochondrial metabolite and energy production is synchronized with the needs of the cell (Denton, 2009). Mitochondrial calcium signaling centers largely

on coordination between calcium influx from the cytosol to the mitochondrial matrix through the mitochondrial calcium uniporter complex, and efflux through the mitochondrial Na^+ / Ca^{2+} exchanger (NCLX) (Palty *et al.,* 2009). The uniporter complex consists of a calcium conducting channel protein, the mitochondrial calcium uniporter (MCU) (Chaudhuri *et al*., 2013), as well as a small, 10-kDa protein essential for pore conductance (EMRE) (Sancak *et al*., 2013), and a heterodimer composed of MICU1 and MICU2 that dissociates from MCU during a calcium signaling event (Csordas *et al*., 2013; Liu *et al*., 2016; Perocchi *et al*., 2010; Pinton *et al*., 2008). A non-pore forming paralog of MCU, MCUB, is sometimes incorporated into the uniporter complex to further regulate calcium dynamics (Huo *et al*., 2020).

Precise control of uniporter complex activity is critical to cellular health, as the calcium concentration of the mitochondrial matrix directly regulates mitochondrial metabolism and energy production. Within the TCA cycle, pyruvate dehydrogenase (PDH), NAD^+-dependent isocitrate dehydrogenase, and 2-oxoglutarate dehydrogenase (part of the oxoglutarate dehydrogenase complex, OGDC), are each activated by Ca^{2+} (Traaseth *et al.*, 2004; Wan *et al.*, 1989). Accordingly, the protein composition of the uniporter complex is regulated by the different metabolic needs of different organisms and their various tissues, in health and illness.

Considering the central role of mitochondrial calcium signaling in cellular health, it was surprising when recent work revealed that organisms can survive without functional MCU and/or EMRE, a regulatory protein essential for MCU Ca^{2+} conductance (Murphy *et al*., 2014; Harrington and Murphy, 2015; Wang *et al*., 2020). In addition to the production of many organisms with tissue-specific MCU knockouts (Bisbach *et al.*, 2020; Gherardi *et*

al., 2019; Rasmussen *et al.*, 2015; Wu *et al.*, 2015; Luongo *et al.*, 2015; Kwong *et al.*, 2015; Flicker *et al*., 2019), viable whole-body $MCU^{-/-}$ organisms have been produced in a variety of non-mammalian organisms including zebrafish (Bisbach *et al.*, 2020), *C. elegans* (Álvarez-Illera *et al.*, 2020), and *Drosophila*. These organisms exhibit broadly normal metabolism and physiology (Bisbach *et al.*, 2020; Álvarez-Illera *et al.*, 2020; Choi *et al.*, 2017). The viability of mammalian MCU and EMRE knockout mammals is less clear cut. While an MCU knockout is embryonic lethal on a C57BL/6 mouse background (Pan *et al.*, 2013), MCU or EMRE knockout mice on a mixed C57BL/6 and CD1 background exhibit normal aerobic respiration, despite having a smaller body size, being unable to take up mitochondrial calcium, and exhibiting depressed mitochondrial matrix calcium (Pan *et al.*, 2013; Liu *et al.* 2020). Though no MCU mutations have yet been observed in humans, two patients with EMRE mutations resulting in a loss of EMRE have been identified. These patients exhibited muscle breakdown in addition to a number of diverse symptoms (Bulthuis *et al*., 2022).

We were intrigued by the fact that organisms and specific tissues are generally able to survive the loss of MCU, and hypothesized that surviving MCU KO organisms employed compensatory metabolic pathways to avoid a metabolic crisis. We reasoned that examining the proteins and pathways altered between wild type and MCU KO cells and organisms could reveal the mechanism for such an adaptation. By pairing data collected using mass spectrometry and RNA-seq with physiological data, we have determined that cells lacking mitochondrial calcium signaling upregulate a series of metabolic pathways that allows them to bypass the calcium-regulated proteins of the citric acid cycle. Instead, cells rely on the catabolism of amino acids and odd-chain fatty acids,

before returning the products of these pathways to the canonical citric acid cycle as succinyl-CoA.

RESULTS

Because we hypothesized that a loss of MCU-mediated mitochondrial calcium signaling would result in altered regulation of metabolic pathways, we began our investigation by collecting mass spectrometry data from wild type and MCU knockout (KO) HeLa cells (**Fig. 1A**). MCU KO cells show downregulation of proteins involved in thiamine metabolism, cysteine and methionine metabolism, purine metabolism, and other assorted metabolic pathways, according to KEGG pathway enrichment (**Fig. S1A**). Meanwhile, the pathways most significantly upregulated in MCU KO cells included those involved in the pentose phosphate pathway and the TCA cycle (**Fig. S1B**), again according to KEGG pathway enrichment.

When looking at individual protein hits within our mass spectrometry results, we were particularly intrigued by the dramatic increase in peptides from the MMSDH (*ALDH6A1* gene) and ACAT1 proteins, as both proteins are involved in the catabolism of amino acids that results in the production of propionyl-CoA and succinyl-CoA. *ALDH6A1* encodes a protein called methylmalonate semialdehyde dehydrogenase (MMSDH) that localizes to the mitochondrial matrix and catalyzes reactions in the distal portions of the valine and pyrimidine catabolic pathways (Kedishvili *et al.*, 2000). Specifically, MMSDH catalyzes the decarboxylation of malonate and methylmalonate semialdehydes to acetyl- and propionyl-CoA. *ACAT1* encodes a protein called ACAT1 which also localizes to the mitochondrial matrix, and which participates in the pathway essential to the catabolism of

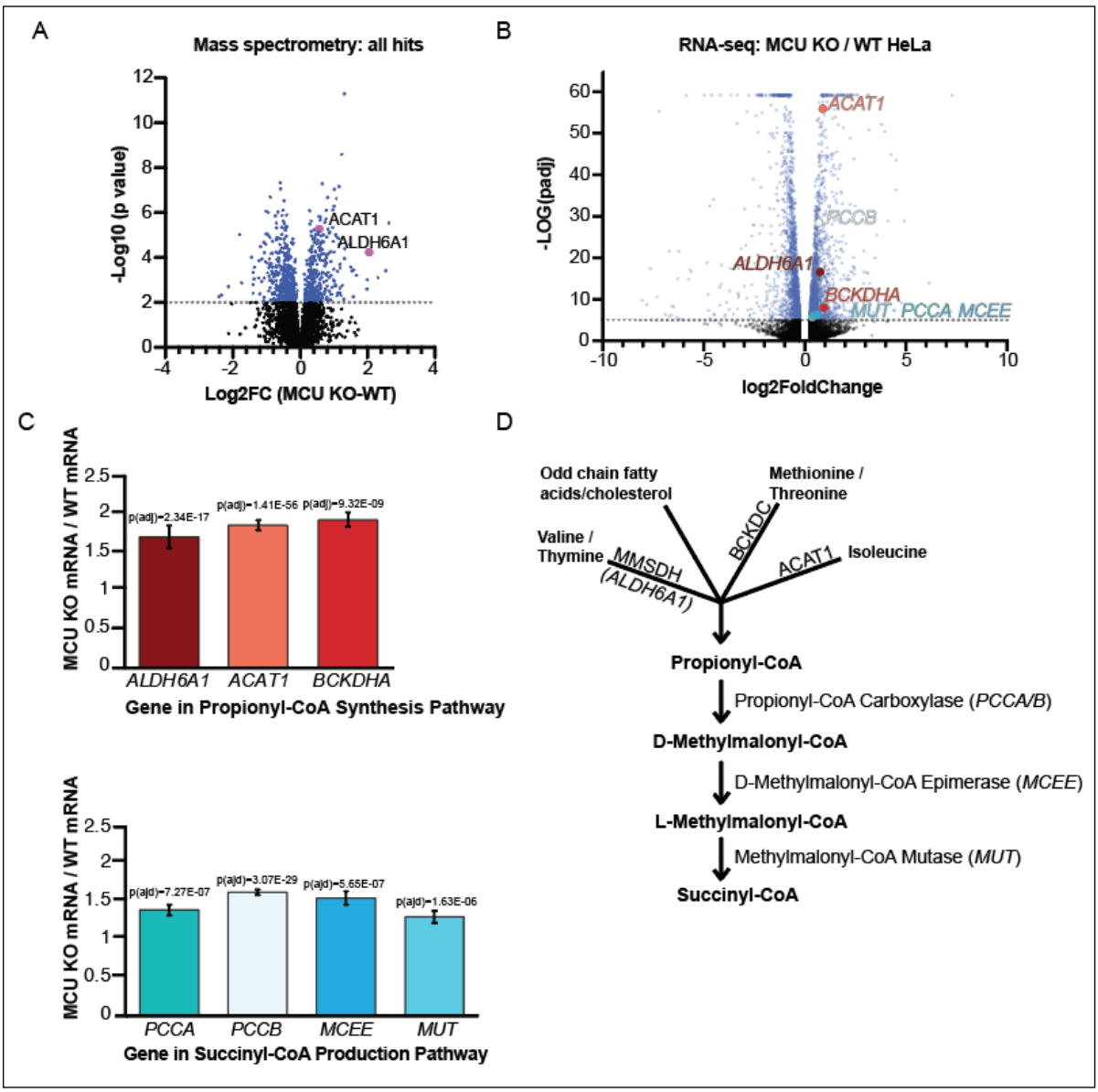

Fig. 1. Knockout of the mitochondrial calcium uniporter (MCU) in HeLa cells causes upregulation of genes central to propionyl-CoA/succinyl-CoA metabolism. (A) In a mass spectrometry data set of wild type versus MCU KO HeLa cells, both ACAT1 and MMSDH (the protein product of the *ALDH6A1* gene) are significantly upregulated. **(B)** In an RNA sequencing data set of wild type versus MCU KO HeLa cells, many genes central to the propionyl-CoA/succinyl-CoA pathways are significantly upregulated. Minimum fold change plotted: 0.25. **(C)** Bar graphs of the genes labeled in **(B)**. **(D)** A schematic illustrating the catabolic pathways that feed into the propionyl-CoA/succinyl-CoA metabolic pathway.

isoleucine by converting 2-methyl-acetoacetyl-CoA into propionyl-CoA and acetyl-CoA. The primary function of acetyl-CoA is to introduce the acetyl group into the TCA cycle. Propionyl-CoA, on the other hand, is further catabolized by a series of enzymes into

succinyl-CoA, which can enter the TCA cycle and be converted to succinate by succinyl-CoA synthetase. We hypothesized that the ACAT1 and MMSDH peptide increases we observed in MCU KO HeLa cells reflected a broader upregulation of the propionyl-CoA and succinyl-CoA pathways. Following a loss of mitochondrial Ca^{2+} signaling, such upregulation could be beneficial as it could provide a bypass to Ca^{2+}-regulated enzymes of the TCA cycle.

We next used RNA-seq to deepen our understanding of the altered metabolic regulation caused by a loss of mitochondrial calcium signaling (**Fig. 1B**). KEGG pathway enrichment performed using this RNA-seq data revealed few noteworthy trends in terms of which pathways were downregulated in MCU KO cells (**Fig. S1C**), while showing the upregulation of pathways similar to those observed in our mass spectrometry data (**Fig. S1D),** most notably the citric acid cycle. We observed that “valine, leucine, and isoleucine degradation” was hit in both our RNA-seq dataset and our mass spectrometry dataset, according to KEGG pathway enrichment (**Fig. S1B; Fig. S1D**). Of the genes that appear in our RNA-seq dataset, the RNA expression of all genes critical to the propionyl-CoA and succinyl-CoA pathways are significantly upregulated. **(Fig 1C)**. A schematic illustrating the propionyl-CoA/succinyl-CoA production pathways is included in **Figure 1D**; this illustration also demonstrates how the propionyl-CoA/succinyl-CoA pathway may bypass Ca^{2+}-regulated steps of the TCA cycle that function improperly during a loss of mitochondrial Ca^{2+} signaling.

We next used a variety of cell lines to validate the increased expression of propionyl-CoA / succinyl-CoA synthesis enzymes that we observed by mass spectrometry

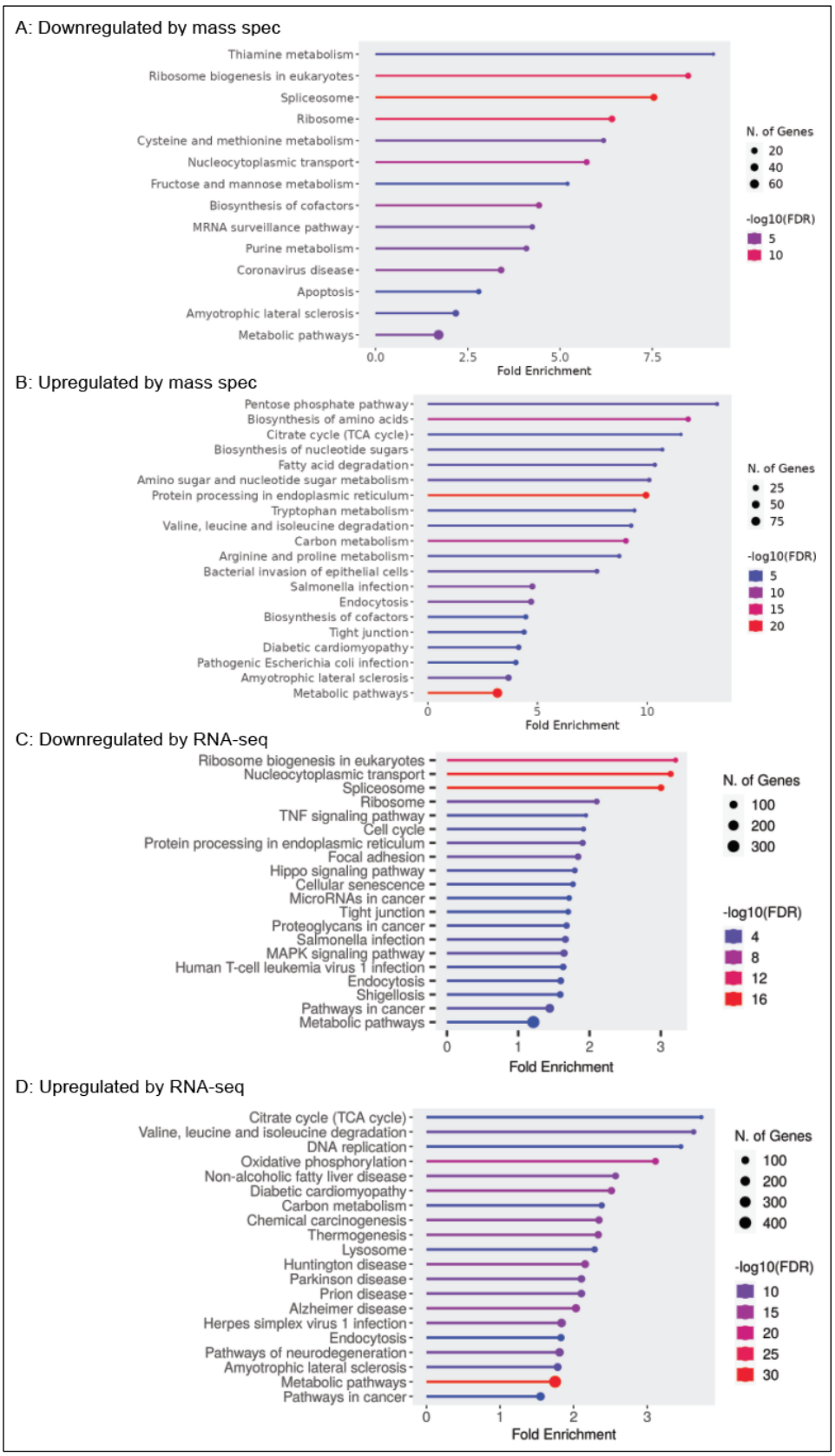

Fig. S1. Pathway enrichment analysis of mass spectrometry and RNA-seq data. Data plotted using Shiny Go. P-value cutoff: 0.5.

and RNA-seq of WT and MCU KO HeLa cells. In western blots of human cells (HeLa and U-2 OS), we observed protein level increases of MMSDH, ACAT1, BCKDHA, PCCB, MCEE, and MUT in MCU and EMRE KO HeLa cells (**Fig. 2A; Fig. 2B**). We also observed increased levels of MMSDH and BCKDHA in U-2 OS MCU KO cells (**Fig. 2C**). These differences between HeLa and U-2 OS cells suggests that these

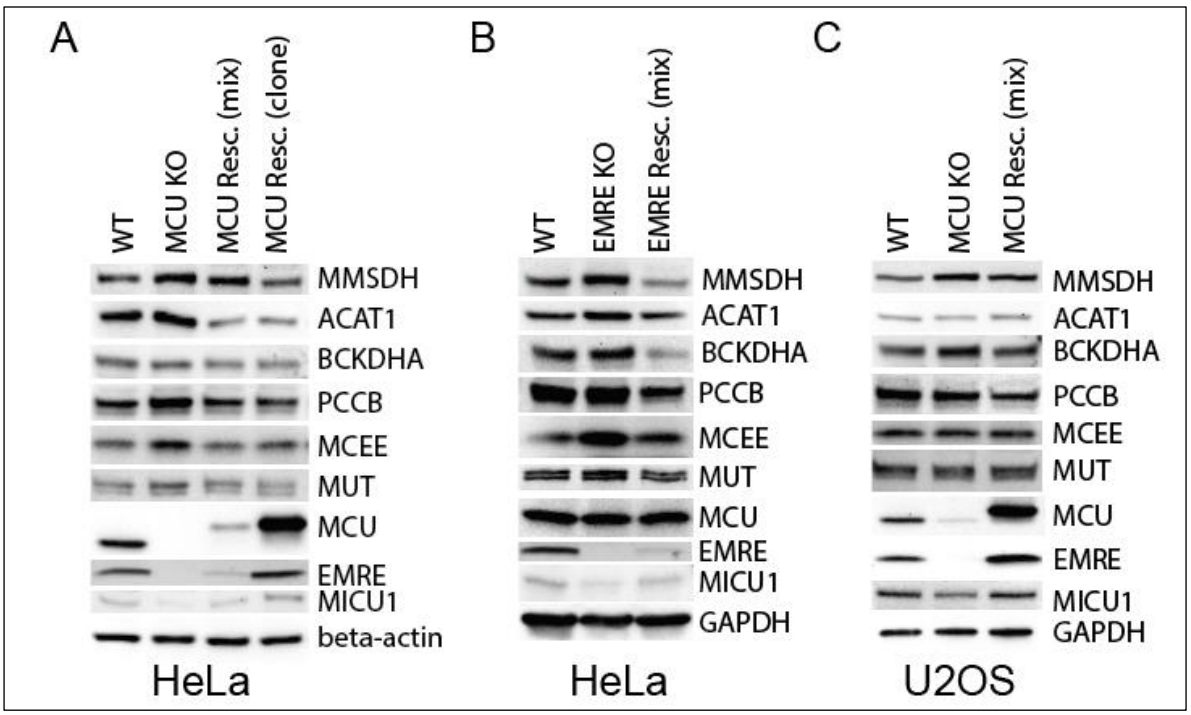

Fig. 2. Western blotting human cell lines confirms increased expression of proteins central to propionyl-CoA/succinyl-CoA metabolism. Western blots of wild type or uniporter knockout/rescue HeLa cells **(A, B)** and U-2 OS **(C)** validate the peptide / mRNA level increases observed for propionyl-CoA/succinyl-CoA metabolism in **Fig. 1.**

proteins may be regulated differently in different cell types. Because the propionyl-CoA production via BCKDHA and MMSDH is redundant with the function of ACAT1 and other enzymes involved in odd-chain fatty acid oxidation, these findings in U-2 OS cells still support our hypothesis. All proteins elevated in HeLa or U-2 OS MCU or EMRE KO cells decreased following the rescue of EMRE or MCU, respectively.

We validated the capacity of our experimental cell lines to participate in mitochondrial calcium signaling by using mitochondrial calcium uptake assays (**Fig. S2A, S2B, S2C**). We also observed an MMSDH protein level increase by western blotting in two different mouse systems. MMSDH increased following two different MCU knockdowns in AML12 cells (a mouse hepatocyte cell line) (**Fig. 3A**), and also increased in liver samples of outbred mice on a C57BL/6 background with a liver-specific MCU

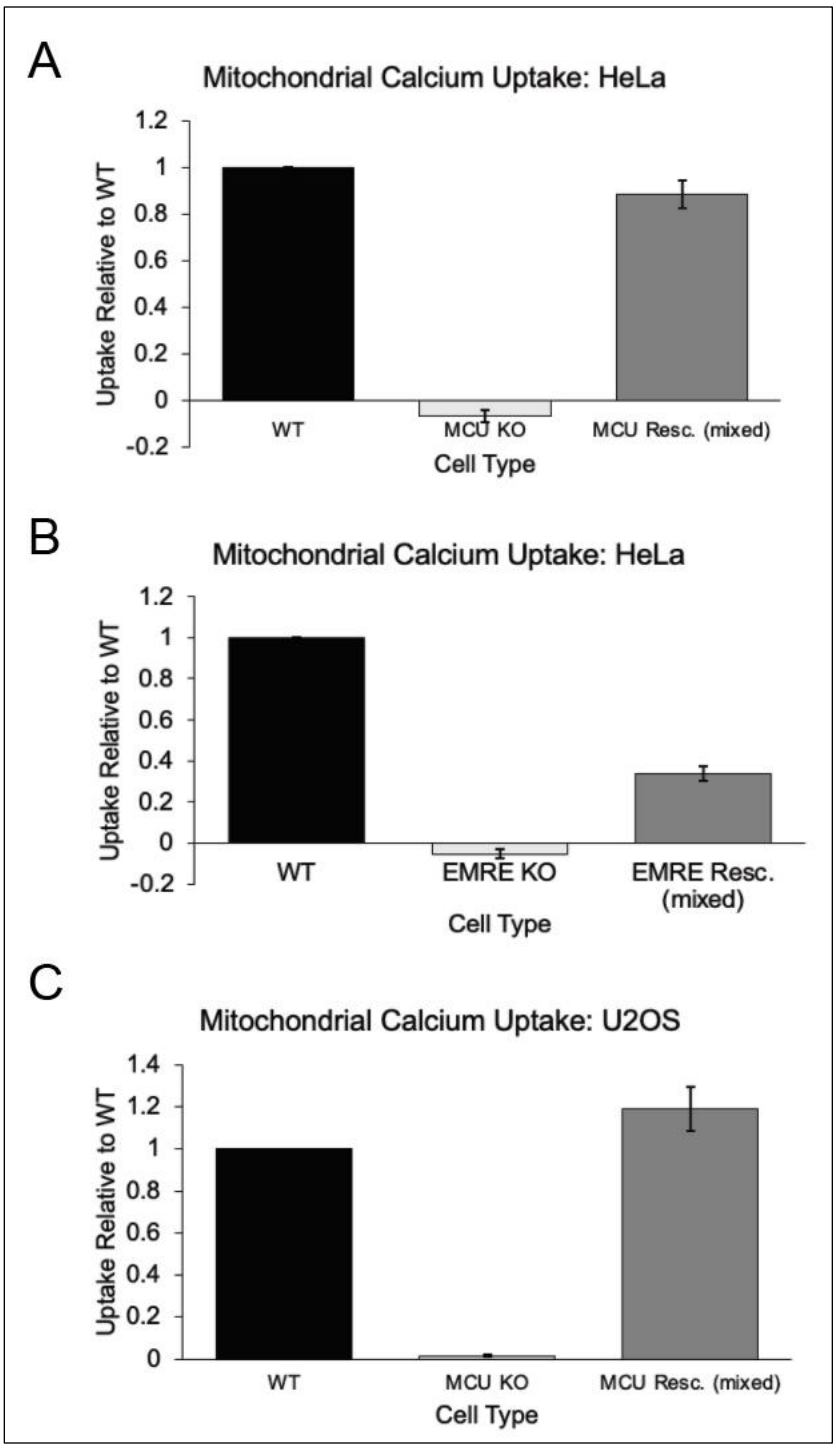

Fig. S2. Mitochondrial calcium uptake assays validate cell lines' ability to perform calcium signaling. Assays performed in HeLa cells (A, B) or U2OS cells (C) confirm that mitochondria from permeabilized WT, MCU or EMRE KO, or MCU rescue / EMRE rescue cells respond as expected to a bolus of extracellular calcium.

knockout (**Fig. 3B**). Because most of our propionyl/succinyl-CoA antibodies are human-specific, we were unable to validate other protein level increases. These data led us to conclude that the propionyl-CoA pathway protein level increases we observe in response to a loss of MCU-mediated mitochondrial Ca^{2+} signaling are neither species specific, nor specific to cancer cell lines.

Our mass spectrometry and RNA-seq data, paired with western blot validation of MMSDH protein level increases, led us to hypothesize that cells with disrupted

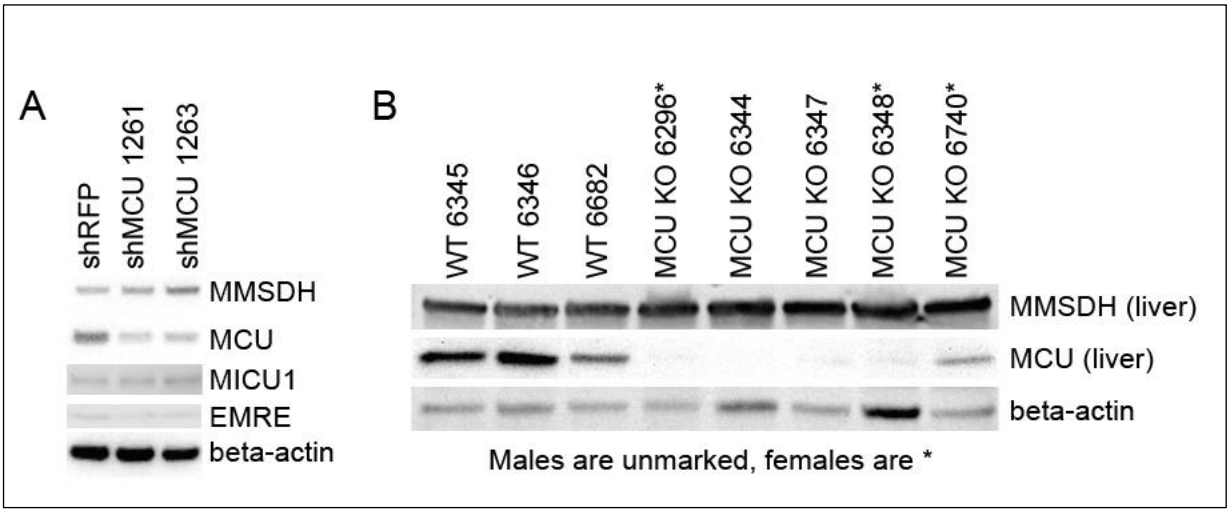

Fig. 3. Western blotting mouse cell lines also links loss of mitochondrial calcium uniporter with upregulation of propionyl-CoA pathway. Western blots of **(A)** MCU knocked down AML12 cells or **(B)** liver-specific MCU knockout mice show an upregulation of MMSDH protein.

mitochondrial calcium signaling rely more heavily on propionyl-CoA and succinyl-CoA synthesis as a means of bypassing two consecutive steps of the TCA cycle that are regulated by calcium: the enzyme isocitrate dehydrogenase (ICDH), and the 2-oxoglutarate dehydrogenase complex (OGDHC).

Because we observe similar data in a variety of cell lines, we hypothesize that this bypass step is not specific to cancer cells or individual species. **Figure 4** illustrates the established metabolic pathways relevant to this model.

We next performed a series of experiments to determine the effect of this proposed bypass mechanism on cellular metabolism and fitness. First, because MMSDH was one of the most significant hits by mass spectrometry, we used short hairpin RNA (shRNA) targeted to *ALDH6A1* to knock down MMSDH protein levels in wild type and MCU KO HeLa cells to determine what impact elevated ALDH6A1 may be having in MCU KO cells. Somewhat surprisingly, knocking down *ALDH6A1* had no significant impact on the

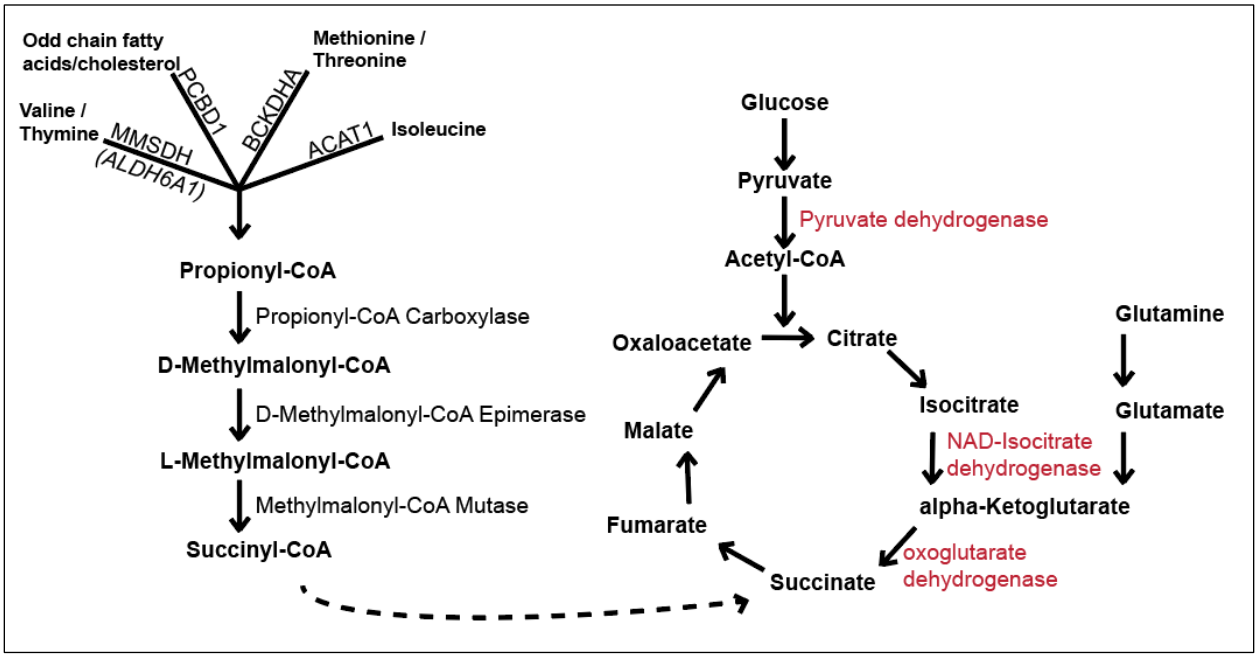

Fig. 4. propionyl-CoA/succinyl-CoA metabolism parallels the TCA cycle, before succinyl-CoA rejoins the cycle downstream of Ca^{2+}-regulated enzymes. Red enzymes are Ca^{2+}-regulated.

doubling time of wild type or MCU KO cells (**Fig. 5A**) when the cells were grown in standard DMEM media supplemented with 10% FBS and GlutaMAX™.

Though glucose is the canonical carbon chain that supplies the citric acid cycle, glutamine metabolism is significantly upregulated in many cancer cell lines and is a major source of ATP produced via oxidative phosphorylation (Altman *et al.*, 2016; Fan *et al.* 2013). Depriving normal human cells of glutamine has also been found to lead to MYC-dependent apoptosis, a fate preceded by a depletion of Krebs cycle intermediates (Yuneva *et al.*, 2007). Glutamine is notable as it contributes not just to the metabolism of carbon, but also of nitrogen; it is the dominant source of nitrogen for nonessential amino acids and hexosamines (Hensley *et al.*, 2013; Yang *et al.*, 2014). The oxidation of glutamine has been found to maintain the TCA cycle when mitochondrial pyruvate transport is impaired (Yang *et al.* 2014). Based on this body of research, we hypothesized that glutamine metabolism may be at least partially regulated by Ca^{2+}. Glutamine is

metabolized to glutamate, before entering the citric acid cycle as 2-oxoglutarate. It bears repeating that 2-oxoglutarate is both preceded and succeeded by Ca^{2+}-regulated enzymes, isocitrate dehydrogenase and the OGDH complex (**Fig. 4**). We therefore predicted that repeating the wild type versus MCU KO *ALDH6A1* knockdown experiment in glutamine-free media might reveal more dramatic differences in the response of wild type versus MCU KO cells, than growing these knocked down cells in normal glutamine-supplemented DMEM.

Our results supported the above prediction. When doubling time is calculated as a readout of cell growth raves, our results showed a significantly different degree of response to *ALDH6A1* knockdown, depending on whether knockdown was performed on WT or MCU KO cells. While the knockdown of *ALDH6A1* increased the doubling time of wild type cells from approximately 31 hours to either 57 or 73 hours, the same knock down in MCU KO cells only increased the doubling time from approximately 39 hours, to either 49 or 51 hours (**Fig. 5B**). This difference could reflect glutamine metabolism being somewhat calcium dependent. Following a conversion from glutamine to glutamate, glutamate is metabolized once again to form 2-oxoglutarate, a TCA cycle intermediate that lies between two calcium-regulated enzymes: isocitrate dehydrogenase, and OGDHC. In the absence of glutamine, wild type HeLa cells responding to *ALDH6A1* knockdown are less able to fall back on the propionyl-CoA and succinyl-CoA pathways that are upregulated in MCU KO cells (**Fig. 4**). A critical counterargument to this model would be evidence that MCU and *ALDH6A1* are inversely regulated – that is, if decreasing levels of *ALDH6A1* expression (MMSDH protein) caused increasing levels of MCU, just

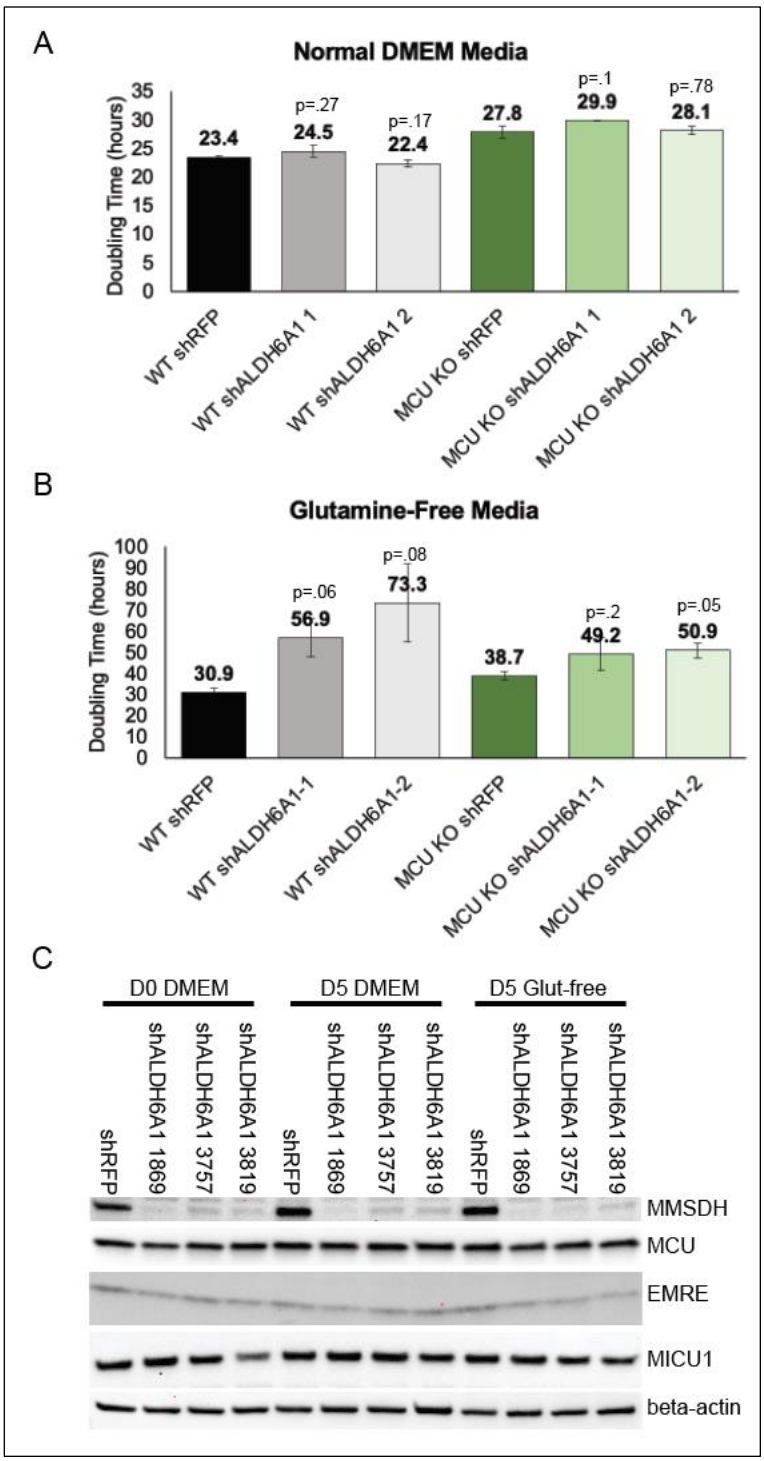

Fig. 5. Doubling times of wild HeLa cells knocked down for *ALDH6A1* slow more than those of knocked down MCU KO cells. Doubling times of wild type and MCU KO HeLa cells knocked down for ALDH6A1, normal DMEM media **(A)** versus glutamine-free DMEM media **(B)**. For **B** and **C**, p-values are calculated relative to WT or MCU shRFP control knockdown. **(C)** Validation of *ALDH6A1* knockdowns, and validation that the proteins of the uniporter complex do not change following knockdown of *ALDH6A1*.

as decreasing levels of MCU cause increased levels of *ALDH6A1* expression. If this "toggle" mechanism were true, decreased MMSDH levels and concomitant increased MCU levels might drive the TCA cycle more aggressively, negating the effects of *ALDH6A1* knockdown. But a follow up experiment examining MCU levels at different time points, in different media conditions, suggests that this is not the case (**Fig. 5C**) – *ALDH6A1* knockdown seems to have no impact on the protein levels of MCU, MICU1, or EMRE.

NEXT STEPS

Though the work shown above is centered on large, well-controlled data sets comprised of mass spectrometry and RNA-seq data, the data from many of the subsequent experiments are relatively preliminary and several key experiments solidifying the mechanistic and physiological implications of this project have not yet been performed.

One of the most informative data sets the author anticipates producing concerns the knockdown of *MUT*. *MUT* is the gene encoding the final enzyme required for metabolism of propionyl-CoA to succinyl-CoA (protein name MMUT). Though the knockdown of *ALDH6A1* was informative, the phenotype of knocked down wild type versus MCU KO cells was unimpressive in normal DMEM media, despite significant differences appearing in glutamine-free media. Multiple "sister" pathways contribute to the production of propionyl-CoA, as this structure can be catabolized from a variety of sources (amino acids; odd-chain fatty acids, etcetera). However, the catabolism pathway between propionyl-CoA and succinyl-CoA is linear and non-redundant. Knocking down MMUT will also allow us to distinguish between the entrance of acetyl-CoA into the TCA cycle from the activity of MMSDH/ACAT1, versus the entrance of succinyl-CoA into the TCA cycle from the activity of MMSDH and all the other enzymes contributing to propionyl-CoA/succinyl-CoA metabolism. These follow-up knockdown experiments will reveal valuable information about how catabolic pathways "parallel" to the citric acid cycle may allow MCU KO cells to bypass Ca^{2+}-sensitive citric acid enzymes, thus avoiding an energy/metabolic crisis.

Subsequent experiments will also explore the metabolic implications of this bypass mechanism in greater detail. By assessing the different amino acid levels, NADH:NAD^+

ratios, and citric acid cycle metabolites of MCU KO and wild type cells grown under different media conditions, as well as under conditions of *ALDH6A1* versus MMUT knockdown, we will be able to further dissect the relative contributions of propionyl-CoA/succinyl-CoA catabolism to the maintenance of cellular energy. For example, NAD^+ is known to be a redox cofactor of many enzymes, including MMSDH (Vidal *et al.* 2018); it will be informative to explore how the NADH:NAD^+ ratio is impacted by MMSDH levels and activity. Recent work by the Chaudhuri lab found that the NADH:NAD^+ ratio was reduced in MCU KO cells, though it remains unclear how this altered ratio may be related to upregulated propionyl-CoA/succinyl-CoA catabolism (Balderas *et al.*, 2022).

To further illustrate the dependence of MCU KO cells on amino acid metabolism and succinyl-CoA production, our peers have suggested that we perform growth curve experiments using media supplemented with succinate, or depleted of valine, methionine, isoleucine, threonine, or thymine, to demonstrate that MCU KO cells would grow substantially better with succinate supplementation, or substantially worse following a loss of amino acids to catabolize. We agree that these are excellent suggestions. In a similar vein, we are also interested in working with a collaborator to quantify the fatty acid levels of wild type versus MCU KO cells. If propionyl-CoA/succinyl-CoA pathways are upregulated in MCU KO cells, we hypothesize that fatty acid levels should be lower in MCU KO cells, as these molecules are being preferentially converted to propionyl-CoA.

Links between the propionyl-CoA/succinyl-CoA pathways and human disease are well established, though no work has been done to explicitly link these diseases to altered Ca^{2+} has yet been performed. For example, a deficiency in MMSDH protein can cause a rare autosomal recessive disorder characterized by metabolic abnormalities as well as

dysmyelination and transient methylmalonic aciduria (Marcadier *et al.*, 2013). *ALDH6A1* has also been identified as a prognostic and diagnostic marker for several forms of cancer. Low levels of *ALDH6A1* expression have been correlated with a worse prognosis in clear cell renal cell carcinoma (Lu *et al.*, 2020), metastatic prostate cancer (Cho *et al.*, 2018), colon adenocarcinoma (Li *et al.*, 2022), bladder cancer tissues (Guo *et al.*, 2022), and hepatocellular carcinoma (Chen *et al.*, 2017). Many of these same publications also found that increasing *ALDH6A1* expression depresses cell proliferation and migration (Lu *et al.*, 2020), or decreases cell migration and invasion, while promoting apoptosis (Li *et al.*, 2022). In a similar vein, ACAT mutations can cause beta-ketothiolase deficiency, which can manifest as episodes of ketoacidosis and damage to the nervous system. Inhibition of ACAT1 has been shown to increase pyruvate dehydrogenase complex (PDC) flux and oxidative phosphorylation, which in turn slows cancer cell proliferation and tumor growth (Fan *et al*., 2016). ACAT1 deficiency also impairs cholesterol metabolism (Dove *et al.*, 2005). Hyperinsulinemia has been linked to the progression of colon cancer (Chen *et al*., 2018), and has been shown to increase the mRNA and protein levels of ACAT1 (Chen *et al*. 2018). Implicating altered mitochondrial Ca^{2+} signaling in the progression of these diseases has the potential to clarify drugging strategies or protein drug targets.

Cancer cells have been found to upregulate the citric acid cycle and glycolysis, thus increasing the metabolites necessary for proliferation (Vasan *et al*., 2020). An emerging therapeutic approach therefore centers on halting the citric acid cycle of cancer cells by inhibiting pyruvate dehydrogenase (PDH) and 2-oxoglutarate dehydrogenase complexes (KGDH) (Pardee *et al.* 2019). Our work has the potential to elucidate the metabolic alterations that transpire when functionality of the citric acid cycle is decreased.

Furthermore, recent work by Shanmughapriya *et al*., 2018 has demonstrated that MICU1 is required for cellular differentiation, which suggests that the restoration of gated mitochondrial calcium signaling may trigger metabolic alterations in these differentiating cells (Shanmughapriya *et al*., 2018). Our work may help clarify the mechanisms underlying this shift.

METHODS and MATERIALS

Cell culture

- DMEM; Thermo Fisher Scientific, cat. no. 11-965-118
- Glutamine-free DMEM; Thermo Fisher Scientific, cat. no. 11960044
- FBS; Sigma-Aldrich, cat. no. TMS-013-B
- GlutaMAX; Thermo Fisher Scientific, cat. no. 35-050-061
- Trypsin; Gibco, cat. no. 12605-010
- PBS; Thermo Fisher Scientific, cat. no. 20012050
- Penicillin/streptomycin solution; VWR cat. no. 45000-652
- Genlantis MycoScope PCR Detection Kit; VWR cat. no. 10497-508

Cell lines

- HeLa cells: HeLa cells were acquired from the Whitehead Institute for Biomedical Research. They were grown in DMEM medium supplemented with 1× GlutaMAX and 10% FBS. The cells were tested for mycoplasma every 3 mo. using the Genlantis MycoScope PCR Detection Kit and were confirmed to be free of mycoplasma contamination. The HeLa cell line has the following short tandem repeat profile: D5S818 (11, 12); D13S317 (12, 13.3); D7S820 (8, 12); D16S539 (9, 10); vWA (16, 18); TH01 (7); AMEL (X); TPOX (8, 12); CSF1PO (9, 10). This

profile matches 94% to HeLa Cervical Adenocarcinoma (Human) (CCL-2; ATCC) according to the analysis performed by the ATCC database.

- U-2 OS cells from ATCC, cat. no. HTB-96
- AML12 cells from ATCC, cat. no. CRL-2254
- HEK cells were acquired from the Sabatini Lab at the Whitehead Institute for Biomedical Research. They were grown in DMEM medium supplemented with 1× GlutaMAX and 10% FBS. The cells were tested for mycoplasma every 3 mo. using the Genlantis MycoScope PCR Detection Kit and were confirmed to be free of mycoplasma contamination. The identity of the HEK293T cells was confirmed using short tandem repeat analysis. The HEK293T cell line has the following short tandem repeat profile: TH01 (7, 9.3); D21S11 (28, 29, 30.2); D5S818 (7, 8, 9); D13S317 (11, 12, 13, 14, 15); D7S820 (11); D16S539 (9, 13); CSF1PO (11, 12, 13); Amelogenin (X); vWA (16, 18, 19, 20); TPOX (11). This profile matches 100% to HEK293T cell line profile (CRL-3216; ATCC) if the Alternative Master's algorithm is used, and 83% if the Tanabe algorithm is used.

Gel electrophoresis and Western blotting Antibodies and dilution used for experiments

- ALDH6A1 antibody; ABclonal, cat. no. A3309 (1:3000)
- ACAT1 antibody; ABclonal, cat. no. A13273 (1:3000)
- BCKDHA antibody; ABclonal, cat. no. A21588 (1:3000)
- PCCB antibody; ABclonal, cat. no. A5415 (1:3000)
- PCBD1 antibody; ABclonal, cat. no. A9426 (1:3000)
- MCEE antibody; ABclonal, cat. no. A14430 (1:3000)
- MUT antibody; ABclonal, cat. no. A3969 (1:3000)

- MCU antibody; Sigma-Aldrich, cat. no. HPA016480-100UL (1:3000)
- EMRE antibody; Bethyl Laboratories, cat. no. A300-BL19208 (1:5000)
- MICU1 antibody; ABclonal, cat. no. A21948 (1:3000)
- Beta-actin antibody; Cell Signaling Technology, cat. no. 3700S (1:5000)
- GAPDH antibody; Cell Signaling Technology, cat. no. 5174S (1:5000)
- HRP-linked antirabbit secondary antibody; Cell Signaling Technology Cat. no. 7074S (1:10,000)
- HRP-linked anti-mouse secondary antibody; Cell Signaling Technology Cat. no. 7076S (1:10,000)

Gel electrophoresis

- 10× Tris/Glycine Buffer; Boston BioProducts, cat. no. BP-150
- 4-15% Mini-PROTEAN TGX Gels; Bio Rad, cat. no. 4561086

Western blotting

- 10× TBST-Standard (10× w/1% Tween-20, pH 7.4); Boston Bio- Products Cat. no. IBB-180
- Ethanol, 200 proof (100%); Thermo Fisher Scientific Cat. no. 04- 355-450
- Trans-Blot Turbo 5× Transfer Buffer; Bio-Rad, cat. no. 10026938
- Bovine serum albumin (BSA); Sigma-Aldrich, cat. no. A2153
- Trans-Blot Turbo RTA Mini PVDF Transfer Kit; Bio-Rad Cat. no. 1704272
- Transfer apparatus for SDS–PAGE; Bio-Rad Trans-Blot Turbo Transfer System

Bio-Rad Mixed Molecular Weight Protein Transfer setting (7 min, 1.3 A, 25 V)

- Blot imager: iBrightCL1000

- Automated Western Blot Development Processor: Precision Bio- systems BlotCycler, Model W5 100-12VAC; S/N 394387
- Clarity Max Western ECL Substrate; Bio-Rad Cat. no. 1705062
- Clarity Western ECL Substrate; Bio-Rad Cat. no. 170-5060

After transfer, the membranes were incubated with 1% BSA in TBST (wt/vol) for a minimum of 1 hour. They were then incubated overnight with primary antibodies diluted in 1% BSA in TBST (wt/vol). Afterward, all membranes were washed with TBST three times, 5 min each, and incubated for 1 h with secondary antibody diluted in 1% BSA in TBST at room temperature. The membranes were then washed four times, 5 min each, using a Precision Biosystems BlotCycler. Membranes were developed using Bio-Rad ECL substrate.

Transfer and PFA cross-linking of EMRE blots

- Transfer apparatus for SDS–PAGE; Bio-Rad Trans-Blot Turbo Transfer System

A custom 3-min transfer protocol with constant 1.3 A and 25 V was used for EMRE Western blotting

- 16% Paraformaldehyde aqueous solution; EMS/Thermo Fisher Scientific Cat. no. 50-980-487
- PBS; Thermo Fisher Scientific, Cat. no. 20012050

Protocol and reagents adapted from (Suzuki *et al.*, 2008). Immediately after transfer of proteins from the electrophoresis gel to a 0.22-μm polyvinylidene difluoride (PVDF) membrane, membranes that were to be immunoblotted for EMRE were soaked in a solution of 0.4% PFA in PBS for 30 min without agitation. The membranes were then blocked and immunoblotted normally, as described above.

Cell lysis, sample preparation, and immunoprecipitation

- Bradford Dye Reagent; Bio-Rad, Cat. no. 5000205
- BioTek Synergy H1 microplate reader
- Protease inhibitors; Sigma-Aldrich, Cat. no. 5892953001
- Lysis buffer reagents:
- 50 mM HEPES–KOH

    HEPES; Sigma-Aldrich cat. no. H3375-1KG

    KOH; Sigma Millipore cat. no. 1050121000
- 40 mM NaCl; Sigma-Aldrich cat. no. 746398-5KG
- 2 mM EDTA; Sigma-Aldrich, cat. no. 607-429-00-8
- 10 mM β-Glycerophosphate disodium salt hydrate; Sigma-Aldrich, cat. no. G9422-100G
- 1.5 mM sodium orthovanadate; Sigma-Aldrich, cat. no. S6508-50G
- 50 mM sodium fluoride; Sigma-Aldrich, cat. no. S7920-500G
- 10 mM sodium pyrophosphate; Sigma-Aldrich, cat. no. 71501-1KG
- Triton X-100; Sigma-Aldrich, Cat. no. X100-1L
- DDM; Sigma-Aldrich, Cat. no. D4641-5G

Reducing sample buffer, pH 6.8:

- SDS; Sigma-Aldrich Cat. no. L4509-1KG
- BME/2-mercaptoethanol; Sigma-Aldrich Cat. no. M3148-25ML Glycerol; Sigma-Aldrich Cat. no. G5516-1L
- Tris–HCl:

    Trizma base; Sigma-Aldrich Cat. no. RDD008

- Bromophenol Blue; VWR Cat. no. 97061-690

For standard lysis, cell plates were placed on ice and washed with cold PBS, which was then aspirated. Cells were harvested in lysis buffer supplemented with 1% Triton X-100 and proteases inhibitors; the volume of lysis buffer used varied based on downstream uses. Cells were triturated in tubes and then centrifuged at 17,000g for 10 min. Cell supernatant was quantified using a Bradford protein assay and a BioTek Synergy H1 plate reader. Sample preparation varied based on downstream applications.

HeLa, U-2 OS MCU or EMRE knockout cell line production

These sequences were generated by the Broad Institute; the human sequences originated in the Brunello genome-wide CRISPR KO library screen.

- MCU gRNA sequence: TGAACTGACAGCGTTCACGC
- EMRE gRNA sequence: GTCTCAGCCAGGTACCGTCG
- Cas plasmid: enhanced SpCas9 was ordered from Addgene, plasmid cat. no. 71814,
- M13R sequencing primer was used to sequence the sgRNA cloned into the U6 T7 minimal sgRNA plasmid.

5 million cells were suspended in 400 µl FBS-supplemented DMEM media (see above) with 2 µg Cas9 plasmid, 500 ng gRNA, and 17.5 µg pUC19 plasmid. The cells and DNA were pipetted into a cuvette, put on ice for 5 min, electroporated, and then returned to a 10 cm plate. Electroporation settings: 950 microF; 200V; pulse length: 23 msec. Electroporated cells were plated on 10 cm plates and allowed to grow to confluence before being were diluted to 1 cell/well and plated on 96-well plates to obtain single cell

clones. MCU or EMRE KO cell clones were verified by Western blotting, functional assays, and by sequencing.

HEK293T EMRE knockout cell line production

- eSpCas9(1.1) plasmid; Addgene plasmid #71814
- QIAquick PCR Purification Kit; QIAGEN, Cat. no. 28106
- dNTP set, PCR grade; QIAGEN, Cat. no. 201913
- QIAprep Spin Miniprep Kit; QIAGEN, Cat. no. 27106
- Q5 High Fidelity DNA polymerase; QIAGEN Cat. no. M0491S
- HsEMRE gRNA: GCCGGAGCCTGGTACCGTCG

MCU KO cell line was described before (Sancak *et al.*, 2013). EMRE gRNA was cloned into a gRNA expression plasmid. 600,000 cells growing on six-well plates were transfected with 250 ng of gRNA expression plasmid and 1 µg of eSpCas9(1.1) plasmid. 2 d later, cells were diluted to 1 cell/well and plated on 96-well plates to obtain single cell clones. EMRE KO cell clones were verified by Western blotting, functional assays, and by sequencing.

Generation of shRNA knockdown constructs

- pLKO.1 knockdown backbone (TRC cloning construct); Addgene plasmid # 10878
- Buffer 2; NEB cat. no. B7002S
- Quick ligase; NEB, cat. no. M2200SVIAL
- Quick ligation reaction buffer; NEB, cat. no. B2200SVIAL
- shALDH6A1 1869 (knockdown #1)
    - FWD oligo:

CCGGCCAATTCTACACTCAGTTAAACTCGAGTTTAACTGAGTGTAGAA
TTGGTTTTTG

- REV oligo:
  AATTCAAAAACCAATTCTACACTCAGTTAAACTCGAGTTTAACTGAGT
  GTAGAATTGG

- shALDH6A1 3757 (knockdown #2)
  - FWD oligo:
    CCGGCCGCTATCAACAACTTATTAACTCGAGTTAATAAGTTGTTGATA
    GCGGTTTTTG
  - REV oligo:
    AATTCAAAAACCGCTATCAACAACTTATTAACTCGAGTTAATAAGTTGT
    TGATAGCGG

shRNA hairpins were created using forward / reverse oligos designed by the RNAi Consortium (TRC) of the Broad Institute. To produce hairpins from the oligos, each oligo was resuspended in dH_2O to a concentration of 20 uM. Then, 5 µL Forward oligo, 5 µL Reverse oligo, 5 µL 10x NEB buffer 2 and 35 µL ddH2O were mixed together in a 1.7 mL Eppendorf tube. The tube was incubated for 4 minutes in a beaker of boiling water, before the heat to the water was turned off and the water was allowed to cool slowly. This slow cooling allows the oligos to anneal into a hairpin structure. 2 µl of this reaction was ligated into the pLKO.1 backbone before being transformed, plated, sequenced and used downstream.

Growth curves

On Day 0, 20,000 cells were plated in each well of a 6-well plate using “normal” (high-glucose DMEM) media and 2 mL media. On Day 1, if the experiment studied the impact of alternative media (for example: glutamine-free), the media of the wells was changed. On Days 2, 3, and 5, for counting, the media was aspirated, the cells were washed using PBS, trypsinized using 0.2 mL trypsin, and then resuspended in 1.8 mL media, for a total volume of 2 mL media. The resuspended cells were then counted.

Cell line sequencing

With the exception of the shRNA knockdown plasmids, the sequences of all genes used in this study were verified by sequencing using CMV forward primer and custom designed reverse primer (TCTCGCACATTCTTCACGTC).

The shRNA knockdown plasmids were sequenced using Azenta’s in-house U6 sequencing primer.

Lentivirus production and infection

- X-treme(GENE) 9 DNA Transfection Reagent; Sigma-Aldrich, cat. no. 6365779001
- psPax2; Addgene cat. no. 12260
- VSV-G; Addgene, cat. no. 8454
- Puromycin dihydrochloride; VWR, cat. no. 62111-170
- Hygromycin B Solution; VWR, cat. no. 45000-806
- Hexadimethrine bromide/polybrene; Sigma-Aldrich cat. no. H9268-10G
- DMEM; Thermo Fisher Scientific, cat. no. 11-965-118
- Filter; VWR, cat. no. 28145-505
- Syringe; VWR, cat. no. 28200-042

Lentivirus production: 1 million HEK293T cells were plated in 6-cm plates in 5 ml of media. 1 d later, the cells were transfected with viral mix. To prepare the viral mix, 100 ng VSV-G, 900 ng psPax2, 1.6 µg viral plasmid, dH2O to 10 µl, and 150 µl DMEM mixed with 7.5 µl X-treme(GENE) and incubated for 30 min at room temperature before being added to the cells and mixed. 2 days later, the medium—which now contained the virus of interest—was filtered through a 0.45 µm sterile filter attached to a syringe. The virus was stored at −80°C until use.

Lentivirus infection: 250K cells (HEK293T, HeLa or otherwise) were plated in a six-well dish containing 2 ml media. The following day, between 200 and 500 µl of the virus-containing media and 2 µl of polybrene from an 8-mg/ml stock solution was added to a final concentration of 8 µg/ml. Polybrene stock solution was prepared in water, filter sterilized and stored at −20°C for long term storage and at 4°C for short term storage. 2 d later, the cells were split and transferred to 10 cm tissue culture plates and selected. Infected cells were selected using either 1 µg/ml puromycin from a 1 mg/ml puromycin stock solution that was prepared in water, filter-sterilized, and stored at −20°C for long-term storage and at 4°C for short-term storage; or 200 µg/ml from a 50 mg/ml hygromycin stock solution that was prepared in water, filter sterilized, and stored at 4°C.

Calcium uptake in permeabilized cells

- Digitonin; Thermo Fisher Scientific, cat. no. BN2006
- Oregon Green 488 Bapta-6F; Invitrogen, cat. no. O23990
- L-Glutamic acid; Sigma-Aldrich cat. no. G1251-1KG
- L-(-)-Malic Acid; Sigma-Aldrich cat. no. M7397-25G
- KCl buffer:

KCl; Sigma-Aldrich, cat. no. 793590-1KG

K2HPO4 Sigma-Aldrich, cat. no. P3786-1KG

MgCl2 Sigma-Aldrich, cat. no. M8266-1KG

HEPES Sigma-Aldrich, cat. no. H3375-1KG

- EGTA; Sigma-Aldrich cat. no. E3889

Protocol and reagents adapted from Sancak *et al.* (2013). For all cell types: cells grown in 10-cm tissue culture plates were trypsinized and resuspended in 10 ml of prepared media. 1 million cells transferred to microcentrifuge tubes and spun down for 3 min at 800g at room temperature to pellet cells. Cells were washed with PBS once and resuspended in KCl buffer (125 mM KCl, 2 mM K2HPO4, 1 mM MgCl2, 20 mM HEPES, pH 7.2), supplemented with 5 mM glutamate/malate from a 500 mM G/M stock solution that was filtered and stored at −20°C, 0.005% digitonin (HEK 293T cells) or 0.01% digitonin (HeLa or U-2 OS cells), and 1 μM Oregon Green Bapta 6F.

Fluorescence was monitored for 137 s every 2 s at room temperature (~25°C) using a BioTek Synergy H1 microplate reader before and after injection of 50 μM CaCl2 from a 500-μM stock prepared in dH2O. Fluorescence was recorded using a fluorescent green filter set to 485/20 excitation, 528/20 emission. Calcium uptake rates were calculated using the linear fit of uptake curves between 20 and 30 s after calcium injection. A maximum of eight samples were assayed together, including one wild type control per assay run. To calculate calcium uptake rates relative to wild type, the wild-type rate for each sample set was set at 100%. Calculating experimental calcium uptake rate yielded the relative calcium uptake rate. For each figure, each proportional experimental calcium uptake rate is plotted relative to its corresponding wild type calcium uptake rate.

RNA sequencing

- RNeasy kit; Qiagen, cat. no. 74106

0.5M HeLa cells were plates in 6-well plates (WT and MCU KO #18 cells.) Two days later, total RNA was isolated using Qiagen RNasy kit. Samples were sent to Genewiz for sequencing and data analysis.

Genewiz performed the following workflow:

First, Genewiz performed mRNA enrichment, mRNA fragmentation, and random priming. Next, they performed first and second strand cDNA synthesis before performing end repair, 5' phosphorylation, and dA-Tailing. Finally, they performed adaptor ligation, PCR enrichment, and sequencing.

Genewiz's bioinformatics analysis workflow consisted of evaluating sequence quality, trimming reads, mapping the reads to the genome, generating hit counts for genes/exons, and then comparing gene hit counts and exon hit counts. Gene ontology of gene hit counts was then analyzed.

For mapping sequence reads to the reference genome: Sequence reads were trimmed to remove possible adapter sequences and nucleotides with poor quality using Trimmomatic v.0.36. The trimmed reads were mapped to the Homo sapiens GRCh38 reference genome available on ENSEMBL using the STAR aligner v.2.5.2b. The STAR aligner is a splice aligner that detects splice junctions and incorporates them to help align the entire read sequences. BAM files were generated as a result of this step.

For extracting gene hit counts: Unique gene hit counts were calculated by using featureCounts from the Subread package v.1.5.2. The hit counts were summarized and reported using the gene_id feature in the annotation file. Only unique reads that fell within

exon regions were counted. Since a strand-specific library preparation was performed, the reads were strand-specifically counted.

Differential gene expression analysis: After extraction of gene hit counts, the gene hit counts table was used for downstream differential expression analysis. Using DESeq2, a comparison of gene expression between the customer-defined groups of samples was performed. The Wald test was used to generate p-values and log2 fold changes. Genes with an adjusted p-value < 0.05 and absolute log2 fold change > 1 were called as differentially expressed genes for each comparison.

Gene ontology analysis: A gene ontology analysis was performed on the statistically significant set of genes by implementing the software GeneSCF v.1.1-p2. The goa_human GO list was used to cluster the set of genes based on their biological processes and determine their statistical significance. A list of genes clustered based on their gene ontologies was generated.

Splice variant expression analysis: To estimate the expression levels of alternatively spliced transcripts, the splice variant hit counts were extracted from the RNA-seq reads mapped to the genome. Differentially spliced genes were identified for groups with more than one sample by testing for significant differences in read counts on exons (and junctions) of the genes using DEXSeq. For groups with only one sample, the exon hit count tables were provided.

Mass Spectrometry (methods adapted from Golkowski et al*., 2017)*

500,000 WT and MCU KO HeLa cells were plated in 10 cm plates, five replicates. 48 hours later, the media was aspirated, cells were washed with cold PBS, and cells were lysed using 350 µl lysis buffer. Cells were sonicated on ice using the following settings:

100 amplitude, 10 min processing, 30 seconds on / 30 seconds off. Samples were then shaken at max speed for 30 min at 37C. Samples were then centrifuged for 10 min at 4C, max speed, before the supernatant was transferred to two 1 mL tubes per sample. The pellet was discarded. Next, 700 µl -20C acetone was added to each tube (acetone was 4X the volume of the cleared lysate). 5% tube volume of trichloroacetic acid (TCA) was then added to each tube. The samples were then vortexed briefly at max speed and stored at -20C overnight.

Samples were spun down at 6000 rcf for 10 min at 4C. The supernatant was aspirated. 500 µl ice-cold acetone was added to the pellet, and the pellet was sonicated in a water bath before being stored on ice for 10-15 min. Tubes were then spun down at 4C for 10 min, 6000 rcf. The supernatant was aspirated, and the tubes were air dried for 2-3 min. 200 µl 8M urea and 100 mM Tris solution was then added to the sample. Samples were then put into a 37C shaker for 1 hour to resuspend pellet in solution. Protein was quantified and 1 mg of protein per sample was used for downstream processing / experiments. Samples were suspended in equal volume 8M urea / 100 mM Tris. 1X sample volume triethyl ammonium bicarbonate (TEAB) was then added to each tube to reduce urea concentration to 4M. Lys-C endoproteinase (stock 2 µg/µl) was added to 1:100 enzyme:protein ratio. Samples were vortexed and shaken at 37C for 2 hours at max speed. 1X total volume TEAB was added to samples once again, to dilute urea concentration to 2M. Trypsin dissolved in 40 mM acetic acid was then added in a 1:100 enzyme:protein ratio; trypsin stored as a 0.5 µg/µl stock. Samples were shaken overnight at 37C, max speed.

The next day, formic acid was added to 2% total sample volume. Digested protein samples were spun down for 5 min at 11000g.

5% of the supernatant was used for stage tipping: Methanol > Buffer B > Buffer A > Sample > Buffer A. Buffer A: 5% Acetonitrile, 0.1% TFA; Buffer B: 80% Acetonitrile (ACN), 0.1% Trifluoracetic Acid (TFA).

For LC-MS/MS and data analysis: Peptides were separated on a Thermo-Dionex RSLCNano UHPLC instrument (Sunnyvale, CA) with 10 cm long fused silica capillary columns made in-house with a laser puller (Sutter, Novato CA) and packed with 3 micron reversed phase C18 beads. The LC gradient was 90 min long with 3–35% B at 200 nL/min. LC solvent A was 0.1% acetic acid and LC solvent B was 0.1% acetic acid, 99.9% acetonitrile. MS data was collected with a Thermo Orbitrap Elite. Data-dependent analysis was applied using Top15 selection with CID fragmentation. Raw files were analyzed by MaxQuant version 1.5.2.8 using protein, peptide and site FDRs of 0.01 and a score minimum of 40 for modified peptides, 0 for unmodified peptides; delta score minimum of 17 for modified peptides, 0 for unmodified peptides. MS/MS spectra were searched against the UniProt human database. MaxQuant search parameters: Variable modifications included Oxidation (M), phosphorylation (STY). Carbamidomethyl (C) was a fixed modification. Max. labeled amino acids was 3, max. missed cleavages was 2, enzyme was Trypsin/P, max charge was 7, multiplicity was 3. The initial search tolerance for FTMS scans was 20 ppm and 0.5 Da for ITMS MS/MS scans. Data was further processed using the Perseus software package (version 1.5.2.6), the R environment, Origin Pro 8.0 and Microsoft Excel. GO term enrichment analysis was performed using the GOrilla web application (http://cbl-gorilla.cs.technion.ac.il/) [23].

Generation of mice with liver-specific MCU knockout:

Mice were produced as in (Flicker *et al*., 2019)

Western blotting of mouse tissue

Animals were sacrificed by CO2 asphyxiation followed by cervical dislocation. Tissues were immediately harvested and snap frozen in liquid N2. For preparation of protein lysates, a small tissue sample was put in 750 µl of RIPA buffer supplemented with either cOmplete EDTA-free protease inhibitor cocktail. The tissue was then lysed with QIAGEN TissueRuptor until no solid tissue was observed (10-40 seconds). The resulting homogenate was centrifuged for 10 mins at maximum speed at 4°C, and the supernatant was centrifuged a second time to remove residual insoluble material, and any fat residue on top of the lysate was aspirated. Protein content of the resulting clarified lysate was determined using a Bradford assay. Appropriate volumes of lysate were boiled for 5 mins in the presence of SDS sample buffer. Lysates were then resolved on Tris-Glycine SDS-PAGE gels, and transferred to PVDF membranes for western blotting as per protocol above.

ACKNOWLEDGEMENTS

We are grateful to Dr. Vishal Gohil and the members of the Seattle Organelle Biology Interest Group (SOBIG) for their thoughtful discussion of this project. MJS MacEwen was supported by grant number 1F31AG072716-01A1 from the National Institute on Aging (NIA), National Institutes of Health (NIH). YS is a Pew Charitable Trust Fellow.

AUTHOR CONTRIBUTIONS

- MJS MacEwen: conceptualization, data collection, data analysis, funding acquisition, validation, visualization, methodology, and writing
- Y Sancak: conceptualization, data collection, data analysis, supervision, funding acquisition, validation, investigation, visualization, methodology, and writing

CONFLICT OF INTEREST STATEMENT

The authors have no conflicts of interest to disclose.

REFERENCES

- Altman, B. J., Stine, Z. E., & Dang, C. V. (2016). From Krebs to clinic: glutamine metabolism to cancer therapy. Nature reviews. Cancer, 16(11), 749. https://doi.org/10.1038/nrc.2016.114
- Álvarez-Illera, P., García-Casas, P., Fonteriz, R. I., Montero, M., & Alvarez, J. (2020). Mitochondrial Ca2+ Dynamics in MCU Knockout C. elegans Worms. International journal of molecular sciences, 21(22), 8622. https://doi.org/10.3390/ijms21228622
- Balderas, E., Eberhardt, D. R., Lee, S., Pleinis, J. M., Sommakia, S., Balynas, A. M., Yin, X., Parker, M. C., Maguire, C. T., Cho, S., Szulik, M. W., Bakhtina, A., Bia, R. D., Friederich, M. W., Locke, T. M., Van Hove, J. L. K., Drakos, S. G., Sancak, Y., Tristani-Firouzi, M., Franklin, S., … Chaudhuri, D. (2022). Mitochondrial calcium uniporter stabilization preserves energetic homeostasis during Complex I impairment. Nature communications, 13(1), 2769. https://doi.org/10.1038/s41467-022-30236-4
- Bisbach, C. M., Hutto, R. A., Poria, D., Cleghorn, W. M., Abbas, F., Vinberg, F., Kefalov, V. J., Hurley, J. B., & Brockerhoff, S. E. (2020). Mitochondrial Calcium

Uniporter (MCU) deficiency reveals an alternate path for Ca2+ uptake in photoreceptor mitochondria. Scientific reports, 10(1), 16041. https://doi.org/10.1038/s41598-020-72708-x

- Bulthuis, E.P., Adjobo-Hermans, M.J.W., de Potter, B., Hoogstraten, S., Wezendonk, L.H.T., Tutakhel, O.A.Z., Wintjes, L.T., van den Heuvel, B., Willems, P.H.G.M., Kamsteeg, E.-J., et al. (2022). SMDT1 variants impair EMRE-mediated mitochondrial calcium uptake in patients with muscle involvement. bioRxiv, 2022.2010.2031.514480. 10.1101/2022.10.31.514480.
- Chaudhuri, D., Sancak, Y., Mootha, V. K., & Clapham, D. E. (2013). MCU encodes the pore conducting mitochondrial calcium currents. eLife, 2, e00704. https://doi.org/10.7554/eLife.00704
- Chen, P., Wang, F., Feng, J., Zhou, R., Chang, Y., Liu, J., & Zhao, Q. (2017). Co-expression network analysis identified six hub genes in association with metastasis risk and prognosis in hepatocellular carcinoma. Oncotarget, 8(30), 48948–48958. https://doi.org/10.18632/oncotarget.16896
- Chen, X., Liang, H., Song, Q., Xu, X., & Cao, D. (2018). Insulin promotes progression of colon cancer by upregulation of ACAT1. Lipids in health and disease, 17(1), 122. https://doi.org/10.1186/s12944-018-0773-x
- Cho, S. Y., Kang, S., Kim, D. S., Na, H. J., Kim, Y. J., Choi, Y. D., & Cho, N. H. (2018). HSP27, ALDH6A1 and Prohibitin Act as a Trio-biomarker to Predict Survival in Late Metastatic Prostate Cancer. Anticancer research, 38(11), 6551–6560. https://doi.org/10.21873/anticanres.13021

- Choi, S., Quan, X., Bang, S., Yoo, H., Kim, J., Park, J., Park, K. S., & Chung, J. (2017). Mitochondrial calcium uniporter in Drosophila transfers calcium between the endoplasmic reticulum and mitochondria in oxidative stress-induced cell death. The Journal of biological chemistry, 292(35), 14473–14485. https://doi.org/10.1074/jbc.M116.765578
- Csordas, G., Golenar, T., Seifert, E.L., Kamer, K.J., Sancak, Y., Perocchi, F., Moffat, C., Weaver, D., Perez, S.F., Bogorad, R., et al. (2013). MICU1 controls both the threshold and cooperative activation of the mitochondrial Ca(2)(+) uniporter. Cell Metab 17, 976-987. 10.1016/j.cmet.2013.04.020.
- Denton R. M. (2009). Regulation of mitochondrial dehydrogenases by calcium ions. Biochimica et biophysica acta, 1787(11), 1309–1316. https://doi.org/10.1016/j.bbabio.2009.01.005
- Dove, D. E., Su, Y. R., Zhang, W., Jerome, W. G., Swift, L. L., Linton, M. F., & Fazio, S. (2005). ACAT1 deficiency disrupts cholesterol efflux and alters cellular morphology in macrophages. Arteriosclerosis, thrombosis, and vascular biology, 25(1), 128–134. https://doi.org/10.1161/01.ATV.0000148323.94021.e5
- Fan, J., Kamphorst, J. J., Mathew, R., Chung, M. K., White, E., Shlomi, T., & Rabinowitz, J. D. (2013). Glutamine-driven oxidative phosphorylation is a major ATP source in transformed mammalian cells in both normoxia and hypoxia. Molecular systems biology, 9, 712. https://doi.org/10.1038/msb.2013.65
- Fan, J., Lin, R., Xia, S., Chen, D., Elf, S. E., Liu, S., Pan, Y., Xu, H., Qian, Z., Wang, M., Shan, C., Zhou, L., Lei, Q. Y., Li, Y., Mao, H., Lee, B. H., Sudderth, J., DeBerardinis, R. J., Zhang, G., Owonikoko, T., … Chen, J. (2016). Tetrameric

Acetyl-CoA Acetyltransferase 1 Is Important for Tumor Growth. Molecular cell, 64(5), 859–874. https://doi.org/10.1016/j.molcel.2016.10.014

- Flicker, D., Sancak, Y., Mick, E., Goldberger, O., & Mootha, V. K. (2019). Exploring the In Vivo Role of the Mitochondrial Calcium Uniporter in Brown Fat Bioenergetics. Cell reports, 27(5), 1364–1375.e5. https://doi.org/10.1016/j.celrep.2019.04.013
- Gherardi, G., Nogara, L., Ciciliot, S., Fadini, G. P., Blaauw, B., Braghetta, P., Bonaldo, P., De Stefani, D., Rizzuto, R., & Mammucari, C. (2019). Loss of mitochondrial calcium uniporter rewires skeletal muscle metabolism and substrate preference. Cell death and differentiation, 26(2), 362–381. https://doi.org/10.1038/s41418-018-0191-7
- Golkowski, M., Shimizu-Albergine, M., Suh, H. W., Beavo, J. A., & Ong, S. E. (2016). Studying mechanisms of cAMP and cyclic nucleotide phosphodiesterase signaling in Leydig cell function with phosphoproteomics. *Cellular signalling*, *28*(7), 764–778. https://doi.org/10.1016/j.cellsig.2015.11.014
- Guo, Q., Zhang, T., Gong, Y., Tao, Y., Gao, Y., Wang, Y., Tian, J., Zhang, S., Wang, H., Rodriguez, R., & Wang, Z. (2022). Aldehyde dehydrogenase 6 family member A1 negatively regulates cell growth and to cisplatin sensitivity in bladder cancer. Molecular carcinogenesis, 61(7), 690–701. https://doi.org/10.1002/mc.23411
- Harrington, J. L., & Murphy, E. (2015). The mitochondrial calcium uniporter: mice can live and die without it. Journal of molecular and cellular cardiology, 78, 46–53. https://doi.org/10.1016/j.yjmcc.2014.10.013

- Hensley, C. T., Wasti, A. T., & DeBerardinis, R. J. (2013). Glutamine and cancer: cell biology, physiology, and clinical opportunities. The Journal of clinical investigation, 123(9), 3678–3684. https://doi.org/10.1172/JCI69600
- Huo, J., Lu, S., Kwong, J.Q., Bround, M.J., Grimes, K.M., Sargent, M.A., Brown, M.E., Davis, M.E., Bers, D.M., and Molkentin, J.D. (2020). MCUb Induction Protects the Heart From Postischemic Remodeling. Circ Res 127, 379-390. 10.1161/CIRCRESAHA.119.316369.
- Kedishvili, N. Y., Goodwin, G. W., Popov, K. M., & Harris, R. A. (2000). Mammalian methylmalonate-semialdehyde dehydrogenase. Methods in enzymology, 324, 207–218. https://doi.org/10.1016/s0076-6879(00)24233-x
- Kwong, J. Q., Lu, X., Correll, R. N., Schwanekamp, J. A., Vagnozzi, R. J., Sargent, M. A., York, A. J., Zhang, J., Bers, D. M., & Molkentin, J. D. (2015). The Mitochondrial Calcium Uniporter Selectively Matches Metabolic Output to Acute Contractile Stress in the Heart. Cell reports, 12(1), 15–22. https://doi.org/10.1016/j.celrep.2015.06.002
- Li, X., Wang, N., Wu, Y., Liu, Y., & Wang, R. (2022). ALDH6A1 weakens the progression of colon cancer via modulating the RAS/RAF/MEK/ERK pathway in cancer cell lines. Gene, 842, 146757. https://doi.org/10.1016/j.gene.2022.146757
- Liu, J. C., Syder, N. C., Ghorashi, N. S., Willingham, T. B., Parks, R. J., Sun, J., Fergusson, M. M., Liu, J., Holmström, K. M., Menazza, S., Springer, D. A., Liu, C., Glancy, B., Finkel, T., & Murphy, E. (2020). EMRE is essential for mitochondrial calcium uniporter activity in a mouse model. JCI insight, 5(4), e134063. https://doi.org/10.1172/jci.insight.134063

- Liu, J.C., Liu, J., Holmstrom, K.M., Menazza, S., Parks, R.J., Fergusson, M.M., Yu, Z.X., Springer, D.A., Halsey, C., Liu, C., et al. (2016). MICU1 Serves as a Molecular Gatekeeper to Prevent In Vivo Mitochondrial Calcium Overload. Cell Rep 16, 1561-1573. 10.1016/j.celrep.2016.07.011.
- Lu, J., Chen, Z., Zhao, H., Dong, H., Zhu, L., Zhang, Y., Wang, J., Zhu, H., Cui, Q., Qi, C., Wang, S., Chen, S., & Shao, J. (2020). ABAT and ALDH6A1, regulated by transcription factor HNF4A, suppress tumorigenic capability in clear cell renal cell carcinoma. Journal of translational medicine, 18(1), 101. https://doi.org/10.1186/s12967-020-02268-1
- Luongo, T. S., Lambert, J. P., Yuan, A., Zhang, X., Gross, P., Song, J., Shanmughapriya, S., Gao, E., Jain, M., Houser, S. R., Koch, W. J., Cheung, J. Y., Madesh, M., & Elrod, J. W. (2015). The Mitochondrial Calcium Uniporter Matches Energetic Supply with Cardiac Workload during Stress and Modulates Permeability Transition. Cell reports, 12(1), 23–34. https://doi.org/10.1016/j.celrep.2015.06.017
- Marcadier, J. L., Smith, A. M., Pohl, D., Schwartzentruber, J., Al-Dirbashi, O. Y., FORGE Canada Consortium, Majewski, J., Ferdinandusse, S., Wanders, R. J., Bulman, D. E., Boycott, K. M., Chakraborty, P., & Geraghty, M. T. (2013). Mutations in ALDH6A1 encoding methylmalonate semialdehyde dehydrogenase are associated with dysmyelination and transient methylmalonic aciduria. Orphanet journal of rare diseases, 8, 98. https://doi.org/10.1186/1750-1172-8-98
- Murphy, E., Pan, X., Nguyen, T., Liu, J., Holmström, K. M., & Finkel, T. (2014). Unresolved questions from the analysis of mice lacking MCU expression.

Biochemical and biophysical research communications, 449(4), 384–385. https://doi.org/10.1016/j.bbrc.2014.04.144

- Palty, R., Silverman, W. F., Hershfinkel, M., Caporale, T., Sensi, S. L., Parnis, J., Nolte, C., Fishman, D., Shoshan-Barmatz, V., Herrmann, S., Khananshvili, D., & Sekler, I. (2010). NCLX is an essential component of mitochondrial Na+/Ca2+ exchange. Proceedings of the National Academy of Sciences of the United States of America, 107(1), 436–441. https://doi.org/10.1073/pnas.0908099107
- Pan, X., Liu, J., Nguyen, T., Liu, C., Sun, J., Teng, Y., Fergusson, M. M., Rovira, I. I., Allen, M., Springer, D. A., Aponte, A. M., Gucek, M., Balaban, R. S., Murphy, E., & Finkel, T. (2013). The physiological role of mitochondrial calcium revealed by mice lacking the mitochondrial calcium uniporter. Nature cell biology, 15(12), 1464–1472. https://doi.org/10.1038/ncb2868
- Pardee, T. S., Luther, S., Buyse, M., Powell, B. L., & Cortes, J. (2019). Devimistat in combination with high dose cytarabine and mitoxantrone compared with high dose cytarabine and mitoxantrone in older patients with relapsed/refractory acute myeloid leukemia: ARMADA 2000 Phase III study. Future oncology (London, England), 15(28), 3197–3208. https://doi.org/10.2217/fon-2019-0201
- Perocchi, F., Gohil, V.M., Girgis, H.S., Bao, X.R., McCombs, J.E., Palmer, A.E., and Mootha, V.K. (2010). MICU1 encodes a mitochondrial EF hand protein required for Ca(2+) uptake. Nature 467, 291-296. 10.1038/nature09358.
- Pinton, P., Giorgi, C., Siviero, R., Zecchini, E., and Rizzuto, R. (2008). Calcium and apoptosis: ER-mitochondria Ca2+ transfer in the control of apoptosis. Oncogene 27, 6407-6418. 10.1038/onc.2008.308.

- Rasmussen, T. P., Wu, Y., Joiner, M. L., Koval, O. M., Wilson, N. R., Luczak, E. D., Wang, Q., Chen, B., Gao, Z., Zhu, Z., Wagner, B. A., Soto, J., McCormick, M. L., Kutschke, W., Weiss, R. M., Yu, L., Boudreau, R. L., Abel, E. D., Zhan, F., Spitz, D. R., … Anderson, M. E. (2015). Inhibition of MCU forces extramitochondrial adaptations governing physiological and pathological stress responses in heart. Proceedings of the National Academy of Sciences of the United States of America, 112(29), 9129–9134. https://doi.org/10.1073/pnas.1504705112
- Sancak, Y., Markhard, A.L., Kitami, T., Kovacs-Bogdan, E., Kamer, K.J., Udeshi, N.D., Carr, S.A., Chaudhuri, D., Clapham, D.E., Li, A.A., et al. (2013). EMRE is an essential component of the mitochondrial calcium uniporter complex. Science 342, 1379-1382. 10.1126/science.1242993.
- Sellés Vidal, L., Kelly, C. L., Mordaka, P. M., & Heap, J. T. (2018). Review of NAD(P)H-dependent oxidoreductases: Properties, engineering and application. Biochimica et biophysica acta. Proteins and proteomics, 1866(2), 327–347. https://doi.org/10.1016/j.bbapap.2017.11.005
- Shanmughapriya, S., Tomar, D., Dong, Z., Slovik, K. J., Nemani, N., Natarajaseenivasan, K., Carvalho, E., Lu, C., Corrigan, K., Garikipati, V. N. S., Ibetti, J., Rajan, S., Barrero, C., Chuprun, K., Kishore, R., Merali, S., Tian, Y., Yang, W., & Madesh, M. (2018). FOXD1-dependent MICU1 expression regulates mitochondrial activity and cell differentiation. Nature communications, 9(1), 3449. https://doi.org/10.1038/s41467-018-05856-4
- Suzuki Y, Takeda Y, Ikuta T (2008) Immunoblotting conditions for human hemoglobin chains. Anal Biochem 378: 218–220. doi:10.1016/ j.ab.2008.04.008

- Traaseth, N., Elfering, S., Solien, J., Haynes, V., & Giulivi, C. (2004). Role of calcium signaling in the activation of mitochondrial nitric oxide synthase and citric acid cycle. Biochimica et biophysica acta, 1658(1-2), 64–71. https://doi.org/10.1016/j.bbabio.2004.04.015
- Vasan, K., Werner, M., & Chandel, N. S. (2020). Mitochondrial Metabolism as a Target for Cancer Therapy. Cell metabolism, 32(3), 341–352. https://doi.org/10.1016/j.cmet.2020.06.019
- Wan, B., LaNoue, K. F., Cheung, J. Y., & Scaduto, R. C., Jr (1989). Regulation of citric acid cycle by calcium. The Journal of biological chemistry, 264(23), 13430–13439.
- Wang, P., Fernandez-Sanz, C., Wang, W., & Sheu, S. S. (2020). Why don't mice lacking the mitochondrial Ca2+ uniporter experience an energy crisis?. The Journal of physiology, 598(7), 1307–1326. https://doi.org/10.1113/JP276636
- Wu, Y., Rasmussen, T. P., Koval, O. M., Joiner, M. L., Hall, D. D., Chen, B., Luczak, E. D., Wang, Q., Rokita, A. G., Wehrens, X. H., Song, L. S., & Anderson, M. E. (2015). The mitochondrial uniporter controls fight or flight heart rate increases. Nature communications, 6, 6081. https://doi.org/10.1038/ncomms7081
- Yang, C., Ko, B., Hensley, C. T., Jiang, L., Wasti, A. T., Kim, J., Sudderth, J., Calvaruso, M. A., Lumata, L., Mitsche, M., Rutter, J., Merritt, M. E., & DeBerardinis, R. J. (2014). Glutamine oxidation maintains the TCA cycle and cell survival during impaired mitochondrial pyruvate transport. Molecular cell, 56(3), 414–424. https://doi.org/10.1016/j.molcel.2014.09.025

- Yuneva, M., Zamboni, N., Oefner, P., Sachidanandam, R., & Lazebnik, Y. (2007). Deficiency in glutamine but not glucose induces MYC-dependent apoptosis in human cells. The Journal of cell biology, 178(1), 93–105. https://doi.org/10.1083/jcb.200703099

CHAPTER 5:

Mathematical modeling and biochemical analysis support partially ordered CaM-MLCK binding

Melissa JS MacEwen[1], Domnita-Valeria Rusnac[1], Henok Ermias[1], Timothy M Locke[1], Hayden E Gizinski[1], Joseph P Dexter[2*], Yasemin Sancak[1*3]

iScience

Published 4 February 2023

DOI: https://doi.org/10.1016/j.isci.2023.106146

[1]Department of Pharmacology, University of Washington, Seattle, WA, 98195, USA.

[2]Data Science Initiative and Department of Human Evolutionary Biology, Harvard University, Cambridge, MA, 02138 USA

[3]Lead contact

*Co-corresponding authors: jdexter@fas.harvard.edu, sancak@uw.edu

ABSTRACT

Activation of myosin light chain kinase (MLCK) by calcium ions (Ca^{2+}) and calmodulin (CaM) plays an important role in numerous cellular functions including vascular smooth muscle contraction and cellular motility. Despite extensive biochemical analysis, aspects of the mechanism of activation remain controversial, and competing theoretical models have been proposed for the binding of Ca^{2+} and CaM to MLCK. The models are analytically solvable for an equilibrium steady state and give rise to distinct predictions that hold regardless of the numerical values assigned to parameters. These predictions form the basis of a recently proposed, multi-part experimental strategy for model discrimination. Here we implement this strategy by measuring CaM-MLCK binding using an *in vitro* FRET system. Interpretation of binding data in light of the mathematical models suggests a partially ordered mechanism for binding of CaM to MLCK. Complementary data collected using orthogonal approaches that directly quantify CaM-MLCK binding further supports this conclusion.

INTRODUCTION

Calmodulin (CaM) is a calcium-binding protein found ubiquitously in the cytosol of eukaryotic cells. CaM contains two globular domains joined by a flexible linker. The N-terminus and C-terminus domains each have a pair of EF-hand motifs and are each capable of binding two calcium ions (Ca^{2+}) (Babu *et al.*, 1985). CaM acts as a regulator or effector in numerous cellular processes, ranging from muscle contraction to glycogen metabolism and synaptic plasticity (Swulius & Waxham, 2008; Webb, 2003; Xia & Storm, 2005). The Ca^{2+}-mediated binding of CaM and either smooth muscle myosin light chain kinase or nonmuscle myosin light chain kinase (henceforth collectively referred to as

"MLCK") is central to functions such as vascular smooth muscle contraction and cell motility. CaM-MLCK binding takes place as follows: Ca^{2+} enters the cytosol and binds to the four Ca^{2+} binding sites of CaM, leading to a dramatic change in CaM protein conformation (Park *et al.*, 2008). CaM then binds to the CaM-binding domain of MLCK, triggering a conformational change in MLCK that activates the kinase by displacing an autoinhibitory sequence from the kinase's catalytic domain (Adelstein & Sellers, 1987; Hong *et al.*, 2011). Finally, activated MLCK phosphorylates the 20-kDa regulatory light chains of myosin II, resulting in contraction caused by myosin cross-bridges moving along actin filaments.

Multiple formal models have been proposed for the activation of MLCK by Ca^{2+} and CaM (Brown *et al.*, 1997; Fajmut, Brumen *et al.*, 2005; Fajmut, Jagodic *et al.*, 2005; Kato *et al.*, 1984). Given the cooperative nature of Ca^{2+} binding at both the C- and N-terminus of CaM, each of these models treats CaM as having two Ca^{2+} binding sites. The model of Brown *et al.*, 1997 and Fajmut, Brumen *et al.*, 2005 makes no further assumptions, giving rise to an eight-state reaction network in which MLCK may bind to CaM before or after Ca^{2+} ("Model 1" in **Fig. 1A**). Other previously proposed models are truncations of this network, in which the binding of Ca^{2+} and MLCK is either partially (Fajmut, Jagodic *et al.*, 2005) or fully (Kato *et al.*, 1984) ordered ("Model 2" and "Model 3" in **Fig. 1A**, respectively). Accordingly, Model 1 corresponds to a fully random binding mechanism (Ca^{2+} and MLCK can bind to CaM in any order), Model 2 to a partially ordered mechanism (MLCK can bind to CaM after Ca^{2+} is bound at the C-terminus), and Model 3 to a fully ordered mechanism (MLCK can bind to CaM only after Ca^{2+} is bound at both the C-terminus and N-terminus).

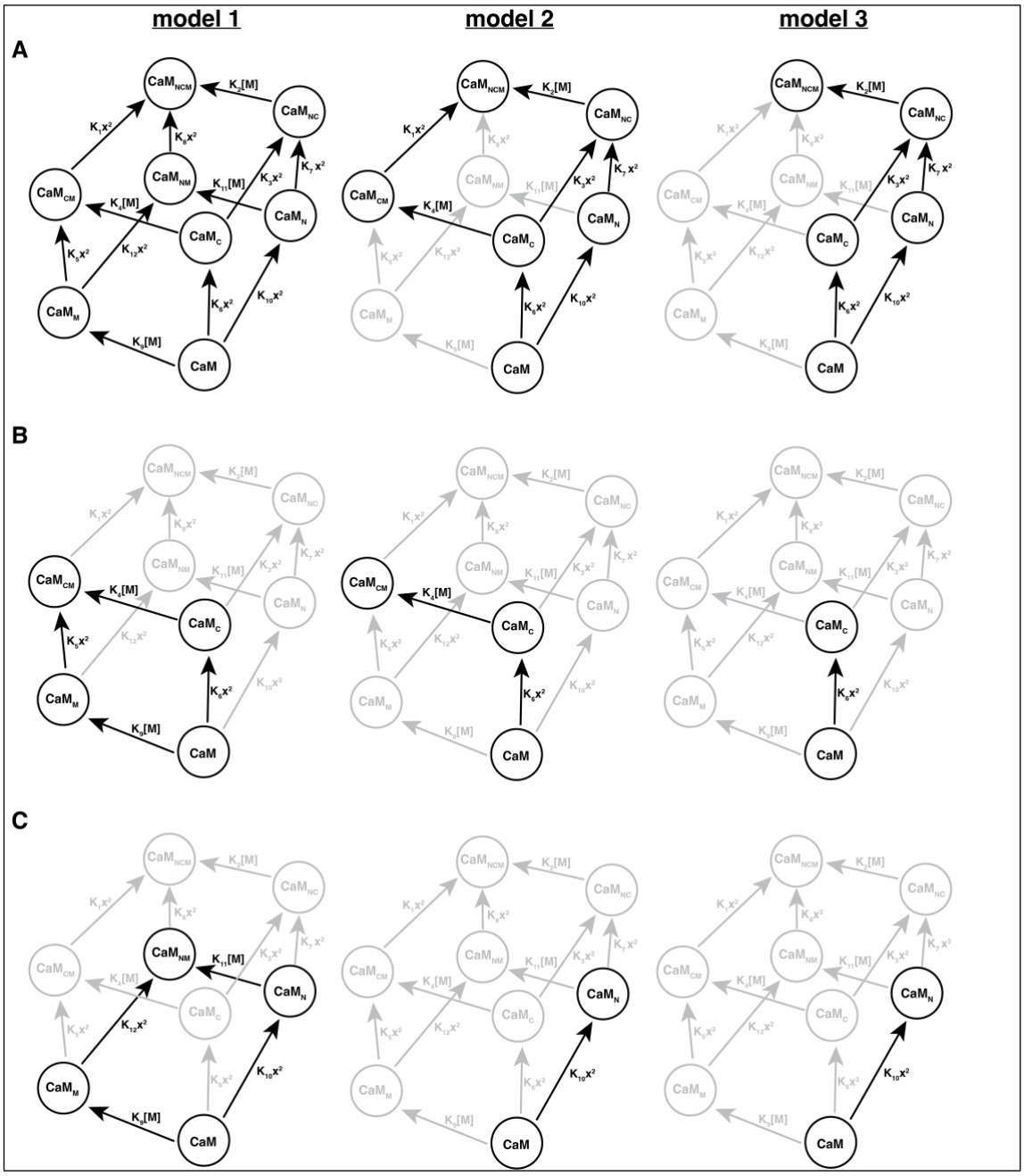

Figure 1: Network diagrams for the binding of Ca^{2+} and MLCK to CaM. Model 1 is the unordered model proposed by Brown *et al.*, 1997 and Fajmut, Brumen *et al.*, 2005; models 2 and 3 correspond to the partially and fully ordered models of Fajmut, Jagodic *et al.*, 2005 and Kato *et al.*, 1984, respectively. **(A)** shows the networks for CaM^{WT}, **(B)** for $CaM^{21A,57A}$, and **(C)** for $CaM^{94A,130A}$ Models 2 and 3 are truncations of Model 1; omitted edges and vertices are shown in gray. In each network *x* denotes $[Ca^{2+}]$, and *M* denotes MLCK. The subscripts N and C indicate Ca^{2+} binding at the N-terminus and C-terminus EF hands of CaM, respectively, and the subscript M indicates MLCK binding. The figure is adapted from Dexter *et al.*, 2018.

In recent work, Dexter *et al*. showed that this class of models is analytically

solvable for a CaM/MLCK system at both thermodynamic equilibrium and steady state, and that each model predicts distinct steady-state behavior in certain Ca^{2+} concentration regimes (Dexter *et al.*, 2018). Importantly, these predictions hold regardless of the numerical values assigned to the model parameters (i.e., the equilibrium constants in **Fig. 1A**), allowing us to develop a strategy for model discrimination that does not require extensive parameter estimation.

Our biochemical approach to testing the predictions of the models centers on the use of an established fluorescence resonance energy transfer (FRET) reporter that we term FR. FR has been employed to characterize CaM- and Ca^{2+}-dependent activation of MCLK both *in vivo* and *in vitro* (Calizo *et al.*, 2020; Geguchadze *et al.*, 2004; Mauban *et al.*, 2014; Raina *et al.*, 2009; Wang *et al.*, 2013; Wier *et al.*, 2008; Zhang *et al.*, 2019). FR acts as a stand-in for the wild-type MLCK protein; it is composed of an EYFP and ECFP

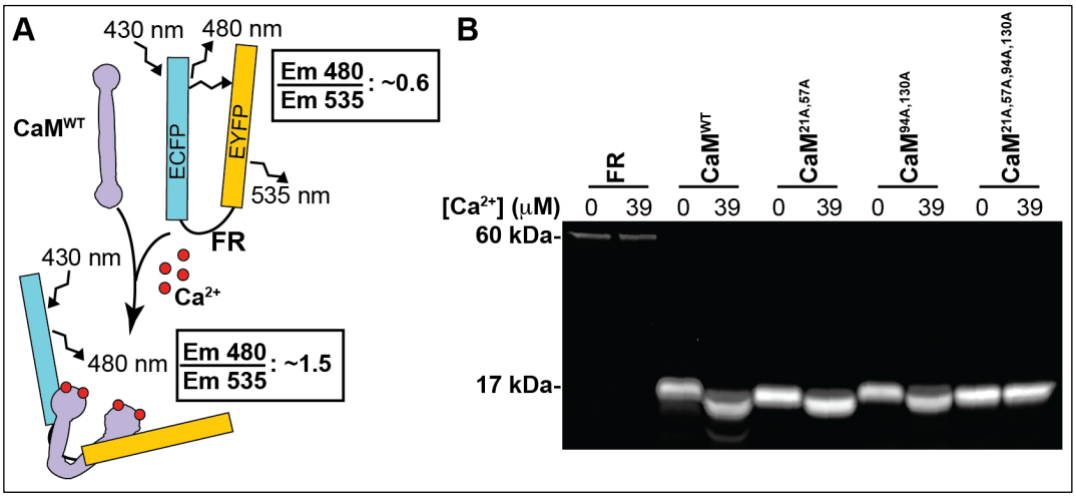

Figure 2: MLCK-based FRET assay reports MCLK-CaM binding. (A) Schematic showing assay principle. In the presence of Ca^{2+}, CaM binds to the CaM-binding domain of FR, leading to a decrease in FRET and reduced emission at 535 nm. **(B)** Representative gel image of purified FR and CaM proteins visualized with SYPRO™ Ruby protein gel stain following SDS-PAGE. Samples were incubated in buffers containing either 0 μM Ca^{2+} or 39 μM free Ca^{2+} before SDS-PAGE. 8 μg of each CaM protein and 800 ng of FR was loaded.

FRET pair, which are linked by the CaM-binding domain of smooth muscle MLCK (Geguchadze *et al.*, 2004). Binding of CaM to FR interferes with FRET, enabling analysis of FR-CaM binding in the form of the ratio of EYFP and ECFP emission (F480/F535) after excitation at 430 nm (**Fig. 2A**). For our FRET-based binding assays, we measure FR-CaM binding across a wide range of [Ca^{2+}] for wild-type CaM (CaM^{WT}) and three different CaM mutants: CaM with its N-terminus EF-hands mutated (D21A and D57A mutations, $CaM^{21A,57A}$; **Fig. 1B**), CaM with its C-terminus EF-hands mutated (D94A and D130A mutations, $CaM^{94A,130A}$; **Fig. 1C**) and CaM with all of its EF-hands mutated (D21A, D57A, D94A, D130A, $CaM^{21A,57A,94A,130A}$). Each of the site-directed Asp to Ala mutations we performed has been demonstrated to prevent Ca^{2+} binding, and to have only a slight impact on the structure of each CaM EF hand (Piazza *et al.*, 2017).

We use a multi-step strategy to discriminate between these models. We first compare Model 1 to Models 2 and 3, and then we compare Model 3 to Models 1 and 2. During the first step, FR-CaM binding at zero [Ca^{2+}] is determined as Model 1, but not Models 2 and 3, predicts binding under these conditions. In the second step, binding of FR to a CaM with impaired N-terminus Ca^{2+} ($CaM^{21A,57A}$) is measured at high [Ca^{2+}]. Models 1 and 2, but not Model 3, predict binding between FR and this mutant CaM at high [Ca^{2+}]. Finally, we use a CaM mutant with impaired C-terminus Ca^{2+} binding ($CaM^{94A,130A}$) to evaluate additional predictions of Model 2. Because this approach assesses binding behavior predicted by the three proposed models, no parameter estimation is required or employed.

Our binding measurements using the FR falsify key predictions of both Model 1 (random binding) and Model 3 (fully ordered binding) but are consistent with multiple

distinct predictions of Model 2, which strongly suggests that CaM-MLCK binding follows a partially ordered mechanism. We further validate our key findings and the utility of the FR system using orthogonal experimental techniques and assessing binding between full length MLCK-FLAG protein and CaM.

RESULTS

For all binding experiments, we purified either FLAG-tagged FR or MLCK from HEK 293T cells after transient transfection, and purified His-tagged CaM^{WT} and CaM mutants ($CaM^{21A,57A}$, $CaM^{94A,130A}$, and $CaM^{21A,57A,94A,130A}$) after bacterial expression. Gel electrophoresis and SYPRO™ Ruby staining of purified proteins (**Fig. 2B**), as well as mass spectrometry analysis (**Fig. S1**), established that the protein preparations were free of major contaminants. It is well documented that the electrophoretic mobility of CaM in SDS-PAGE changes following Ca^{2+} binding-induced conformational change. This gel mobility shift is commonly used as a readout of Ca^{2+}-CaM binding [21-24]. We observed an expected Ca^{2+}-dependent gel mobility shift in our CaM^{WT}, $CaM^{21A,57A}$, and $CaM^{94A,130A}$

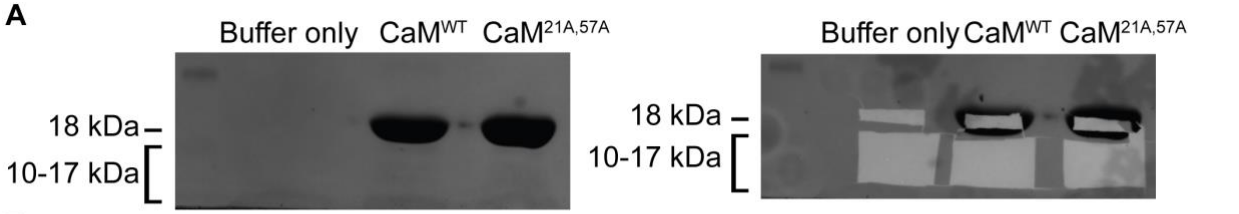

B

	% CaM intensity			% Keratin, E.coli proteins		
Molecular Weight	Buffer only	CaM^{WT}	$CaM^{21A,57A}$	Buffer only	CaM^{WT}	$CaM^{21A,57A}$
18 kDa	17%	96%	99%	34%	0%	0%
10-17 kDa	53%	91%	66%	11%	3%	15%
Lane total	51%	96%	96%	13%	1%	2%

Supplemental Figure 1: Mass spectrometry analysis of purified calmodulin proteins, Related to Figure 2. Semi-quantitative mass spectrometry was performed to assess the purity of purified CaM^{WT} and $CaM^{21A,57A}$ proteins; a "loading buffer only" lane was used as a control. **(A)** Following SDS-PAGE, the gel was Coomassie stained, and bands of interest were excised and analyzed by mass spectrometry. **(B**) The identified peptides were categorized as CaM or a contaminating protein (keratin or *E. coli* protein) using their annotations. Finally, the percent abundance of either CaM or contaminants in each band was determined using their intensity in mass spectrometry data.

proteins (**Fig. 2B**) (Wallace *et al.*, 1982), but observed no gel mobility shift for FR or $CaM^{21A,57A,94A,130A}$ in the presence of Ca^{2+}. These data suggest that our purified CaM proteins each retain their expected Ca^{2+} -binding affinity.

Having validated our experimental tools, we collected FRET-based FR-CaM binding data to use in our model discrimination strategy. The previous theoretical analysis identified a two-part strategy for distinguishing between the three models of CaM-MLCK binding, which is described in detail in Dexter *et al.,* 2018. The analysis involves deriving algebraic expressions for the fraction of total MLCK (*F*) that is predicted to bind to CaM as a function of free [Ca^{2+}] for each of the models. Plots of *F* are shown in **Fig. 3A** for CaM^{WT}, $CaM^{21A,57A}$, $CaM^{94A,130A}$, and $CaM^{21A,57A,94A,130A}$ (assuming the reference values for the equilibrium constants compiled by Fajmut, Brumen *et al.,* 2005 and the concentrations of CaM and MLCK used in our experiments). The model discrimination strategy rests on two predictions that differ between the three models and that hold true regardless of the specific numerical values assigned to the model parameters, such as the equilibrium constants in **Fig. 1**. The first is that only Model 1 predicts non-zero binding of MLCK in zero [Ca^{2+}], with the fraction bound given by the following expression:

$$F_1^{WT}(0) = \frac{2K_9 CaM_{tot}}{1+K_9(CaM_{tot}+M_{tot})+\sqrt{1+2K_9(CaM_{tot}+M_{tot})+K_9^2(CaM_{tot}-M_{tot})^2}}, \quad (1)$$

where CaM_{tot} and $MLCK_{tot}$ denote total CaM and total MLCK, respectively. The second is that only Model 3 predicts zero binding of MLCK to a CaM mutant with nonfunctional N-terminal EF hands, such as $CaM^{21A,57A}$, at any free [Ca^{2+}]. In contrast, both Models 1 and 2 predict non-zero binding, with the fraction in the high-[Ca^{2+}] limit given by

$$\lim_{[Ca^{2+}]\to\infty} F_1^N = \lim_{[Ca^{2+}]\to\infty} F_2^N = \frac{2K_4 CaM_{tot}}{1+K_4(CaM_{tot}+M_{tot})+\sqrt{1+2K_4(CaM_{tot}+M_{tot})+K_4^2(CaM_{tot}-M_{tot})^2}}. \quad (2)$$

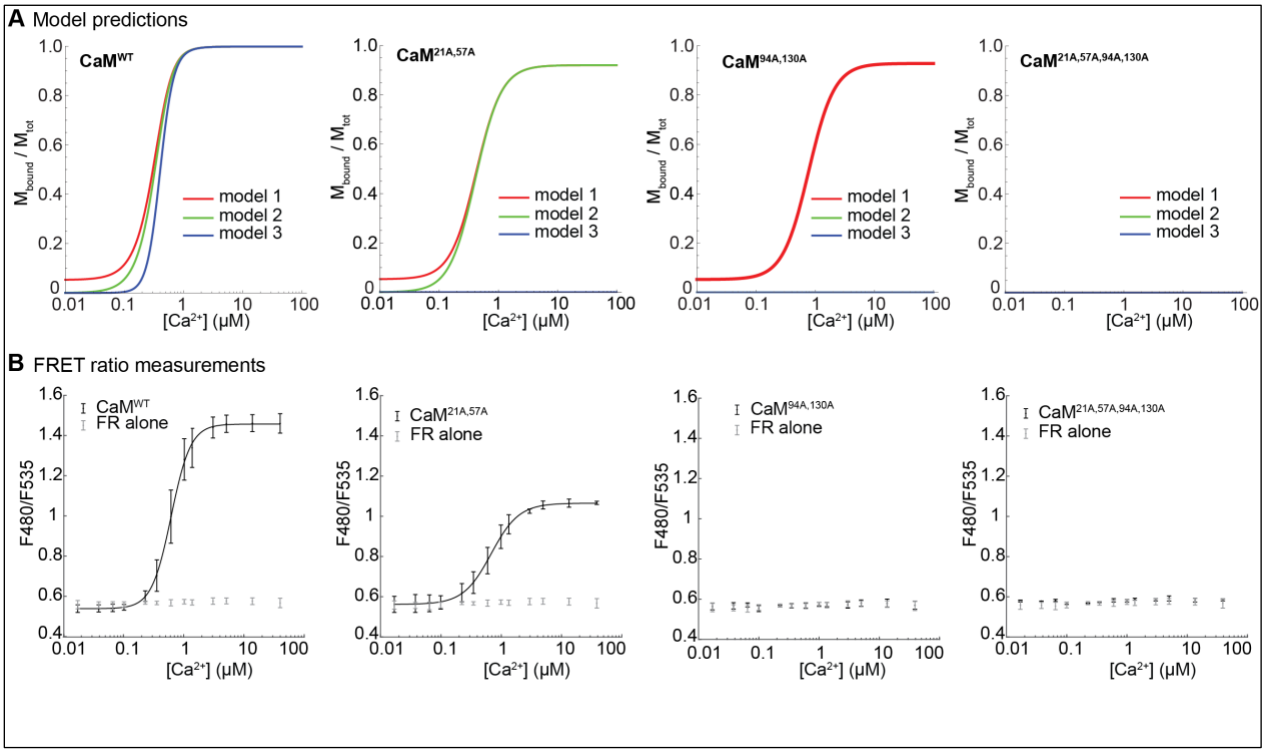

Figure 3: Predictions of mathematical models of MLCK binding and FRET measurements in the presence of excess CaM relative to FR. (A) Theoretical CaM-MLCK binding curves for CaM^{WT}, $CaM^{21A,57A}$, $CaM^{94A,130A}$, and $CaM^{21A,57A,94A,130A}$. The predicted curves were calculated assuming [CaM] = 0.713 μM and [MLCK] = 0.0237 μM (the concentrations of CaM and FR used in the main experiments) and the reference parameter values from Fajmut, Brumen *et al.*, 2005. **(B)** Experimental binding curves showing FRET ratio measurements CaM proteins. For the experiments, FR was incubated either alone, or with a 30-fold excess of CaM^{WT}, $CaM^{21A,57A}$, $CaM^{94A,130A}$, $CaM^{21A,57A,94A,130A}$, in the presence of indicated [Ca^{2+}] in 96-well plates. Emission at 480 nm and 535 nm was measured after excitation at 430 nm using a plate reader. The [Ex 430, Em 480] fluorescence intensity was then divided by the [Ex 430, Em 535] intensity to yield an emission ratio, which is plotted. Shown are mean ± standard deviation of 17 replicates for FR only, 15 replicates for CaM^{WT}, 15 replicates for $CaM^{21A,57A}$, 8 replicates for $CaM^{94A,130A}$, and 3 replicates for $CaM^{21A,57A,94A,130A}$.

The algebraic structure of Eqs. 1 and 2 is identical; the only difference between the two expressions is which equilibrium constant appears (K_9 in Eq. 1, K_4 in Eq. 2). As discussed

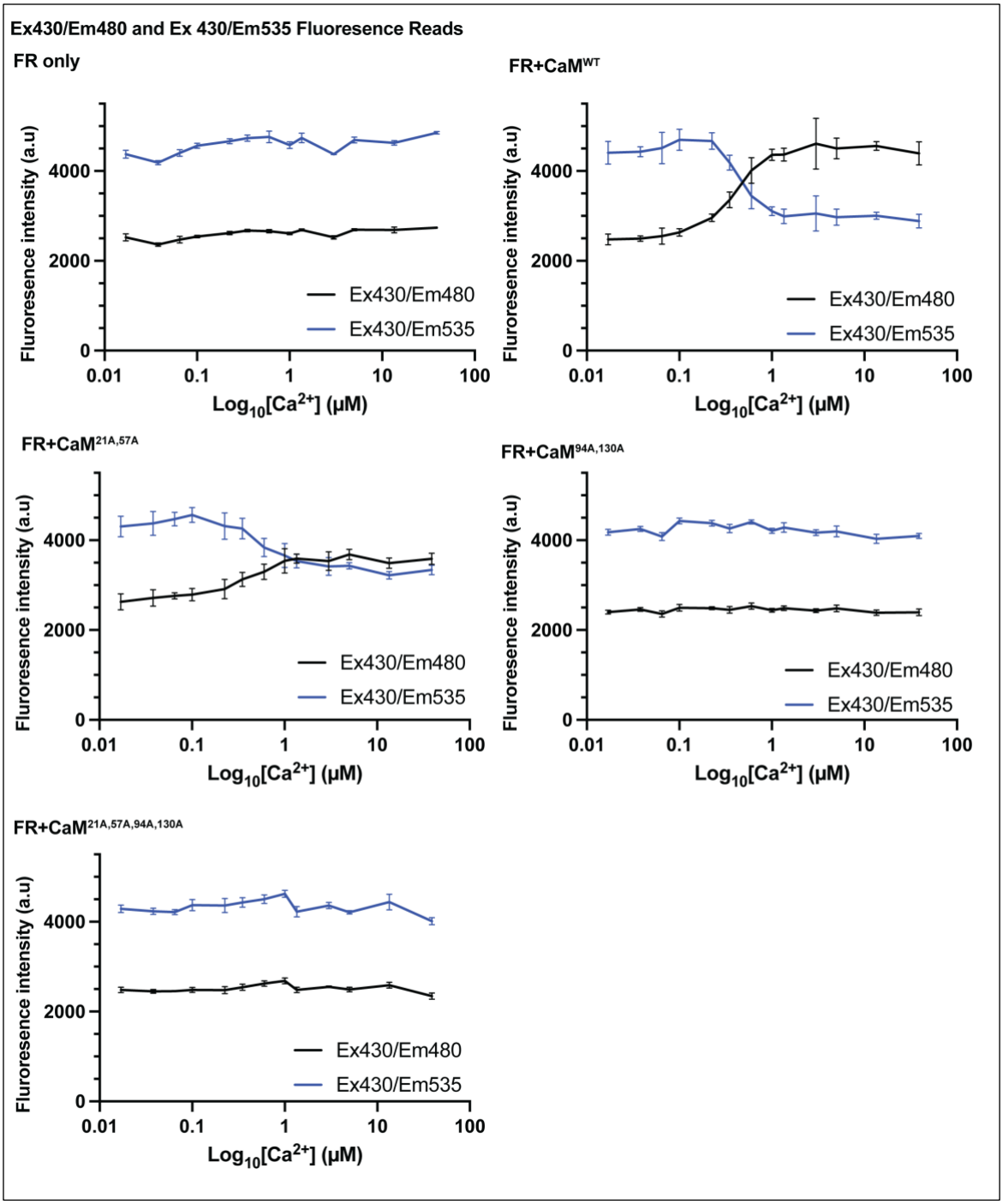

Supplemental Figure 2: Fluorescence intensities of FR-CaM binding assay, Related to Figure 3. For each of the indicated CaM-FR combinations, 673 nM CaM and 22.9 nM FR were combined in 150 µl of Ca^{2+} buffer (14 conditions between 0 µM and 39 µM). Fluorescence intensity of [Ex 430, Em 480], followed by intensity of [Ex 430, Em 535], was measured using a plate reader. Shown are mean ± standard deviation of raw data from at least 5 replicates for CaM^{WT}, $CaM^{21A,57A}$, and $CaM^{94A,130A}$, and 3 replicates for $CaM^{21A,57A,94A,130A}$ and FR only. **Fig. 3** shows the full dataset following analysis.

in Dexter *et al.*, 2018, this similarity is a consequence of the fact that the reaction network

reduces to a bimolecular reaction in both the low- and high-[Ca^{2+}] limits.

To test these predictions experimentally, we used a plate reader to detect changes in FR- CaM binding as a function of free [Ca^{2+}] with a 30-fold molar excess CaM^{WT}, $CaM^{21A,57A}$, $CaM^{94A,130A}$, or $CaM^{21A,57A,94A,130A}$ relative to FR. [CaM] was 673 nM (13 ng/µl), and [FR] was 22.9 nM (1.3 ng/µl). After collecting Ex 430/Em 480 and Ex 430/Em 535 data from different FR-CaM pairs (**Fig. S2**), we divided each [Ex 430/Em 480] fluorescence intensity value by its corresponding [Ex 430/Em 535] value to yield a ratio, which is plotted in **Fig. 3B**. We confirmed the presence of excess CaM compared to FR, and equal protein amount across experiments, by SDS-PAGE and SYPRO™ Ruby staining of the samples after FRET measurement (**Fig. S3**).

For the first model discrimination test, we compared the FRET ratio of CaM^{WT}-FR pair with baseline in zero and low [Ca^{2+}]. Contrary to the prediction of Model 1, we find no evidence that the signal in zero [Ca^{2+}], or the area under the binding curve for 0 µM ≤ [Ca^{2+}] ≤ 0.038 µM, is higher than baseline (p = 0.994 and p = 0.995, respectively, by a one-tailed Mann-Whitney U test). For the second test, we compared the FRET ratio of $CaM^{21A,57A}$ -FR pair in high [Ca^{2+}]. We found that FRET ratio in the maximum concentration used (39 µM [Ca^{2+}]) is significantly higher than baseline ($p = 2.83*10^{-6}$ by a one-tailed Mann-Whitney U test), as is the area under the complete binding curve ($p = 2.83*10^{-6}$ by a one-tailed Mann-Whitney U test). These observations are sufficient to falsify Model 3, which predicts zero binding of MLCK to any CaM mutant with impaired N-terminus Ca^{2+} binding. As such, only the predictions of Model 2 are consistent with the full set of experimental results. As an additional test of Model 2, we examined binding of C-terminus mutant $CaM^{94A,130A}$ in high [Ca^{2+}]; consistent with the predictions of the model,

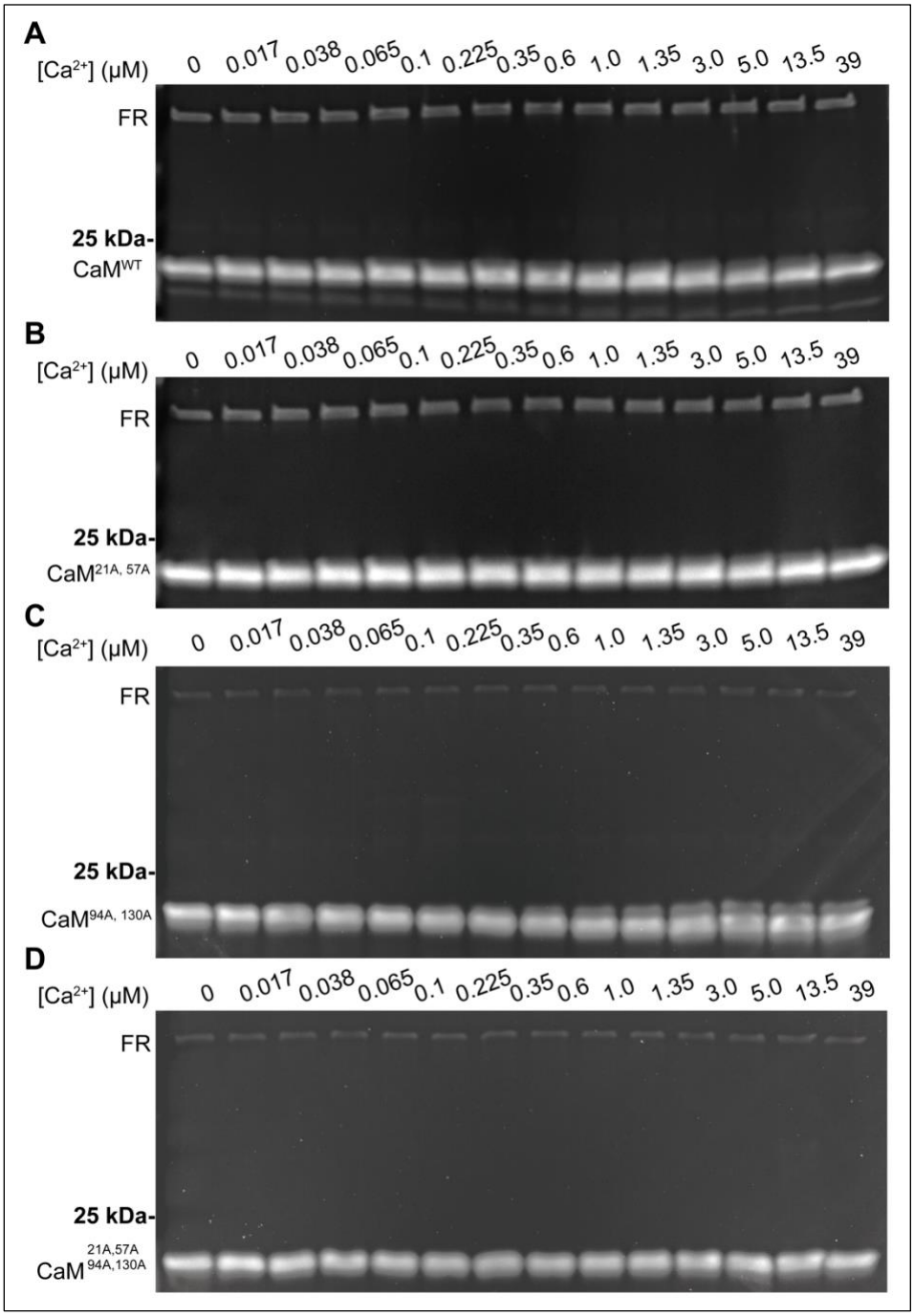

Supplemental Figure 3: Purified FR and CaM used in data collection. Related to Figure 3. A portion of each sample for fluorescent detection of FR-CaM binding was recovered from the wells. SDS-PAGE and SYPRO™ Ruby staining confirmed the presence of excess CaM compared to FR in the FRET-based binding assay for **(A)** CaM^{WT} and FR, **(B)** $CaM^{21A,57A}$ and FR, **(C)** $CaM^{94A,130A}$ and FR, and **(D)** $CaM^{21A,57A,94A,130A}$

we found no significant difference over baseline for the FRET ratio in 39 μM [Ca^{2+}] or for the area under the complete binding curve (p = 0.345 and p = 0.294, respectively, by a one-tailed Mann-Whitney U test).

A striking feature of the experimental binding curves is the significant difference in maximum binding between CaM^{WT} and $CaM^{21A,57A}$ ($p = 1.16*10^{-6}$ by a one-tailed Mann-Whitney *U* test); this difference is also consistent with the predictions of Model 2 (**Fig. 3A**). Assuming Model 2, the fraction of $CaM^{21A,57A}$ bound in the high-$[Ca^{2+}]$ limit is given by Eq. 2. For CaM^{WT}, the limiting expression is the same as Eq. 2 but with K_2 instead of K_4 (for the reasons explained above), so that the model predicts equal maximum binding if $K_2 = K_4$. In the reference parameter set, $K_2 = 1{,}000$ and $K_4 = 16.7$, corresponding to predicted binding of 99.9% for CaM^{WT} and 92.0% for $CaM^{21A,57A}$ in 39 μM $[Ca^{2+}]$. As such, the experimentally observed difference is also predicted by our mathematical analysis, assuming that the literature parameter values are correct within an order of magnitude.

The validity of our experimental approach for model discrimination depends on the ability of the FR-CaM interaction to accurately mirror CaM-MLCK binding with sufficient sensitivity, as well as other considerations related to the experimental perturbations. To address these, we performed a series of control experiments and tested the robustness of our experimental design and data.

First, to confirm that the FRET ratio of FR is only altered by the binding of Ca^{2+}-bound CaM, we collected 460 nm - 700 mm emission spectra with Ex 430 of the FR in 0 and 39 μM $[Ca^{2+}]$. When FR was assayed alone, FR showed no changes in FRET ratio as a function of $[Ca^{2+}]$ and produced fluorescence peaks at Em 480 and Em 535 (**Fig. S4A**). Incubating FR with either CaM^{WT} or N-terminus mutant $CaM^{21A,57A}$ in the presence of 39 μM Ca^{2+} caused FR fluorescence to increase at ~Em 480 and decrease at ~Em 535 (**Fig. S4B** and **S4C**). No change to FR fluorescence was observed in the absence of Ca^{2+} at any wavelength following FR incubation with CaM^{WT} or N-terminus mutant $CaM^{21A,57A}$.

C-terminus mutant CaM^{94A,130A} did not noticeably change the FR spectra at any wavelength, with or without Ca^{2+} (**Fig. S4D**).

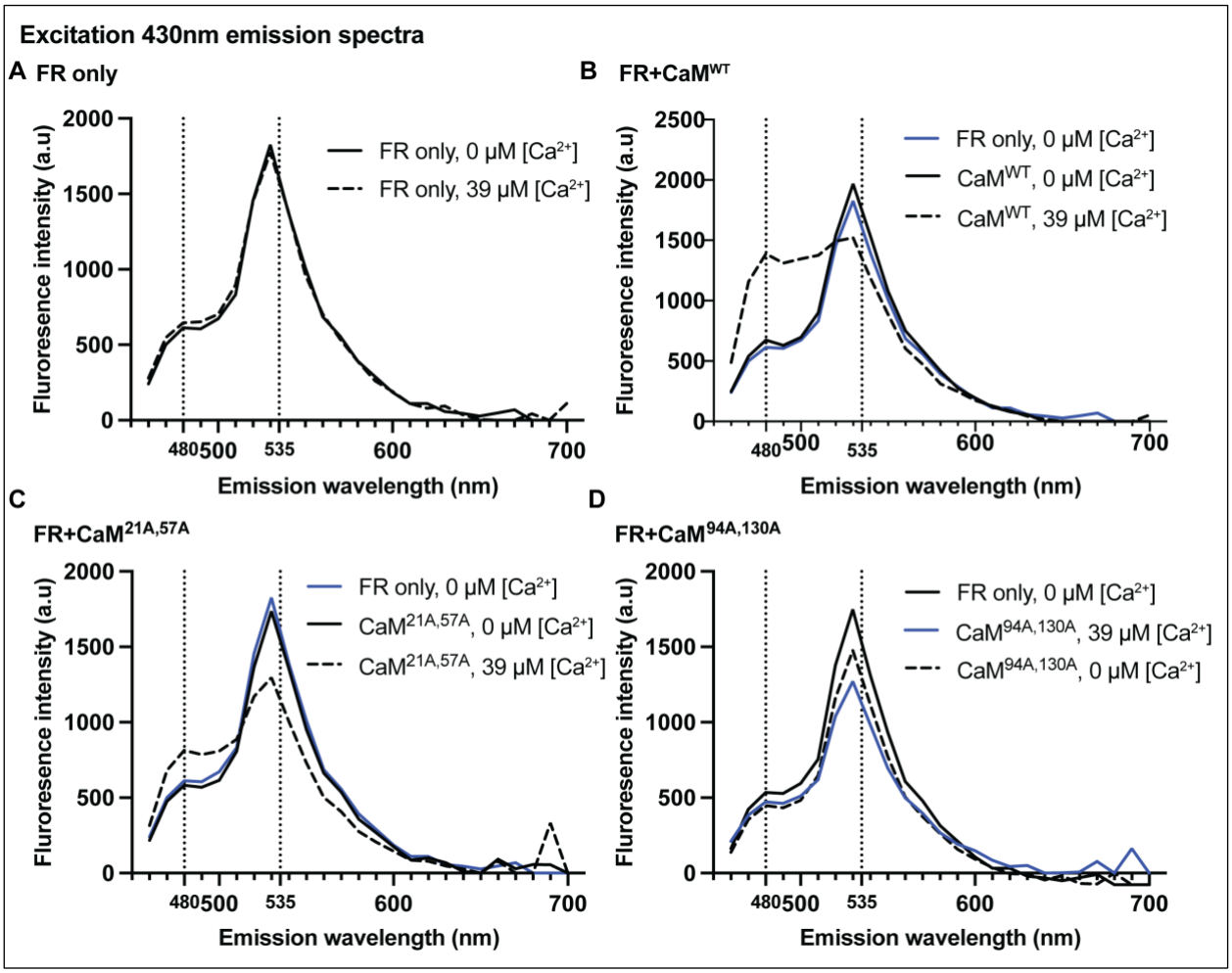

Supplemental Figure 4. Emission spectra of FR at Ex 430, Related to Figure 3. The emission spectra (460 nm - 700 nm, 10 nm steps) of **(A)** FR alone or with **(B)** CaM^{WT}, **(C)** CaM^{21A,57A}, or **(D)** CaM^{94A,130A} was measured at either 0 or 39 μM [Ca^{2+}]. Dotted lines indicate the Em 480 and Em 535 wavelengths, which were used in FRET-based FR-CaM binding assays. One representative read for each condition is shown. FR-only spectra are included in the CaM graphs as a reference.

Having observed no interactions between FR and CaM^{94A,130A} or CaM^{21A,57A,94A,130A} during our FRET-based binding assays, we wanted to confirm that the interactions we observed between FR-CaM^{WT} and FR-CaM^{21A,57A} are specific, Ca^{2+}-dependent, and representative of binding between CaM and MLCK. To do so, we performed several on-bead binding assays using either FR or MLCK-FLAG. When bead-bound FR was

incubated in 50 µl of buffer with 505 nM CaM^{WT} (approximately 20 ng/µl), the fraction of CaM^{WT} bound to FR increased proportionally with free [Ca^{2+}]. At 39 µM [Ca^{2+}], the majority of the CaM^{WT} input was bound to the FR (**Fig. 4A**). When the same experiment was repeated using N-terminus mutant $CaM^{21A,57A}$, more than half of $CaM^{21A,57A}$ bound to FR at 39 µM Ca^{2+} (**Fig. 4B**). These results suggest that the purified CaM proteins are

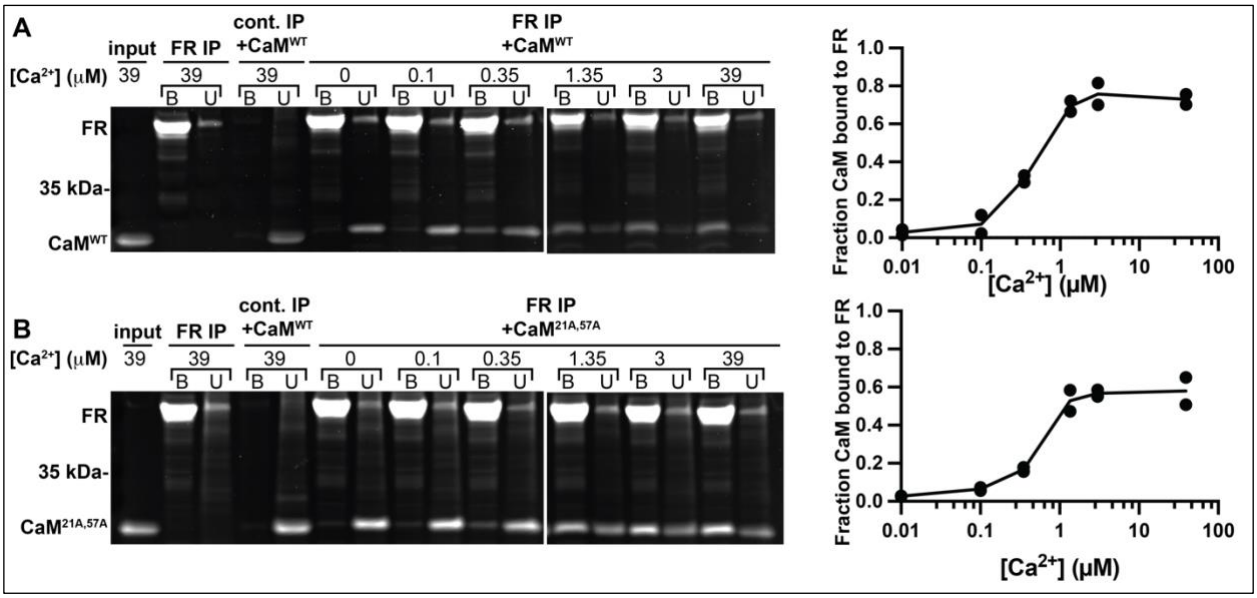

Figure 4: Purified CaM^{WT} and $CaM^{21A,57A}$ show Ca^{2+}-dependent interaction with FR. Representative images showing binding between bead-immobilized FR and **(A)** CaM^{WT} or **(B)** $CaM^{21A,57A}$ in buffers with the indicated free [Ca^{2+}]. Unbound and bound fractions were analyzed by SDS-PAGE followed by SYPRO™ Ruby protein gel stain. Fraction of CaM bound to the FR was quantified using ImageJ. The binding graph shows quantification of two experimental replicates; curve shows the average of the two data points at each [Ca^{2+}]. FR without CaM addition and a control binding experiment using non-transfected HEK 293T cells serve as controls. The input lane shows the purified CaM^{WT} or $CaM^{21A,57A}$ added to the on-bead binding assay.

functional and bind to Ca^{2+} and the FR, and that there is negligible non-specific binding between the FR and the purified CaM proteins. To determine if FR-CaM binding is representative of binding between CaM and full-length MLCK, we performed an on-bead binding assay after transient expression and purification of MLCK-FLAG protein. Despite the presence of several background bands, we observed the same CaM binding pattern

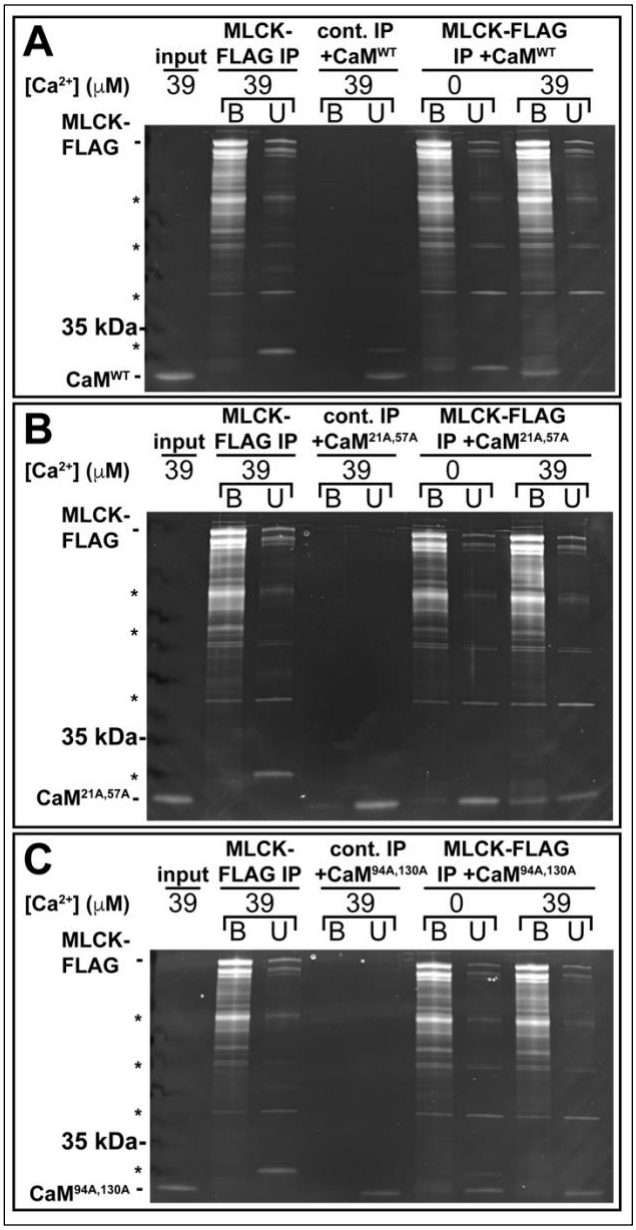

Supplemental Figure 5: Purified CaM^{WT} and $CaM^{21A,57A}$ show Ca^{2+}-dependent interaction with MLCK-FLAG; $CaM^{94A,130A}$ does not, Related to Figure 4. Representative images showing binding between bead-immobilized MLCK-FLAG and **(A)** CaM^{WT}, **(B)** $CaM^{21A,57A}$, and **(C)** $CaM^{94A,130A}$ in buffers with the indicated free [Ca^{2+}]. Unbound and bound fractions were analyzed by SDS-PAGE followed by SYPRO™ Ruby protein gel stain. MLCK-FLAG without CaM addition and a control binding experiment using non-transfected HEK 293T cells serve as controls. The input lane shows the purified CaM^{WT}, $CaM^{21A,57A}$, or $CaM^{94A,130A}$ added to the on-bead binding assay. Asterisks (*) indicates background bands.

to MLCK-FLAG, as to FR. At 39 μM [Ca^{2+}], the majority of the CaM^{WT} input appeared bound to MLCK-FLAG (**Fig. S5A**), and there was partial binding of N-terminus mutant $CaM^{21A,57A}$ to MLCK-FLAG (**Fig. S5B**). There was no apparent interaction between C-terminus mutant $CaM^{94A,130A}$ and MLCK-FLAG at 39 μM [Ca^{2+}] (**Fig. S5C**). None of the CaM proteins bound to MLCK-FLAG at 0 μM [Ca^{2+}].

We also investigated the relationship between the “fraction bound” calculated in the modeling analysis and the FRET ratio we use as a proxy for FR-CaM interaction. Although the Em 480/Em 535 ratio may not have a one-to-one relationship to “fraction bound” described in the models, this ratio correlates closely with FR-CaM binding at high and low [Ca^{2+}], as calculated using on-bead binding assays **(Fig. S6)**. Moreover, the same FRET ratio has been shown to mirror MLCK phosphorylation *in vivo* (Geguchadze *et al.*,

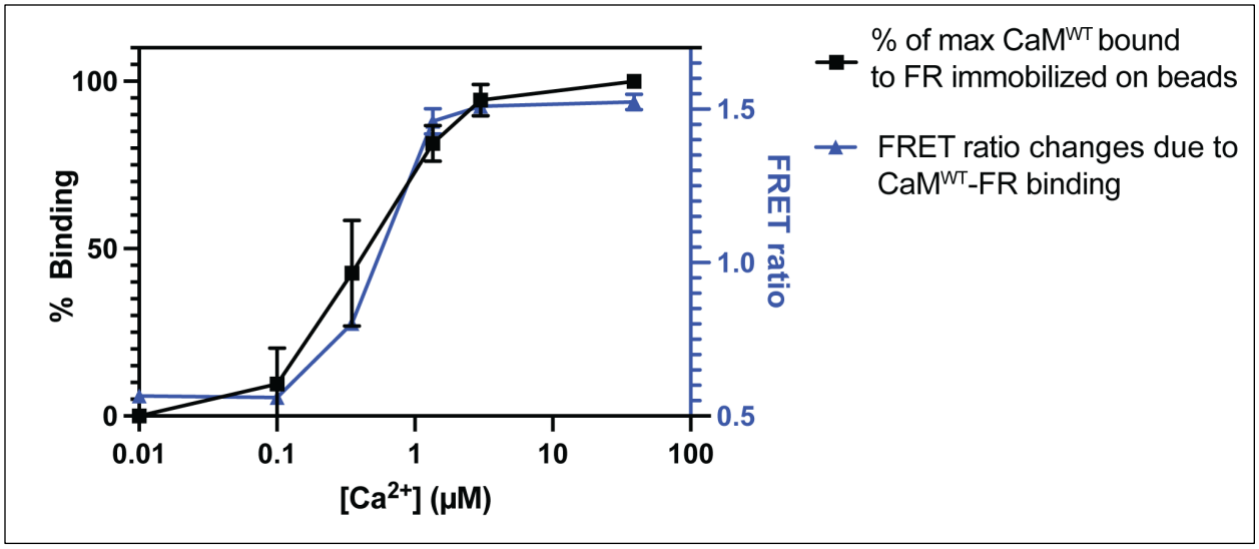

Supplemental Figure 6. Comparison of on-bead and FRET-based binding assessment between FR and CaM^{WT} as a function of [Ca^{2+}], Related to Figure 4. Data collected using FRET-based binding assay for CaM^{WT}-FR was plotted alongside data collected using on-bead binding assay. To quantify the relative amount of CaM bound to FR, CaM^{WT}-FR binding at 39 μM [Ca^{2+}] was set to 100%, binding at other [Ca^{2+}] relative to this maximum signal were calculated. Two replicates of images of on-bead binding were quantified using ImageJ; mean and ± standard deviation are shown. 15 replicates of FRET ratio changes due to CaM^{WT}-FR binding are shown as mean ± standard deviation.

2004). As a result, we conclude that the ratio can be used to characterize CaM-FR interaction for our model discrimination strategy, which rests on differential binding predictions in zero and high [Ca^{2+}].

We do not observe binding between FR and C-terminus mutant $CaM^{94A,130A}$ in our FRET-based binding assays. To investigate the possibility that $CaM^{94A,130A}$ might bind to the FR but fail to interfere with FRET, we used a Bio-Layer Interferometry (BLI) assay as

an orthogonal method to measure binding between FR and CaM. Binding detection in the BLI assay is independent of FRET measurement, which enabled us to decouple binding and FRET interference. The BLI assay showed robust binding between FR and CaM^{WT} at high [Ca^{2+}], an intermediate degree of binding between FR and $CaM^{21A,57A}$ at high [Ca^{2+}], and no detectable binding between FR and $CaM^{94A,130A}$ at high [Ca^{2+}] (**Fig. 5A**). Performing a BLI assay using CaM^{WT}, $CaM^{21A,57A}$ and $CaM^{94A,130A}$ with purified MLCK-FLAG yielded comparable results (**Fig. 5B**).

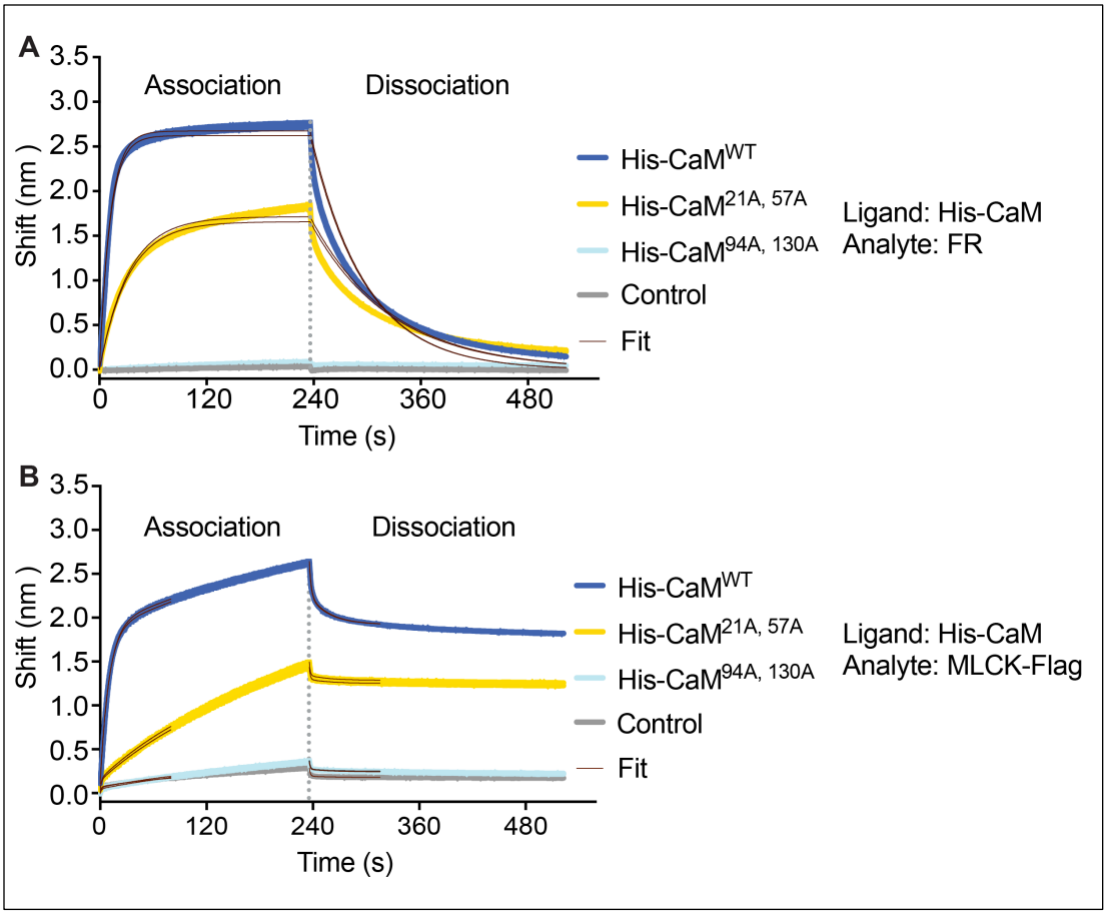

Figure 5: Bio-Layer Interferometry (BLI) binding assays show no binding between FR or MLCK-FLAG and $CaM^{94A,130A}$. BLI was performed using purified His-tagged calmodulin (CaM^{WT}, $CaM^{21A,57A}$, or $CaM^{94A,130A}$) as a ligand immobilized to a Ni-NTA biosensor, and either **(A)** FR or **(B)** MLCK-FLAG as an analyte. Two replicates of each condition are shown. "Control" refers to the analyte binding to the ligand-free probe. Data was analyzed using the Octet data analysis software (Octet® Analysis Studio).

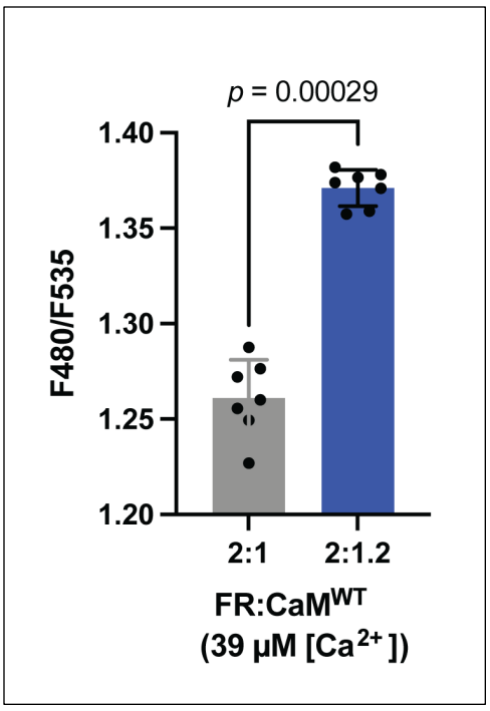

Supplemental Figure 7: FR-CaM binding assay is sensitive enough to detect a calculated 8.5% increase in CaM-FR binding, Related to Figure 5. A modified version of the FR-CaM FRET-based binding assay using a FR:CaM^{WT} ratio of either 2:1 or 2:1.2 (22.9 nM FR and 11.45 nM or 13.75 nM CaM) in high [Ca^{2+}] was performed. The Em 480/Em F535 ratio increased significantly between conditions (p = 0.00029 by a one-tailed Mann-Whitney U test), from an average of 1.26 to 1.37 (an 8.7% increase in FRET ratio). Assuming Model 2 and the reference parameter values from Fajmut, Brumen *et al.*, 2005, the fraction of FR bound to CaM^{WT} is predicted to differ by 8.5% between the two conditions (46.2% vs. 54.7% bound). Mean ± standard deviation of 7 replicates for each condition are shown.

We next assessed the intrinsic sensitivity of the FRET assay. To test if our assay can detect small changes in binding, which is necessary for many of the comparisons involved in our model discrimination analysis, we measured FRET at 39 µM [Ca^{2+}] with different FR:CaM ratios. Assuming Model 2 and the reference parameter values from Fajmut, Brumen *et al.*, 2005, if the FR:CaM molar ratio is increased from 2:1 to 2:1.2, the amount of CaM-bound FR in 39 µM [Ca^{2+}] is predicted to increase by 8.5% (from 46.2% bound to 54.7% bound). When we repeated our FRET-based FR-CaM binding assay using these ratios (22.9 nM FR and 11.45 nM or 13.75 nM CaM), we observed a significant increase in F480/F535 **(Fig. S7)** (p = 0.00029 by a one-tailed Mann-Whitney U test), with a calculated 8.7% difference in FRET ratios between the two conditions**.** We therefore conclude that, under our experimental conditions, the assay is sensitive enough to detect at least a 9% increase in the fraction of CaM-bound FR.

The predictions of zero MLCK binding in a particular [Ca^{2+}] hold for any set of numerical values assigned to the model parameters (the equilibrium constants K_1...K_{11} in

Fig. 1), as shown in Dexter *et al.*, 2018. For predictions of non-zero binding, however, the magnitude of binding does depend on the choice of parameters. As such, it is theoretically possible that the model could predict a binding fraction that is non-zero but too small to detect experimentally in an important concentration regime. To address this potential concern, we undertook a sensitivity analysis of the two key predictions of non-zero MLCK binding. For numerical calculations with the models, we used the set of reference parameter values compiled by Fajmut, Brumen *et al.*, 2009 from previous biochemical studies. As shown in Eq. 1, the prediction of Model 1 for the fraction of MLCK bound in zero [Ca^{2+}] depends on the value of a single parameter (K_9). Assuming the parameter value selected by Fajmut, Brumen *et al.*, 2009 based on several prior studies (K_9 = 0.078 μM^{-1}) and the concentrations of CaM^{WT} and FR used in the main experiment, the model predicts 5.2% binding in zero [Ca^{2+}]. As is clear from the structure of Eq. 1, the fraction of MLCK predicted to bind in zero [Ca^{2+}] increases with the ratio of total CaM to total MLCK. To confirm our falsification of Model 1, we therefore repeated the binding experiment in zero [Ca^{2+}] with a much higher [CaM] (35.65 μM), for which 73.5% binding is predicted with the reference parameter values and 21.7% binding is predicted with K_9 = 0.0078 μM^{-1} (i.e., 10-fold lower than the reference value). As in the main experiment, the FRET ratio did not increase above baseline in zero [Ca^{2+}] (**Fig. S8**), providing strong evidence against Model 1 even if previous parameter estimates are incorrect by an order of magnitude (p =0.998 by a one-tailed Mann-Whitney U test).

For Model 2, the fraction of MLCK predicted to bind to the N-terminus mutant $CaM^{21A,57A}$ depends on two parameters, K_4 and K_6 (Eq. 2). We confirmed the robustness of the key prediction of non-zero binding in 39 μM [Ca^{2+}] by calculating F_2^N for 200,000

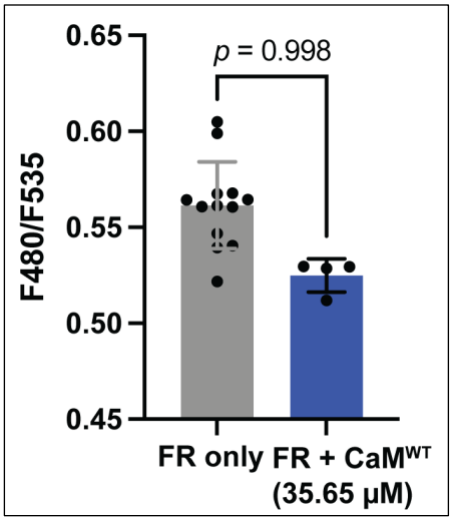

Supplemental Figure 8: CaM^{WT} does not bind to FR in the absence of Ca^{2+} even at high concentrations, Related to Figure 5. To test the robustness of our observation of no binding in zero [Ca^{2+}], we repeated the FRET-based binding assay with 35.65 µM CaM^{WT}, for which Model 1 predicts 21.7% binding even if previous estimates of a key parameter value are incorrect by an order of magnitude. CaM^{WT} was concentrated to 66.6 µg/µl so that the volume of protein solution used was comparable to previous assays. As in the original assay, the F480/F535 ratio was not higher than baseline (p = 0.998 by a one-tailed Mann-Whitney U test). Mean ± standard deviation of 13 replicates for FR only read and 4 replicates for FR+ CaM^{WT} reads are shown.

combinations in which values for each of the two parameters were chosen at random from the interval [0.1v, 10v], where v is the reference value from Fajmut, Brumen *et al*. [9]. Across the combinations F_2^N was never less than 18%, a level of binding straightforward to distinguish from baseline; the full distribution is shown in **Fig. S9**.

Finally, we confirmed that the addition of the purified proteins to the prepared Ca^{2+} buffers did not significantly alter the buffers' free [Ca^{2+}]. We measured the fluorescence intensity of two Ca^{2+} indicator dyes with different Ca^{2+} affinities (Fluo-4

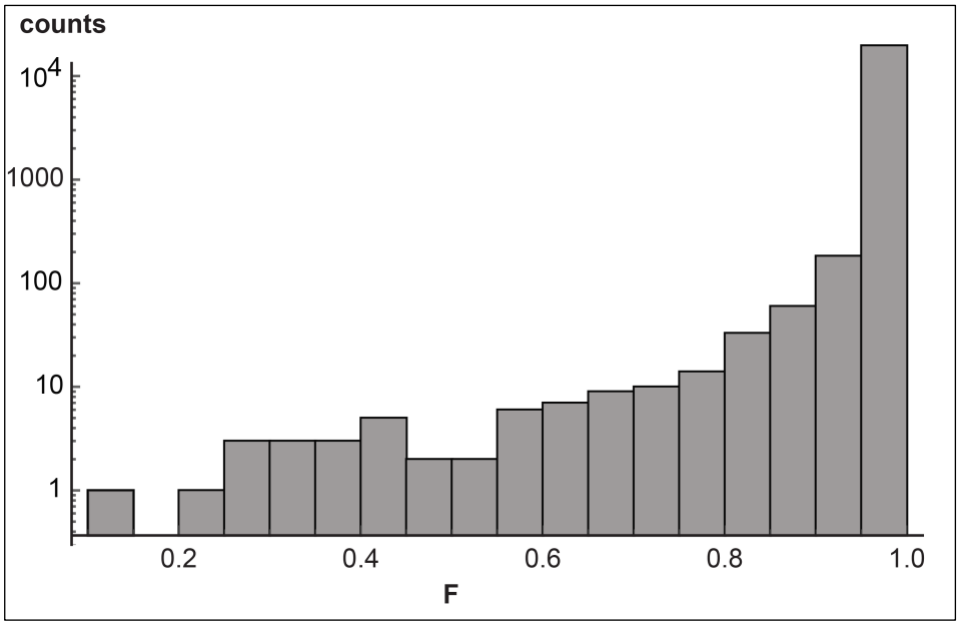

Supplemental Figure 9. Histogram from sensitivity analysis of model of CaM^{21A,57A}, Related to Figure 5. The histogram shows the distribution of predicted binding fractions for 200,000 combinations of K_4 and K_6 chosen at random from the interval [0.1v, 10v], where v is the reference value from Fajmut, Brumen *et al.*, 2005.

and Calcium Green), before and after addition of the buffer in which our CaM proteins were stored. The largest volume of protein added to any of our FRET-based binding experiments was 1.3 µl per assay, so this was the volume that we tested. We did not observe a significant change in indicator dye fluorescence intensity after CaM storage buffer addition, which suggests that any changes to free [Ca^{2+}] that are experimentally introduced are smaller than can be detected reliably with Fluo-4, a dye that has a very high Ca^{2+} affinity (17 nM) **(Fig. S10)** (*p* =0.23-0.99 by a two-tailed Mann-Whitney *U* test).

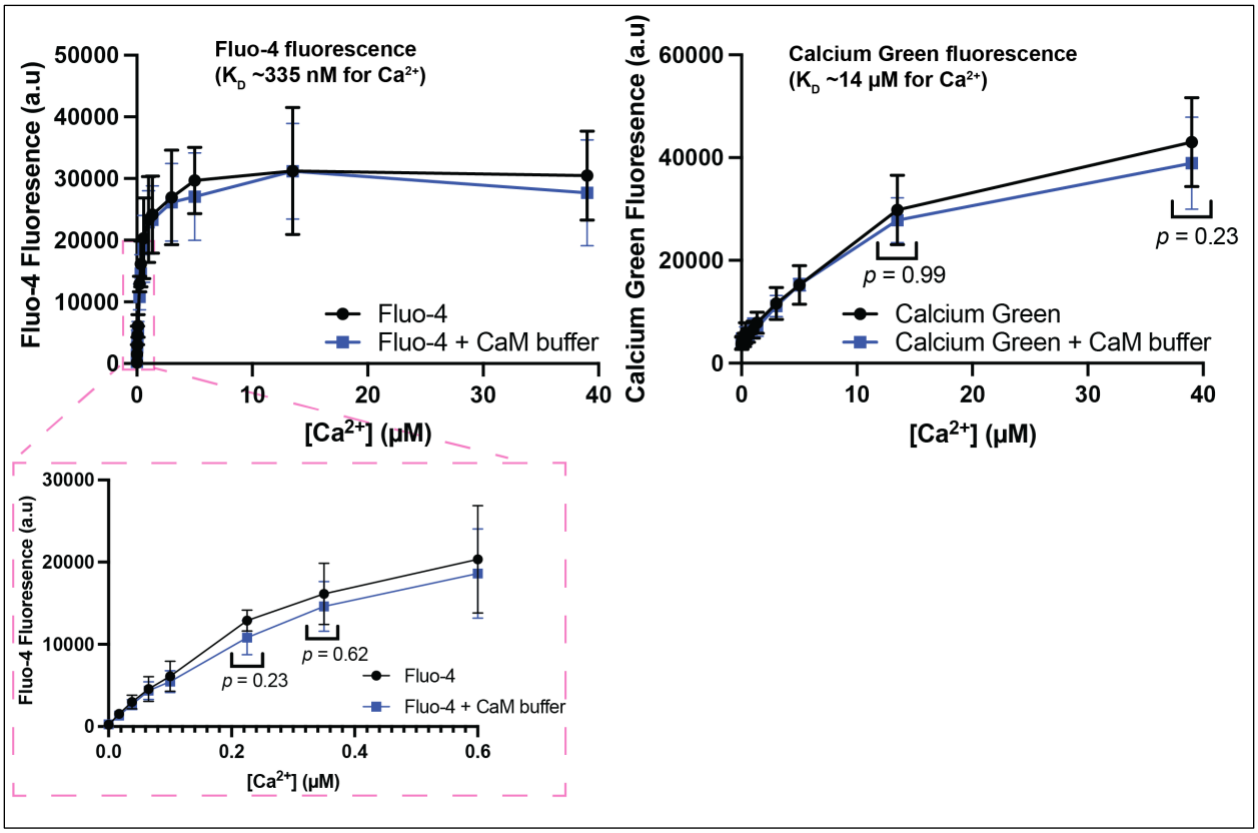

Supplemental Figure 10. Buffer addition to FR-CaM binding assay does not change assay free [Ca^{2+}], Related to Figure 5. Ca^{2+} indicator dyes Fluo-4 or Calcium Green were added to the 14-buffer series of the FR-CaM binding assay; data was collected using a plate reader with a GFP filter. The same buffer/Ca^{2+} indicator dye combinations were then assayed following the addition of a "dummy buffer" composed of the buffer in which all CaM proteins were stored. The area of interest (magnified region in red dotted line) highlights the data corresponding to [Ca^{2+}] most relevant to Fluo-4, which has K_D~335 nM. Calcium Green has K_D~14 µM. Mean ± standard deviation of four replicates for each condition are shown. *P* values were calculated using a two-tailed Mann-Whitney *U* test.

These sets of control experiments and sensitivity analyses show that our experimental system is robust and rigorously controlled. The FRET-based binding assay that we used as the core of our model discrimination strategy is well validated. Furthermore, the FR and CaM proteins we used are free of major contaminants. SYPRO® stained SDS-PAGE gels of the CaM proteins also confirm that these proteins display the predicted altered electrophoretic mobility upon binding to Ca^{2+}, which strongly suggests that they bind [Ca^{2+}] as expected. Follow-up plate reader experiments confirmed that FRET interference is sensitive enough to allow discrimination between candidate CaM-MLCK binding models. We also show that a change in FRET ratio is caused only by binding of Ca^{2+}-bound CaM proteins. Conversely, orthogonal BLI experiments confirm that a lack of FRET interference accurately reflects a lack of FR-CaM binding. We have also confirmed that the [Ca^{2+}] of our experimental buffers is not altered by the addition of our experimental proteins. Critically, on-bead binding experiments with both FR and MLCK-FLAG reproduced the key findings of our FRET-based binding assays. These data, in combination with the MLCK-FLAG data from our BLI assays, suggests that FR-CaM binding accurately mirrors binding between CaM and full-length MLCK protein, and suggests that our FR data can confidently be used for our model discrimination strategy.

In sum, our binding measurements using the FR falsify key predictions of both the fully random binding mechanism (Model 1) and the fully ordered binding mechanism (Model 3). Our data instead support Model 2, which predicts partially ordered binding between CaM and MLCK (**Fig. 1**). As predicted by Model 2, we observe zero binding in low [Ca^{2+}] for CaM^{WT} and all CaM mutants, non-zero binding in high [Ca^{2+}] for CaM^{WT}, non-zero binding in high [Ca^{2+}] for N-terminus mutant $CaM^{21A,57A}$, and zero binding in high

[Ca^{2+}] for both of our CaM mutants containing mutations in the C-terminus domain ($CaM^{94A,130A}$ and $CaM^{21A,57A,94A,130A}$). Model 2 makes six correct predictions and no incorrect predictions (**Table 1**). Model 1 makes two falsified predictions: non-zero binding in low [Ca^{2+}] for CaM^{WT}, and non-zero binding in high [Ca^{2+}] for the C-terminus mutant, $CaM^{94A,130A}$. Finally, Model 3 makes one falsified prediction: zero binding in high [Ca^{2+}] for the N-terminus mutant, $CaM^{21A,57A}$.

	model 1	model 2	model 3	observed
zero Ca^{2+}				
CaM^{WT}	**B**	NB	NB	NB
$CaM^{21,57A}$	**B**	NB	NB	NB
$CaM^{94A,103A}$	**B**	NB	NB	NB
high Ca^{2+}				
CaM^{WT}	B	B	B	B
$CaM^{21,57A}$	B	B	**NB**	B
$CaM^{94A,103A}$	**B**	NB	NB	NB

Table 1: Summary of model discrimination results for CaM and MLCK binding. B denotes binding, NB denotes no binding. Bolded entries indicate experimentally falsified predictions.

DISCUSSION

In recent work, Dexter *et al.* analyzed a class of previously developed theoretical models of CaM-MLCK binding and proposed a multi-part strategy for distinguishing between them (Dexter *et al.*, 2018). Our primary contribution here is an experimental implementation of this model discrimination strategy, which suggests a partially ordered mechanism for binding. Our analysis sheds new light on a controversy that has persisted for several decades and demonstrates a productive interplay between mathematical modeling and biochemical analysis.

It is important to remember that model discrimination strategies of this kind work by process of elimination. Models can be ruled out when their predictions contradict experimental data, but the failure of some models does not guarantee the correctness of others. We present here evidence sufficient to falsify all but one of the models of CaM-MLCK binding in the literature (**Table 1**). Data collected using wild-type and mutant CaM proteins in three different binding experiments (FRET, BLI and on-bead binding) in zero and high [Ca^{2+}], using both FR and MLCK-FLAG when possible, rule out both Model 1 and Model 3. Our data is consistent with Model 2, which makes six correct predictions. Taken together, these results strongly support a partially ordered mechanism in which MLCK can bind to CaM after Ca^{2+} is bound at the C-terminus (Model 2).

To investigate MCLK-CaM binding, we centered our experimental design on a FR system that uses the CaM-binding domain of smooth muscle MLCK. Prior studies have demonstrated that this reporter accurately reflects the CaM-MLCK binding in a variety of *in vivo* and *in vitro* contexts (Calizo *et al.*, 2020; Geguchadze *et al.*, 2004; Mauban *et a.l*, 2014; Raina *et al.*, 2009; Wang *et al.*, 2013; Wier *et al.*, 2008; Zhang *et al.*, 2019). Moreover, our FRET-based FR-CaM binding assay enabled collection of robust and reproducible data using purified CaM and FR proteins, with minimal risk of interference from endogenous proteins or contaminants. This system is also amenable to complementary, non-FRET-based biochemical techniques to assess FR-CaM binding, which allowed us to confirm the FRET-based binding data we obtained. Although the FR we used has been extensively validated to be a good proxy for CaM-MLCK binding, the use of an MLCK fragment still does raise concerns about the behavior of the fragment relative to the full-length protein. To allay these concerns, we repeated two key

experiments – on-bead binding experiments and BLI – with a full-length MLCK-FLAG protein in lieu of the FR protein. In each of these experiments, FR and MLCK-FLAG performed similarly, showing the utility of the FRET-based binding assay for our model discrimination strategy.

In HEK 293T lysates, changing myosin phosphorylation has been shown to correspond to changes in the FRET ratio produced by FR. Changes to the FRET ratio can therefore be used as a proxy for MLCK activation (Geguchadze *et al.*, 2004). It is important to note that changes in FRET ratio do not necessarily correspond 1:1 with changes to fraction of FR bound to CaM across all of the Ca^{2+} concentrations. Nevertheless, this fact does not impede our model discrimination strategy. The FRET ratios measured at 0 μM [Ca^{2+}] and 39 μM [Ca^{2+}] are the data points most critical to our model discrimination strategy. We also complement this FRET-based binding assay data with on-bead binding assays showing that in 39 μM [Ca^{2+}], the majority of CaM^{WT} binds to either FR or full length MLCK protein (MLCK-FLAG) expressed using human smooth muscle MLCK gene *MYLK1*, while a negligible amount of CaM binds to FR or MLCK-FLAG in 0 μM [Ca^{2+}]. We therefore conclude that FRET ratio data represents CaM^{WT}-MLCK binding in 0 μM [Ca^{2+}] and 39 μM [Ca^{2+}].

It should be noted that mammalian myosin light chain kinases are a group of serine/threonine kinases encoded by at least four genes: *MYLK1*, *MYLK2*, *MYLK3*, and *MYLK4* (Chang *et al.*, 2016). *MYLK1* has alternative initiation sites that enable expression of at least four protein products including nonmuscle (long isoform) MLCK and smooth muscle (short isoform) MLCK. *MYLK2* encodes an MLCK isoform expressed solely in skeletal muscle, *MYLK3* encodes a cardiac-specific MLCK (MLCK3), and the

gene product(s) of *MYLK4* remain largely uncharacterized (Wallace *et al.*, 1982; Chang *et al.*, 2016). All MLCK proteins, except MLCK4, have a CaM-binding peptide that shows sequence homology to both the peptide used in our FR, which is derived from avian smooth muscle MLCK, and to the CaM-binding domain of our MLCK-FLAG protein. As a result, we expect that our findings here can be generalized to other MLCK proteins and their interaction with CaM and Ca^{2+}.

In addition to providing a blueprint for future model discrimination efforts that integrate mathematical and biochemical approaches, our work may also prove useful in a translational or pharmaceutical context, as MLCK and its activation by CaM have been linked to the pathogenesis of human disease. For example, increased organization of the sarcomere, the contractile unit of the striated muscle, is observed during the onset of cardiomyocyte hypertrophy. CaM-activated MLCK has been shown to mediate sarcomere organization induced by a hypertrophic agonist in cultured cardiomyocytes and *in vivo* (Aoki *et al.*, 2000). Fuller characterization of the Ca^{2+}-CaM-MLCK interaction network may therefore prove relevant for future drug discovery efforts.

LIMITATIONS of STUDY

Although our data consistently supports partially ordered binding between MLCK and CaM, there are meaningful limitations to our study. Our experimental strategy does not infer MLCK activation in response to CaM-Ca^{2+} binding; binding data should not be interpreted as MLCK activation. In addition, MLCK is but one of the many binding partners of CaM. Future work is needed to determine mechanisms of CaM-Ca^{2+} binding to other CaM-Ca^{2+} regulated proteins.

ACKNOWLEDGEMENTS

We would like to thank Dr. Ning Zheng and Dr. Haibin Mao for their help with protein purification, Dr. Martin Golkowski for his help with mass spectrometry, Dr. Anthony Persechini for providing the MLCK FR construct, and Dr. Zenon Grabarek and Dr. John Biddle for comments on the manuscript. The authors are also grateful to UW's elevator maintenance team for rescuing MJSM (and several liters of induced bacteria) from a stalled elevator during the writing of this manuscript. MJSM was supported by NIH grant T32GM007750; JPD was supported by a Neukom Fellowship and a Harvard Data Science Fellowship.

AUTHOR CONTRIBUTIONS

MJSM, JPD, and YS designed the experiments and wrote the manuscript. MJSM, HE, and YS performed cloning, binding assays, and other biochemical experiments. DVR performed BLI experiments. TL and HG contributed to experimental design. MJSM, JPD, and YS analyzed the data. JPD developed the mathematical models.

DECLARATION OF INTEREST

The authors declare no conflicts of interest.

STAR★METHODS

RESOURCE AVAILABILITY

Lead Contact

Information and requests for resources and reagents should be directed to and will be fulfilled by the lead contact, Dr. Yasemin Sancak (sancak@uw.edu).

Materials availability

All plasmids generated in this study at University of Washington, Seattle, WA, USA are available upon request.

Data and code availability

- The original data reported in this paper will be shared by the lead contact upon request.
- This paper does not report original code
- Any additional information required to reanalyze the data reported in this paper is available from the lead contact upon request.

EXPERIMENTAL MODEL AND SUBJECT DETAILS

HEK 293T cells were acquired from the Sabatini Lab at the Whitehead Institute for Biomedical Research. The identity of the cell line was confirmed using STR analysis; cell line is of female origin. Cells were grown in DMEM supplemented with 1X GlutaMAX and 10% fetal bovine serum. Cells were tested for mycoplasma every 3 months and were confirmed to be free of mycoplasma contamination. Cells were cultured at 37°C with 5% CO2.

BL21(DE3) *E. coli* bacteria were acquired from the Zheng Lab at the University of Washington, Department of Pharmacology solely for the purpose of protein expression. Bacteria are stored as a flash frozen stock at -80C.

METHOD DETAILS

Cell Culture

- DMEM; Thermo Fisher Scientific, cat. no. 11-965-118
- Glutamax; Fisher Scientific, cat. no. 35-050-061
- PBS; Thermo Fisher Scientific, cat. no. 20012050
- Penicillin/streptomycin solution; VWR cat. no. 45000-652
- Fetal bovine serum; Life Technologies, cat. no. 26140087

- Genlantis MycoScope PCR Detection Kit; VWR cat. no. 10497-508

Gel Sample Preparation, Running, and Imaging

Reducing sample buffer, pH 6.8

- SDS; Sigma-Aldrich Cat. no. L4509-1KG
- BME/2-mercaptoethanol; Sigma-Aldrich Cat. no. M3148-25ML
- Glycerol; Sigma-Aldrich Cat. no. G5516-1L
- Tris–HCl: Sigma-Aldrich cat. no. T5941
- Bromophenol Blue; VWR Cat. no. 97061-690

Gel Electrophoresis

- 10X Tris/Glycine Buffer; Boston BioProducts Cat. no. BP-150-4L
- Tris-Glycine 12% Gel, 10-well or 15-well; Bio-Rad Cat. No. 4561043 or 4561046

Gel Imaging

- Methanol; Sigma-Aldrich cat. no. 32213-2.5L
- Acetic Acid; Sigma-Aldrich cat. no. A6283-500ML

Gels were stained with SYPRO® Ruby Protein Gel Stain (# S12000) following manufacturer's instructions and imaged with iBrightCL 1000 on fluorescent protein gel setting.

Expression of FR and MLCK-FLAG via transient transfection

- Transfection reagent; X-treme(GENE) 9, Sigma-Aldrich, cat. no. 6365779001

Day 1: Either 5 million (purification) or 2 million (on-bead binding assays) HEK 293T cells were plated on 15 cm or 10 cm plates, respectively. Day 2: 5 µg FR plasmid (purification), 1.5 µg FR plasmid (on-bead binding assays with FR) or 3 µg MLCK-FLAG plasmid (on-bead binding assays with MLCK-FLAG) was transfected using transfection reagent. *Day*

4: Cells were harvested, and FR or MLCK-FLAG was either purified (see below, “Purification of FR”) or used for on-bead binding assays.

Purification of FR and MLCK-FLAG

Lysis Buffer

- 50 mM HEPES-KOH **(**HEPES, Sigma-Aldrich, # H3375-1KG KOH, Sigma Millipore, # 1050121000)
- 150 mM NaCl, Sigma-Aldrich, # 746398-5KG
- 5 mM Ethylenediaminetetraacetic acid (EDTA): Sigma-Aldrich, # 607-429-00-8
- 1% Triton X-100: Sigma, # X100-1L
- FLAG Peptide Elution Buffer: 50 mM HEPES, 500 mM NaCl, pH 7.4
- Protease Inhibitor Tablets; Complete™, Mini, EDTA-free Protease Inhibitor Cocktail, Sigma-Aldrich cat. no. 5892953001
- Anti-FLAG affinity gel; Sigma-Aldrich, cat. no. A2220-5ML
- 3X FLAG peptide; Sigma-Aldrich cat. no. F4799-4MG
- Chromatography spin column; Bio-Rad cat. no. 7326204

Cells were lysed using lysis buffer supplemented with proteases inhibitors. Lysates were triturated in tubes and then centrifuged at 17000 g for 10 minutes. Cell supernatant was divided into three tubes with 200 µl of anti-FLAG affinity gel slurry (50:50 bead/lysis buffer). These tubes were rocked at 4 °C for 1 hour, and beads were washed three times with lysis buffer. A 22.5-gauge syringe was used to aspirate all remaining liquid from the tubes. FLAG-tagged protein was eluted with 90 µl of elution buffer, and 10 µl of 3XFLAG peptide prepared at 5 mg/mL for 30 minutes at 30 °C. The gel/elution buffer slurry from

all three tubes was then pipetted into one spin column and spun at max speed for 5 minutes.

Expression and Purification of Wild-type and Mutant CaM via Bacterial Induction

- Low-salt LB broth: Millipore Sigma, # L3397-1KG
- Isopropyl beta-D-1-thiogalactopyranoside (IPTG): Sigma-Aldrich, # I5502-5G
- HiTrap Q HP anion exchange chromatography column: Cytiva, # 17115301
- Centrifugal protein concentrator, 10K cutoff: Amicon, # UFC8010

Lysis Buffer

- 20 mM Tris-HCl, Sigma-Aldrich cat. no. T5941
- 100 mM NaCl, Sigma-Aldrich, cat. no. 746398-5KG
- 20 mM imidazole, Sigma-Aldrich, cat. no. I5513
- 0.4 mM EGTA, Sigma-Aldrich cat. no. 324626-25GM
- 0.5 mM TCEP, Sigma-Aldrich cat. no. C4706-2G

Elution Buffer

- 20 mM Tris-HCl, Sigma-Aldrich cat. no. T5941
- 100 mM NaCl, Sigma-Aldrich, cat. no. 746398-5KG
- 200 mM imidazole, Sigma-Aldrich, cat. no. I5513
- 0.4 mM EGTA, Sigma-Aldrich cat. no. 324626-25GM
- 0.5 mM TCEP, Sigma-Aldrich cat. no. C4706-2G

Buffer A:

- 100 mM NaCl, Sigma-Aldrich, cat. no. 746398-5KG
- 20 mM Tris-HCl, Sigma-Aldrich cat. no. T5941

Buffer B:

- 1M NaCl, Sigma-Aldrich, cat. no. 746398-5KG
- 20 mM Tris-HCl, Sigma-Aldrich cat. no. T5941

BL21 (DE3) bacteria transformed with a CaM expression vector were grown at 37 ^{o}C, 200 RPM until OD600 reached 0.8-1.0. Cultures were cooled to 18 ^{o}C and supplemented with IPTG to a final concentration of 0.3 mM before incubation at 18 ^{o}C, 200 RPM for 18 hours. Bacteria were pelleted, frozen, and stored at -80 °C until protein purification. Cells were lysed using sonication for 5 minutes at 40% power before being centrifuged at 17,400 RPM for 40 minutes to separate the soluble and insoluble portions of the lysate. The clarified lysate was loaded onto a Ni-NTA gravity column and then washed with 10 column volumes of lysis buffer before elution with 5 column volumes of elution buffer. The eluted protein was loaded manually into a 1 ml anion exchange chromatography column. HPLC was performed using buffers A and B. The HPLC fractions that contained the highest concentrations of protein were collected and concentrated to their final concentrations using a centrifugal filter with a 10 kDa molecular weight cutoff. Stock protein concentrations were as follows: CaM^{WT}: 3.98 µg/µl; $CaM^{21A,57A}$: 4.96 µg/µl; $CaM^{94A,130A}$: 1.36 µg/µl; $CaM^{21A,57A,94A,130A}$: 1.52 µg/µl. Purified protein was aliquoted, flash frozen in a liquid nitrogen dewar, and then stored at -80 °C until use.

FRET-Based CaM-FR Binding Assay

- Calcium calibration buffer kit; Invitrogen cat. no. C3008MP
- Microplate reader; BioTek Synergy H1
- Black 96-well plates; Greiner Bio-One cat. no. 655076

For each CaM-FR binding assay condition, 2 µg of CaM (either wild-type or mutant) and 200 ng FR was thoroughly mixed with 150 µl of Ca^{2+} buffer (14 conditions between 0 µM

and 39 μM). 150 μl of the resulting mixture was pipetted into 1 well of a 96-well plate (Greiner Bio-One, # 655076). CaM was used at a final concentration of 673 nM (13 ng/μl); FR was used at a final concentration of 22.9 nM (1.3 ng/μl). All protein preps (FR and CaM) were at sufficiently high concentrations that each protein addition added negligible volume; stock protein concentrations were as follows: CaM^{WT}: 3.98 μg/μl; $CaM^{21A,57A}$: 4.96 μg/μl; $CaM^{94A,130A}$: 1.36 μg/μl; $CaM^{21A,57A,94A,130A}$: 1.52 μg/μl; FR: 0.52 μg/μl. Follow-up experiments with Ca^{2+} indicator dyes confirmed that the final [Ca^{2+}] were unaffected by the addition of CaM or FR to the Ca^{2+} buffer (see "CaM and Ca^{2+} Buffer with Ca^{2+} Indicator Dye Assay" below). For functional assay, all 14 Ca^{2+} conditions were tested together, batch-wise. All wells were read at 430, 480 excitation/emission, and then again at 430, 535 excitation/emission using a microplate reader. The [430, 480] read was divided by the [430, 535] read to yield an emission ratio, which was plotted relative to [Ca^{2+}]. A small portion of each prepared Ca^{2+} condition was conserved and prepared with sample buffer, to be loaded onto a gel and stained.

CaM-FR FRET-Based Binding Sensitivity Assays

- Microcon concentrator column, Millipore cat. No. 42407

To test the robustness of the falsification of Model 1 to uncertainty in parameter values, we repeated the binding assay in zero [Ca^{2+}] using 35.65 μM CaM^{WT}. CaM^{WT} was concentrated to a stock concentration of 66.6 μg/μl using a concentrator column so that a comparable volume of protein stock (relative to previous assays) could be used. The "FRET-Based CaM-FR Binding Assay" was then performed as described above, except using 35.65 μM CaM^{WT}.

To determine a lower sensitivity limit for the CaM-FR binding assay, 22.9 nM FR was added to 150 µl of high Ca^{2+} buffer along with either 11.45 or 13.74 nM CaM^{WT}, which resulted in a CaM^{WT}:FR molar ratio of either 1:2 or 1.2:2. 150 µl of the resulting mixture was then read in a plate reader using the program employed by the "FRET-Based CaM-FR Binding Assay" (see above) and analyzed accordingly.

CaM-FR Spectral Scanning

- Calcium calibration buffer kit; Invitrogen cat. no. C3008MP
- Microplate reader; BioTek Synergy H1
- Black 96-well plates; Greiner Bio-One cat. no. 655076

CaM and FR were added to either 0 or 39 µM [Ca^{2+}] as per "FRET-Based CaM-FR Binding Assay" above. CaM was used at a final concentration of 673 nM (13 ng/µl); FR was used at a final concentration of 22.9 nM (1.3 ng/µl). Using an excitation wavelength of 430 nm, the wells were read using spectral scanning between wavelengths 460 nm and 700 nm, with an emission step of 10 nm. The fluorescence intensity of each wavelength was then plotted.

CaM-FR and CaM-MLCK-FLAG On-Bead Binding Assays

For assays utilizing FR, assay data was collected under 8 different conditions: FR bound to anti-FLAG M2 affinity gel beads and CaM under 6 different [Ca^{2+}] (0 µM, 0.1 µM, 0.35 µM, 1.35 µM, 3 µM, and 39 µM) and two controls (bead-bound FR alone in 39 µM [Ca^{2+}]; beads with CaM in 39 µM [Ca^{2+}]). For assays utilizing MLCK-FLAG, assay data was collected under 4 different conditions: MLCK-FLAG bound to anti-FLAG M2 affinity gel beads and CaM under 2 different [Ca^{2+}] (0 µM and 39 µM) and two controls (bead-bound MLCK-FLAG alone in 39 µM [Ca^{2+}]; beads with CaM in 39 µM [Ca^{2+}]).

Binding Assay Protocol: Transiently transfected cells were washed once with chilled PBS, and then harvested in 1% Triton buffer using a cell scraper. Cells were triturated to ensure complete lysis, and then were spun down at maximum speed (17,000g) for 10 minutes using a 4 ^{o}C centrifuge. 160 µl bead:glycerol M2 FLAG slurry was prepared for FLAG-tagged protein binding by washing three times with 1 ml 1% Triton buffer before being divided evenly between 8 tubes. The cleared lysate from the transiently transfected cells was divided evenly between 7 of the tubes, while cleared lysate from control WT HEK 293T was added to the 8th tube (control lysate). The beads were incubated with the lysate on a rocker at 4 ^{o}C for 45 minutes. After incubation, the two control tubes were washed twice with 200 µl 39 µM [Ca^{2+}], while the tubes for the 6 different Ca^{2+} conditions were each washed with the appropriate Ca^{2+} buffer. 50 µl of the appropriate Ca^{2+} buffer was then added to each experimental tube, while 50 µl of 39 µM Ca^{2+} was added to each control tube. Finally, for FR assays, 0.5 µg of CaM was added to all tubes except the reporter-only condition; final CaM concentration was approximately 505 nM (10 ng/µl). For MLCK-FLAG assays, 0.25 µg of CaM was added to all tubes except the MLCK-FLAG-only condition; final CaM concentration was approximately 24 nM (5 ng/µl) (NOTE: CaM concentration for MLCK-FLAG assays was decreased to compensate for decreased MLCK-FLAG expression relative to FR expression). CaM stock was at a sufficiently high concentration to ensure the addition of CaM did not meaningfully alter Ca^{2+} buffer concentration (see “CaM and Ca^{2+} Buffer with Ca^{2+} Indicator Dye Assay below”) (**Fig. S5**). All tubes were incubated at room temperature for 15 minutes and were flicked occasionally. Following incubation, the tubes were spun for 1 minute at 1,000 g to pellet the beads. 40 µl of the unbound portion was conserved and prepared with 10 µl 5X

reducing sample buffer. The beads for all conditions were then washed with 50 µl of the appropriate Ca^{2+} buffer and all liquid was aspirated from the beads using a syringe to remove residual unbound CaM. The beads were then incubated with 40 µl of FLAG peptide prepared in elution buffer for 30 minutes at 30°C to elute FLAG tagged FR. After elution, the beads were loaded to a spin column and spun for 1 minute at 1000g at room temperature to recover the eluate without the beads. This eluted sample was then boiled with 10 µl 5X reducing sample buffer. Finally, an "input" sample was prepared by adding 0.5 µg of CaM to 40 µl of 39 µM [Ca^{2+}] solution and 10 µl 5X reducing sample buffer.

Binding quantification: Bands were quantified using ImageJ. A rectangle was drawn around the unbound CaM band in the FR / CaM assay at 0 µM [Ca^{2+}]. This same rectangle was used to quantify the mean gray value within the rectangle for each binding condition. A measurement was also taken of the gel background, from the "input" lane containing only calmodulin. The background intensity measurement was subtracted from each quantified region. % binding was calculated using the following equation: % binding = bound fraction / [unbound CaM fraction + bound CaM fraction]. For **Fig. S6**, binding fraction was normalized by setting binding at 0 µM [Ca^{2+}] to 0% and at 39 µM [Ca^{2+}] to 100%, and calculating the % bound in the rest of the samples by normalizing to this scale.

CaM and Ca^{2+} Buffer with Ca^{2+} Indicator Dye Assay

- Calcium Green 5N, Hexapotassium Salt, Cell Impermeant; Thermo Fisher Scientific, cat. no. C3737
- Fluo-4 Cell Impermeant; Thermo Fisher Scientific, cat. no. F14200
- Microplate reader; BioTek Synergy H1
- Calcium calibration buffer kit; Invitrogen cat. no. C3008MP

- Black 96-well plates; Greiner Bio-One cat. no. 655076

CaM Storage Buffer ("Dummy Buffer")

- 250 mM NaCl, Sigma-Aldrich, cat. no. 746398-5KG
- 20 mM Tris, pH 8, Sigma-Aldrich cat. no. T5941

This assay was performed to confirm that the addition of CaM protein to the Ca^{2+} buffer used for the CaM-FR binding assay did not change the final [Ca^{2+}]. Two "sets" of each of the 14 different Ca^{2+} buffers used for CaM-FR binding assay were prepared, with dye (Calcium Green or Fluo-4) added to a final concentration of 1 μM. For one set of buffers, the buffer in which the CaM proteins was stored was added ("dummy buffer"). The amount of "dummy buffer" added was equal in volume to the maximum volume of CaM added per reaction (ie the C-terminus mutant CaM was the most dilute CaM prep, and approximately 1.5 μl CaM was added to each assay well, so an equivalent amount of "dummy buffer" was used for these experiments). 150 μl of each of these prepared buffers was added to wells of a black 96-well plate and data was collected using the GFP filter of a plate reader.

Mass Spectrometry Analysis of CaM Proteins

- Calcium calibration buffer kit, Invitrogen cat. no. C3008MP
- Chloroacetamide, Sigma cat. no. C0267
- TCEP, Sigma-Aldrich cat. no. C4706-2G
- Rappsilbers Stage tipping Paper (23), C-18 material: CDS Empore C18 Extraction Disks, Fisher cat. no. 13-110-016
- Formic acid for HPLC LiChropur, Sigma cat. no. 5438040100
- Trifluoroacetic acid (TFA), HPLC Grade, 99.5+%, Alfa Aesar, cat. no. AA446305Y
- Acetonitrile (ACN), Sigma-Aldrich cat. no. 271004-100ML

- Mass spectrometer: LC-MS: Orbitrap Fusion Lumos Tribrid (Thermo Fisher Scientific) and EASY-nLC™ 1200 System (Thermo Fisher Scientific)
- Triethylammonium bicarbonate buffer 1.0 M, pH 8.5±0.1, Sigma cat. no. T7408
- Ethanol for HPLC, Sigma cat. no. 459828
- Promega trypsin, cat no. V5111
- Methanol for HPLC, Sigma cat. No. 494291

StageTip Buffer A

- 5% ACN
- 0.1% TFA
- MQ water

StageTip Buffer B

- 0.1% TFA
- 80% ACN
- MQ water

Extraction solution

- 0.1% TFA, diluted in MQ water

Running the Gel

30 µg of wild-type CaM and N-terminus mutant CaM were each mixed with high Ca^{2+} calibration buffer to a final volume of 20 µl. A blank control consisting of CaM storage buffer and Ca^{2+} calibration buffer was also prepared. All samples were reduced using 1 mM final concentration of TCEP and alkylated using 2 mM final concentration of chloroacetamide (CAM) at 37C for 20 min on a shaker. They were then quenched using 1 mM final concentration of TCEP at 37C for 20 min on a shaker. Next, they were mixed

with 5X gel loading buffer, boiled for five minutes, and loaded into a 10% gel (see "**Gel Electrophoresis**" above). The samples were run until the dye front reached the bottom of the gel. The gel was then rinsed and stained using Coomassie stain for one hour, and de-stained overnight.

In-gel Digestion Protocol

The next day, two bands from each lane were excised and cut into small cubes using a single-use scalpel; one band was comprised of the gel at ~18 kDa (where the major CaM band is located) and one was comprised of the gel between ~10 and 17 kDa, the area under the major band. The rest of the in-gel digestion was performed as previously described in Lau *et al.*, 2014.

Extraction of Peptides and StageTip Purification

StageTip extraction of peptides was performed as described previously in Rappsilber *et al.*, 2007.

nanoLC-MS/MS Analyses

LC-MS analyses were performed as described previously with the following minor modifications (Cox *et al.*, 2011). Peptide samples were separated on an EASY-nLC 1200 System (Thermo Fisher Scientific) using 20 cm long fused silica capillary columns (100 µm ID) packed with 3 µm 120 Å reversed phase C18 beads (Dr. Maisch, Ammerbuch, DE). The LC gradient was 90 min long with 5−35% B at 300 nL/min. LC solvent A was 0.1% (v/v) aq. acetic acid and LC solvent B was 20% 0.1% (v/v) acetic acid, 80% acetonitrile. MS data was collected with a Thermo Fisher Scientific Orbitrap Fusion Lumos Tribrid mass spectrometer. Data-dependent analysis was applied using Top15 selection with CID fragmentation

Computation of MS raw files

Data .raw files were analyzed by MaxQuant/Andromeda (Cox *et al.*, 2011) version 1.5.2.8 using protein, peptide, and site FDRs of 0.01 and a score minimum of 40 for modified peptides, 0 for unmodified peptides; delta score minimum of 17 for modified peptides, 0 for unmodified peptides. MS/MS spectra were searched against the UniProt human database (updated July 22nd, 2015). MaxQuant search parameters: Variable modifications included Oxidation (M) and Phospho (S/T/Y). Carbamidomethyl (C) was a fixed modification. Maximum missed cleavages was 2, enzyme was Trypsin/P and max. charge was 7. The MaxQuant "match between runs" feature was disabled. The initial search tolerance for FTMS scans was 20 ppm and 0.5 Da for ITMS MS/MS scans.

Semi-quantitative analysis of contaminants and CaM protein

The intensity of peptides annotated as CaM, keratin, or bacterial protein was summed up and their relative intensities were calculated by dividing them to the total peptide intensity in the samples.

Octet BioLayer Interferometry (BLI) measurement

- Octet Red 96 (ForteBio, Pall Life Sciences)
- Bovine Serum Albumin (BSA), Sigma-Aldrich cat. no. A3294-100G
- Calcium chloride, Sigma-Aldrich cat. no. 746495-1KG
- Tris-HCl, Sigma-Aldrich cat. no. T5941
- NaCl Sigma-Aldrich, # 746398-5KG

The binding of His-CaM to FR or FL-MLCK-FLAG protein in the presence of Ca^{2+} was analyzed using the Octet Red 96 (ForteBio, Pall Life Sciences) following the manufacturer's procedures in duplicates. The reaction was carried out in black 96 well

plates maintained at 30 °C. The reaction volume was 200 µL in each well. The Octet buffer contained 20 mM Tris-HCl, 200 mM NaCl, and 0.1% BSA, pH 8.0. The Association buffer contained 20 mM Tris-HCl, 200 mM NaCl, 1.5 mM Ca^{2+} and 0.1% BSA, pH 8.0. The Dissociation buffer contained 20 mM Tris-HCl, 200 mM NaCl, and 0.1% BSA, pH 8.0. The concentration of ligand – His-CaM^{WT}, His-$CaM^{21A, 57A}$, or His-$CaM^{94A, 130A}$ – in the Octet buffer was 2 µM. The concentration of His-GST as the quench in Octet Buffer was 0.68 µM. The concentration of FR or MLCK-FLAG as the analyte in the Association buffer was 1.5 µM. Ni-NTA optical probes were loaded with His-CaM^{WT}, His-$CaM^{21A, 57A}$, or His-$CaM^{94A, 130A}$ as ligands for 110 seconds and quenched with His-GST for 80 seconds prior to binding analysis. While not loaded with ligand, the control probes were quenched with His-GST. In each experiment, “Control” refers to the analyte (either FR or MLCK-FLAG) binding to the ligand-free probe. This control is performed to demonstrate that the association seen in the ligand bound probes is not due to nonspecific binding but is, in fact, specific. The binding of the analyte (either FR or MLCK-FLAG) to the optical probes was measured simultaneously using instrumental defaults for 236 seconds. The dissociation was measured for 287 seconds. There was no binding of FR to the unloaded probes; however, slight binding of MLCK-FLAG to the unloaded probes was observed. The data were analyzed by the Octet data analysis software. The association and dissociation curves for FR binding were globally fit with a 1:1 ligand model, and the curves for MLCK-FLAG binding were locally fit for 80s. The data was plotted using Prism 7.

DNA Sequences

CaM Sequences

Red highlighting: mutations

His-CaM^{WT} DNA Sequence (protein molecular weight: ~19.8 kDa)

atgggcagcagccatcatcatcatcacagcagcggcctggtgccgcgcggcagccatagcgaaaacctctacttcc
aatcgatggctgaccagctgactgaggagcagattgcagagttcaaggaggccttctccctctttgacaaggatggagat
ggcactatcaccaccaaggagttggggacagtgatgagatccctgggacagaaccccactgaagcagagctgcagga
tatgatcaatgaggtggatgcagatgggaacgggaccattgacttcccggagttcctgaccatgatggccagaaagatga
aggacacagacagtgaggaggagatccgagaggcgttccgtgtctttgacaaggatgggaatggctacatcagcgccg
cagagctgcgtcacgtaatgacgaacctgggggagaagctgaccgatgaggaggtggatgagatgatcagggaggct
gacatcgatggagatggccaggtcaattatgaagagtttgtacagatgatgactgcaaagtga

His-CaM^{21A,57A} DNA Sequence (protein molecular weight: ~19.8 kDa)

atgggcagcagccatcatcatcatcacagcagcggcctggtgccgcgcggcagccatagcgaaaacctctacttcc
aatcgatggctgaccagctgactgaggagcagattgcagagttcaaggaggccttctccctctttgccaaggatggagat
ggcactatcaccaccaaggagttggggacagtgatgagatccctgggacagaaccccactgaagcagagctgcagga
tatgatcaatgaggtggcagcagatgggaacgggaccattgacttcccggagttcctgaccatgatggccagaaagatg
aaggacacagacagtgaggaggagatccgagaggcgttccgtgtctttgacaaggatgggaatggctacatcagcgcc
gcagagctgcgtcacgtaatgacgaacctgggggagaagctgaccgatgaggaggtggatgagatgatcagggagg
ctgacatcgatggagatggccaggtcaattatgaagagtttgtacagatgatgactgcaaagtga

His-CaM^{94A,130A} DNA Sequence (protein molecular weight: ~19.8 kDa)

atgggcagcagccatcatcatcatcacagcagcggcctggtgccgcgcggcagccatagcgaaaacctctacttcc
aatcgatggctgaccagctgactgaggagcagattgcagagttcaaggaggccttctccctctttgacaaggatggagat
ggcactatcaccaccaaggagttggggacagtgatgagatccctgggacagaaccccactgaagcagagctgcagga
tatgatcaatgaggtggatgcagatgggaacgggaccattgacttcccggagttcctgaccatgatggccagaaagatga
aggacacagacagtgaggaggagatccgagaggcgttccgtgtctttgccaaggatgggaatggctacatcagcgccg
cagagctgcgtcacgtaatgacgaacctgggggagaagctgaccgatgaggaggtggatgagatgatcagggaggct
gccatcgatggagatggccaggtcaattatgaagagtttgtacagatgatgactgcaaagtga

His-CaM^{21A,57A,94A,130A} DNA Sequence (protein molecular weight: ~19.8 kDa)

atgggcagcagccatcatcatcatcacagcagcggcctggtgccgcgcggcagccatagcgaaaacctctacttcc
aatcgatggctgaccagctgactgaggagcagattgcagagttcaaggaggccttctccctctttgccaaggatggagat
ggcactatcaccaccaaggagttggggacagtgatgagatccctgggacagaaccccactgaagcagagctgcagga

tatgatcaatgaggtggcagcagatgggaacgggaccattgacttcccggagttcctgaccatgatggccagaaagatg
aaggacacagacagtgaggaggagatccgagaggcgttccgtgtctttgccaaggatgggaatggctacatcagcgcc
gcagagctgcgtcacgtaatgacgaacctgggggagaagctgaccgatgaggaggtggatgagatgatcagggagg
ctgccatcgatggagatggccaggtcaattatgaagagtttgtacagatgatgactgcaaagtga

MLCK FRET REPORTER (FR) DNA Sequence (protein molecular weight: ~58.2 kDa)

Yellow highlighting: EYFP

Light grey highlighting: Calmodulin binding domain

Blue highlighting: ECFP

Dark grey highlighting: Flexible linker

Green highlighting: FLAG tag

Atggtgagcaagggcgaggagctgttcaccggggtggtgcccatcctggtcgagctggacggcgacgtaaacggcca
caagttcagcgtgtccggcgagggcgagggcgatgccacctacggcaagctgaccctgaagttcatctgcaccaccgg
caagctgcccgtgccctggcccaccctcgtgaccaccttcggctacggcctgatgtgcttcgcccgctaccccgaccacat
gcgccagcacgacttcttcaagtccgccatgcccgaaggctacgtccaggagcgcaccatcttcttcaaggacgacggc
aactacaagacccgcgccgaggtgaagttcgagggcgacaccctggtgaaccgcatcgagctgaagggcatcgactt
caaggaggacggcaacatcctggggcacaagctggagtacaactacaacagccacaacgtctatatcatggccgaca
agcagaagaacggcatcaaggtgaacttcaagatccgccacaacatcgaggacggcagcgtgcagctcgccgacca
ctaccagcagaacaccccatcggcaacggccccgtgctgctgcccgacaaccactacctgagctaccagtccgccct
gagcaaagaccccaacgagaagcgcgatcacatggtcctgctggagttcgtgaccgccgccgggatcactctcggcat
ggacgagctgtacaagggtaccgccgctcgtcagaaatggcagaaaaccggacatgcggtgcgtgcgattggccgtct
ggctgctaccggtagcaagggcgaggagctgttcaccggggtggtgcccatcctggtcgagctggacggcgacgtaaa
cggccacaggttcagcgtgtccggcgagggcgagggcgatgccacctacggcaagctgaccctgaagttcatctgcac
caccggcaagctgcccgtgccctggcccaccctcgtgaccaccctgacctggggcgtgcagtgcttcagccgctacccc
gaccacatgaagcagcacgacttcttcaagtccgccatgcccgaaggctacgtccaggagcgtaccatcttcttcaagga
cgacggcaactacaagacccgcgccgaggtgaagttcgagggcgacaccctggtgaaccgcatcgagctgaagggc
atcgacttcaaggaggacggcaacatcctggggcacaagctggagtacaactacatcagccacaacgtctatatcacc
gccgacaagcagaagaacggcatcaaggcccacttcaagatccgccacaacatcgaggacggcagcgtgcagctcg
ccgaccactaccagcagaacaccccatcggcgacggccccgtgctgctgcccgacaaccactacctgagcacccag

tccgccctgagcaaagaccccaacgagaagcgcgatcacatggtcctgctggagttcgtgaccgccgccgggatcact
ctcggcatggacgagctgtacaagcccgggggtggatctggtggatctggtggatctatggattacaaggatgacgatga
caag

Full-length MLCK DNA Sequence (Protein molecular weight: ~212.0 kDa)

Light grey highlighting: Calmodulin binding domain

Dark grey highlighting: Flexible linker

Green highlighting: FLAG tag

atgggggatgtgaagctggttgcctcgtcacacatttccaaaacctccctcagtgtggatccctcaagagttgactccatgcc
cctgacagaggcccctgctttcattttgccccctcggaacctctgcatcaaagaaggagccaccgccaagttcgaagggc
gggtccggggttacccagagccccaggtgacatggcacagaaacgggcaacccatcaccagcgggggccgcttcctg
ctggattgcggcatccgggggactttcagccttgtgattcatgctgtccatgaggaggacaggggaaagtatacctgtgaa
gccaccaatggcagtggtgctcgccaggtgacagtggagttgacagtagaaggaagttttgcgaagcagcttggtcagc
ctgttgtttccaaaaccttaggggatagattttcagcttcagcagtggagacccgtcctagcatctgggggggagtgcccacc
aaagtttgctaccaagctgggccgagttgtggtcaaagaaggacagatgggacgattctcctgcaagatcactggccgg
ccccaaccgcaggtcacctggctcaagggaaatgttccactgcagccgagtgcccgtgtgtctgtgtctgagaagaacgg
catgcaggttctggaaatccatggagtcaaccaagatgacgtgggagtgtacacgtgcctggtggtgaacgggtcgggg
aaggcctcgatgtcagctgaactttccatccaaggtttggacagtgccaataggtcatttgtgagagaaacaaaagccacc
aattcagatgtcaggaaagaggtgaccaatgtaatctcaaaggagtcgaagctggacagtctggaggctgcagccaaa
agcaagaactgctccagcccccagagaggtggctccccaccctgggctgcaaacagccagcctcagcccccaaggg
agtccaagctggagtcatgcaaggactcgcccagaacggccccgcagactccggtccttcagaagacttccagctccat
caccctgcaggccgcaagagttcagccggaaccaagagcaccaggcctgggggtcctatcaccttctggagaagaga
ggaagaggccagctcctccccgtccagccaccttccccaccaggcagcctggcctggggagccaagatgttgtgagca
aggctgctaacaggagaatccccatggagggccagagggattcagcattccccaaatttgagagcaagccccaaagc
caggaggtcaaggaaaatcaaactgtcaagttcagatgtgaagtttccgggattccaaagcctgaagtggcctggttcctg
gaaggcacccccgtgaggagacaggaaggcagcattgaggtttatgaagatgctggctcccattacctctgcctgctgaa
agcccggaccagggacagtgggacatacagctgcactgcttccaacgcccaaggccaggtgtcctgtagctggaccct
ccaagtggaaaggcttgccgtgatggaggtggccccctccttctccagtgtcctgaaggactgcgccgttattgagggcca
ggattttgtgctgcagtgctccgtacgggggaccccagtgccccggatcacttggctgctgaatgggcagcccatccagta
cgctcgctccacctgcgaggccggcgtggctgagctccacatccaggatgccctgccggaggaccatggcacctacac

ctgcctagctgagaatgccttggggcaggtgtcctgcagcgcctgggtcaccgtccatgaaaagaagagtagcaggaag
agtgagtaccttctgcctgtggctcccagcaagcccactgcacccatcttcctgcagggcctctctgatctcaaagtcatgga
tggaagccaggtcactatgactgtccaagtgtcagggaatccacccccctgaagtcatctggctgcacaatgggaatgaga
tccaagagtcagaggacttccactttgaacagagaggaactcagcacagcctttgtatccaggaagtgttcccggaggac
acgggcacgtacacctgcgaggcctggaacagcgctggagaggtccgcacccaggccgtgctcacggtacaagagc
ctcacgatggcacccagccctggttcatcagtaagcctcgctcagtgacagcctccctgggccagagtgtcctcatctcctg
cgccatagctggtgacccctttcctaccgtgcactggctcagagatggcaaagccctctgcaaagacactggccacttcg
aggtgcttcagaatgaggacgtgttcaccctggttctaaagaaggtgcagccctggcatgccggccagtatgagatcctgc
tcaagaaccgggttggcgaatgcagttgccaggtgtcactgatgctacagaacagctctgccagagcccttccacgggg
gagggagcctgccagctgcgaggacctctgtggtggaggagttggtgctgatggtggtggtagtgaccgctatgggtccct
gaggcctggctggccagcaagagggcagggttggctagaggaggaagacggcgaggacgtgcgaggggtgctgaa
gaggcgcgtggagacgaggcagcacactgaggaggcgatccgccagcaggaggtggagcagctggacttccgaga
cctcctggggaagaaggtgagtacaaagaccctatcggaagacgacctgaaggagatcccagccgagcagatggatt
tccgtgccaacctgcagcggcaagtgaagccaaagactgtgtctgaggaagagaggaaggtgcacagcccccagca
ggtcgattttcgctctgtcctggccaagaaggggacttccaagacccccgtgcctgagaaggtgccaccgccaaaacctg
ccaccccggattttcgctcagtgctgggtggcaagaagaaattaccagcagagaatggcagcagcagtgccgagaccc
tgaatgccaaggcagtggagagttccaagcccctgagcaatgcacagccttcagggcccttgaaacccgtgggcaacg
ccaagcctgctgagaccctgaagccaatgggcaacgccaagcctgccgagaccctgaagcccatgggcaatgccaa
gcctgatgagaacctgaaatccgctagcaaagaagaactcaagaaagacgttaagaatgatgtgaactgcaagagag
gccatgcagggaccacagataatgaaaagagatcagagagccaggggacagccccagccttcaagcagaagctgc
aagatgttcatgtggcagagggcaagaagctgctgctccagtgccaggtgtcttctgacccccagccaccatcatctgga
cgctgaacggaaagaccctcaagaccaccaagttcatcatcctctcccaggaaggctcactctgctccgtctccatcgag
aaggcactgcctgaggacagaggcttatacaagtgtgtagccaagaatgacgctggccaggcggagtgctcctgccaa
gtcaccgtggatgatgctccagccagtgagaacaccaaggccccagagatgaaatcccggaggcccaagagctctctt
cctcccgtgctaggaactgagagtgatgcgactgtgaaaaagaaacctgcccccaagacacctccgaaggcagcaat
gccccctcagatcatccagttccctgaggaccagaaggtacgcgcaggagagtcagtggagctgtttggcaaagtgaca
ggcactcagcccatcacctgtacctggatgaagttccgaaagcagatccaggaaagcgagcacatgaaggtggagaa
cagcgagaatggcagcaagctcaccatcctggccgcgcgccaggagcactgcggctgctacacactgctggtggaga
acaagctgggcagcaggcaggcccaggtcaacctcactgtcgtggataagccagacccccagctggcacaccttgtg
cctctgacattcggagctcctcactgaccctgtcctggtatggctcctcatatgatgggggcagtgctgtacagtcctacagc
atcgagatctgggactcagccaacaagacgtggaaggaactagccacatgccgcagcacctctttcaacgtccaggac

ctgctgcctgaccacgaatataagttccgtgtacgtgcaatcaacgtgtatggaaccagtgagccaagccaggagtctga
actcacaacggtaggagagaaacctgaagagccgaaggatgaagtggaggtgtcagatgatgatgagaaggagccc
gaggttgattaccggacagtgacaatcaatactgaacaaaaagtatctgacttctacgacattgaggagagattaggatct
gggaaatttggacaggtctttcgacttgtagaaaagaaaactcgaaaagtctgggcagggaagttcttcaaggcatattca
gcaaaagagaaagagaatatccggcaggagattagcatcatgaactgcctccaccaccctaagctggtccagtgtgtgg
atgcctttgaagaaaaggccaacatcgtcatggtcctggagatcgtgtcaggaggggagctgtttgagcgcatcattgacg
aggactttgagctgacggagcgtgagtgcatcaagtacatgcggcagatctcggagggagtggagtacatccacaagc
agggcatcgtgcacctggacctcaagccggagaacatcatgtgtgtcaacaagacgggcaccaggatcaagctcatcg
actttggtctggccaggaggctggagaatgcggggtctctgaaggtcctctttggcaccccagaatttgtggctcctgaagtg
atcaactatgagcccatcggctacgccacagacatgtggagcatcggggtcatctgctacatcctagtcagtggcctttccc
ccttcatgggagacaacgataacgaaaccttggccaacgttacctcagccacctgggacttcgacgacgaggcattcgat
gagatctccgacgatgccaaggatttcatcagcaatctgctgaagaaagatatgaaaaaccgcctggactgcacgcagt
gccttcagcatccatggctaatgaaagataccaagaacatggaggccaagaaactctccaaggaccggatgaagaag
tacatggcaagaaggaaatggcagaaaacgggcaatgctgtgagagccattggaagactgtcctctatggcaatgatct
cagggctcagtggcaggaaatcctcaacagggtcaccaaccagcccgctcaatgcagaaaaactagaatctgaagaa
gatgtgtcccaagctttccttgaggctgttgctgaggaaaagcctcatgtaaaaccctatttctctaagaccattcgcgatttag
aagttgtggagggaagtgctgctagatttgactgcaagattgaaggatacccagaccccgaggttgtctggttcaaagatg
accagtcaatcagggagtcccgccacttccagatagactacgatgaggacgggaactgctctttaattattagtgatgtttgc
ggggatgacgatgccaagtacacctgcaaggctgtcaacagtcttggagaagccacctgcacagcagagctcattgtgg
aaacgatggaggaaggtgaaggggaaggggaagaggaagaagaggtcgacatggactacaaggacgacgacga
caag

QUANTIFICATION AND STATISTICAL ANALYSIS

Analysis of FR-CaM Binding Assay (Fig. 3): For CaM^{WT} and $CaM^{21A,57A}$, each data point is presented as the mean ± s.d. of 15 independent experiments. For $CaM^{94A,130A}$, each data point is presented as mean of ± s.d. of 8 independent experiments, and for $CaM^{21A,57A,94A,130A}$, each data point is presented as mean of ± s.d. of 3 independent experiments. For reporter-only data, each data point is presented as a mean ± s.d. of 17 independent experiments. Curve fits were computed using the Matlab (version R2020a) package doseResponse. Algebraic calculations involving the mathematical models were

done in Wolfram Mathematica (version 12.1). Statistical calculations were performed using Matlab. AUC was computed using the trapz built-in Matlab function.

Comparison of on-bead and FRET-based binding assessment between FR and CaM^{WT} as a function of [Ca^{2+}] (Fig. S6): Fraction of calmodulin bound to FR was quantified using ImageJ; GraphPad Prism 7 was used to plot mean and standard deviation.

Bio-Layer Interferometry (BLI) binding assays (Fig. 5): Following data collection, the data were analyzed using the Octet data analysis software (Octet® Analysis Studio) and plotted using GraphPad Prism 7.

FR-CaM binding sensitivity assay (Fig. S7): Following the determination of the mean and standard deviation using GraphPad Prism, a one-tailed Mann-Whitney *U* test was performed to determine the significance (*P* value) of the ratio increase.

High concentration FR-CaM^{WT} binding quantification (Fig. S8): Following the determination of the mean and standard deviation using GraphPad Prism, a one-tailed Mann-Whitney *U* test was performed to determine the significance (*P* value) of the ratio increase.

Impact of buffer addition on free [Ca^{2+}] (Fig. S10): Following the determination of the mean and standard deviation using GraphPad Prism, a two-tailed Mann-Whitney *U* test was performed to determine the significance (*P* value) of the fluorescence change.

Statistical Analysis: Statistical calculations were performed using Matlab. AUC was computed using the trapz built-in Matlab function.

KEY RESOURCES TABLE

REAGENT or RESOURCE	SOURCE	IDENTIFIER

Bacterial and Virus Strains		
BL21(DE3) *E. coli* bacteria	New England BioLabs (note: for the purpose of these experiments, BL21(DE3) bacteria were obtained from the Ning Zheng Lab at the University of Washington)	cat. no. C2527I
Chemicals, Peptides, and Recombinant Proteins		
DMEM	Thermo Fisher Scientific	cat. no. 11-965-118
Glutamax	Fisher Scientific	cat. no. 35-050-061
PBS	Thermo Fisher Scientific	cat. no. 20012050
Penicillin/streptomycin solution	VWR	cat. no. 45000-652
Fetal bovine serum	Life Technologies	cat. no. 26140087
SDS	Sigma-Aldrich	cat. no. L4509-1KG
BME/2-mercaptoethanol	Sigma-Aldrich	cat. no. M3148-25ML
Glycerol	Sigma-Aldrich	cat. no. G5516-1L

Tris–HCl	Sigma-Aldrich	cat. no. T5941
Bromophenol Blue	VWR	cat. no. 97061-690
10X Tris/Glycine Buffer	Boston BioProducts	cat. no. BP-150-4L
Tris-Glycine 12% Gel, 10-well or 15-well	Bio-Rad	cat. no. 4561043 or 4561046
Methanol	Sigma-Aldrich	cat. no. 32213-2.5L
Acetic Acid	Sigma-Aldrich	cat. no. A6283-500ML
Transfection reagent; X-treme(GENE) 9	Sigma-Aldrich	cat. no. 6365779001
SYPRO™ Ruby Protein Gel Stain	Thermo Fisher Scientific	cat. no. S12000
HEPES	Sigma-Aldrich	cat. no. H3375-1KG
KOH	Sigma Millipore	cat. no. 1050121000
NaCl	Sigma-Aldrich	cat. no. 746398-5KG
Ethylenediaminetetraacetic acid (EDTA)	Sigma-Aldrich	cat. no. 607-429-00-8
Triton X-100	Sigma-Aldrich	cat. no. X100-1L
Protease Inhibitor Tablets; Complete™, Mini, EDTA-free Protease Inhibitor Cocktail	Sigma-Aldrich	cat. no. 5892953001
Anti-FLAG affinity gel	Sigma-Aldrich	cat. no. A2220-5ML
3X FLAG peptide	Sigma-Aldrich	cat. no. F4799-4MG
Low-salt LB broth	Millipore Sigma	cat. no. L3397-1KG
Isopropyl beta-D-1-thiogalactopyranoside (IPTG)	Sigma-Aldrich	cat. no. I5502-5G

imidazole	Sigma-Aldrich	cat. no. I5513
EGTA	Sigma-Aldrich	cat. no. 324626-25GM
TCEP	Sigma-Aldrich	cat. no. C4706-2G
Calcium calibration buffer kit	Invitrogen	cat. no. C3008MP
Calcium Green 5N, Hexapotassium Salt, Cell Impermeant	Thermo Fisher Scientific	cat. no. C3737
Fluo-4 Cell Impermeant	Thermo Fisher Scientific	cat. no. F14200
Chloroacetamide	Sigma	cat. no. C0267
TCEP	Sigma-Aldrich	cat. no. C4706-2G
Rappsilbers Stage tipping Paper (23), C-18 material; CDS Empore C18 Extraction Disks	Fisher	cat. no. 13-110-016
Formic acid for HPLC LiChropur	Sigma	cat. no. 5438040100
Trifluoroacetic acid (TFA), HPLC Grade, 99.5+%	Alfa Aesar	cat. no. AA446305Y
Acetonitrile (ACN)	Sigma-Aldrich	cat. no. 271004-100ML
Triethylammonium bicarbonate buffer 1.0 M, pH 8.5±0.1	Sigma	cat. no. T7408
Ethanol for HPLC	Sigma	cat. no. 459828
trypsin	Promega	cat no. V5111
Methanol for HPLC	Sigma	cat. no. 494291
Bovine Serum Albumin (BSA)	Sigma-Aldrich	cat. no. A3294-100G
Calcium chloride	Sigma-Aldrich	cat. no. 746495-1KG
Critical Commercial Assays		

Genlantis MycoScope PCR Detection Kit	VWR	cat. no. 10497-508
Deposited Data		
Data was uploaded to BioRxiv on 1 December 2022 prior to iScience acceptance	bioRxiv	doi: https://doi.org/10.1101/2022.06.08.495195
Experimental Models: Cell Lines		
HEK-293T cell line	acquired from the Sabatini Lab at the Whitehead Institute for Biomedical Research.	This cell line has been published extensively. For example PMID: 29074583
Recombinant DNA		
His-CaMWT DNA in bacterial expression plasmid	this paper	plasmid available upon request
His-CaM21A,57A DNA in bacterial expression plasmid	this paper	plasmid available upon request
His-CaM94A,130A DNA in bacterial expression plasmid	this paper	plasmid available upon request
His-CaM21A,57A,94A,130A DNA in bacterial expression plasmid	this paper	plasmid available upon request
MLCK FRET Reporter (FR) DNA in mammalian expression plasmid	this paper	plasmid available upon request. FR was firt developed by Dr. Anthony Persechini, and was cloned in mammalian expression vector; see PMID: **14741352** for reference.
Full-length MLCK DNA in mammalian expression plasmid	this paper	plasmid available upon request. MLCK gene was amplified from Addgene plasmid # 46316, from the Bresnick Lab, and cloned into a mammalian expression vector.
Software and Algorithms		

Andromeda version 1.5.2.8	MaxQuant	https://www.maxquant.org/
trapz; doseResponse	MATLAB R2020a	https://www.mathworks.com/products/new_products/release2020a.html
Octet® Analysis Studio	Sartorius	https://www.sartorius.com/en/products/protein-analysis/octet-bli-detection/octet-systems-software
Prism 7	Graphpad	https://www.graphpad.com/support/prism-7-updates/
Mathematica 12.1	Wolfram	https://support.wolfram.com/51966
ImageJ	National Insitutes of Health	https://imagej.net/ij/index.html

REFERENCES

- Adelstein, R.S., and Sellers, J.R. (1987). Effects of calcium on vascular smooth muscle contraction. Am J Cardiol 59, 4B-10B. 10.1016/0002-9149(87)90076-2.
- Aoki, H., Sadoshima, J., and Izumo, S. (2000). Myosin light chain kinase mediates sarcomere organization during cardiac hypertrophy in vitro. Nat Med 6, 183-188. 10.1038/72287.
- Babu, Y.S., Sack, J.S., Greenhough, T.J., Bugg, C.E., Means, A.R., and Cook, W.J. (1985). Three-dimensional structure of calmodulin. Nature 315, 37-40. 10.1038/315037a0.
- Brown, S.E., Martin, S.R., and Bayley, P.M. (1997). Kinetic control of the dissociation pathway of calmodulin-peptide complexes. J Biol Chem 272, 3389-3397. 10.1074/jbc.272.6.3389.
- Calizo, R.C., Bell, M.K., Ron, A., Hu, M., Bhattacharya, S., Wong, N.J., Janssen, W.G.M., Perumal, G., Pederson, P., Scarlata, S., et al. (2020). Cell shape regulates subcellular organelle location to control early Ca(2+) signal dynamics in vascular smooth muscle cells. Sci Rep 10, 17866. 10.1038/s41598-020-74700-x.

- Chang, A.N., Mahajan, P., Knapp, S., Barton, H., Sweeney, H.L., Kamm, K.E., and Stull, J.T. (2016). Cardiac myosin light chain is phosphorylated by Ca2+/calmodulin-dependent and -independent kinase activities. Proc Natl Acad Sci U S A 113, E3824-3833. 10.1073/pnas.1600633113.
- Cox, J., Neuhauser, N., Michalski, A., Scheltema, R.A., Olsen, J.V., and Mann, M. (2011). Andromeda: a peptide search engine integrated into the MaxQuant environment. J Proteome Res 10, 1794-1805. 10.1021/pr101065j.
- Dexter, J.P., Biddle, J.W., and Gunawardena, J. (2018). Model discrimination for Ca(2+) -dependent regulation of myosin light chain kinase in smooth muscle contraction. FEBS Lett 592, 2811-2821. 10.1002/1873-3468.13207.
- Fajmut, A., Brumen, M., and Schuster, S. (2005). Theoretical model of the interactions between Ca2+, calmodulin and myosin light chain kinase. FEBS Lett 579, 4361-4366. 10.1016/j.febslet.2005.06.076. (A)
- Fajmut, A., Jagodic, M., and Brumen, M. (2005). Mathematical modeling of the myosin light chain kinase activation. J Chem Inf Model 45, 1605-1609. 10.1021/ci050177i. (B)
- Geguchadze, R., Zhi, G., Lau, K.S., Isotani, E., Persechini, A., Kamm, K.E., and Stull, J.T. (2004). Quantitative measurements of Ca(2+)/calmodulin binding and activation of myosin light chain kinase in cells. FEBS Lett 557, 121-124. 10.1016/s0014-5793(03)01456-x.
- Geiser, J.R., van Tuinen, D., Brockerhoff, S.E., Neff, M.M., and Davis, T.N. (1991). Can calmodulin function without binding calcium? Cell 65, 949-959. 10.1016/0092-8674(91)90547-c.

- Hong, F., Haldeman, B.D., Jackson, D., Carter, M., Baker, J.E., and Cremo, C.R. (2011). Biochemistry of smooth muscle myosin light chain kinase. Arch Biochem Biophys 510, 135-146. 10.1016/j.abb.2011.04.018.
- Kato, S., Osa, T., and Ogasawara, T. (1984). Kinetic model for isometric contraction in smooth muscle on the basis of myosin phosphorylation hypothesis. Biophys J 46, 35-44. 10.1016/S0006-3495(84)83996-X.
- Lau, H.T., Suh, H.W., Golkowski, M., and Ong, S.E. (2014). Comparing SILAC- and stable isotope dimethyl-labeling approaches for quantitative proteomics. J Proteome Res 13, 4164-4174. 10.1021/pr500630a.
- Mauban, J.R., Fairfax, S.T., Rizzo, M.A., Zhang, J., and Wier, W.G. (2014). A method for noninvasive longitudinal measurements of [Ca2+] in arterioles of hypertensive optical biosensor mice. Am J Physiol Heart Circ Physiol 307, H173-181. 10.1152/ajpheart.00182.2014.
- Paranjape, V., Roy, B.G., and Datta, A. (1990). Involvement of calcium, calmodulin and protein phosphorylation in morphogenesis of Candida albicans. J Gen Microbiol 136, 2149-2154. 10.1099/00221287-136-11-2149.
- Park, H.Y., Kim, S.A., Korlach, J., Rhoades, E., Kwok, L.W., Zipfel, W.R., Waxham, M.N., Webb, W.W., and Pollack, L. (2008). Conformational changes of calmodulin upon Ca2+ binding studied with a microfluidic mixer. Proc Natl Acad Sci U S A 105, 542-547. 10.1073/pnas.0710810105.
- Piazza, M., Taiakina, V., Dieckmann, T., and Guillemette, J.G. (2017). Structural Consequences of Calmodulin EF Hand Mutations. Biochemistry 56, 944-956. 10.1021/acs.biochem.6b01296.

- Raina, H., Zacharia, J., Li, M., and Wier, W.G. (2009). Activation by Ca2+/calmodulin of an exogenous myosin light chain kinase in mouse arteries. J Physiol 587, 2599-2612. 10.1113/jphysiol.2008.165258.
- Rappsilber, J., Mann, M., and Ishihama, Y. (2007). Protocol for micro-purification, enrichment, pre-fractionation and storage of peptides for proteomics using StageTips. Nat Protoc 2, 1896-1906. 10.1038/nprot.2007.261.
- Sengprasert, P., Amparyup, P., Tassanakajorn, A., and Wongpanya, R. (2015). Characterization and identification of calmodulin and calmodulin binding proteins in hemocyte of the black tiger shrimp (Penaeus monodon). Dev Comp Immunol 50, 87-97. 10.1016/j.dci.2015.02.003.
- Swulius, M.T., and Waxham, M.N. (2008). Ca(2+)/calmodulin-dependent protein kinases. Cell Mol Life Sci 65, 2637-2657. 10.1007/s00018-008-8086-2.
- Wallace, R.W., Tallant, E.A., Dockter, M.E., and Cheung, W.Y. (1982). Calcium binding domains of calmodulin. Sequence of fill as determined with terbium luminescence. J Biol Chem 257, 1845-1854.
- Wang, Y., Chen, L., Wier, W.G., and Zhang, J. (2013). Intravital Forster resonance energy transfer imaging reveals elevated [Ca2+]i and enhanced sympathetic tone in femoral arteries of angiotensin II-infused hypertensive biosensor mice. J Physiol 591, 5321-5336. 10.1113/jphysiol.2013.257808.
- Wang, N., Zhong, X., Song, X., Gu, X., Lai, W., Xie, Y., Peng, X., and Yang, G. (2017). Molecular and biochemical characterization of calmodulin from Echinococcus granulosus. Parasit Vectors 10, 597. 10.1186/s13071-017-2545-2.

- Webb, R.C. (2003). Smooth muscle contraction and relaxation. Adv Physiol Educ 27, 201-206. 10.1152/advan.00025.2003.
- Wier, W.G., Rizzo, M.A., Raina, H., and Zacharia, J. (2008). A technique for simultaneous measurement of Ca2+, FRET fluorescence and force in intact mouse small arteries. J Physiol 586, 2437-2443. 10.1113/jphysiol.2008.151522.
- Xia, Z., and Storm, D.R. (2005). The role of calmodulin as a signal integrator for synaptic plasticity. Nat Rev Neurosci 6, 267-276. 10.1038/nrn1647.
- Zhang, J., Wang, Y., Chen, L., Wier, W.G., and Blaustein, M.P. (2019). Na(+)/Ca(2+) exchanger overexpression in smooth muscle augments cytosolic Ca(2+) in femoral arteries of living mice. Am J Physiol Heart Circ Physiol 316, H298-H310. 10.1152/ajpheart.00185.2018.

CONCLUSION

Research into cellular and mitochondrial Ca^{2+} signaling has revolutionized our understanding of chemistry, basic biology, and human disease. Nevertheless, the field of mitochondrial Ca^{2+} signaling is relatively young; indeed, much of the mitochondrial machinery central to this signaling was only identified within the past two decades. Much work remains to better understand the complex interplay between Ca^{2+}, mitochondrial function, and the rest of the cell.

Fortunately, this field is developing rapidly. Diseases with a mitochondrial component – such as Alzheimer's Disease, Parkinson's Disease, and obesity – are on the rise around the world, and interest in mitochondrial biology is rising with them. As the body of research for this field grows, so too will ideas for novel therapeutic strategies, research technologies, and medical interventions. A new mitochondria era is dawning.